

DOI: <https://doi.org/10.15388/vu.thesis.472>

<https://orcid.org/0000-0002-6772-5693>

VILNIUS UNIVERSITY

CENTER FOR PHYSICAL SCIENCES AND TECHNOLOGY

Joanna Stocka

# Vibrational spectroscopic study of non-aromatic heterocyclic molecular compounds

**DOCTORAL DISSERTATION**

Natural Sciences

Physics (N 002)

---

VILNIUS 2023

This dissertation was written between 2015 and 2022 at the Institute of Chemical Physics, Vilnius University. The research was supported by the Research Council of Lithuania, Erasmus+ Programme and CEDC award.

**Scientific supervisor:**

**Prof. Dr. Valdas Šablinskas** (Vilnius University, Natural Sciences, Physics, N 002).

**Scientific consultant:**

**Assoc. Prof. Habil. Dr. Paweł Rodziewicz** (Jan Kochanowski University, Natural Sciences, Chemistry, N 003).

**Dissertation Defense Panel:**

**Chairman - Prof. Habil. Dr. Jūras Banys** (Vilnius University, Natural Sciences, Physics, Physics, N 002).

**Members:**

**Prof. Habil. Dr. Vidmantas Gulbinas** (Vilnius University, Natural Sciences, Physics, N 002),

**Assoc. Prof. Dr. Kęstutis Aidas** (Vilnius University, Natural Sciences, Physics, N 002),

**Dr. Martynas Talaikis** (Center for Physical Science and Technology, Natural Sciences, Chemistry N 003),

**Assoc. Prof. Habil. Dr. Aneta Jezierska** (Wroclaw University, Natural Sciences, Chemistry, N 003).

The dissertation shall be defended at a public meeting of the Dissertation Defense Panel at 15:00 on 24th May 2023 in Room B336 of the National Center for Physical Sciences and Technology.

Address: Saulėtekio al. 3, NFTMC, Room B336, Vilnius, Lithuania.

Tel. +370 5 264 8884; e-mail: office@ftmc.lt;

The text of this dissertation will be accessed at the Vilnius University Library, as well as on the website of Vilnius University:

[www.vu.lt/naujienos/ivykiu-kalendorius](http://www.vu.lt/naujienos/ivykiu-kalendorius).

DOI: <https://doi.org/10.15388/vu.thesis.472>

<https://orcid.org/0000-0002-6772-5693>

VILNIAUS UNIVERSITETAS  
FIZINIŲ IR TECHNOLOGIJOS MOKSLŲ CENTRAS

Joanna Stocka

# Nearomatinių heterociklinių molekulių darinių tyrimas virpesinės spektroskopijos metodais

**DAKTARO DISERTACIJA**

Gamtos mokslai  
Fizika (N 002)

---

VILNIUS 2023

Disertacija rengta 2015-2022 metais Vilniaus universiteto Cheminės fizikos institute. Disertacijos ruošimą parėmė Lietuvos mokslo taryba, Erasmus+ programa ir CEDC.

**Mokslinis vadovas - prof. dr. Valdas Šablinskas** (Vilniaus universitetas, gamtos mokslai, fizika, N 002).

**Mokslinis konsultantas - prof. habil. dr. Paweł Rodziewicz** (Jano Kochanovskio universitetas, gamtos mokslai, chemija, N 003).

### **Gynimo taryba:**

**Pirmininkas – prof. habil. dr. Jūras Banys** (Vilniaus universitetas, gamtos mokslai, fizika, N 002).

### **Nariai:**

**Prof. habil. dr. Vidmantas Gulbinas** (Vilniaus universitetas, gamtos mokslai, fizika, N 002),

**Prof. dr. Kęstutis Aidas** (Vilniaus universitetas, gamtos mokslai, fizika, N 002),

**Dr. Martynas Talaikis** (Vilniaus universitetas, gamtos mokslai, chemija, N 003),

**Prof. habil. dr. Aneta Jezierska** (Vroclavo universitetas, gamtos mokslai, chemija, N 003).

Disertacija ginama viešame Gynimo tarybos posėdyje 2023 m. gegužės 24 d. 15 val., Nacionalinio fizinių ir technologijų mokslų centro B336 auditorijoje. Adresas: Saulėtekio al. 3, NFTMC, B336 auditorija, Vilnius, Lietuva. Tel. +370 5 264 8884; el. paštu: office@ftmc.lt;

Disertaciją galima peržiūrėti Vilniaus universiteto, Fizinių ir technologijos centro bibliotekose ir VU interneto svetainėje adresu: [www.vu.lt/naujienos/ivykiu-kalendorius](http://www.vu.lt/naujienos/ivykiu-kalendorius).

## ACKNOWLEDGEMENTS

I am thrilled to express my gratitude for the opportunity to experience the magnificence of Vilnius and Lithuania during the exceptional phase of my doctoral dissertation. My heart brims with deep gratitude to Vilnius University and the Institute of Chemical Physics for embracing me with open arms.

I would like to extend my sincere appreciation to Professor Valdas Šablinskas, my supervisor, for his exceptional guidance, unyielding motivation, and unflinching support throughout the entire journey. I cannot thank him enough for his invaluable tips during the experiments and data analysis, which significantly contributed to the successful completion of my research. I would also like to thank him for his constant willingness to help.

Additionally, I express immense gratitude to Professor Paweł Rodziewicz for introducing me to computational methodology and creating a safe space where no question was ever considered 'stupid.' The scientific discussions we had enriched my knowledge and contributed immensely to my research.

I want to thank Professor Justinas Čeponkus for his exceptional guidance in the laboratories, numerous brilliant ideas, and explanations of concepts that were previously unknown to me. His contributions were invaluable, and I cannot thank him enough for his unwavering support.

It is with great pleasure that I extend my appreciation and gratitude to Rasa Platakytė for her companionship during laboratory work and the time we shared whenever it was possible, making the entire experience even more enjoyable and memorable.

I would like to thank Professor Gamil Guirgis and his esteemed group at Charleston College for their invaluable contributions to my research. Without their expertise in the synthesis of heterocyclic compounds, my research would not have been possible.

I would like to thank every member of the Institute of Chemical Physics at Vilnius University for their kindness, numerous insightful discussions, and deep insights into high-level science.

Last but not least, I would like to express my deep gratitude to my family. My Husband Marek, who played a crucial role in the successful completion of my research. Without his support, patience, and understanding, I would not have been able to accomplish my goals. Thank you, Romek and Zbyszek, for being my pillars of strength and for reminding me that nothing is impossible. I am immensely proud to be your parent and grateful for the love and joy you bring to my life. To my dear Mother, thank you for your belief in me and your constant encouragement. To my Sisters, thank you for always being there for me.

## LIST OF ABBREVIATIONS

1-ClM-1-F-SiCH	1-chloro-1-chloromethyl-silacyclohexane $C_6H_{12}ClFSi$
1-ClM-1-F-SiCP	1-chloromethyl-1-fluoro-silacyclohexane $C_6H_{12}Cl_2Si$
1-ClM-1-F-SiCP	1-chloromethyl-1-fluoro-silacyclopentane $C_5H_{10}ClSi$
1-M-GeCH	1-methyl-germacyclohexane $C_6H_{11}CH_3$
3A3S	1,3,5,2,4,6-triazatrisilinane $Si_3(NH)_3H_6$
6M3A3S	2,2,4,4,6,6-hexamethyl-1,3,5,2,4,6-triazatrisilinane $Si_3(NH)_3(CH_3)_6$
ATR	attenuated total reflectance
B	boat
B3LYP	hybrid Becke, Lee, Yang, Parr functional
BLYP	Becke, Lee, Yang, Parr functional
C	chair
CP-MD	Car-Parrinello Molecular Dynamics
DFT	Density Functional Theory
E	envelope
FT-IR	Fourier-transform infrared spectroscopy
H	half-chair
MP2	Møller-Plesset perturbation theory 2nd order
PBE	Perdew, Burke, Ernzerhof functional
PES	potential energy surface
PW	plane wave
RDF	radial distribution function
S	skew-boat
T	twist
THF	oksolan (tetrahydrofuran) $C_4H_8O$

# CONTENTS

ACKNOWLEDGEMENTS	5
LIST OF ABBREVIATIONS	6
CONTENTS	7
INTRODUCTION	10
GOALS AND TASKS OF THE WORK	14
PRACTICAL AND SCIENTIFIC NOVELTY	15
STATEMENTS TO BE DEFENDED	16
CONTRIBUTION OF THE AUTHOR	17
LIST OF PUBLICATIONS	18
1 CHAPTER: HETEROCYCLIC COMPOUNDS	21
1.1 Conformational diversity of five- and six-member ring molecules . . .	21
1.2 Structure and energetics of oxolanes . . . . .	23
1.3 Properties of silicon and Si containing heterocyclic molecules . . .	24
1.3.1 Conformational analysis and energetics of silacyclopentanes . . .	26
1.3.2 Conformational analysis and energetics of silacyclohexanes . . .	27
1.4 Structure and energetics of $\text{Si}_n\text{-N}_m$ clusters . . . . .	29
1.5 Properties of germanium and Ge containing heterocyclic molecules	31
2 CHAPTER: INTRODUCTION TO EXPERIMENTAL AND THEORETICAL METHODS USED	33
2.1 Experimental methods . . . . .	33
2.1.1 Raman spectroscopy . . . . .	33
2.1.2 Infrared spectroscopy . . . . .	35
2.1.3 Attenuated total reflectance infrared spectroscopy . . . . .	36
2.1.4 Matrix isolation technique . . . . .	37
2.2 Computational methods . . . . .	40
2.2.1 Hartree-Fock approach and other approximations . . . . .	41
2.2.2 Global and local energy minima . . . . .	42
2.2.3 Density Functional Theory . . . . .	43
2.2.4 Car-Parrinello Molecular Dynamics . . . . .	48
2.2.5 Boltzmann probability distribution function . . . . .	50
2.2.6 Python based proprietary programs . . . . .	51
3 CHAPTER: MATERIALS AND METHODS	52
3.1 Experimental methods . . . . .	52
3.2 Computational methods . . . . .	53
4 CHAPTER: RESULTS AND DISCUSSION ON FIVE MEMBER RING HETEROCYCLES	55

4.1	Tetrahydrofuran (THF) . . . . .	55
4.1.1	Static Density Functional Theory based calculations . . . . .	55
4.1.2	Car-Parrinello molecular dynamics simulations . . . . .	55
4.1.3	Matrix isolation experiment . . . . .	58
4.1.4	Vibrational analysis . . . . .	59
4.1.5	Conclusions . . . . .	61
4.2	1-chloromethyl-1-fluoro-silacyclopentane (1-CIM-1-F-SiCP) . . . . .	62
4.2.1	Density Functional Theory and Møller–Plesset based calculations . . . . .	62
4.2.2	Potential energy surface scan . . . . .	63
4.2.3	FT-IR spectra in the gas phase . . . . .	65
4.2.4	Matrix isolation experiment . . . . .	66
4.2.5	Conclusions . . . . .	68
5	CHAPTER: RESULTS AND DISCUSSION ON SIX MEMBER RING HETEROCYCLES . . . . .	70
5.1	1-chloromethyl-1-fluoro-silacyclohexane (1-CIM-1-F-SiCH) . . . . .	70
5.1.1	Density Functional Theory and Møller–Plesset based calculations . . . . .	70
5.1.2	Potential energy surface scan . . . . .	71
5.1.3	FT-IR vibrational analysis of sample in the liquid and gas phase . . . . .	73
5.1.4	Matrix isolation experiment . . . . .	74
5.1.5	Conclusions . . . . .	75
5.2	1-chloro-1-chloromethyl-silacyclohexane (1-Cl-1-CIM-SiCH) . . . . .	76
5.2.1	Density Functional Theory and Møller–Plesset based calculations . . . . .	76
5.2.2	Potential energy surface scan . . . . .	78
5.2.3	FT-IR vibrational analysis of sample in the liquid and gas phase . . . . .	81
5.2.4	Matrix isolation experiment . . . . .	82
5.2.5	Conclusions . . . . .	84
5.3	Car-Parrinello molecular dynamics of the 1-Cl-1-CIM-SiCH and 1-CIM-1-F-SiCH molecules . . . . .	85
5.4	1-methyl-germacyclohexane . . . . .	90
5.4.1	Density Functional Theory and Møller–Plesset based calculations . . . . .	90
5.4.2	Potential energy surface scan . . . . .	91
5.4.3	Matrix isolation experiment . . . . .	92
5.5	Conclusions . . . . .	94
5.6	1,3,5,2,4,6-triazatrisilane and hexamethyl derivate . . . . .	95
5.6.1	Density Functional Theory and Møller–Plesset based calculations . . . . .	95
5.6.2	Potential energy surface scan . . . . .	96
5.6.3	Matrix isolation experiment . . . . .	97
5.7	Conclusions . . . . .	99
5.8	Summary on the influence of heteroatom/substituent to conformational stability . . . . .	99
	CONCLUSIONS . . . . .	106



SANTRAUKA LIETUVIŲ KALBA	109
APPENDIX I TABLES	121
BIBLIOGRAPHY	139
CURRICULUM VITAE	155

## INTRODUCTION

Conformational diversity of heterocyclic molecules plays a very important role in chemical and biochemical processes. Complete understanding of the majority of chemical reactions involves taking into account the liquid or solid environment. Therefore, one has to treat the chemical process as a complex set of mutually interacting molecular systems. From this perspective we have to consider hundreds, thousands, millions or even more atoms to construct a proper model of the investigated process. In many cases such approach is either a tedious task or it is simply impossible. One of the most common ways to overcome this problem is to represent a complex system using a much smaller model with the same properties. Five- and six-member saturated heterocyclic molecules form a group of chemical compounds which are crucial in various natural processes as well as in industrial applications. Following the idea presented above one can try to understand the structural and energetic properties of selected, characteristic, molecules which belong to this wide group of species and to draw conclusions on the influence of structural parameters on the stability of the systems belonging to this group. Therefore, in order to find the structural-energetic correlations of the five- and six-member saturated heterocyclic molecules some specific chemical compounds have been selected for the detailed studies.

On the basis of the structure and its composition, including heteroatoms, the following compounds have been chosen: tetrahydrofuran, silicon and germanium based five and six-member ring saturated heterocycles and Si-N six-member ring neutral clusters.

Tetrahydrofuran (THF) finds its usage in industry applications [1, 2], can be a precursor in the synthesis of biologically active molecules [3], or be used as a monomer in polymerization [4]. The small size of the molecule makes it a perfect model of the deoxyribose in the DNA chain. [5] Ring of the tetrahydrofuran molecule can exist in two conformations, as envelope with  $C_s$  symmetry and as twisted with  $C_2$  symmetry. The low energy barrier between conformers causes the  $C_s \longleftrightarrow C_2$  interconversion (pseudorotation). This process was described for the first time for the cyclopentane molecule. [6, 7] Many mutually exclusive scientific experimental and computational results on the stability of the tetrahydrofuran conformers have sparked lively discussion, considering which conformer is the true global energy minimum structure.

Investigation of the properties of the small heterocycles chosen as model systems can give insight into the more complex macrocycles guest-host interaction and can be used in the drug design. [8–16] The wide usage of silicon based compounds makes them important models to investigate. The most common use of such compounds is as constituents in the production of more sophisti-

cated materials, including glasses, ceramics, cement, fiber optics, liquid crystal, silicones, and many other polymers. [17–26]

The five and six- member ring molecules with one silicon atom can be considered as part of larger biologically active molecules with vast medical applications. They were comprehensively studied during the search for a variety of drugs. [27–32] Due to the good adsorption properties, the silicon-containing molecules are hydrophobic and have potential use in the novel hydrophobic coatings. The silicon containing materials are usually less toxic and might be used as a Teflon replacement. [17, 33]

The investigation of the spectroscopic properties and conformational diversity of the silacyclohexanes and silacyclopentanes is crucial, for developing the molecules with desired medical and industrial applications.

Germanium, called a "technology-critical element", has its applications in the fiber-optics industry, infrared optics, as a polymerization catalyst, and for electronics and solar electric applications, as well as in metallurgy and chemotherapy. [34, 35] Introduction of the germanium atom to the cyclohexane ring causes changes in the structural parameters, conformational stability, and reactivity. The nature and detailed description of the conformational variety of germanocyclohexanes is still unclear. Generally, germanium has lower electronegativity than carbon, and its atom van der Waals radius is longer, leading to the formation of longer chemical bonds. Elongation of the bonds in the cyclic rings can cause an increase in the ring flexibility.

By now, germacyclohexane was the subject of the electron diffraction, [36] as well as infrared and Raman spectroscopy experiments supported by the DFT calculations [37] studies. It was found that stable conformers have chair and skew-boat type structures, but due to the low population, the less stable structure can not be traced under experimental conditions.

Six-membered ring  $\text{Si}_n\text{N}_m$  systems also called mixed silicon clusters, have received a great deal of attention both experimentally and theoretically. [38–42] These clusters are often investigated due to their prominent roles in the development of materials with astrophysical, environmental, and biomedical applications. [38] Silicon nitride six-membered ring systems have been studied to gain insight into the morphology and properties of bulk silicon nitride. Ye and co-workers studied a series of  $\text{Si}_n\text{N}_m$  clusters using DFT with a TZ2P basis set. They reported that the structures evolve from planar to three dimensions as the number of atoms increases.

In the last century, the majority of scientific studies on structural and energetic properties of five- and six-membered heterocyclic molecules focused on experimental techniques, mainly diffraction and spectroscopy-based methods. For the samples in the gas phase, the spectroscopic techniques can deliver precise structural parameters based on the rotational spectra. Investigation of the chemical compounds in the liquid phase utilizing spectroscopic methods is

much more complex due to the environment. FT-IR spectra can become very complicated due to the large number of spectral bands and their mutual overlapping. Such effects lead to loss and/or uncertainty of the information, such as the spectroscopic parameters. Among several experimental methods used for conformational diversity analysis, the matrix isolation infrared absorption spectroscopy is used. The cryogenic temperature of the molecule:matrix mixture causes rapid solidification of the sample, thus reflecting the thermodynamic stability of the room temperature gaseous sample. The molecule can be investigated as a non-interacting system, excluding or minimizing the environmental influence. This technique uses inert matrix materials such as noble gasses, to prohibit the inter- and intra-molecular interactions. [43–45] The spectral bands obtained from the matrix isolation spectroscopic experiments are much narrower than the standard approach and well separated allowing for the search of the characteristic bands belonging to different conformers. Even though the matrix isolation technique provides good insight into the properties of the isolated systems, the analysis of FT-IR spectra gets much more complicated when the size of the system under study increases.

In the last two decades, we observe a enormous increase in computational resources worldwide. Rapid development of new high-performance computing clusters with a combination of parallelized software enabled the usage of quantum-mechanics-based methods to model chemical processes. Nowadays, one can compute the energetic properties of systems of the size of hundreds of atoms with good precision. Therefore, a natural way to resolve FT-IR spectra and assign respective vibrational bands is to combine experimentally obtained spectroscopic parameters and results of the computational vibrational analysis.

Five- and six-member heterocyclic molecules are a good target for combined computational and experimental investigations due to their moderate size. The selected group of the molecules contains different heteroatoms and might serve as a good representation of five- and six-member ring heterocyclic species. Investigation of all possible canonical ring shapes and position of the substituents is crucial to performing detailed conformational analysis. Up to now the most common combination of experimental and theoretical methods was based on FT-IR matrix isolation spectra and static DFT/MP2 calculations. The introduction of Car-Parrinello molecular dynamics simulations enables the description of the *kinetics* of molecular systems, contrary to the *thermodynamic picture* present in the static calculations. With the help of molecular dynamics simulations, it is possible to trace the *dynamics* of the molecular changes, in particular, to obtain a qualitative and quantitative description of intra- and inter-molecular interactions at the atomistic level.

The present dissertation addresses two primary challenges. Firstly, it aims to overcome the deficiency of structural and spectroscopic data concerning selected novel heterocyclic compounds. Secondly, it seeks to improve the accuracy

of static calculations by accounting for the dynamic behavior of molecules in their environment. To achieve this, we introduce a time-dependent explicit model of molecules isolated in a nitrogen matrix with the use of the Car-Parrinello molecular dynamics simulations, which provides insights into the conformational changes of these molecules over time.

## GOALS AND TASKS OF THE WORK

The main goal of this dissertation is a complete description of the saturated heterocyclic molecular compounds in terms of their structural, energetic and IR and Raman spectroscopic properties for systematic analysis of conformational diversity of canonical five- and six-member ring heterocyclic molecules using both- advanced spectroscopic experimental and computational methods. The goals of the work were achieved by accomplishing the tasks listed below:

- Conformational studies of tetrahydrofuran, 1-chloromethyl-1-fluoro-silacyclopentane, 1-chloromethyl-1-fluoro-silacyclohexane, 1-chloro-1-chloromethyl-silacyclohexane, 1-methyl-1germacyclohexane and 2,2,4,4,6,6-hexamethyl-1,3,5,2,4,6-triazatrisilinane by means of matrix isolation FTIR spectroscopy.
- Complete theoretical conformational analysis of all investigated molecules utilizing DFT and MP2 static computational methods employing potential energy surface scans for the conformer interconversion and calculations of energy barriers.
- Complete CP-MD simulations of explicit matrix isolation experiment model and for tetrahydrofuran, 1-chloromethyl-1-fluoro-silacyclohexane and 1-chloro-1-chloromethyl-silacyclohexane.
- Unification of computational methodology for a systematic investigation of conformational stability of six member ring saturated heterocycles. Influence of heteroatoms (Ge, Si) and substituents (-Cl, -F, -CH<sub>3</sub>, CH<sub>2</sub>Cl) on the conformational landscape.
- Systematic theoretical study of conformational stability for the Si<sub>3</sub>(NH)<sub>3</sub>H<sub>6</sub> (1,3,5,2,4,6-triazatrisilinane) and its ligated counterpart Si<sub>3</sub>(NH)<sub>3</sub>(CH<sub>3</sub>)<sub>6</sub> (2,2,4,4,6,6-hexamethyl-1,3,5,2,4,6-triazatrisilinane) neutral clusters utilizing DFT and MP2 methods.

## PRACTICAL AND SCIENTIFIC NOVELTY

The research concerning substituted and unsubstituted heterocyclic saturated compounds focuses on tetrahydrofuran, 1-chloromethyl-1-fluoro-silacyclohexane, 1-chloro-1-chloromethyl-silacyclohexane, 1-chloromethyl-1-fluoro-silacyclopentane and 2,2,4,4,6,6-hexamethyl-1,3,5,2,4,6-triazatrisilane. Apart from the tetrahydrofuran, all other aforementioned molecules were newly synthesized, in the course of searching for new hydrophobic coating materials. These novel species were investigated with state-of-the-art spectroscopic and theoretical methods for the first time.

The matrix isolation technique was used for the complete and systematic assignment of vibrational modes in the FT-IR absorption spectra for investigated species. Annealing experiments allowed to find the marker bands for particular low-energy conformers' and the conformational rearrangements.

The scientific novelty of the research originates also from a unique approach based on a combination of experimental results and static DFT/MP2 calculations supported with Car-Parrinello molecular dynamics simulations.

Systematic computational studies covered all possible canonical ring shapes and axial/equatorial, *trans/gauche* substituents positions of investigated molecules. In the case of silacyclomolecules, blue-shifting weak hydrogen bonds and their effect on the conformers structure have been observed for the first time.

With the help of periodic boundary conditions, a realistic model of the nitrogen matrix has been proposed with explicit nitrogen atoms located as in the alpha or beta phase of the N<sub>2</sub> crystal, depending on the temperature. Car-Parrinello molecular dynamics simulations also allowed a deeper understanding of the kinetics of conformational stability with respect to the temperature changes, namely obtaining the lifetime of the specific conformers and the time of their mutual interconversion. Analysis of trajectories from molecular dynamics simulations required the creation of new software, thus the scripts based on the Python programming language were implemented to automatize some procedures and now can be shared and used within the scientific community.

The investigated molecules belong to the class of six-member heterocyclic systems and there are many other examples of such kind of compounds. It was however difficult to compare the results of these studies to other data present in the literature due to the different methods used. Therefore in this work, some of the results for already existing molecules were recalculated at the same level of theory in order to draw general conclusions on the energetic, structural, and spectroscopic properties of six-member ring heterocyclic species.

## STATEMENTS TO BE DEFENDED

1. The matrix isolation experiments allow to observing not overlapping characteristic spectral bands of different conformers for heterocyclic five- and six-member ring molecules. The annealing experiment prove the existence of the conformer interconversion under experimental conditions.
2. Car-Parrinello molecular dynamics simulations are very informative for estimating of the ratio between envelope and twisted conformations with respect to a change in temperature. Simulations at finite temperatures describe the lifetime of the tetrahydrofuran conformations and the  $C_2 \rightarrow C_s$  and  $C_s \rightarrow C_2$  rearrangements.
3. The type of the media used as a host-material in the matrix isolation experiment influences axial *gauche*  $\rightarrow$  axial *trans* conformational changes in five and six membered saturated heterocycles, the polar  $N_2$  matrix stabilizes conformers with a higher dipole moment.
4. A newly proposed model of the matrix isolation experiment from Car-Parrinello molecular dynamics simulations, based on explicit nitrogen molecules, confirms the existence of weak C-H $\cdots$ N hydrogen bonds between host and guest species.
5. The introduction of methyl substituents to silicon ring atoms of 1,3,5,2,4,6-triazatrisilinane molecular cluster affects the conformational stability, reducing the number of stable conformers.



## CONTRIBUTION OF THE AUTHOR

The experimental work was performed in the Laboratories of the Institute of Chemical Physics at Vilnius University, Lithuania. The experiments were performed by the author or with Rasa Platakytė, under the supervision of Justinas Čeponkus and Valdas Šablinskas.

All static quantum-mechanical (DFT, MP2) calculations and Car-Parrinello molecular dynamics simulations were performed by the author, under the supervision of Paweł Rodziewicz. The supercomputer resources were delivered by the High Performance Computing Center (HPCC) of the Lithuanian National Center of Physical and Technology Sciences (NCPTS) at Vilnius University and Jan Kochanowski University of Kielce. Python-based programs were written and have been applied for the analysis of results by the author.

Publications of this work were written by the author [A1, A2, A4, A5, A6] and revised and corrected by co-authors. The paper on the 1-chloromethyl-1-fluoro-silacyclohexane [A3] was written by the author and Rasa Platakytė and revised and corrected by co-authors.

## LIST OF PUBLICATIONS

On the dissertation topic

- [A1] **J. Stocka**, J. Čeponkus, V. Šablinskas, P. Rodziewicz, Conformational diversity of the THF molecule in N<sub>2</sub> matrix by means of FTIR matrix isolation experiment and Car-Parrinello molecular dynamics simulations, *Spectrochimica Acta Part A: Molecular and Biomolecular Spectroscopy* **238**, 2020, 118425.
- [A2] T.M.C McFadden, R. Platakytė, **J. Stocka**, J. Čeponkus, V. Aleksa, T. Carrigan-Broda, V. Šablinskas, P. Rodziewicz, G.A. Guirgis, Experimental (Raman and IR) and computational (DFT, MP2) studies of conformational diversity of 1-chloromethyl-1-fluorosilacyclohexane, *Journal of Molecular Structure*, **1221**, 2020, 128786.
- [A3] **J. Stocka**, R. Platakytė, T.M.C. McFadden, J. Čeponkus, V. Aleksa, A.G. Hanna, V. Šablinskas, P. Rodziewicz, G.A. Guirgis, Conformational diversity of 1-chloro-1-chloromethyl-silacyclohexane with experimental (Raman and IR) and computational (DFT, MP2) methods, *Journal of Molecular Structure*, **1249**, 2022, 131644.
- [A4] **J. Stocka**, R. Platakytė, D. Hickman, T. Carrigan-Broda, J. Čeponkus, V. Šablinskas, P. Rodziewicz, G.A. Guirgis, Experimental (Raman and IR) and computational (DFT, MP2) studies of the conformational diversity of 1-chloromethyl-1-fluorosilacyclopentane molecule, *Journal of Molecular Structure*, **1272**, 2023, 134125).
- [A5] **J. Stocka**, R. Platakytė, J. Macyte, V. Šablinskas, P. Rodziewicz, G.A. Guirgis, Influence of heteroatoms and substituents on structural and spectroscopic parameters of saturated six-member ring heterocycles: experimental and theoretical study of 1-methyl-1-germacyclohexane, *Journal of Molecular Structure*, 2023, peer-reviewed.
- [A6] **J. Stocka**, J. Čeponkus, V. Šablinskas, P. Rodziewicz, G.A. Guirgis, Influence of methyl substituents on the conformational stability of Si<sub>3</sub>N<sub>3</sub>(CH<sub>3</sub>)<sub>6</sub> cluster: first principles and FT-IR matrix isolation study, *Journal of Molecular Structure*, 2023, submitted.

## Other publications

- [A7] **J. Lach (Stocka)**, J. Goclon, P. Rodziewicz, Structural flexibility of the sulfur mustard molecule at finite temperature from Car-Parrinello molecular dynamics simulations, *Journal of Hazardous Materials* **306**, 2016, 269-277.
- [A8] Y. Vaskivskiy, Y. Chernolevska, A. Vasylieva, V. Pogorelova, R. Platakytė, **J. Stocka**, I. Doroshenko, 1-Hexanol conformers in a nitrogen matrix: FTIR study and high-level ab initio calculations, *Journal of Molecular Liquids* **278**, 2019, 356-362.

## Research abroad, Traineeships

- [B1] **Research at the University of Białystok** Erasmus Practice Internship, Białystok, Poland, April – September 2016.
- [B2] **Toruń School of Molecular Modelling**, Molecular Modelling Traineeship, Supraśl, Poland, 11-15 April 2016.
- [B3] **Research at the Jan Kochanowski University of Kielce**, Erasmus Practice Internship, Kielce, Poland Erasmus Internship, February – September 2020.
- [B4] **From theory to the experiment: role of the molecular interactions in the self-organization of the molecules**, Seminar/Webinar, The Chemistry Department, University of Wrocław, Poland, 16 February 2022.
- [B5] **The practical approach of the classical molecular dynamics**, Traineeship, The Chemistry Department, University of Wrocław, Poland, 16 February 2022.

## Conference presentations

- [C1] **J. Lach (Stocka)**, P. Rodziewicz, M. Kozłowska, M. Baradyn, Differences in the structural flexibility of the sulfur and oxygen mustards molecules from Car-Parrinello molecular dynamics simulations, *Deutsche Physikalische Gesellschaft, Regensburg, Germany*, 2016.
- [C2] **J. Lach (Stocka)**, J. Čeponkus, V. Šablinskas, P. Rodziewicz, Tetrahydrofuran conformational diversity: FT-IR matrix isolation spectra and the theoretical study, *EUCMOS 2016 33rd European Congress on Molecular Spectroscopy, Szeged, Hungary*, 2016.

- [C3] **J. Lach (Stocka)**, J. Čeponkus, V. Šablinskas, P. Rodziewicz, FT-IR matrix isolation and theoretical study of tetrahydrofuran pseudorotation, Deutsche Physikalische Gesellschaft, Regensburg, Germany, 2016.
- [C4] **J. Lach (Stocka)**, R. Platakytė, J. Čeponkus, V. Šablinskas, V. Pavardenis, Conformational analysis of tetrahydrofuran by means of FT-IR matrix isolation spectra - hot nozzle experiment, Open Readings, Vilnius, Lithuania, 2016.
- [C5] R. Platakytė, **J. Lach (Stocka)**, J. Čeponkus, C. Crepin-Gilbert, A. Gutierrez, M. Chevalier, V. Šablinskas, Study of water-acetylacetone complexes by the means of matrix isolation infrared absorption spectrometry, Open Readings, Vilnius, Lithuania, 2016.
- [C6] **J. Stocka**, FTIR Matrix Isolation and CPMD methods in conformational analysis of THF molecule, Open Readings, Vilnius, Lithuania, 2017.
- [C7] **J. Stocka**, THF pseudorotation under FTIR Matrix Isolation and CPMD study, COINS International conference of Life sciences, Vilnius, Lithuania, 2017.
- [C8] **J. Stocka**, R. Platakytė, J. Čeponkus, V. Šablinskas, G. A. Guirgis, P. Rodziewicz, Computational and experimental vibrational study of 1-chloromethyl-1-fluorosilacyclohexane and its rearrangements, Open Readings, Vilnius, Lithuania, 2021.
- [C9] **J. Stocka**, R. Platakytė, J. Macyte, J. Čeponkus, V. Šablinskas, P. Rodziewicz, Kinetics of the conformational changes of the valeric acid in the nitrogen matrix: experiment meets theory at finite temperature, ACCORD 2022. Interdisciplinary Conference on Drug Sciences Synergy of interdisciplinary innovations - **awarded as the best presentation**, Warsaw, Poland, 26-28 May, 2022.
- [C10] **J. Stocka**, V. Šablinskas, Conformational diversity of non-aromatic heterocyclic molecular compounds as studied by means of matrix isolation infrared spectroscopy, International Symposium on Molecular Spectroscopy, Champaign-Urbana, 20-24 June, 2022.
- [C11] **J. Stocka**, P. Rodziewicz, V. Šablinskas, G. A. Guirgis, Kinetics of the conformational changes of the nitrogen matrix isolated disubstituted silacyclohexanes: experiment meets theory at finite temperatures, Open Readings, Vilnius, Lithuania, 18-21 April, 2023.
- [C12] Jovilė Mačytė, Rasa Platakyte, **J. Stocka**, Valdas Šablinskas, Structural analysis of the valeric acid structure using matrix isolation FTIR spectroscopy and *ab initio* calculations, Open Readings, Vilnius, Lithuania, 18-21 April, 2023.

# 1. CHAPTER: HETEROCYCLIC COMPOUNDS

## 1.1. Conformational diversity of five- and six-member ring molecules

The shape of the heterocyclic molecules play a very important role in the chemical and biochemical reactions, for example, glycosidase reactions. Modeling of the small heterocycles can give insight into the more complex macrocycles, their guest-host interaction, and drug design. [8–16]

The ring shape variety is dictated by the out-of-plane ring atoms bending, as a result of the rotation of bonds in the ring. This is called ring puckering. The ring puckering motion produce the canonical structures. For simple unsubstituted cycloalkanes, the representative structures are degenerated, but the introduction of the heteroatom produces a larger number of possible conformers. [46]

Ring puckering might be developed through many methods. One of them is based on the displacement of the ring atoms from the ring plane in perpendicular direction measurements. [7, 47–50] Another method in common usage is the investigation of the ring torsion angles, but can not be used while the pseudorotation is investigated. [51]

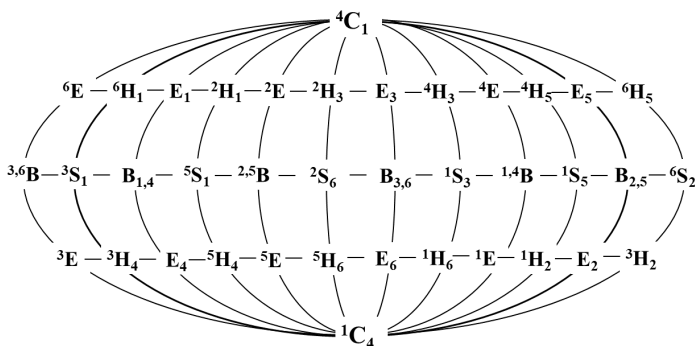


Figure 1.1: 2-dimensional scheme of the Cremer-Pople sphere: 38 canonical cyclohexane structures.

Among these methods the Cremer-Pople puckering coordinates [47, 49] are frequently used [48, 52] this approach allows for reducing the number of parameters to  $N-3$  ( $N$ -number of atoms in the ring), to describe the geometry of the ring. The description of the conformational space of five-member and six-member ring is then limited to 2 (5-3) and 3 (6-3) parameters, respectively. [47, 48]

The 5-member ring unsubstituted molecules can exist in two stable conformers, namely envelope ( $C_s$ ) and twisted ( $C_2$ ) (see Fig. 1.2). While one the heteroatom is introduced to the cyclic ring, the number of canonical ring

conformers rise to 20. [48]

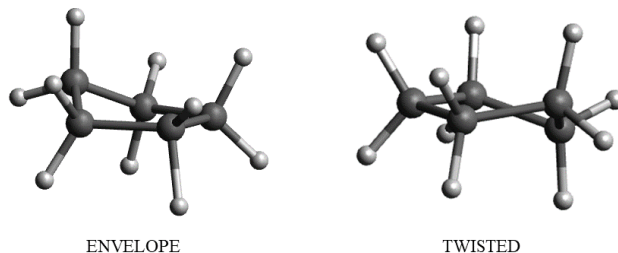


Figure 1.2: The envelope (left) and twisted (right) conformations of five member ring molecule i.e. cyclopentane.

For 6-member ring molecules substituted with 1 heteroatom, this method gives 38 canonical conformers. Among them, we can distinguish chair (2), boat (6), skew-boat (6), half-chair (12), and envelope (12). [50, 53]

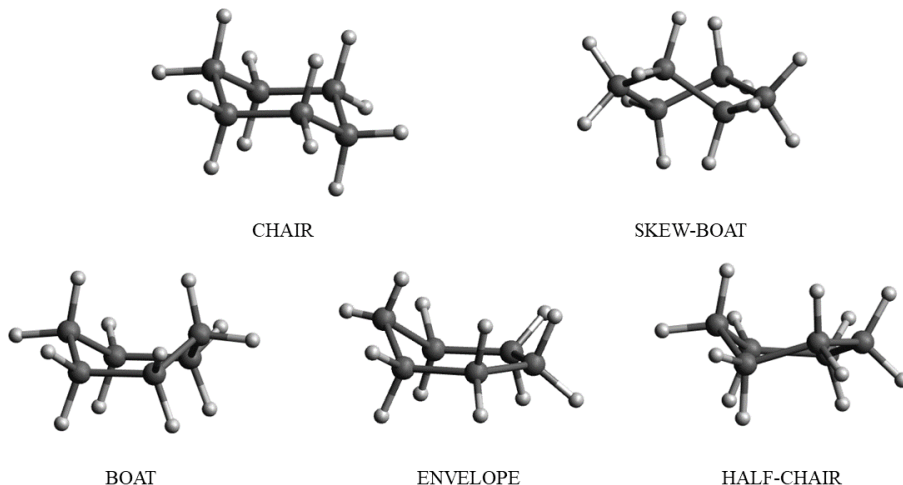


Figure 1.3: The chair, skew-boat, boat, envelope and half-chair conformers of six member ring molecule i.e. cyclohexane.

The nomenclature for the investigated five- and six-member ring molecules was used pyranoses. The chair, boat, twist-boat, half-chair, and envelope are described with C, B, T, H, and E letters, respectively. [54, 55] The number with super-, sub-script denote atoms that are above or below the ring plane. [55] Additionally, in the ring numbering we introduce the Si/Ge without number. For example,  $^{Si}C_4$  is the conformer with the chair ring conformation, where atom silicon atom is above and atom number 3 is below the ring plane).

Despite the canonical ring shape it is crucial to consider differences in conformations based on the axial/equatorial and *cis/trans/gauche-/gauche+* positions of the substituents. The *cis/trans/gauche-/gauche+* positions are present

in the molecules containing  $-\text{CH}_3\text{X}$  group and are caused by its rotation, explicitly describing the position of the X atom with respect to the second substituent attached to the heteroatom as in Fig.1.4.

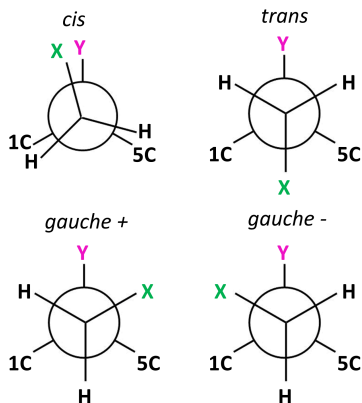


Figure 1.4: The Newman projection of the X-C-Si/Ge/C-Y dihedral angle for  $-\text{CH}_3\text{X}$  substituted heterocyclic molecules.

In this work, we did not investigate the *cis* position of the X-C-Si/Ge/C-Y dihedral angle. The steric hindrance and repulsive interaction of F/Cl make this conformation unfavorable. [56–58]

## 1.2. Structure and energetics of oxolanes

Tetrahydrofuran (THF) known as oxolane is cyclic ether its structure is depicted in Fig. 1.5. THF finds its usage in industry applications [1, 2], can be a precursor in the synthesis of biologically active molecules [3], or used as a monomer in polymerization. [4] The tetrahydrofuran molecule was used as a model of the deoxyribose in the DNA chain. [5] The THF ring (like other cyclopentane molecules), is not planar and can exist in two conformations, envelope (E) with  $C_s$  symmetry and twisted (T) with  $C_2$  symmetry.

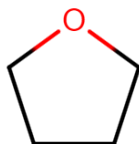


Figure 1.5: Structure of the tetrahydrofuran molecule.

The energy barrier between conformers is low, leading to the constant  $C_s \longleftrightarrow C_2$  interconversion. Such a process is called a pseudorotation and was

described for the first time for the cyclopentane molecule. [6, 7] Small energy difference and the presence of many mutually exclusive scientific experimental and computational results have sparked lively discussion, trying to answer which conformer is true global energy minimum structure.

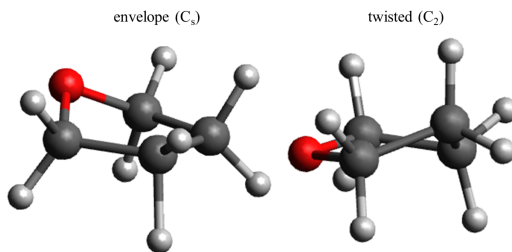


Figure 1.6: Tetrahydrofuran molecule in envelope ( $C_s$ ) and twisted ( $C_2$ ) conformations.

Despite the fact, that several computational studies on the THF conformational stability utilizing DFT and *ab initio* methods indicate that twisted conformer is the global minimum [59–62], some of the researchers point that the lowest energy conformer is envelope structure [63, 64]. These differences are based mostly on the level of theory used during the computational investigation. The CCSD(T) method gives accurate results for small molecules, such as tetrahydrofuran. This method was used for THF monomer, dimer, trimer, and tetramer analysis. [65] The envelope  $C_s$  conformer was found to be the true global energy minimum structure, with the  $C_2$  conformer as the local energy minimum with a calculated relative energy difference equal to 0.14 kcal/mol. The conformational stability of the THF molecule was investigated with experimental methods as well.

Due to the electron momentum (EMS) [66] and infrared (IR) [67] spectroscopy, the  $C_2$  conformer distribution in the experimental gas-phase sample is bigger than  $C_s$ . The rotational spectra of the tetrahydrofuran proved the coexistence of two conformers but do not derive any detailed information about the conformer ratio or stability. [68, 69] In the liquid and condensed phase, the THF molecule tends to be more populated in the  $C_2$  conformation. [70, 71]

### 1.3. Properties of silicon and Si containing heterocyclic molecules

Silicon in the elemental form at room temperature exists as a crystalline solid with a blue-gray metallic color, with melting and boiling point values equal to 1414°C and 3265°C, respectively. The electron configuration of silicon is [Ne] 3s<sup>2</sup> 3p<sup>2</sup> being in most cases tetravalent. [72] The properties of the silicon atom in comparison with the carbon atom shed some light on the differences in properties of the silacyclic and cyclic molecules. The greater reactivity the of silanes



is caused by the larger size of the silicon atom, lower electronegativity, and the availability of low-energy orbitals occupation. The larger size of the molecule, the longer possible bonds formed. These differences affect the structural properties and conformational diversity. The electronegativity differences, Si (1.90) and C (2.55). [73] Such a difference in the electronegativity cause the reverse polarity in the Si-H, when compared with the C-H bond. [73]

The lower electronegativity of silicon (1.90) compared to carbon (2.55) results in more polar bonds, and in the case of silanes, results in a reverse polarity in the Si-H bond compared to the C-H bond. In most cases, the polarity of the bonds formed with the Si atom is greater when that C-H bond. The polarity of the Si-bond increase in the bonds formed with oxygen and halogens, among which the strongest is the Si-F bond. In contrary to that, silicon bonds formed with hydrogen, carbon, silicon, or sulfur have lower strength. The C-X (X = H, C, Si, S) bonds are stronger when compared with analogous Si-X bonds. [74–76] The carbon atom easily forms unsaturated bonds, while silicon atom unsaturated bonds are rare. [77] The analogous Si-C bond is longer in comparison to C-C, this cause the lower  $\pi$  orbital overlap.

Silicon occurs naturally in the earth crust (2nd most popular) and in all universe (8th most popular). Its physicochemical properties caused its wide usage in technology, medical, and industrial applications. [78] The technological application of the silicon speed up with the semiconductor emergence. [79–82]

The silicon atom properties make it an important feature of the biologically active molecules. [17, 18] The silicon-based compounds find usage in the production of many materials, like glasses, ceramics, cement, fiber optics, liquid crystal, silicones, and many other polymers. [17–26] The silicon-containing cyclic molecules has a potential use in medicine. The replacement of the carbon atom with silicon, in the bioisosteres has several advantages. Such a change increases the lipophilicity of the molecule and make the membrane penetration easier. [83–86] Additionally, the Si atom is not toxic. [17, 33]

The carbon replacement in the biologically active molecules with silicon influences the electronic structure and may lead to different interactions with enzymes in the human body. This allows for designing specific pharmaceuticals, like enzyme inhibitors including silanediols and silanetriol. [87–91]

The silicon-containing five and six- member ring molecules (see Fig. 1.7) can be considered as a part of big biologically active molecules with vast medical applications. The investigation of the nature and conformational diversity of the silacyclopentanes and silacyclopentanes is crucial, for developing the molecules with desired medical applications. Five- and six-member ring cyclic molecules were investigated during the search for fungicidal, anti-tumor, anti-malarial, and steroid-mimicking drugs. [27–32]

The functionalized cyclohexane compounds display good adsorption properties. The silicon containing molecules are hydrophobic. This is why are

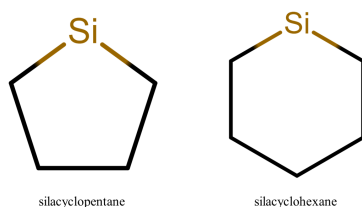


Figure 1.7: Structures of the silacyclopentane and silacyclohexane molecules.

potential materials for novel hydrophobic coatings fabrication. The silicon-containing materials are usually less toxic and thought to be used as a Teflon replacement.

### 1.3.1. Conformational analysis and energetics of silacyclopentanes

The silacyclopentanes may serve as a surface modification coating substances [92] especially since the silicon presence improves the adhesion by covalent bonding with glass. The attachment of the radicals (halogen atoms or methyl group) boosts the hydrophobicity of substituted organic compounds. [93, 94] The hydrophobicity of the silicon-containing cyclic molecules depends on the ring size and type of substituents which affects the conformational diversity. The substitution of the cyclic ring even with small radicals can be essential [95, 96] for the dynamic conformational equilibrium and chemical [97] or biological [98] activity.

Cyclopentane and its substituted derivatives were studied by both computational and experimental techniques. [48, 95, 96, 99–103] The most populated conformer is the twisted ( $C_2$ ) conformer, but the small relative energy difference of the envelope ( $C_1$ ) conformer cause pseudorotation. The pseudorotation process origin is still not fully understood. [48, 101–103]

The introduction of the heteroatom into five member cyclic ring as well as the substitution of the ring hydrogen atoms with various radicals changes its stability and conformational preferences. The oxolane or thiophene molecules favor the envelope conformation. [96] For the disubstituted silacyclopentanes, the twisted conformation is the most populated when both radicals are the same. The planar ( $C_{2v}$ ) and envelope ( $C_s$ ) conformations were found to be transition state structures. [100, 104–106]

Silicon containing five-member ring molecules substituted with Cl, Br and F radicals have only one stable structure, namely twisted conformer. [107–111] Substituents with high electronegativity like halogen atoms, are more stable in the pseudo-axial position, while bigger organic substituents (methyl group) prefer the pseudo-equatorial position. [101]

Homodisubstituted silacyclopentanes (1,1-difluoro-silacyclopentane and 1,1-

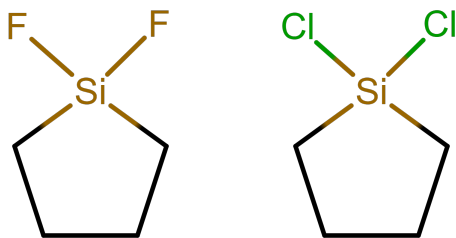


Figure 1.8: Structures of the 1,1-difluoro-silacyclopentane and 1,1-dichloro-silacyclopentane molecules.

dichloro-silacyclopentane), depicted in Fig. 1.8 form only one stable conformer, namely twisted structure. Both experimental (IR and Raman spectroscopy) in the liquid and solid samples and computational (MP2 and B3LYP methods) studies proved the existence of only one T (trans) [112] with the envelope structure as a transition state (TS). The assignment of the vibrational modes was performed for conformers with  $C_{2v}$  [113] and  $C_2$  [112] symmetry of the molecules.

### 1.3.2. Conformational analysis and energetics of silacyclohexanes

Conformational analysis and energetic stability was the field of interest for many scientists due to their impact on the basic knowledge of organic chemistry. [114, 115] The understanding of the interconversion pathways and structural properties enables and support the synthesis of molecule and materials with desired properties. [115] The cyclohexane is the simplest model for six-member ring molecules and was the subject of extensive studies utilizing both experimental and computational methods. [50, 53, 116–125] Among experimental methods used we can find IR, Raman, microwave spectroscopy [114–118, 126–130], or electron diffraction experiment. [131] Despite the method used it was found that the chair structure is the most energetically stable and abundant. The relative energy difference between chair (C) and boat (B) structures is caused by the eclipsing  $\text{CH}_2\text{--CH}_2$  interactions and the distortions that decrease the flagpole interactions. [119] The conformational path for the chair-to-chair inversion was found to be either chair  $\rightarrow$  half-chair  $\rightarrow$  skew-boat  $\rightarrow$  boat  $\rightarrow$  skew-boat  $\rightarrow$  half-chair  $\rightarrow$  chair [127] (see Fig.1.9) or chair  $\rightarrow$  half chair  $\rightarrow$  skew-boat  $\rightarrow$  half chair  $\rightarrow$  chair without going through the boat conformation. [114, 132] The calculated free energy for the chair  $\rightarrow$  half-chair transition is about 2.4-2.5 kcal/mol. [127]

In the case of the substituted cyclohexanes. In the substituted cyclohexanes, the attached radicals prefer the equatorial position. In the disubstituted cyclohexanes, the equatorial position is favored with the bulkier substituent,

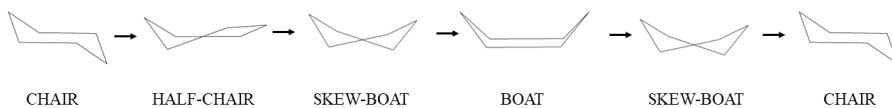


Figure 1.9: Chair to chair conformational rearrangement pathway for the cyclohexane molecule.

caused by 1,3-syn-diaxial interactions hyperconjugation. [133] The substituent in the axial position interacts with axial ring hydrogen atoms, thus bigger radicals avoid this position to reduce the repulsion. [50, 134–136] The radical itself does not destabilize the ring structure, the strain is minimized by the orientation change of the substituent. [56] The final conformation of the substituted cyclohexanes is an equilibrium between the ring shape and the attached radical position. The axial stabilization of the substituent may be supported by the charge transfer from the ring to the substituent. [57]

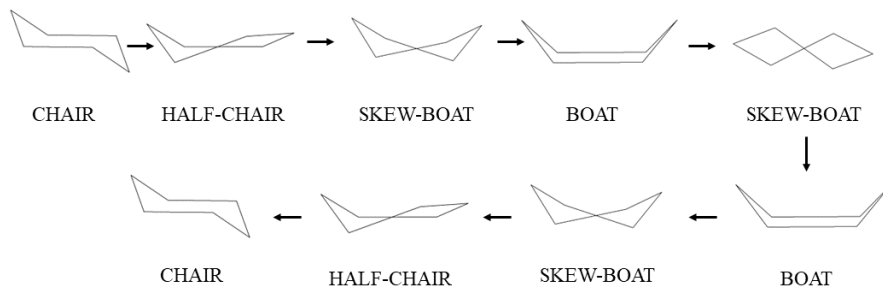


Figure 1.10: Chair to chair conformational rearrangement pathway for the silacyclohexane molecule.

Replacing one of the carbon atom with silicon, has a great impact on the molecular properties, causing differences in the conformational and energetic stability. The detailed analysis of the silacyclohexane was performed utilizing experimental (IR, Raman, microwave, gas electron diffraction spectroscopy) and computational methods. [137–141] The global energy minimum is the chair (C) conformations, while the skew-boat (S) and boat (B) conformer differ in energy by about 1.7–2.2 kcal/mol and 1.9–2.5 kcal/mol, respectively. Further analysis showed that the skew-boat conformer exists in two stable isomers with  $C_1$  and  $C_2$  symmetry. [58] The energy of the silacyclohexane conformers increases in order: B  $\rightarrow$  T ( $C_1$  symmetry)  $\rightarrow$  T ( $C_2$  symmetry)  $\rightarrow$  C. The chair-to-chair inversion, results from C-Si-C-C and C-C-C-C dihedral angles changes and follow the pattern: chair  $\rightarrow$  half-chair (TS)  $\rightarrow$  skew-boat ( $C_1$  symmetry)  $\rightarrow$  boat  $\rightarrow$  skew-boat ( $C_2$  symmetry)  $\rightarrow$  boat  $\rightarrow$  skew-boat ( $C_1$  symmetry)  $\rightarrow$  half-chair (TS)  $\rightarrow$  chair (see Fig. 1.10). [57, 58, 123] Where the chair, boat, and skew-boat conformers are the local energy minima and the sofa-like structure

is a transition state (TS). The H $\cdots$ H non-bonded distances are greater than the sum of van der Waals hydrogen atom radius in the silacyclohexane molecules and equal to 2.4 Å, thus any repulsive interactions do not occur.

The conformational energy differences might be explained by [74, 142–145]:

- hyperconjugative effect,
- overall eclipsed conformations bond orbitals interactions,
- bonding–antibonding orbitals influence.

The proof of the stereoelectronic hyperconjugation effect is the elongation of the axially oriented Si-H and C–H bonds. Synthesis of new compounds with desired properties usually begins with the functionalization of the existing materials, which structure and properties are well known. Thus, further analysis describes the substituted heterocyclic six-member ring compounds. The axial orientation of the monosubstituents (Br, I, F, Cl, At, trifluoromethyl, methoxy group, hydroxy group) is caused by the anomeric effect. [58, 146–154] Contrary to that, the methyl substituent prefers the equatorial orientation, because the steric effect is only one of several interactions, being responsible for the spatial structure of the conformer. [57, 136, 148, 155, 156]

The 1-fluoro-1-methyl-silacyclohexane and 1-methyl-1-trifluoromethyl-1-silacyclohexane, were already investigated. Results from gas electron diffraction, low-temperature NMR, temperature-dependent Raman spectroscopy experimental methods, and quantum chemical calculations indicates the C axial and equatorial structures are almost equally populated. [150] The  $C_{ax}$  to  $C_{eq}$  rearrangement along the pattern: chair  $_{ax}$   $\rightarrow$  half-chair (TS)  $\rightarrow$  skew-boat ( $C_1$  symmetry)  $\rightarrow$  boat (TS)  $\rightarrow$  skew-boat ( $C_2$  symmetry)  $\rightarrow$  boat (TS)  $\rightarrow$  ( $C_1$  symmetry)  $\rightarrow$  half-chair (TS)  $\rightarrow$  chair  $_{eq}$ . [150] Where the local energy minima structures are chair (C) and skew-boat (S -  $C_1$  and  $C_2$  symmetry), and the transition state structures (TS) are half-chair (H) and boat (B). The pattern of the ring rearrangements is the same as in Fig. 1.10.

#### 1.4. Structure and energetics of $Si_n-N_m$ clusters

Atomic clusters are comprised of three to hundreds of atoms and hve intrigued scientists for many years. [157, 158] Clusters are of interest due to the unique electronic, optical, and often magnetic properties associated with their size, which differs from their bulk counterparts. It is well-known that with increasing cluster size from molecular to bulk values, cluster properties tend to evolve and can at times reveal surprising physical morphology and chemical properties, providing insight into observed chemical phenomena. However, it is also becoming increasingly important to observe the interactions and stability of sub-nanometer-sized clusters to not only fundamentally understand properties

at the sub-nanometer scale but also to further develop breakthroughs in nanotechnology and nanochemistry. Mixed silicon clusters, in particular, have received a great deal of attention both experimentally and theoretically. [38–42] These clusters are often investigated due to their prominent roles in the development of materials with astrophysical, environmental, and biomedical applications. [38] Silicon nitride clusters specifically have been studied to gain insight into the morphology and properties of bulk silicon nitride which is then used in technological applications. For example, Ye and co-workers studied a series of  $\text{Si}_n\text{N}_m$  clusters using DFT with a TZ2P basis set. They reported that the structures evolve from planar to three dimensions as the number of atoms increases. [41] Owusu-Ansah and co-workers investigated small  $\text{Si}_n\text{N}_m$  ( $n+m = 4$ ) clusters using density functional theory (DFT) and reported the first ten electronic transitions using time-dependent DFT (TDDFT). [42] Other studies have focused on doping silicon nitride clusters in an effort to understand the role of electron donors and acceptors in these systems. [159] While most studies have focused on doping, to our knowledge, no study has examined the role of incorporating ligands into silicon-nitrogen-based clusters.

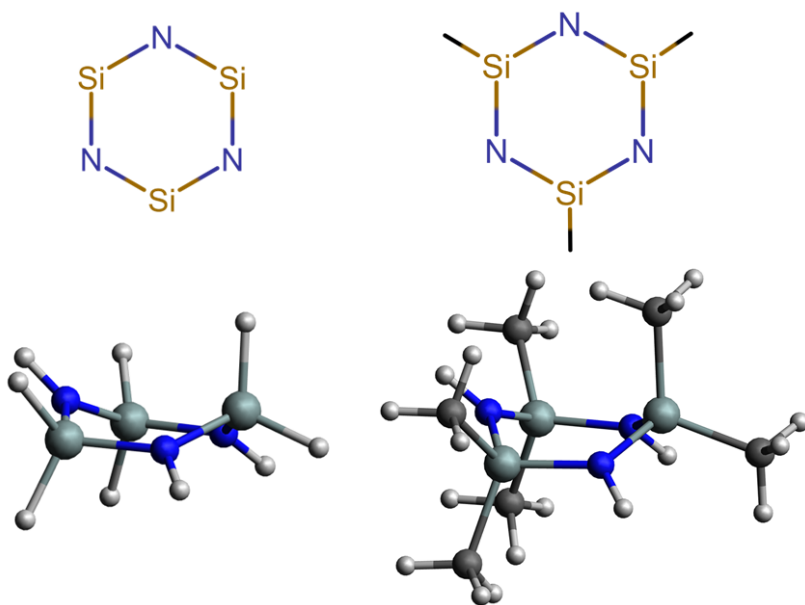


Figure 1.11: Structures of the 1,3,5,2,4,6-triazatrisilinane (left) and 2,2,4,4,6,6-hexamethyl-1,3,5,2,4,6-triazatrisilinane (right) molecules and the boat conformers derived from DFT/aug-cc-pVTZ calculations. [A6]

In this study, we present theoretical results on the neutral six-membered ring  $\text{Si}_3(\text{NH})_3\text{H}_6$  (1,3,5,2,4,6-triazatrisilinane abbr. 3A3S) and its ligated counterpart  $\text{Si}_3(\text{NH})_3(\text{CH}_3)_6$  (2,2,4,4,6,6-hexamethyl-1,3,5,2,4,6-triazatrisilinane abbr. 6M3A3S) neutral clusters (see Fig.1.11). The calcu-

lations provided the most stable isomers which yield detailed structural information and vibrational spectra. The calculations were confirmed by the matrix isolation experiments performed in neon and argon matrix. The experiments give insight to the possible conformational changes in the inert media and detailed vibrational analysis of the  $\text{Si}_3(\text{NH})_3(\text{CH}_3)_6$  cluster.

### 1.5. Properties of germanium and Ge containing heterocyclic molecules

Germanium (Ge) is a lustrous, grayish-white metalloid. At room temperature crystalline solid, in appearance similar to silicon. In nature reacts with oxygen-forming complexes. The melting and boiling point temperatures are  $938.25\text{ }^\circ\text{C}$  and  $2833\text{ }^\circ\text{C}$ , respectively. The electron configuration is  $3d^{10}4s^2 4p^2$ . [72, 160] The electronegativity of germanium is equal to 2.01. [73] Germanium in organic compounds is tetravalent.

Germanium is used very frequently in the fiber-optics industry, infrared optics, as a polymerization catalyst, and for electronics and solar electric applications, on a smaller scale in metallurgy and chemotherapy. [34] Germanium, due to its vast applications is called a "technology-critical element". [35]

Replacing one of the carbon atom in the cyclohexane molecule with the germanium atom influence the structural parameters, conformational stability and reactivity. In the literature there are limited information on the nature and detailed description of the conformational variety. Germanium has lower electronegativity than carbon, the van der Waals radius is longer leading to the formation of longer bonds. Elongation of the bonds in the cyclic ring can cause bigger ring flexibility. Germacyclohexane is very important as a backbone of the nematic liquid crystals for displays. By now, germacyclohexane ( $\text{GeCH}$ ), (see Fig. 1.12) was the subject of the gaseous electron diffraction, microwave spectroscopy [36], and Infrared and Raman spectroscopy supported by the DFT-calculations [37] studies. It was found that  $\text{GeCH}$  stable conformers are chair and skew-boat structures, but due to the low population can not be traced under experimental conditions.

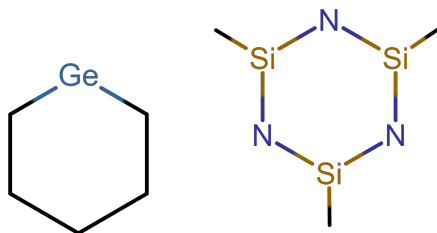


Figure 1.12: Structures of the germacyclohexane and methyl-germacyclohexane molecules.

The monosubstituted 1-methyl-1-germacyclohexane (1-M-GeCH), see Fig. 1.12 is more unstable than its 1-methyl-cyclohexane analog and was not investigated in detail yet. The NMR chemical shifts and MM calculations for 1-M-GeCH proved that methyl substituent favor the axial (60%) over equatorial(40%) position. [161] The dynamic NMR experiment showed that above a certain temperature (140 K) we can observe constant chair  $\longleftrightarrow$  chair interconversion. While the temperature is decreased two stable conformers can be detected. The conformational pathway for chair axial  $\longleftrightarrow$  chair equatorial inversion is: C axial  $\rightarrow$  H  $\rightarrow$  S ( $^1S_3$ )  $\rightarrow$  B  $\rightarrow$  S ( $^1S_5$ )  $\rightarrow$  S ( $^1S_3$ )  $\rightarrow$  H  $\rightarrow$  C equatorial. [162]



## 2. CHAPTER: INTRODUCTION TO EXPERIMENTAL AND THEORETICAL METHODS USED

### 2.1. Experimental methods

#### 2.1.1. Raman spectroscopy

Raman spectroscopy is a powerful analytical technique used to study the molecular vibrations of a wide range of materials, including solids, liquids, and gases. The technique is based on the Raman effect, which is the inelastic scattering of light by a molecule. In this effect, the energy of the scattered light changes, resulting in a shift in the wavelength of the scattered photons. This shift in wavelength, known as the Raman shift, provides information about the molecular vibrations of the sample. [163]

The Raman shift can be expressed with spectral wavelengths, with use of the equation 2.1 where  $\Delta\tilde{\nu}$  is the Raman shift in  $\text{cm}^{-1}$ ,  $\lambda_0$  is the excitation wavelength and  $\lambda_1$  denote Raman spectrum wavelength.

$$\Delta\tilde{\nu} = \left( \frac{1}{\lambda_0} - \frac{1}{\lambda_1} \right) \quad (2.1)$$

The principles of Raman spectroscopy can be explained by considering the interaction of light with matter. When a beam of light is directed onto a sample, some of the photons in the beam interact with the molecules in the sample. Most of the photons are scattered elastically, meaning that they retain their original energy and wavelength. However, a small fraction of the photons undergo inelastic scattering, in which the energy and wavelength of the scattered photons are different from those of the incident photons. [164]

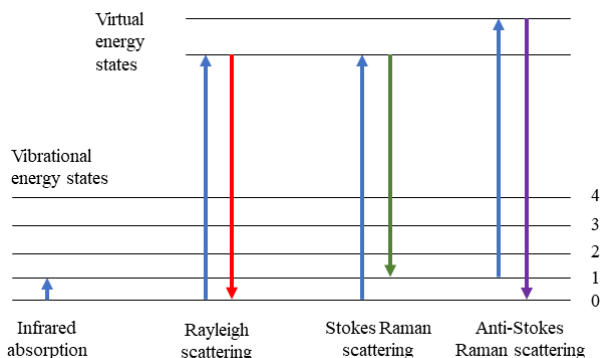


Figure 2.1: Energy-level diagram showing the states involved in Raman spectra.

In Raman spectroscopy, a monochromatic laser beam is directed onto the sample. The photons emitted by laser interact with the sample molecules, the molecules are excited to the vibrational energy levels. As a result of this vibration, the energy of the scattered photons changes, resulting in the Raman shift (See Fig. 2.1). The Raman shift provides information about the vibrational modes of the molecules in the sample, which in turn can be used to identify the chemical composition of the sample. [163,164]

The Raman effect is caused by the interaction of the laser light with the polarizability of the sample molecules. When a molecule vibrates, its polarizability changes, resulting in a change in the distribution of charge within the molecule. This change in the distribution of charge affects the electric field of the molecule, leading to the Raman effect. [163,164]

The induction of the dipole moment occurs when the incident monochromatic electromagnetic field interacts with the material, and this phenomenon can be mathematically described by the 2.2 equation with  $\alpha$  - molecular polarizability.

$$P = \alpha E \tag{2.2}$$

The equation 2.3 is a mathematical representation of a monochromatic electromagnetic wave, where  $E$  represents the electric field strength,  $E_0$  is the maximum amplitude of the electric field,  $\omega_0$  is the angular frequency, and  $t$  is time. The cosine function describes the oscillating behavior of the electric field over time.

$$E = E_0 \cdot \cos(\omega_0 t) \tag{2.3}$$

The induction of a time-dependent dipole moment can serve as a source for the production of secondary radiation, given by the equation 2.4.

$$P = \alpha E_0 \cdot \cos(\omega_0 t) \tag{2.4}$$

The intensity of the Raman scattering is proportional to the concentration of the molecules that are vibrating at a particular frequency. Therefore, Raman spectroscopy can be used to quantify the amount of a particular molecule in a sample. Raman spectra are typically recorded over a range of Raman shifts, with each peak in the spectrum corresponding to a particular vibrational mode of the molecule. [163,164]

Raman spectroscopy can be used to study a wide range of materials, including organic and inorganic compounds, polymers, and biological molecules

including heterocyclic five- and six-member ring molecules. [107,110,111,156,165–168]

### 2.1.2. Infrared spectroscopy

Infrared spectroscopy is analytical technique used for assessing the chemical composition of a sample. This technique is based on the interaction of infrared (IR) radiation with the molecular vibrations of a sample.

Molecules are composed of atoms held together by chemical bonds, and these bonds can vibrate in different ways. Each type of bond has a characteristic vibrational frequency, which can be excited by electromagnetic radiation of specific frequencies. Infrared radiation possesses the appropriate energy to excite these vibrations, leading to the stretching or bending of the bonds in the molecule. Infrared spectroscopy operates by passing an infrared beam through the sample and detecting the amount of infrared radiation absorbed by the sample. The detector measures the intensity of the transmitted radiation, and the data is then plotted as a spectrum of the frequencies of the absorbed radiation. [169,170]

In the IR spectroscopy the transmittance is given by Beer–Lambert law (see Eq. 2.5). The  $I(\tilde{\nu})$  refer to the intensity of transmitted radiation,  $I_0(\tilde{\nu})$  to incident radiation intensity,  $a(\tilde{\nu})$  to coefficient of linear absorption,  $b$  - sample thickness and  $\tilde{\nu}$  refers to wavenumber.

$$T(\tilde{\nu}) = \frac{I(\tilde{\nu})}{I_0(\tilde{\nu})} = e^{(-a(\tilde{\nu})b)} \quad (2.5)$$

The absorbance (A) of material (optical density) is logarithmic ratio of the intensity of the light shining upon the material, to the light transmitted through the material:

$$A = \log_{10} \frac{1}{T} = -\log_{10} \frac{1}{I_0} \quad (2.6)$$

The resulting IR spectrum provides information on the functional groups present in the sample, as well as the types of chemical bonds and their relative abundance. The spectrum is typically divided into three regions: the fingerprint region (400-1500  $\text{cm}^{-1}$ ), the functional group region (1500-4000  $\text{cm}^{-1}$ ), and the overtone region (above 4000  $\text{cm}^{-1}$ ). The fingerprint region contains numerous overlapping peaks unique to each molecule and is used to identify the compound. The functional group region contains peaks that correspond to specific functional groups such as carbonyl, hydroxyl, and amino groups. The overtone region contains peaks that correspond to harmonic overtones of the fundamental vibrational modes. [163,164,169,170]

In summary, infrared spectroscopy is a potent technique for analyzing the chemical composition of samples. It is a non-destructive and non-invasive method for identifying functional groups and chemical bonds present in a sample, making it a versatile tool for a broad range of applications such as pharmaceuticals, forensics, and materials science. [170]

### 2.1.3. Attenuated total reflectance infrared spectroscopy

Attenuated Total Reflectance Infrared (ATR-IR) Spectroscopy is a potent analytical method used to analyze solid and liquid samples. It relies on measuring the infrared radiation absorbed by a sample using an attenuated total reflectance accessory.

The ATR accessory is a specialized crystal, usually made of diamond or zinc selenide, which is brought into contact with the sample. The crystal functions as an optical waveguide, allowing the infrared radiation to penetrate into the sample, where it interacts with the molecular vibrations. [169]

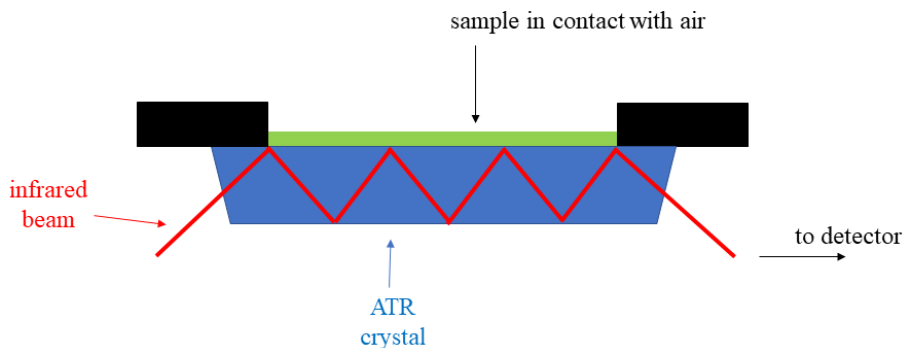


Figure 2.2: Attenuated total reflectance.

As the infrared radiation penetrates the sample, its intensity is reduced by the sample's absorption, reflection, and scattering. The intensity of the radiation that reflects back to the crystal surface is measured, and the resulting spectrum is employed to identify the functional groups and chemical bonds present in the sample. [169]

One of the primary benefits of ATR-IR spectroscopy is that it enables the analysis of solid samples without requiring sample preparation or destruction. The technique can analyze difficult-to-dissolve samples, such as polymers and minerals, as well as small samples, such as microscopic particles. [171–173]

ATR-IR spectroscopy is utilized in various fields, including material science, pharmaceuticals, forensic science, and environmental monitoring. The technique is highly sensitive and provides valuable information on the chemical composition of a sample, making it a useful tool for identifying unknown compounds, characterizing materials, and monitoring chemical reactions. [169]

In conclusion, Attenuated Total Reflectance Infrared Spectroscopy is a robust analytical method for analyzing solid and liquid samples. It is a non-destructive and non-invasive technique for identifying the functional groups and chemical bonds present in a sample, making it an invaluable tool for various applications. [164, 169, 171–173]

#### 2.1.4. Matrix isolation technique

The matrix isolation experiment is a technique in which the guest molecules or atoms of the analyte are trapped in the rigid inert host material. A small amount of the gas phase guest molecule is mixed in the gas chamber with the larger amount of the matrix gas and then sprayed on a surface. The cryogenic temperature of the aforementioned surface causes rapid solidification of the mixture. The conformational ratio of the molecules trapped in the sample reflects the thermodynamic stability of the gaseous sample. The "father" of this methodology was George Pimentel who along with George Porter made extensive studies on this methodology. [43–45]

The spectroscopy of the liquid and gas samples does not describe the molecule itself but a system where molecules are affected by the environment. The spectra can become very complicated due to the large number of bands and the spectral bands overlapping. Such effects lead to loss and uncertainty of the information.

Two approaches that can be used to study the species under ambient conditions. The first one is to look at them for a very short period of time immediately after formation, the second is to trap them and immobilize and study them with simpler spectroscopic methods. The time-resolver approach can give us an insight into the kinetics of the system but with the lowering of the spectroscopic detail, while the stable conditions give us more information on the electronic and molecular properties. It is crucial to remember that species in the matrix isolation experiment are studied as in the "native", not a "natural" environment. Despite the fact that the molecules are separated, the time-dependent measurements with the temperature change allow for controlling the diffusion. If we increase the temperature in a small temperature range and register the spectra at every step we can have insight into the changes in the conformational stability and equilibrium. It is important that after reaching the melting point the structure of the sample layer is destroyed. The matrix isolation technique separates the molecules and prevents intermolecular interactions. Additionally, the temperature is low enough to prevent the diffusion of the analyte. Firstly, the lowest possible temperature reached was 66 K (xenon) but the usage of the closed-cycle cryostat (see Fig. 2.3) allowed to use of temperatures down to 2 K. [174–176]

Among the advantages of the matrix isolation experiment are the use of weak intermolecular interactions, inert gas usage, the transparency of the host

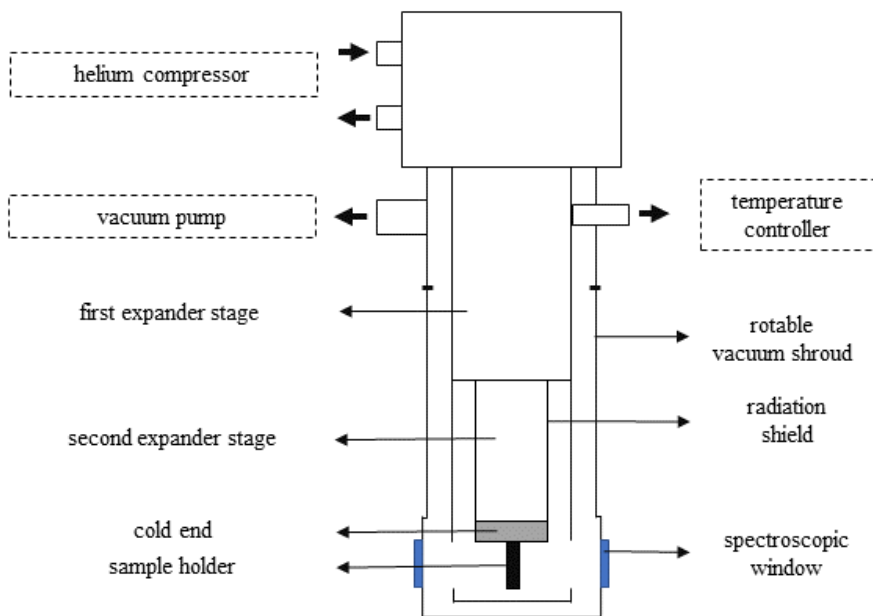


Figure 2.3: Scheme of the closed-cycle cryostat without compressor

materials, possibility to investigate reactive intermediates.

The inert medium prohibits or lowers the rotation of the molecular bonds for large organic compounds thus, the rovibrational bands are not present. Small molecules (e. g. water) still rotate and the number of the present rovibrational bands depends on the matrix temperature. The matrix isolation spectral bands are narrower, the spectral bands width is in most cases lower than  $5\text{ cm}^{-1}$ , thus we do not observe big bands overlap. [174–176]

The matrix isolation technique has its usage in conformational equilibrium studies. The first experiments used the hot-nozzle technique (the heating up of the sample before the deposition on the cryostat cold window surface). Fast cooling of the substance-matrix gas mixture to 4-15K allows trapping the conformers with energy differences higher than 1.5 kcal/mol. This method allows for an insight into the non-equilibrium conformational population in the obtained spectra. The annealing of the sample (heating up the matrix to temperatures below the melting point, and cooling down again) leads to the conformational equilibrium of the molecules.

The energy barriers of conformational transitions can be easily calculated. It is possible to investigate several conformers with various energy differences. The conformers with energy barrier below 1.2 kcal/mol, easily inter-convert, thus the barrier height between conformers is impossible to detect.

IR spectra obtained from matrix isolation experiment are sharp, and do not

overlap (as in the vapor or liquid phase), thus it is possible to observe more bands belonging to different conformers. [177–179]

Even though, that the matrix isolation technique has many advantages, there are several limitations as well. While the typical spectroscopic measurement are fast methods, this technique takes more time including the sample preparation and the measurements itself. The deposition of the mixture or cooling down of the system take much more time. At the very beginning, before the experiment, we should consider the size and the nature of investigated molecules. The molecules should be volatilizable without decomposition. The sample, to be deposited on the cold window, must remain in the gas phase. Molecules which are in the gas phase or have high vapor pressure are perfect candidates for this experiment. That is why many interesting organic compounds are excluded, due to the low vapor pressure. It is impossible to deposit them on the cryostat spectral window without e.g. heating of the sample or usage of more complex methods. [43, 44, 174]

Polar substances even in a gas phase may form dimers or higher aggregates. The self-association, with a lower tendency, may occur in the matrix when too high concentration of the analyte is used, thus we need to carefully choose the substance-matrix gas ratio. When dimers or higher aggregates are formed we can observe additional spectral bands in the obtained spectrum. While we observe the aggregates formation in the matrix it is possible to reduce it by increasing of the matrix gas or sample volumes.

In the spectra obtained in cryogenic matrices, we observe shift of the spectral bands when comparing with the gas or liquid phase spectral bands. This is called a matrix effect, and is caused by the van der Waals interactions formed between the investigated molecules and the matrix gas molecules. The nature of shift depends on the investigated vibration and the matrix gas type. These interactions influence the vibrational levels of the investigated molecules. While looking at the spectra obtained for the same molecule, but with use of argon and nitrogen host gas, we can see some differences. Nitrogen matrix has stronger influence on the guest molecules (due to its quadrupole moment) than argon matrix. In the spectra obtained from matrix isolation experiment the position and shape of bands are changed when comparing spectral bands before and after the annealing process. In most cases we can observe the red-shift (shift to lower frequency numbers), but in case of non-stretching vibrational modes the blue shift can be observed as well. [174]

The change of the type of matrix gas, used during the experiment, influences the molecule and causes the site effect (i.e. cage effect). Different conformers may need more "space" in between the molecules of the matrix. Additionally, even for the same conformer such cages, in which the molecule is nested, can differ. Thus, the interaction of the molecule and surrounding matrix may differ reflecting the obtained spectrum. As a result we can observe the splitting of the

spectral bands in the vibrational spectra. This effect can be investigated with the change of the matrix gas, and analysis of the splitting effect pattern.

Gases used in the matrix isolation experiment must fulfill several conditions:

- be chemically inert,
- form clear glasses,
- be transparent in the IR, Vis, and UV regions of the spectrum.

Typically host materials, that does not interact (or interact very poorly) with the guest molecules, are solid noble gases (Ne, Ar, Kr, and Xe), nitrogen and hydrogen. Aforementioned gases do not absorb radiation in the infrared and visible regions. Additionally, the spectra have good spectral resolution. [174, 175, 180]

The matrix gas type imposes the temperatures used during the experiment and is limited by the gas diffusion temperature, above which the molecules can form aggregates.

Argon and nitrogen are the most commonly used matrix gasses. But apart from them neon, krypton and xenon are used. Recently, para-hydrogen gas has become a popular matrix host gas. [181, 182]

#### 2.1.4.1. Experiment description

The usage of such a small temperatures in the matrix isolation experiment would be impossible without closed cycle cryostat (see Fig. 2.3). Nowadays the three cycle cryostats are used and allow for obtaining temperatures as low as 2-3K.

The cryostat consists of a compressor and expander. The expander is cooled down with helium, which is delivered from compressor with steel tubes. After first expander stage, there is, a surrounded by radiation shield second expander stage. The coldest spot in the apparatus setup is the cold end and attached to it a sample holder (cold window). The expander stages, cold end and sample holder are placed under rotatable vacuum shroud in which just in front of cold window we can find the spectroscopic window. [174, 175, 180]

For performing of the annealing process or deposition of the mixture in higher temperatures, the resistance heater must be used. Then the temperature can be controlled independently and with higher accuracy. The temperature of the sample can be controlled with a thermocouple or silicone diode inside the cryostat.

## 2.2. Computational methods

The computational methods utilized during my work can be divided with respect to the time dependency and methodology of the energy calculations,



namely to so called, static calculations (not time-dependent) and the molecular dynamics (MD) simulations (time-dependent). In this work both static calculations and Car-Parrinello molecular dynamics simulations were used. Due to the accuracy, computational methods can be divided into classical (molecular mechanics (MM) utilizing force-field (FF)) and (*ab initio*) or half-empirical (utilizing quantum mechanics methods). Very important aspect of the computational studies is to choose appropriate level of theory, which is the best compromise between the computational cost and the accuracy of the method. For small systems (few to hundreds of atoms) quantum mechanics based methods can be used, for larger systems it is necessary to decrease the level of the theory to semi-empirical calculations or even molecular mechanics. Introduction of the approximations cause the changes in the computational cost of the calculations defined as a scaling, namely, correlation between the time needed to perform the calculations and the number of electrons in the investigated system.

The basic *ab initio* method, namely Hartree-Fock (HF), has scaling factor  $N^3$ . This method is quite fast but does not describe the antiparallel spin electron correlation, thus its usage is limited. The correct description of the electron correlation needs a usage of the post-Hartree-Fock (post-HF) methods. Post-HF methods are more demanding, the computational cost varies from  $N^5$  for methods based on the perturbation theory (e.g. by Møller–Plesset perturbation theory) to  $N^8$  for couple clusters (CC) method. The CC method is considered as the gold standard in computational chemistry. Another branch of the theoretical methods is the density functional theory (DFT) which has its origin in the band theory of solids. From the 80’s the usage of DFT methods grows very fast and now it is widely used approach in the molecular modeling. The scaling factor for DFT is  $N^3$ . The weak point of this method is the way the electron correlation is included. That is why different functionals are in use, each carries some information about the electronic correlation. From this point of view the DFT method is sometimes classified as a semi-empirical.

### 2.2.1. Hartree-Fock approach and other approximations

Most quantum chemical approaches are based on the approximate solution of the time independent, Schrödinger equation. The Hamiltonian  $\hat{H}$  is not time dependent and acts on the wavefunction  $\Psi_i$ , the same wavefunction  $\Psi_i$  is the ground state wavefunction with energy  $E_i$ .

$$\hat{H}\Psi_i(\vec{x}_1, \vec{x}_2, \dots, \vec{x}_N, \vec{R}_1, \vec{R}_2, \vec{R}_M) = E_i\Psi_i(\vec{x}_1, \vec{x}_2, \dots, \vec{x}_N, \vec{R}_1, \vec{R}_2, \vec{R}_M) \quad (2.7)$$

Hamiltonian ( $\hat{H}$ ) describes a system consisted of M nuclei and N electrons, where magnetic and electric forces are absent. The  $\vec{x}_N$  and  $\vec{R}_M$  are the spatial

positions of the  $N$  electrons and  $M$  nuclei. [183]

$$\hat{H} = -\frac{1}{2} \sum_{i=1}^N \nabla_i^2 - \frac{1}{2} \sum_{A=1}^M \frac{1}{M_A} \nabla_A^2 - \sum_{i=1}^N \sum_{A=1}^M \frac{Z_A}{r_{iA}} + \sum_{i=1}^N \sum_{j>i}^N \frac{1}{r_{ij}} + \sum_{A=1}^M \sum_{B>A}^M \frac{Z_A Z_B}{R_{AB}} \quad (2.8)$$

Hamiltonian is a differential operator, which represents the total energy of the system. In equation (2.8)  $A$  and  $B$  run over the  $M$  nuclei,  $i$  and  $j$  denote the  $N$  electrons. Kinetic energies of the nuclei and electrons are described within the first two terms. Laplacian operator  $\nabla_i^2$  is a sum of differential operators in three dimensions. The last three terms of the Hamiltonian describe attractive electrostatic interactions (nuclei-electrons) and repulsive potential (electron-electron and nucleus-nucleus).  $R_{AB}$  and  $r_{ij}$  are the distances between particles. [183]

Only few basic systems can be analytically solved utilizing Schrödinger equation, for example hydrogen atom or harmonic oscillator. If the ground state geometry of the system and its electron density are known, we can obtain many properties of the system, like for example the spectroscopic parameters (IR) of the investigated system as a derivative of the energy with respect to internal coordinates.

The mass of electron is approximately 1840 times smaller than the mass of the proton. Thus, the electrons move much faster than the nuclei. We can consider the electrons as moving in the electro-static field generated by fixed nuclei. In the Born-Oppenheimer approximation the movement of the electrons and the nuclei is separated. It is possible to divide wave function of a molecule into the two components: electronic and nuclear. The Hamiltonian  $\hat{H}$  operator is reduced to [184]:

$$\hat{H} = -\frac{1}{2} \sum_{i=1}^N \nabla_i^2 - \sum_{i=1}^N \sum_{A=1}^M \frac{Z_A}{r_{iA}} + \sum_{i=1}^N \sum_{j>i}^N \frac{1}{r_{ij}} \quad (2.9)$$

In this approximation the potential energy of nuclei is constant, thus terms describing kinetic energy of the nuclei and repulsive potential nuclei-nuclei are absent.

### 2.2.2. Global and local energy minima

Chemical reactions, as well as the conformational changes, are often determined by the presence of the energy barriers between different conformers. It is important to understand all elementary steps along the reaction or conformational change coordinate.

Hypersurface presenting a relation of the geometry and the energy of a

molecule is called a potential energy surface (PES). Hyperspace of the PES has  $3N-6$  degrees of freedom, where  $N$  represents number of atoms in the investigated molecule. PES can also be used to investigate rearrangements between different conformations of the molecule. Every conformation of the molecule has different energy. The most stable conformer (conformer with the lowest energy) is the global minimum. Other stable structures with higher energy are known as a local minima.

The local and global minima are the stationary points. The optimization procedure is used to search the local structures which refer to the equilibrium structures. [185] If we focus on the conformational changes of the molecule, the transition state is a metastable conformation which will change into global or local minimum. If we consider the structural rearrangements of the molecule as chemical reaction, local minima correspond to reactive intermediates. Transition state is a metastable structure, where one bond is formed instead of the other which have been broken. [183, 186]

Every conformation of the molecule has different energy. Initial structure of investigated system is usually not a stationary point in the PES. That is why in the conformational analysis the first step is the geometry optimization of a set of initial structures. [185] The geometry optimization is based on the stepwise numerical procedure with a different algorithms inside. The most popular are: steepest descent and Newton-Raphson methods.

### 2.2.3. Density Functional Theory

The electron density  $\rho(r)$  defines the ground-state energy of the investigated system. Hartree and Fock proposed many-electron wavefunction  $\psi$ , where  $\psi\psi^*$  has the same meaning as the electron density. The density functional theory (DFT) is based on a electron density  $\rho(r)$  which depends only on the  $x, y, z$  coordinates. In the case of the periodic DFT calculations there are additional terms needed: plane waves, energy cutoff, periodic boundary conditions. [183, 186]

#### 2.2.3.1. The Hohenberg-Kohn Theorems

Hohenberg and Kohn in 1964 proved the two theorems. First theorem implies that the electron density determine the external potential (to within an additive constant). When this statement is true the density determine the Hamiltonian operator. It means that the Hamiltonian is described by the external potential and the total number of electrons  $N$ . This can be computed from the density by integration over all space. External potential  $v$  is unequivocal with the ground state electron density functional:

$$v = v[\rho_0] \quad (2.10)$$

The defined ground state electron density identify at the same time quantum mechanical state described with the wave function  $\psi_1$ .

$$\rho_1 \Leftrightarrow \psi_1 \quad (2.11)$$

Thus, relation between  $\rho_1$  and  $\psi_1$  is reversible. [187] The ground state density determine the Hamiltonian operator, which characterizes all states of the system (ground and excited). [188] It is possible to calculate the total energy of the system by minimization of the charge density functional ( $E[\rho]$ ) which depends on the electron density. [188] Second Hohenberg-Kohn Theorem implies that in the N-electron system the variational principle of the density is described with: The ground state energy  $E_0$  is the lower limit of the energy for probe electron density in the N-electron system. [187]

### 2.2.3.2. Kohn-Sham (KS) method

It is unknown how energies depends on the density but very important in the ground-state energy calculations. Kohn and Sham proposed a method to calculate these terms. They proposed the Schrödinger equation of a fictitious N electron system without any interactions which gives the same density as any investigated system of interacting particles. N non-interacting electrons were described by a single determinant wavefunction in N "orbitals"  $\phi$ . [189] Kohn-Sham electron density functional of the energy is described with Eq. [187] (2.12)

$$E_v[\rho] = T_s[\rho] + \int v(r)\rho(r)dr + \frac{1}{2} \int \int \rho(r)\rho(r') |r - r'|^{-1} drdr' + E_{xc}[\rho] \quad (2.12)$$

$$\equiv T_s[\rho] + V_{ee}[\rho] + J_{ee}[\rho] + E_{xc}[\rho] \quad (2.13)$$

Kinetic energy  $T_s[\rho]$  of the electrons is defined in advance.  $V_{ee}[\rho]$  and  $J_{ee}[\rho]$  energy terms represents the electrons repulsion. Exchange-correlation functional  $E_{xc}$  is the rest of the electron energy and correction of the kinetic energy and electron repulsion energy. [187]

The Kohn-Sham approach presents the exact correspondence of the density and the ground state energy for many body systems described by Schrödinger. The big advantage is that the functional is universal - for any particular system we can solve the Schrödinger equation and determine the energy functional and its potential. [183] The problem is that the correct formula of the

exchange-correlation energy is unknown. These days, main aim of researches is to find new functionals which gives the exact energy value. The major types of exchange-correlation functionals are: LDA (local density approximation), GGA (general gradient approximation) and these employing the exact HF exchange as a component. [184]

### 2.2.3.3. Jacob's Ladder of density functional theory

Perdew and Schmidt (2001) described a ladder of the approximations for the exchange-correlation energy which is the functional of the electron density (in the ground state energy and density calculations with Kohn-Sham functionals). The higher rung of the ladder we step the more complex ingredients are combined. Every additional condition makes the method more accurate and more computationally demanding. The ladder is stepping out of the "Hartree World" to the chemical accuracy "heaven". [190]

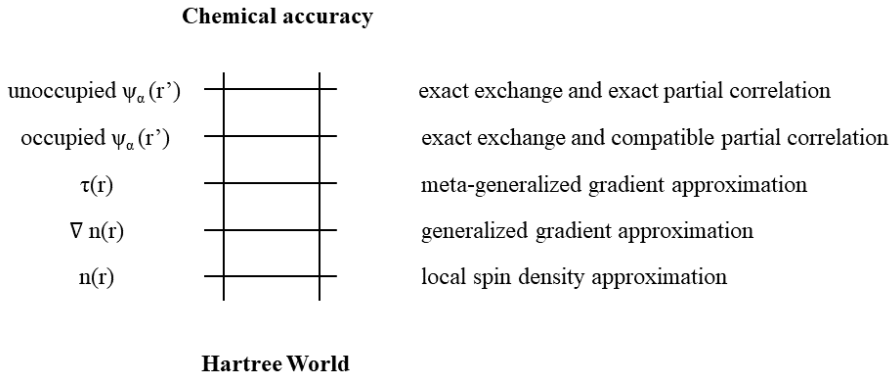


Figure 2.4: Jacobs ladder of density functional theory

At the lowest rung of ladder the contribution to the total energy from 3-dimensional space is determine by the local density. In the local spin density (LSD) approximation the exchange-correlation functional is accurately known and parametrized. [190]

At the second rung the density gradient  $\nabla n(r)$  is introduced. The generalized gradient approximation (GGA) reduce the atomization energy errors. The parametrization of the non-empirical GGA Perdew, Burke, Ernzerhof (PBE) introduce only fundamental constants. GGA require the density in the infinitesimal neighborhood, thus, it is semi-local functional. Utilizing the LSD and GGA we can immediately perform self-consisted calculations, for higher levels we need to introduce the process of averaging over the orbitals to construct an optimized effective potential. [190]

Adding the next natural set of ingredients  $\tau(r)$  to the  $E_{xc}$  produces the meta-GGA – third rung of Jacob's ladder. Meta-GGA is a completely nonlocal

functional of the density but semi-local functional of the occupier orbitals. [190,191]

The exact exchange is nonlocal functional of the occupied Kohn-Sham orbitals which demand a usage of compatible fully nonlocal correlation energy functional. The  $E_{xc}$  with full freedom from self-interaction error and the correct high-density limit under uniform scaling are achieved. [191]

The exact exchange and exact partial correlation include the random phase approximation with suitable short-range corrections. This combination allows to use the occupied and unoccupied Kohn-Sham orbitals. [190,191]

#### 2.2.3.4. Grimme dispersion energy correction

Stefan Grimme proposed a general empirical dispersion correction for density functional calculations. When the Grimme dispersion energy correction is used, total energy of system is described with equation (2.14).

$$E_{DFT_D} = E_{KS-DFT} + E_{disp} \quad (2.14)$$

In (2.14) the  $E_{KS-DFT}$  is a self-consistent Kohn-Sham energy, obtained from chosen functional, the empirical dispersion correction  $E_{disp}$  is described with (2.15). [192]

$$E_{disp} = -s_6 \sum_{i=1}^{N_{at}-1} \sum_{j=i+1}^{N_{at}} \frac{C_6^{ij}}{R_{ij}^6} f_{dmp}(R_{ij}) \quad (2.15)$$

In Eq. 2.15  $N_{at}$  is number of atoms in the investigated system,  $C_6^{ij}$  refers to the dispersion coefficient for pair of the atoms  $i$  and  $j$ ,  $s_6$  is the global scaling factor depend on the utilized functional and  $R_{ij}$  is the distance between  $i$  and  $j$  atoms. [193]

For small distances between  $i$  and  $j$  atoms, to avoid near-singularities, damping function  $f_{dmp}$  must be used, where  $R_r$  refers to the sum of atomic vdW radii. [194]

In this work the BLYP, B3LYP and the PBE functionals were utilized. In the BLYP functional the exchange part was defined by Becke whereas the correlation by Lee, Yang and Parr. The B3LYP functional is a hybrid functional (Becke, 3-parameter, Lee–Yang–Parr). PBE functional also belongs to the class of GGA functionals where the exchange and correlation part were proposed by Perdew, Burke and Ernzerhof.

### 2.2.3.5. Pseudopotentials

Core electrons of the atoms usually are not affected by the chemical environment. The contribution of core electrons in the total energy is not changing when we compare the energy of separate atoms or atoms in molecule or crystals. The biggest changes in the energy are caused by valence electrons.

It is important to describe the valence orbitals properly. Modeling of the core electrons by a proper functions and treating valence electrons separately lower the cost of the calculations (shorter time of the calculation and smaller computer power needed). Usage of the pseudopotentials (PP) allows to minimize the size of the plane wave basis. [186,195] There are two main types of the pseudopotentials, namely norm-conserving and ultrasoft first-principles pseudopotentials. Norm-conserving pseudopotentials impose the conditions, to make every pseudo-wavefunction be identical to its primer all-electron wavefunction. The norm-conserving pseudopotential wavefunction reproduce potential wavefunction properly in the valence region. [196] Vanderbilt ultrasoft pseudopotential was used for the OM molecule, in which the basis-set size is reduced by relaxing the norm-conserving constraint. Norm conserving Troulier-Martins pseudopotentials were used for the SM molecule. [197,198]

### 2.2.3.6. Bloch's theorem

Periodic system is a fictitious set of points given by the translation of the unit cell by every possible vector. Periodic systems are described with wave function written as the product of a cell-periodic part and a wavelike part, due to the Bloch's theorem. Value of the single-electron function  $\psi_k$  in k-point shifted by vector  $R_j$  is given by [199]:

$$\psi_k(r - R) = e^{-ikR_j} \psi_k(r) \quad (2.16)$$

Due to Eq. (2.16) the shift by a vector cause that the function  $\psi_k$  is multiplied by phase factor  $e^{-ikR_j}$ .

The Bloch's function is described with  $\chi(r)$  function which can be the atomic orbital:

$$\phi(r) = \sum_j e^{-ikR_j} \chi(r - R_j) \quad (2.17)$$

The Bloch's function is a orbital of the symmetry given by  $\chi(r - R_j)$  function. Every electronic wave function over a region of k point space can be described by the wave function at a single k point. [199] It is required to obtain electronic state at a finite number of k points to calculate electronic potential.

The electronic wave function at every point can easily be expanded to whole plane-wave basis set. By introducing the energy cutoff to the plane-wave basis set a finite basis set is produced. [200]

Primarily the plane waves have been used only for periodic systems (crystals, solvents), but they can be used as well for separated molecules. By using supercell approach we can investigate molecule in a large box, that the self-interactions of the molecule are absent. [186]

### 2.2.3.7. Energy cutoff

The plane wave basis set is characterized by the highest energy, namely the energy cutoff  $E_{cut}$ . The energy cutoff of 80 eV correspond to a basis set which approximately 8000 functions. Increasing of the energy cutoff  $E_{cut}$  is a way to improve the quality of the plane wave basis set. [186]

$$\frac{\hbar^2}{2m_e} |G + k|^2 < E_{cut} \quad (2.18)$$

Only the plane waves that fulfill equation (2.18) are included in the basis set.

## 2.2.4. Car-Parrinello Molecular Dynamics

Investigation of the structural changes of the molecule in the real conditions should go beyond the usage of static calculations. The proper way to predict how the molecules "behave" at finite temperature is the usage of the molecular dynamics. As a result of molecular dynamics simulations we obtain the trajectory – a set of positions and velocities of atoms as a function of a time. Temperature is defined as the average value from the trajectory in the phase space. Similarly we can obtain physicochemical properties of the investigated system like: dipole moment, density or viscosity.

The main idea of the CP–MD method is a transformation of the quantum adiabatic time-scale separation of fast electron and slow nuclear motion into adiabatic energy-scale separation for the molecular dynamic instead of solving the time-independent Schrödinger equation at each step. [200–202]

### 2.2.4.1. Equation of motion

The parameters which define the shape and size of the unit cell can be presented as the dynamical variables in the molecular-dynamics Lagrangian. Car and Parrinello have postulated Lagrangians as presented below:

$$L_{CP} = \sum_I \frac{1}{2} M_I \dot{R}_I^2 + \sum_i \frac{1}{2} \mu \langle \dot{\psi}_i | \dot{\psi}_i \rangle - \langle \dot{\psi}_i | H_e | \dot{\psi}_i \rangle + constraints \quad (2.19)$$



Equations of motions:

$$M_I \ddot{R}_I(t) = -\frac{\partial}{\partial R_I} \langle \psi_i | H_e | \psi_i \rangle + \frac{\partial}{\partial R_I} (\text{constraints}) \quad (2.20)$$

$$\mu_i \ddot{\psi}_i(t) = -\frac{\partial}{\partial \langle \psi_i |} \langle \psi_i | H_e | \psi_i \rangle + \frac{\partial}{\partial \langle \psi_i |} (\text{constraints}) \quad (2.21)$$

The equations of motion (Fig. (2.20) and Fig. (2.21)) is related to the acceleration of the forces influencing the system.  $\mu_i$  is the fictitious mass assigned to the orbitals (electronic) degrees of freedom. In pursuance of the Car-Parrinello equations of motion the energy involved by nuclei is proportional to  $\sum_I M_I \dot{R}_I^2$  and the fictitious electronic sub-system involves temperature proportional to  $\sum_i \mu \langle \dot{\psi}_i | \dot{\psi}_i \rangle$ . [200]

#### 2.2.4.2. Nosé thermostat

To compensate the irreversible heat flow between the slow nuclei and fast electrons we can introduce the Nosé thermostat.

If we solve the Newton's equation of motion for molecules with fixed initial positions and velocities with chosen algorithm we can obtain micro canonical ensemble (NVE). [203] When we introduce Nosé thermostat the equations of motion are modified, so our system becomes a canonical ensemble (NVT).

$$M_I \ddot{R}_I(t) = -\frac{\partial}{\partial R_I} \langle \psi_i | H_e | \psi_i \rangle + \frac{\partial}{\partial R_I} (\text{constraints}) - M_I \dot{R}_I \dot{x}_R \quad (2.22)$$

$$\mu_i \ddot{\psi}_i(t) = -\frac{\partial}{\partial \langle \psi_i |} \langle \psi_i | H_e | \psi_i \rangle + \frac{\partial}{\partial \langle \psi_i |} (\text{constraints}) - \mu \dot{\psi}_i \dot{x}_e \quad (2.23)$$

The frictions terms,  $M_I \dot{R}_I \dot{x}_R$  and  $\mu \dot{\psi}_i \dot{x}_e$ , are implemented to the equation of motion to merge the atoms and/or wave function motions to the thermostat. Last parts of the equations are dependent on the variable  $x_R$  and  $x_e$  being described with the equations (2.24) and (2.25).

$$Q_R \ddot{x}_R = 2 \left[ \sum_I \frac{1}{2} M_I \dot{R}_I^2 - \frac{1}{2} g k_b T \right] \quad (2.24)$$

Where  $k_b$  is the Boltzmann constant, T is the temperature and  $\frac{1}{2} g k_b T$  is average kinetic energy of the ionic sub-system with  $g=3N$  degrees of freedom. The physical temperature T and mass  $Q_R$  are the basic value for the thermostat

to control degrees of freedom for the ions.

$$Q_e \ddot{x}_e = 2 \left[ \sum_I \mu \langle \dot{\psi}_i | \dot{\psi}_i \rangle \right] - E_{kin,e} \quad (2.25)$$

The kinetic energy  $E_{kin,e}$  of the fictitious sub-system is related to velocities of the atom. Using the  $E_{kin,e}$  and  $Q_e$  helps to control electronic degrees of freedom.

The time scale of the thermal fluctuations of the thermostats are determined by the masses  $Q_R$  and  $Q_e$ . With increase of the masses, the frequencies of the thermal fluctuations associated to the thermostat will decrease. [203]

### 2.2.4.3. Radial Pair Distribution Function

The radial distribution function (RDF)  $g(R)$ , in statistical mechanics, describes how density varies as a function of distance from a reference particle in a group of particles.

When one molecule is treated as the origin  $O$ , and the  $\rho = N/V$  is the average number density of particles, the local time-averaged density at a given distance  $R$  from  $O$  is  $\rho g(R)$ . The above mention simple definition is true when we consider homogeneous and isotropic systems.

Generally it is a measure of the probability of finding a particle at a given distance from a reference particle, relative to that for an ideal gas. The general algorithm involves determining how many particles are within a distance of  $r$  and  $r+dr$  away from a particle. [204]

### 2.2.5. Boltzmann probability distribution function

Based on the relative energy differences it is possible to calculate the population of each conformer. The contribution of the conformers is described with the Boltzmann distribution equation:

$$\frac{N_i}{N_{tot}} = \frac{D_i e^{-\frac{\Delta G_i}{RT}}}{\sum_{i=1}^{23} \frac{\Delta G_i}{RT}} \quad (2.26)$$

where:

- $\Delta G_i = \Delta E_i + RT \ln \sigma_i$ ,
- $D$  - degeneracy of  $i$ -th conformer,
- $\sigma_i$  - symmetry number of the  $i$ -th conformer,
- $T$  - temperature in Kelvin set to 298 K,

- $R = 8.314 \frac{J}{molK}$  - gas constant

The relative energies ( $\Delta E$ ), were calculated as a differences between the global energy minimum and local energy minima structures. The  $N_i$  is the population of the given conformer with respect to the overall amount of the molecules  $N_{tot}$ .

### 2.2.6. Python based proprietary programs

Python is an interpreted, high-level, general-purpose programming language with dynamic semantics, strong typing, and a large standard library, known for its readability and ease of use. Designer of the Python is Guido von Rossum. This programming language allows to write the script quickly and to integrate systems much more effectively. [205] It means that Python is multi-platform that allows to run programs that have been written in other computer systems when the required modules are installed. It is an open source language, one can download and modify the source code, although there are various licenses that allow different uses. [206]

The main reasons why I used Python in the analysis of the CP-MD simulations are:

- big range of library code can possibly be obtained from other sources,
- high level productivity, when large projects are done,
- the Python supports Linux and other platforms,
- comprehensive set of data types.

In this research Python programming was used in the post-processing analysis. First program allows to check which structures are present in the every step of the trajectory. Second program produces the list of conformational changes from one conformer to another.

### 3. CHAPTER: MATERIALS AND METHODS

#### 3.1. Experimental methods

Tetrahydrofuran sample was purchased from Sigma Aldrich (purity 99.9%). Nitrogen (99.995%), Argon (99.995%), Neon, Xenon from Elme Messer Gaas were used as the matrix gases.

The heterocyclic compounds, namely: 1-methyl-germacyclohexane, 1-chloro-1-chloromethyl-silacyclohexane, 1-chloromethyl-1-fluoro-silacyclohexane, 1-chloromethyl-1-fluoro-silacyclopentane and 2,2,4,4,6,6-hexamethyl-1,3,5,2,4,6-triazatrisilinane were recently synthesized by the Guirgis Group at the College of Charleston (Charleston SC). The synthesis procedure is out of the scope of the dissertation.

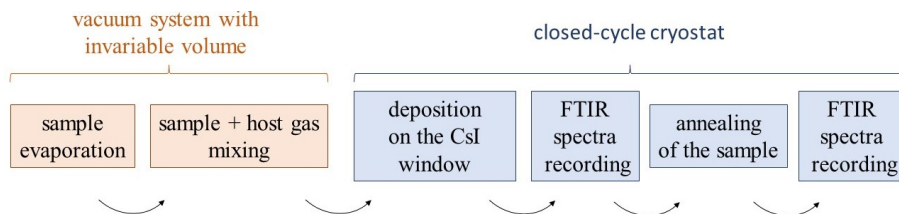


Figure 3.1: Scheme of the closed-cycle cryostat without compressor

The heterocyclic molecules were evaporated in the vacuum system with freeze-pump-thaw cycle. All matrix isolation samples were prepared in the vacuum system with invariable volume (in the mixture chamber). The vapors of investigated compounds were mixed with matrix gas in specific ratios, controlling the pressure of the gases in the gas chamber. Prepared analyte:matrix gas mixture was deposited on the CsI window. For the Tetrahydrofuran molecule the He cryostat (Leybold-Heraeus RW2) was used. For the rest of the molecules new three stage cooling system (Janis SHI-4-1) cryostat (operating temperature 3–300 K) was used. The deposition time was chosen depending on the molecule used, usually 1 hour. The deposition speed was controlled by adjusting needle value in the deposition line. The IR spectra were recorded right after deposition, and after annealing process. The temperatures during deposition on the mixture and during annealing process were chosen depending on the matrix gas used. The schematic description of the experiment steps is presented in Fig. 3.1. The annealing process temperature was driven by the matrix gas type, bearing in mind that while certain temperatures are reached, matrix can be damaged by the irreversible processes (clusterization of the analyte molecules or fast evaporation of the mixture from deposited surface).

During matrix isolation experiments the infrared spectrometer Bruker IFS 113 (Bruker Optik GmbH, Ettlingen, Germany) with  $1\text{ cm}^{-1}$  resolution, KBr

beamsplitter, global source and MCT detector was used. 256 spectra were averaged for each measurement. Both background and sample spectra were measured at the same conditions.

Raman experiments were done with use of the FT-Raman spectrometer MultiRAM from Bruker (Bruker Optik GmbH, Ettlingen, Germany), using Nd:YAG (1064 nm) laser as the excitation source and germanium diode cooled with liquid nitrogen as a detector. The laser power was set to 1000 mW. Spectra were recorded with 4  $\text{cm}^{-1}$  resolution and 1000 spectra were averaged. During the measurements the sample was in the closed glass vial in liquid state.

The attenuated total reflection (ATR) method was used to obtain the IR absorption spectra of the samples in liquid state. All spectra were recorded with Bruker Alpha spectrometer with a single reflection diamond accessory, global source and DTGS detector. The resolution of the spectra was 4  $\text{cm}^{-1}$ , during the measurement 256 spectra were averaged.

### 3.2. Computational methods

All static calculations were performed using the ORCA 4.1.1 software package. [207] The energies and vibrational frequencies were calculated. During calculations for the heterocyclic compounds density functional theory (DFT), utilizing the hybrid B3LYP [208] functional and Dunning’s augmented triple zeta correlation consistent basis sets [209] were used. The Grimme (DFT-D3) general dispersion correction was implemented for better description of the non-covalent interactions. [193, 210] The computational setup of the potential energy surface (PES) scans and the interconversion barriers was as described above. During the PES scans the structures were optimized at every scan step.

Normal vibrational modes derived from DFT/B3LYP/aug-cc-pVTZ method were described with use of the Vibrational Mode Automatic Relevance Determination (VMARD) method. The Automatic Relevance Determination (ARD) method is a variant of Bayesian Ridge Regression and gives a good estimation of the most prominent internal coordinates. [211]

For the tetrahydrofuran, 1-chloro-1-chloromethyl-silacyclohexane and 1-chloromethyl-1-fluoro-silacyclohexane molecules Car-Parrinello molecular dynamics (CP-MD) simulations were done with use of the gradient-corrected Becke-Lee-Yang-Parr (BLYP) exchange-correlation functional. [212, 213]

For isolated THF conformers ( $C_2$  and  $C_s$ ) additional DFT plane-waves (PW) calculations were performed. The 70 Ry cut-off and other parameters like in molecular dynamics simulations were applied.

Car-Parrinello molecular dynamics (CP-MD) [214] simulations were performed using CPMD program package [215] with parameters listed below:

- standard norm-conserving Troullier–Martins pseudopotentials for atomic cores description [216],

- Brillouin zone sampling restricted to the  $\Gamma$ -point,
- empirical D2 dispersion correction by Grimme [192],
- the canonical ensemble (NVT), Nosé–Hoover chain thermostats [203,217] for the nuclear degrees of freedom,
- fictitious electronic mass set at 400 a.u.,
- the equations of motion integrated with a 4 a.u time step,
- temperature set to 20 K for THF, and to 20, 50, 70K for 1-Cl-1-CIM-SiCP and 1-CIM-1-F-SiCP,
- molecules placed in cubic box with side length set to 11.288 Å- to mimic the single crystal of solid nitrogen in the cubic  $\alpha$ -phase [218],
- the CP-MD simulations duration for tetrahydrofuran: 50 ps (equilibration procedure) 100 ps (production run), and for the 1-chloro-1-chloromethyl-silacyclohexane and 1-chloromethyl-1-fluoro-silacyclohexane: 50 ps (equilibration procedure), and 50 ps (70K), 100 ps (20, 50K) simulation time.

For the isolated  $C_2$  and  $C_s$  tetrahydrofuran conformers, additional CP-MD simulations were done with 15.0 Å cubic box length and temperature set to 10 K, to prohibit any conformational rearrangements. The simulations length was 10 ps (equilibrium procedure) and 80 ps (production run).

The anharmonic frequencies for isolated THF conformers and molecule embed in the nitrogen matrix were calculated with the Fourier Transformation of the dipole moment autocorrelation function (program package developed by Kohlmeyer [219]) derived on-the-fly from the CP-MD simulation and further adjusted by the harmonic quantum correction factor. [220]

The visualization of the trajectory was performed using VMD program package [221], for the visualization of the results obtained for the static calculations ChemCraft [222] and Avogadro [223] programs were used.

## 4. CHAPTER: RESULTS AND DISCUSSION ON FIVE MEMBER RING HETEROCYCLES

### 4.1. Tetrahydrofuran (THF)

#### 4.1.1. Static Density Functional Theory based calculations

For the static calculations the BLYP non-hybrid functional was used. The BLYP non-hybrid functional allow to obtain a proper relative energy order for the THF local minima and accurate description of the possible weak hydrogen bonds. The results indicates that the envelope ( $C_s$ ) structure is the global minimum while the twisted ( $C_2$ ) is the first local energy minimum (see Fig. 4.1) with energy difference equal to 0.15 kcal/mol.

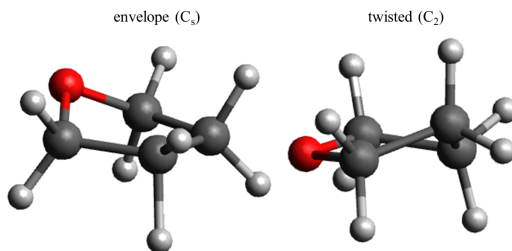


Figure 4.1: Tetrahydrofuran molecule in envelope ( $C_s$ ) and twisted ( $C_2$ ) conformations.

Obtained results are in a very good agreement with CCSD(T) benchmark calculations where the energy difference between global minimum ( $C_s$ ) and first local minimum was found to be 0.14 kcal/mol. Additionally, to test the influence of the basis set used for CP-MD simulations, the DFT plane waves (PW) DFT(PW)/BLYP calculations with Grimme D2 dispersion correction method was used for static calculations. As a results, the proper order of conformers was obtained with energy difference equal to 0.12 kcal/mol.

For the assignment of the experimental vibrational bands the harmonic (static) and anharmonic (CP-MD) infrared spectra were obtained from static DFT calculations and molecular dynamics simulations.

#### 4.1.2. Car-Parrinello molecular dynamics simulations

The main goal of the theoretical calculations is explicit experimental conditions description and insight into molecules behavior. In this particular case the tetrahydrofuran pseudorotation and conformer stability at given temperature. Most of the static calculations omit the temperature impact to the properties of the molecules. That is why the performed CP-MD simulations

for an experimental model of the tetrahydrofuran molecules embedded in the nitrogen matrix utilizing periodic boundary condition is so important. The performed matrix isolation experiment use temperature range of 9-20K, thus for CP-MD calculations temperature equal to 20K was chosen, to mimic the annealing temperature from the experiment. The supercell model consist of a one THF molecule placed in between 31 molecules of the nitrogen in the cubic  $\alpha$ -phase. The THF molecule position was adjusted so its geometrical center fits the geometrical center of  $N_2$  molecule removed from the supercell. Produced supercell was optimized and then used as a starting point for the CP-MD simulations. The size of the supercell was chosen to prohibit any interactions between two tetrahydrofuran molecules.

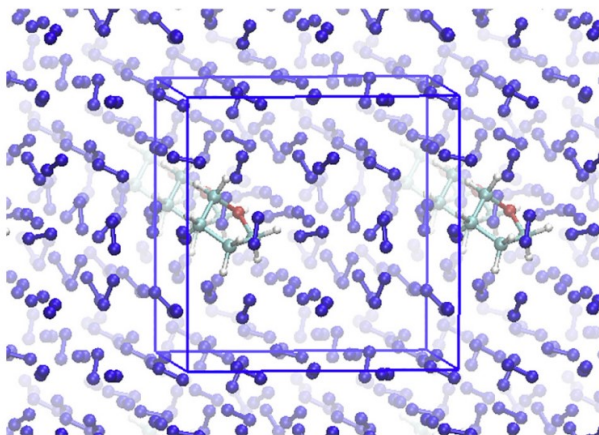


Figure 4.2: THF@N model. For better visibility only two layers are depicted. Atoms colors for the carbon, nitrogen, oxygen and hydrogen are gray, blue, red and white, respectively. [A1]

For the conformational changes investigation the C-C-C-C dihedral angle of the tetrahydrofuran molecule was traced within the CP-MD simulation trajectory. Figure 4.3 depict the time evolution of the mentioned dihedral angle during the production of the simulation. The envelope and twisted conformers are represented by 0 and  $\pm 35.8^\circ$  dihedral angle values, respectively. These values are hardly occupied in the trajectory, so this might be incorrect to describe the structure of the tetrahydrofuran molecule in nitrogen matrix in terms of conformers obtained from the static calculations.

To find the accurate, most populated structure of the THF molecule at nitrogen matrix, the 1-dimensional histogram (see Fig. 4.4) was created. The most populated THF structure in the CP-MD simulations is a structure with the C-C-C-C dihedral angle value around  $24^\circ$ . Such a structure is not an envelope or twisted, rather a superposition of both.

The CP-MD simulations (Fig. 4.3) allow to trace the dynamics of the con-



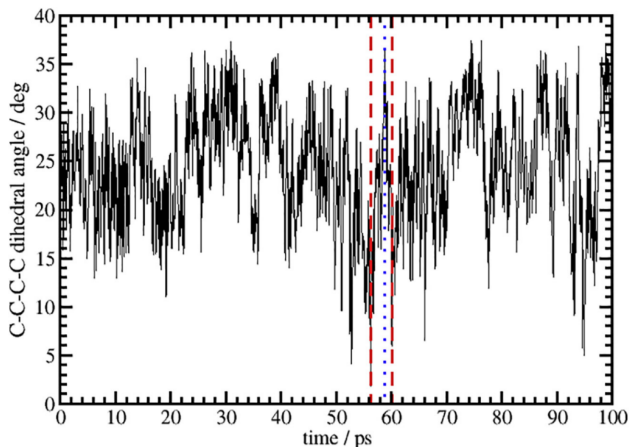


Figure 4.3: The conformational changes of the THF@N system. The C-C-C-C dihedral angle values in the trajectory of the CP-MD simulations. Vertical red and blue lines describe the chosen ( $C_s$ ) envelope and ( $C_2$ ) twisted conformations occurrence. [A1]

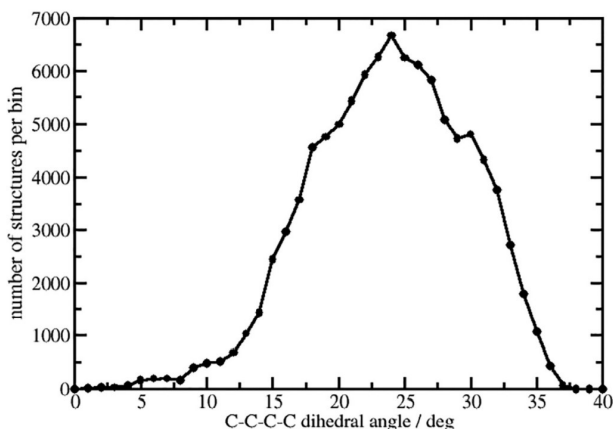


Figure 4.4: One dimensional histogram of the C-C-C-C dihedral angle obtained from the CP-MD trajectory for the THF@N<sub>2</sub> system at temperature of 20 K. [A1]

stant conformational rearrangements (pseudorotation) and estimate the time of the  $C_2 \rightarrow C_s$  and  $C_s \rightarrow C_2$  transitions. The first red dashed line (58 ps) represents the  $C_s$  conformer, change to the  $C_2$  conformer (blue dotted line) takes approximately 2.6 ps. The reverse interconversion, namely  $C_s \rightarrow C_2$  (blue dotted line to second red dashed line) takes around 1.2 ps.

Additionally, CP-MD simulations of the isolated THF system, but with the temperature increased to 100K, revealed that the  $C_2 \rightarrow C_s \rightarrow C_2$  interconversion is much faster, and equals to 0.4 ps. This leads to conclusion that the

pseudorotation process is affected by the matrix environment, explicitly by the formations of the C-H $\cdots$ N interactions.

#### 4.1.3. Matrix isolation experiment

In case of tetrahydrofuran, for which the structure of possible conformers is well known, the matrix isolation experiment was introduced to study the pseudorotation phenomena. The tetrahydrofuran molecules were embedded in the nitrogen matrix at 9K, then the annealing process was performed. The low (fingerprint) and a high (C-H stretch) frequency regions of the FT-IR obtained spectra are depicted in Fig. 4.5 and Fig. 4.6. The 9K spectra represents the equilibrium at room temperature population and the annealing process (heating up to 25K and cooling back to 9K) allow for insight into the temperature impact to conformational stability. The most prominent changes are enlarged and presented below the spectrum window for better visibility. All vibrational frequencies from the matrix isolation experiment are presented in Table 5 in the APPENDIX I.

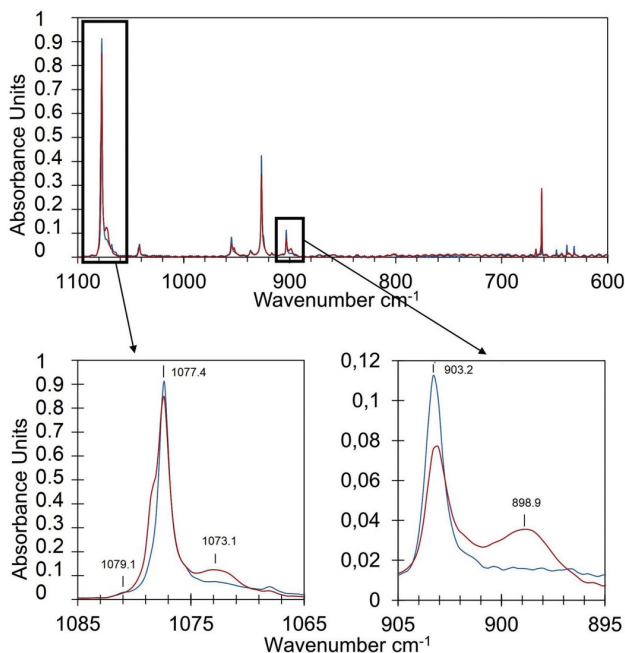


Figure 4.5: The fingerprint frequency region obtained from matrix isolation experiment for THF at nitrogen system at 9 K before (red) and 9 K after the annealing process (blue). [A1]

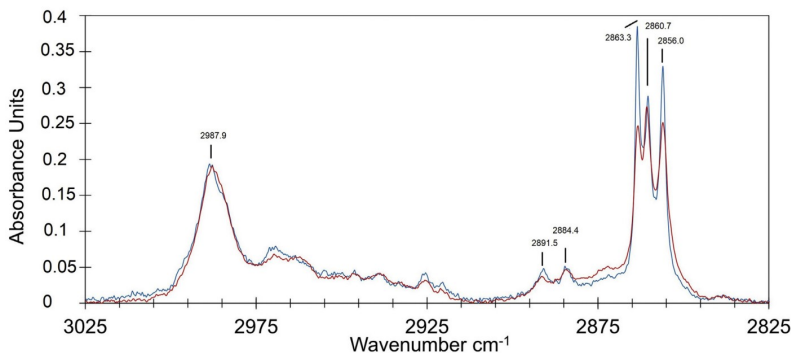


Figure 4.6: FTIR spectra (C-H stretch frequency region) obtained from matrix isolation experiment for THF@N<sub>2</sub> system at 9 K before (red) and 9 K after annealing process (blue). [A1]

#### 4.1.4. Vibrational analysis

The harmonic computational vibrational analysis was performed for both conformers, namely envelope ( $C_s$ ) and twisted ( $C_2$ ), with use of the localized Dunning’s correlation consistent basis set. The obtained vibrational modes with assignment are listed in Table 6 in the APPENDIX I.

The anharmonic vibrational analysis for both isolated conformers and the tetrahydrofuran molecule trapped in the nitrogen matrix at 20K were produced with the Fourier Transform of the dipole moment autocorrelation function, and are depicted in Fig. 4.7. The anharmonic spectrum for isolated envelope ( $C_s$ ) and twisted ( $C_2$ ) structure are related to temperature equal to 10K, to prevent the possible conformational changes.

The biggest changes related to the conformational changes are present in two regions of the experimental spectrum, namely fingerprint (low) 700–1100  $\text{cm}^{-1}$  and C-H (high) 2800–3000  $\text{cm}^{-1}$  frequency.

In the fingerprint region most of the bands are ring vibrational modes. The most intense 1077.4  $\text{cm}^{-1}$  experimental band according to the anharmonic and harmonic approximations correspond to the C-O stretching vibration. It’s intensity does not change upon annealing. This intense band has two subbands at 1079.1  $\text{cm}^{-1}$  and 1073.1  $\text{cm}^{-1}$  which disappear upon annealing. The frequencies calculated with both methods for the envelope structure are higher, thus experimental subband at 1079.1  $\text{cm}^{-1}$  can be attributed to the envelope conformer.

In the harmonic and anharmonic spectra for the isolated molecules, we can find only two bands, the third band is not present. In contrary to that in the spectrum obtained for the THF@N model, we can find aforementioned subband. Thus, the band at 1073.1  $\text{cm}^{-1}$  and its disappearing after annealing can be explained with the change of the symmetry of the nitrogen matrix. In

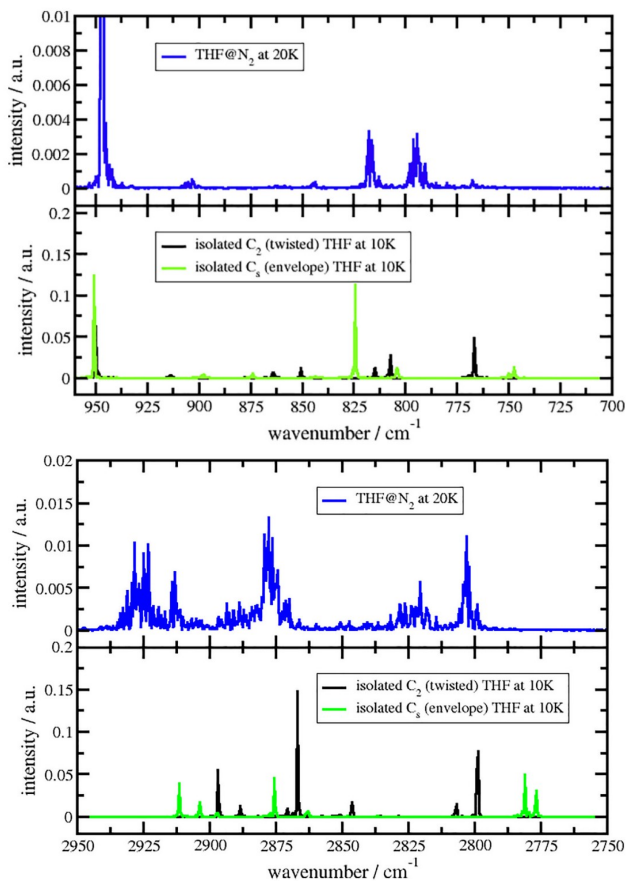


Figure 4.7: Anharmonic IR spectra of the fingerprint and C-H stretch frequency regions, derived from CP-MD simulations. [A1]

the lower temperatures (9 K) the nitrogen matrix structure is  $\alpha$ -phase, with the temperature increase, the structure can change to hexagonal close packed structure in the  $\beta$ -phase.

Despite the fact, that the envelope structure is the global energy minimum, intensity of the band related with this conformer decreases. Such a behavior would be a proof that after annealing process the amount of the envelope conformer decreases. Such effect can be explained by the fact that the THF molecule in the nitrogen matrix undergo constant  $C_2 \rightarrow C_s \rightarrow C_2$  rearrangements. This was explained with the CP-MD calculations and is described in the Car-Parrinello molecular dynamics (CP-MD) simulations section.

The harmonic approximation does not give clear assignment for other bands, but with use of the anharmonic vibrational frequencies we can assign some bands to particular conformer. The band at  $898.9 \text{ cm}^{-1}$  from the experimental spectrum can assigned to the  $C_s$  conformer, while bands  $926.6 \text{ cm}^{-1}$ ,  $926.7$

$\text{cm}^{-1}$  and  $903.2 \text{ cm}^{-1}$  to the  $C_2$  conformer.

In the C-H stretch frequency region the intensity of majority of the bands changes upon annealing. Both conformers are present under experimental conditions, before and after annealing, but the population is different. For the accurate description of the vibrational modes both harmonic and anharmonic spectra were calculated.

The respective bands in the THF@N<sub>2</sub> anharmonic spectrum are blue-shifted in comparison to those for isolated tetrahydrofuran conformers. Such a blue-shift in the C-H stretch frequencies is an evidence of the blue-shifting hydrogen bonds. [224] Formation of blue-shifting hydrogen bonds cause the decrease of C-H bonds lengths of the hydrogen bond donor. To prove the existence of such effect, the C-H bonds length was calculated and averaged. For the isolated THF molecule, the C-H bond length is equal to  $1.0999 \text{ \AA}$ , while for the THF embedded in the nitrogen matrix  $1.0982 \text{ \AA}$ . One may say such a difference is too small, but  $0.0017 \text{ \AA}$  is typical bond length decrease value to be a proof of the weak blue-shifting hydrogen bond existence. While one of such a contact does not influence the molecule, the increase in the C-H $\cdots$ N hydrogen bonds number makes the THF - matrix interactions stronger. The experimental bands in the region  $2856.0\text{-}2863.3 \text{ cm}^{-1}$  are associated with envelope conformer ( $2776.7\text{-}2781.0 \text{ cm}^{-1}$   $\nu(\text{C-H})$  symmetric stretching vibrations). Bands in the  $2884.4\text{-}2891.5 \text{ cm}^{-1}$  region in the experimental spectrum are caused by the  $\nu(\text{C-H})$  symmetric stretching vibrations of the twisted conformer and attributed to the  $2798.3\text{-}2806.1 \text{ cm}^{-1}$  anharmonic bands. The peak at  $2987.9 \text{ cm}^{-1}$  can be attributed to the  $\nu(\text{C-H})$  asymmetric band at  $2911.4 \text{ cm}^{-1}$  from the envelope anharmonic spectrum.

#### 4.1.5. Conclusions

Both tetrahydrofuran conformers, namely envelope  $C_s$  and twisted  $C_2$ , are present under nitrogen matrix experiment conditions, independent from the annealing process. Analysis performed of the experimental spectrum allows for conformer energy difference estimation which was found to be  $-0.11 \text{ kcal/mol}$ . This value corresponds very well with the theoretically obtained values.

The Car-Parrinello molecular dynamics simulations at finite temperature indicate that the full cycle  $C_s \rightarrow C_2 \rightarrow C_s$  conformational change occur within several ps. These changes are steered by the formation of a weak blue-shifted C-H $\cdots$ N contacts between the C-H groups of the THF molecule and the surrounding nitrogen species.

The most probable conformation of the THF molecule in the nitrogen matrix is a transition structure between the envelope and twisted configurations. The  $C_s$  and  $C_2$  local minima predicted by the static DFT calculations which refer to temperature of  $0 \text{ K}$  are hardly present in the THF@N<sub>2</sub> system

## 4.2. 1-chloromethyl-1-fluoro-silacyclopentane (1-CIM-1-F-SiCP)

The synthesis of the 1-chloromethyl-1-fluoro-silacyclopentane (1-CIM-1-F-CP) was done in the laboratory in the College of Charleston. It was synthesized for the first time during the search of novel hydrophobic coatings. The synthesis procedure is not in the scope of this thesis, thus described elsewhere. [A2]

### 4.2.1. Density Functional Theory and Møller–Plesset based calculations

The several envelope ( ${}^1E$ ,  ${}^2E$  and  ${}^{Si}E$ ) and twisted ( ${}^2T_3$ ,  ${}^1T_2$ ,  ${}^{Si}T_1$ ) conformers with Cl-C-Si-F in *gauche+*, *gauche-* and *trans* positions were optimized with use of the DFT/B3LYP/aug-cc-pVTZ method. The optimization procedure revealed that only stable conformers are  ${}^2T_3$  *trans*,  ${}^2T_3$  *gauche-* and  ${}^2T_3$  *gauche+* (see Fig. 4.8) structures. Note that we do not use axial/equatorial position nomenclature. It was omitted due to the axial and equatorial conformers. For mentioned twisted structures the optimization was performed again with more accurate method, namely MP2/aug-cc-pVTZ.

The global energy minimum was found to be  ${}^2T_3$  *trans* structure with  ${}^2T_3$  *gauche-* and  ${}^2T_3$  *gauche+* as a local energy minima with relative energy difference equal to 3.5 MP2 (1.4 DFT) and 4.2 MP2 (1.5 DFT) kcal/mol, respectively. All energy structural parameters are listed in Table 7 in the APPENDIX I.

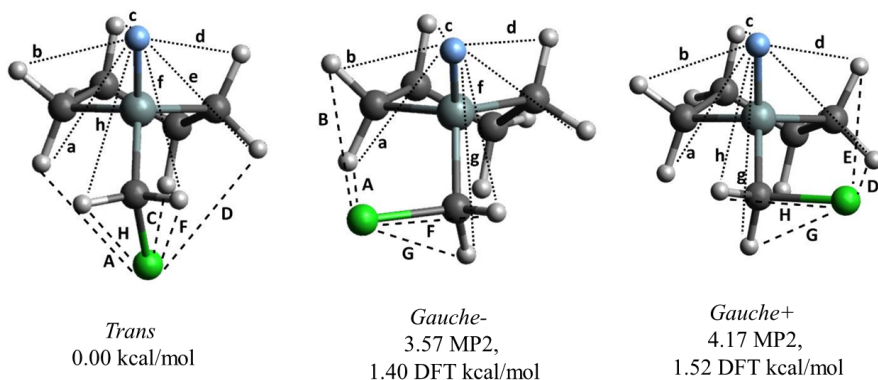


Figure 4.8: Non-degenerated  ${}^2T_3$  *trans*,  ${}^2T_3$  *gauche-* and  ${}^2T_3$  *gauche+* conformers of the 1-chloromethyl-1-fluoro-silacyclopentane additionally marked Si-F...H and CH<sub>2</sub>-Cl...H and relative energy differences resulted from MP2/aug-cc-pVTZ and DFT/B3LYP/aug-cc-pVTZ calculations. [A2]

In the optimized structures the non-bonded H...H lengths, have values similar to the sum of van der Waals hydrogen radius (2.4 Å), this leads to conclusion that during conformational stability analysis we need to consider the repulsive interactions. The structure of the local energy minima conformers is

dictated by the hyperconjugative interactions, the eclipsed conformations of the bond orbitals [142], interaction of bonding–antibonding orbitals [74, 144, 145] and the relative destabilizing non-bonded interactions in the eclipsed CH<sub>2</sub>-CH<sub>2</sub> fragments. The elongation of the axially oriented C-H bond in the ring is a strong proof of the stereoelectronic hyperconjugative effect.

The Boltzmann distribution population calculated with use of obtained relative energy values indicates that the amounts of 84%, 8.6% and 7.1% for the <sup>2</sup>T<sub>3</sub> *trans*, <sup>2</sup>T<sub>3</sub> *gauche*- and <sup>2</sup>T<sub>3</sub> *gauche*+ conformers, respectively.

The structure and stability of the *trans* conformers might be explained as well with analysis of the structural parameters and possible Si-F···H and CH<sub>2</sub>-Cl···H interactions (see Fig. 4.8). In the global energy minimum structure the fluorine atom can interact with axial and equatorial hydrogen atoms attached to the 1C, 2C and 4C carbon atoms resulting in 5 hydrogen bond like contacts. Similar pattern for fluorine atom is present for the *gauche*- and *gauche*+ structures, thus do not give any explanation on the conformational stability. The bigger influence may have interactions of the fluorine atom with the hydrogen atoms from the CH<sub>2</sub>Cl group. In the *trans* form 5C-H···F-Si and 5C-Hg···F-Si contacts. The exact values of all possible contacts are listed in Table 8 in the APPENDIX I.

Fluorine and chlorine atoms have different values of van der Waals radius (Cl-1.95 Å, F-1.60 Å, Si-2.10 Å [225]) and electronegativity (Cl-3.16, F-3.98, Si- 1.9 [73]). The presence of the blue-shifting hydrogen bonds can be detected with the decrease of the C-H bonds lengths. The decrease of number of formed hydrogen bonds and the increase in the hydrogen bond length is a reason of the lower stability of the *gauche* conformers.

#### 4.2.2. Potential energy surface scan

The Potential energy surface scans were performed for the ring (C-C-C-C) and the substituents (Cl-5C-Si-F) containing dihedral angles with use of the DFT/B3LYP/aug-cc-pVTZ method. The results are shown in Fig. 4.9. As it is visible on the top panel the <sup>2</sup>T<sub>3</sub> to <sup>3</sup>T<sub>2</sub> inversion leads through the envelope structure, which is a transition state. The potential energy barrier for this rearrangement is equal to 4.01 kcal/mol. During this rearrangement the position of the substituents remain the same, which is the *trans* position. At the lower panel of Fig. 4.9 the potential energy surface scan describing the CH<sub>2</sub>Cl group rotation is presented. The rotation from *gauche*- and *gauche*- to *trans* position occurs through the *cis* transition state position. The potential energy barriers for the *gauche*- → *trans* and *gauche*+ → *trans* are 1.30 and 1.23 kcal/mol, while the revers processes *gauche*-/*gauche*+ → *trans* are isoenergetic and equal to 2.71 kcal/mol.

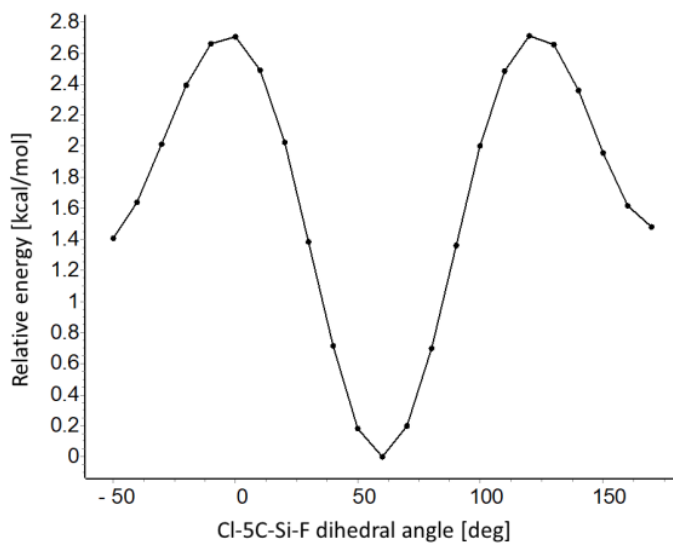
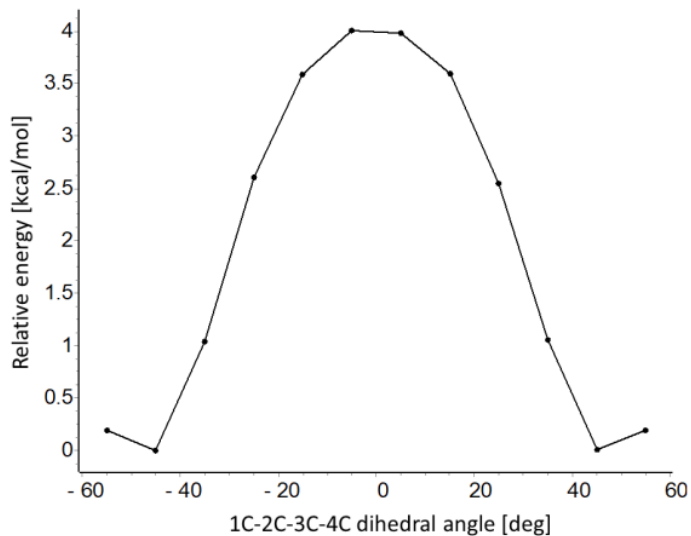


Figure 4.9: The relaxed potential energy surface scans along the C-C-C-C and Cl-C-Si-F (rotation of the CH<sub>2</sub>Cl group) dihedral angle change derived with DFT/B3LYP/aug-cc-pVTZ approach. The relative energy was calculated with respect to the lowest energy from particular surface scan. [A2]



### 4.2.3. FT-IR spectra in the gas phase

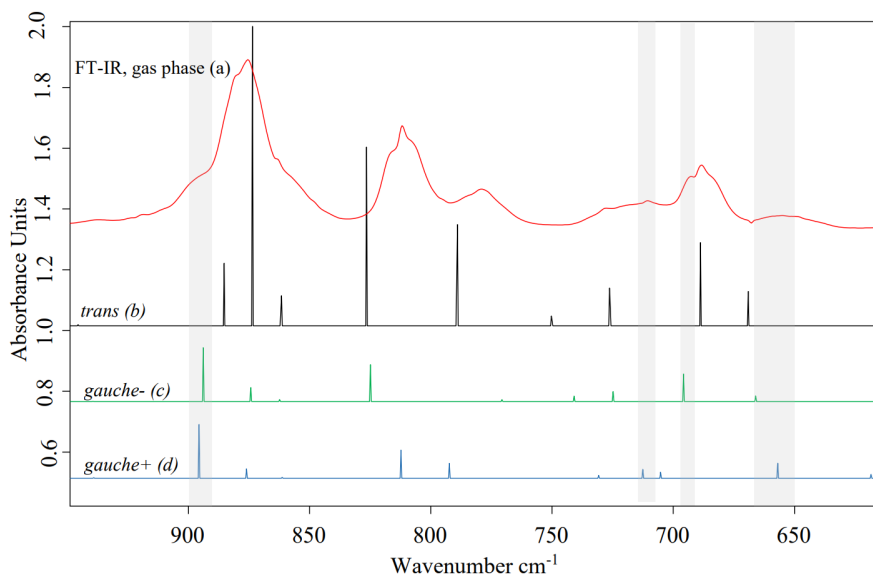


Figure 4.10: FT-IR spectrum of the 1-chloromethyl-1-fluoro-silacyclopentane in the gas phase (a) at room temperature with computational vibrational frequencies for the  ${}^2T_3$  *trans* (b),  ${}^2T_3$  *gauche-* (c) and  ${}^2T_3$  *gauche+* (d) conformers. Intensities of the computational vibrational frequencies were scaled and reflect the population of the conformers. [A2]

The gas phase IR spectra were recorded two times, directly after evaporation in the gas chamber, and after 1 hour. The gas chamber was exposed to the sun light. The results indicate that the CIM-F-CP does undergo any changes under sun light and is stable in the closed chamber. Obtained spectral bands are broad and in most cases overlapped, thus only general assignment of the vibrational band is possible. Despite the band overlap, basing on the computational results we can attribute some bands to the lower energy conformers. The computationally obtained vibrational modes are listed in Table 9 in the APPENDIX I.

The intensity of the computationally obtained spectra during the assignment was scaled according to the Boltzmann distribution based on energy differences of the twisted conformers (See Static Calculations section). Intensity of the bands depends on the conformer amount in the experimental sample, thus the intensity of the bands from *gauche* conformers will be smaller and in some cases overlapped by the *trans* conformer bands with higher intensity.

Shoulder band at  $899\text{ cm}^{-1}$  can be described with the  $929\text{ cm}^{-1}$  Si-F and ring C-C stretching vibrations from both *gauche* conformers. The band at  $812\text{ cm}^{-1}$  from the experimental spectra can be described with  $816\text{ cm}^{-1}$  ( ${}^2T_3$

*trans*) and  $814\text{ cm}^{-1}$  ( ${}^2T_3$  *gauche-*) conformers. The broad band with low intensity at  $693\text{ cm}^{-1}$  is described with the combination of the computational band of the ( ${}^2T_3$  *gauche+*) conformer.

#### 4.2.4. Matrix isolation experiment

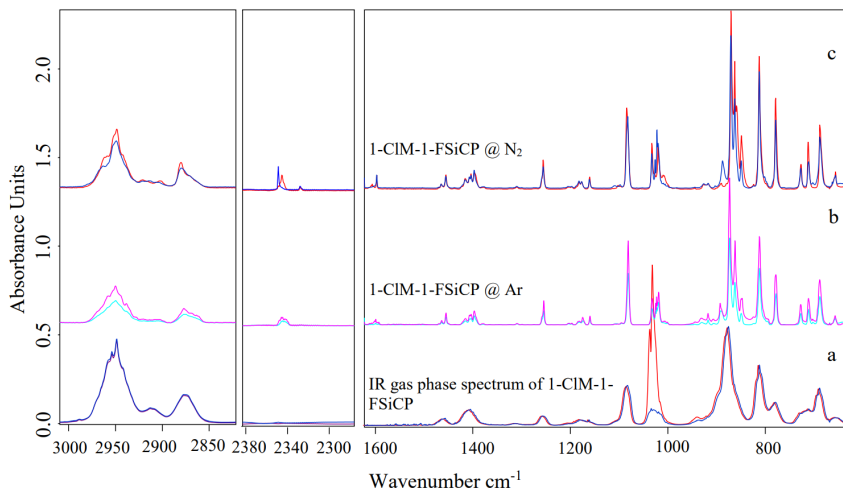


Figure 4.11: (a) FT-IR spectra of 1-ClM-1-FSiCH gas sample: after evaporation (red) and after 1 hr (blue), (b) 1-ClM-1-FSiCH@Ar at 17 K (light blue) and 17 K after annealing to 30 K (pink), (c) 1-ClM-1-FSiCH@N<sub>2</sub> at 17 K (blue) and at 17 K after annealing to 35 K (red). [A2]

The matrix isolation experiments for 1-chloromethyl-1-fluoro-silacyclopentane was done with use of the argon and nitrogen matrix gasses. Samples of the guest-host mixtures were prepared under vacuum conditions. For both method 1:500 ratio of the 1-ClM-1-FSiCH:host gas was prepared in the same volume. The annealing process was done at 30K (Ar) and 35K (N<sub>2</sub>) for 10 minutes. The spectra were collected after annealing process at 17K.

The argon matrix experiment does not give any information on the conformational stability. In the spectrum we can observe only general increase in bands intensities (middle part of Fig. 4.11 spectrum). This can be an effect of the overlapping of the low intensity bands belonging to the *gauche* conformers with very intense bands from the *trans* conformer and we observe only increase of the *trans* conformer population.

In the spectrum obtained from 1-ClM-1-FSiCH@N<sub>2</sub> experiment we can observe more narrow and well separated spectral bands. After annealing many changes can be traced, and the assignment of the bands belonging to particular conformer is possible.

The detailed vibrational assignment of the IR vapor, Raman, 1-CIM-1-FSiCH@Ar and 1-CIM-1-FSiCH@N<sub>2</sub> FT-IR spectra is presented in Table 10 in the APPENDIX I.

In the 3000-2850 cm<sup>-1</sup> region bands related with C-H symmetric and asymmetric stretching, are dominated by the *trans* conformer. Despite the fact that the computational vibrational modes for this conformer have lower intensities than those for *gauche* conformers, their overall amount cause the covering of the bands belonging to the lower energy conformers. This is the reason why we can observe only general increase of the bands intensity after annealing.

In the 1480-1380 cm<sup>-1</sup> spectral range (see Fig. 4.12) there are overlapped bands from both *gauche+* and *gauche-* conformers. Several bands can be explicitly assigned to one of three stable conformers. Band at 1420 cm<sup>-1</sup> can be attributed to the 1453 cm<sup>-1</sup> band of the *gauche+*. Band at 1416 cm<sup>-1</sup>, 1407 cm<sup>-1</sup> and 1404 cm<sup>-1</sup> increases upon annealing and are related to computational bands of the *trans* structure. The 1397 cm<sup>-1</sup> band with decreasing intensity splits to 1397 cm<sup>-1</sup> and 1395 cm<sup>-1</sup> after annealing which can be assigned to *gauche-* and *gauche+* bands, respectively. At lower frequency regions we can observe the overlap of the bands belonging to the *gauche* conformers, so we can not find the characteristic bands for any of them, but the clear decrease of the intensity indicated that their amount after annealing becomes lower.

Additionally, 1084 cm<sup>-1</sup> spectral band increases and is a little shifted to higher frequencies upon annealing. This is a proof of the *gauche* → *trans* inversion. The bands obtained computationally have lower frequencies than those for the *trans* conformer. In this region the *gauche-* structure has only one characteristic band, namely very weak band at 760 cm<sup>-1</sup>, while the *gauche+* explains the existence of the : 801, 784, 702 and 692 cm<sup>-1</sup>. For all above mentioned bands the intensity decrease upon annealing.

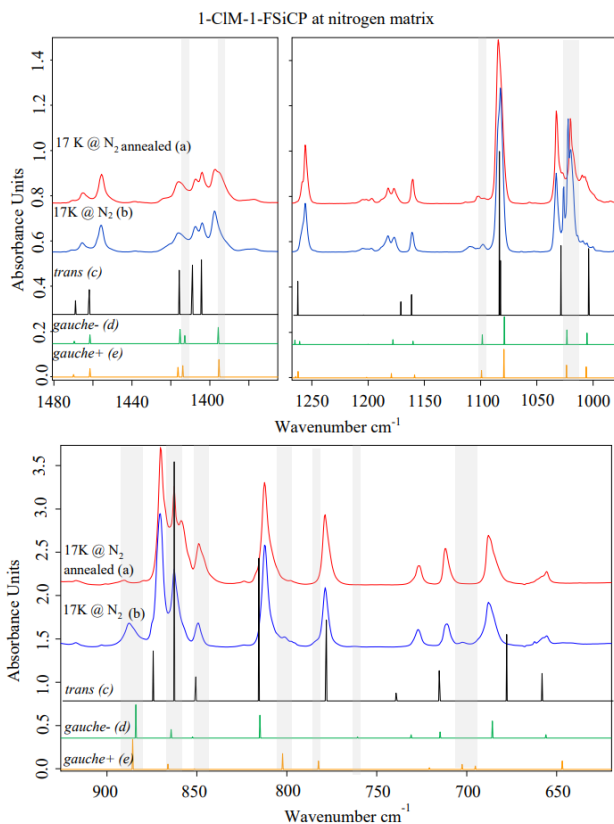


Figure 4.12: FT-IR absorption spectra of  $N_2$  matrix isolated 1-CIM-1-FSiCP: at 17K (b) and at 17K after annealing to 35 K (a), computational spectra (DFT/B3LYP/aug-cc-pVTZ) of twisted *trans* (c), twisted *gauche-* (d) and twisted *gauche+* (e) conformers. The intensities of the theoretical spectra were scaled taking in to account Boltzmann distribution calculated from the DFT relative energy differences. [A1]

#### 4.2.5. Conclusions

As a result of the systematic computational studies of 1-chloromethyl-1-fluoro-silacyclopentane three stable conformers, namely twisted *trans* (global energy minimum), twisted *gauche-* (3.57 kcal/mol MP2, 1.40 kcal/mol DFT) and twisted *gauche+* (4.17 kcal/mol MP2, 1.52 kcal/mol DFT) have been found.

The conformational diversity of these conformers originates from the change of the Cl-C-Si-F dihedral angle. The stability of the *trans* conformer has its origin in the  $5C-Cl \cdots H_{ax}-3C$  (2.779 Å) interaction. The 5C-Cl bond lengths are 1.787 Å (*trans*), 1.783 Å (*gauche-*) and 1.781 Å (*gauche+*), the increase of this bond length proves that in the *trans* conformer, hydrogen bond interactions are stronger.

The ring inversion from  ${}^2T_3$  to  ${}^3T_3$  isoenergetic conformers includes the envelope conformer with unchanged position of the substituents. The potential energy barrier of this process is 4.01 kcal/mol. The potential energy barriers of the *gauche+*/*gauche-* to *trans* rearrangement are 1.30 and 1.23 kcal/mol, respectively. The reverse processes, from *trans* to *gauche+*/*gauche-*, are isoenergetic for both *gauche* positions with energy value of 2.71 kcal/mol.

The matrix isolation experiments proved the existence of twisted *trans* global energy minimum and *gauche+* and *gauche-* local energy minima. Most of the twisted *gauche-*/*gauche+* conformer bands have the same wavenumbers thus overlapping in the experimental spectra but several spectral bands belonging only to *gauche+* or *gauche-* conformers were found in the experimental spectra

## 5. CHAPTER: RESULTS AND DISCUSSION ON SIX MEMBER RING HETEROCYCLES

### 5.1. 1-chloromethyl-1-fluoro-silacyclohexane (1-C1M-1-F-SiCH)

#### 5.1.1. Density Functional Theory and Møller–Plesset based calculations

Originally, the static calculations were performed with use of the DFT/B3LYP/aug-cc-pVDZ and MP2/aug-cc-pVDZ methods [A3], but for easier comparison with other results, all structures were recalculated with the DFT/B3LYP/aug-cc-pVTZ. All structural parameters and energy for the chair conformers are listed in Table 11 in the APPENDIX I. [A5] The results do not cause any qualitative or quantitative differences in the computational results for the 1-chloromethyl-1-fluoro-silacyclohexane conformers. The vibrational analysis was performed with use of the DFT/BLYP/aug-cc-pVDZ method. In this section the axial/equatorial nomenclature refer to the position of the fluorine atom.

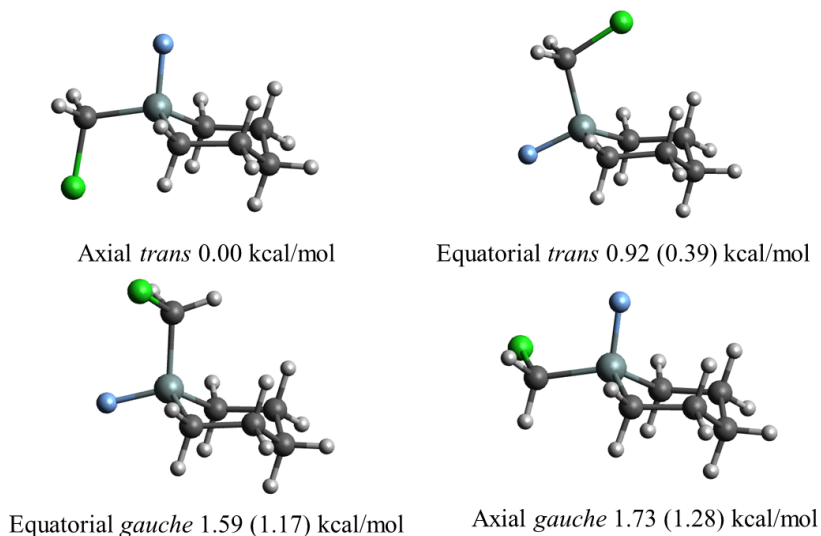


Figure 5.1: Structures of the chair conformers of 1-chloromethyl-1-fluoro-silacyclohexane namely, axial *trans* (top left), equatorial *trans* (top right), equatorial *gauche* (top right) and axial *gauche* (bottom right) with relative energy differences [kcal/mol] obtained from MP2/aug-cc-pVDZ and DFT/B3LYP/aug-cc-pVTZ methods, DFT in parenthesis.

During the conformational analysis the representative boat, skew-boat and chair conformers were taken as the initial geometries. All boat conformers resulted in the chair ring conformation (see Fig. 5.1). The *gauche+* and *gauche-* conformers for the chair structures are degenerated, thus in further analysis we

omit the +/- nomenclature. The optimized skew-boat structures have higher energy (3.50 - 5.32 kcal/mol) and can not be observed under experimental conditions. More about these conformers is elaborated in the "Influence of the heteroatom and substituent change on the conformational stability" section.

All results indicate that the global energy minimum structure is the chair axial *trans* conformer. The differences between the energy values of the respective local minima obtained from the DFT and MP2 method were very similar and the order of structures is the same. The relative energy values for the local energy minima are equal to 0.92 (0.39), 1.59 (1.17) and 1.73 (1.28) kcal/mol for the equatorial *trans*, equatorial *gauche* and axial *gauche*, respectively for MP2(DFT) methods. The *trans* conformers, despite the ring shape, are more stable than *gauche*. It is caused by the presence of the 1/4C-H<sub>ax/eq</sub>...Cl interactions. The fluorine atom form two types of C-H...F interactions, with the hydrogen atoms from ring (3.0, 3.2 Å) and CH<sub>2</sub>Cl group (2.4 Å). The presence of the C-H...F and C-H...Cl interaction influence the C-H bonds lengths. The axial C-H bonds become shorter when the interactions are present about 0.002 Å relative to unbonded one in *gauche* conformers. Such effect is called a blue-shifting or improper hydrogen bonds. [226,227] For the equatorial C-H bonds the shortening is not present, thus C-H...F does not have an impact to conformational stability of the molecules. The presence of the improper hydrogen bonds cause the shift in the spectral band. The equatorial *trans* conformer is stabilized with two different types of C-H...F and four C-H...Cl contacts. The H...F are shorter (2.9, 3.0 Å) than H...F (3.1, 3.7 Å) distances. The equatorial *gauche* conformer is stabilized by the C-H...F bond formation as in the *gauche trans* conformer, but the position of the Cl atom from CH<sub>2</sub>Cl group disable formation of so many C-H...Cl contacts. For the C-H bonds not involved in the C-H...Cl interactions on the one side of the molecule we do not observe any change in lengths. The all non-interactive with Cl atom bonds (2C-H<sub>ax</sub>, 4C-H<sub>ax</sub>) are the same as the nonbonded 3C-H<sub>ax</sub>. In this conformer the only possible contact is 5C-H<sub>eq</sub>...Cl contact. The big energy barrier for the *trans* to *gauche* inversion for the axial conformer cause the significant difference in energy. Despite the fact that the pattern of the C-H...F is the same for both axial conformers, the C-H...Cl contact is only one.

### 5.1.2. Potential energy surface scan

The ring inversion process was traced with the potential energy surface scans. The equatorial *trans* → axial *trans* inversion is presented in Fig. 5.2

During the potential energy surface scans the structures were optimized at every scan step which is the dihedral angle change about 10 deg. The barrier of the equatorial *trans* → axial *trans* inversion is equal to 4.68 kcal/mol. The *gauche* → *trans* inversion was studied for both axial and equatorial conformers. In the middle panel of Fig. 5.2 the axial *gauche* → axial *trans* transition is

presented, and the energy barrier for such a process is equal to 0.95 kcal/mol. The reverse process energy barrier is 2.24 kcal/mol. The energy barrier for the equatorial *trans* → equatorial *gauche* transition is equal to 1.55 kcal/mol, while the reverse process is characterized with 0.76 kcal/mol and more probable to occur.

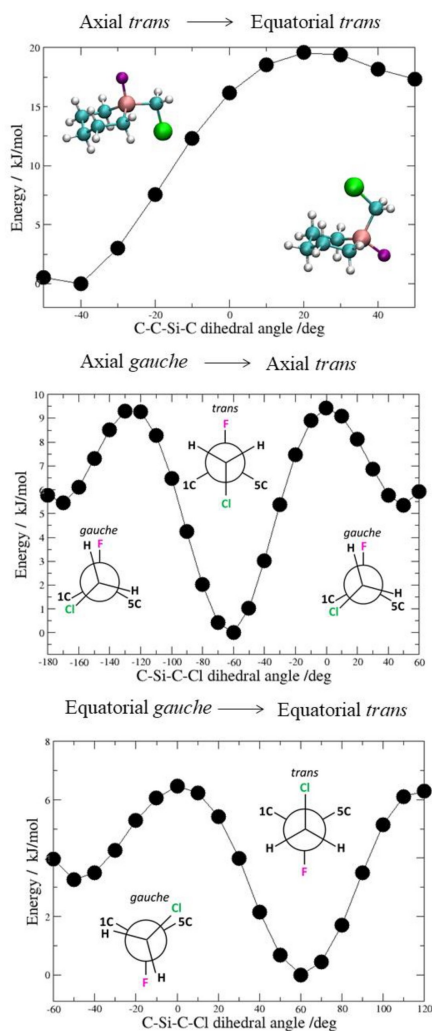


Figure 5.2: Potential energy surface scans, obtained from DFT/B3LYP/ method. Top: axial *trans* → equatorial *trans* inversion, middle: axial *gauche* → axial *trans*, bottom: equatorial *gauche* → equatorial *trans* [A3]



### 5.1.3. FT-IR vibrational analysis of sample in the liquid and gas phase

The liquid sample of the 1-chloromethyl-1-fluoro-silacyclohexane was investigated with the ATR and Raman spectroscopic methods (Fig. 5.3, Table 12 in the APPENDIX I).

As it was expected the number of bands exceed  $3N-6$ , bands are broad and overlapped. This usually is caused by the presence of more than one conformer, interaction of the formed complexes or sample contamination. Despite the fact that the low energy conformers bands should be covered we can find two spectral regions with partially overlapped bands belonging to the specific conformers in  $890\text{ cm}^{-1}$  - and  $750\text{ cm}^{-1}$  frequency range.

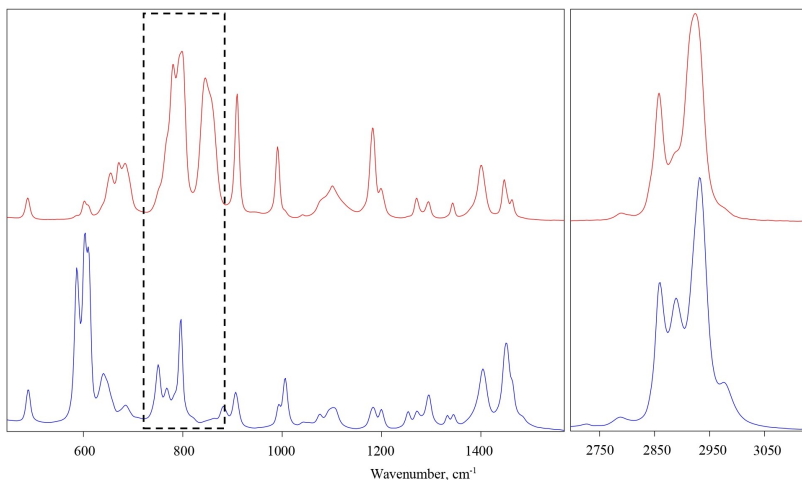


Figure 5.3: ATR FTIR (upper) and Raman (bottom) spectra of the 1-chloromethyl-1-fluoro-silacyclohexane liquid sample

In this spectral region according to the calculations we expect several bands for each conformer, but most of the bands are not enough intense to be observable in the experimental spectrum. The first band (Fig. 5.4) with use of the multiple peak fitting can be described with five bands, namely  $751.3$ ,  $766.4$ ,  $779.6$ ,  $793.5$  and  $801.3\text{ cm}^{-1}$ .

The first band ( $751.3\text{ cm}^{-1}$ ) can be attributed to the  $755.9\text{ cm}^{-1}$  band of the axial *trans* conformer and low intensity band  $747.5\text{ cm}^{-1}$  for the equatorial *trans* conformer. The band at  $766.4\text{ cm}^{-1}$  can be described with  $777\text{ cm}^{-1}$  of the axial *trans* structure. The band at  $779.6\text{ cm}^{-1}$  is assigned to  $783\text{ cm}^{-1}$  equatorial *gauche* conformer mode. Two last fitted bands are described with high intensity bands of three lowest energy conformers band located around  $810\text{ cm}^{-1}$ . The multiple peak fitting predict presence of three bands ( $843$ ,  $855$  and  $863\text{ cm}^{-1}$ ) in region  $880-820\text{ cm}^{-1}$ . There are no characteristic bands that can be assigned to the axial *gauche* conformer. The infrared absorption spectrum

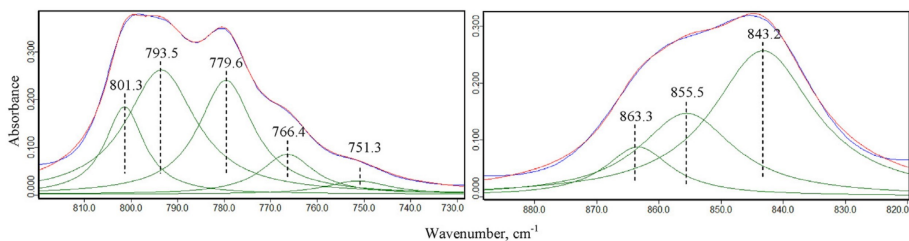


Figure 5.4: The predicted bands in the 750-890  $\text{cm}^{-1}$  region of the ATR FTIR spectrum, (blue - experimental, red - multiple peak fitting).

of the gas phase sample we can prove the existence of three conformers. The presence of the fourth conformer can not be excluded

#### 5.1.4. Matrix isolation experiment

Matrix isolation samples were prepared as described in the Experimental Methods section. The spectra were collected for the 1-chloromethyl-1-fluoro-silacyclohexane (1-C1M-F-CH) embedded in the argon and nitrogen matrices, with concentration ratio 1-C1M-F-CH:matrix gas equal to 1:500. The annealing process was performed at 30K for argon and for 35K for nitrogen matrix.

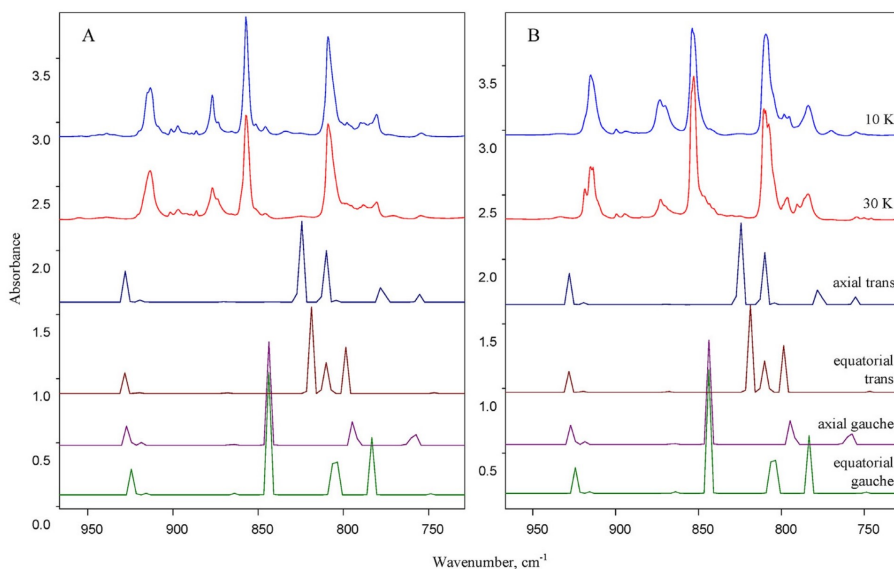


Figure 5.5: FTIR spectra of 1-chloromethyl-1-fluoro-silacyclohexane at argon (A) and nitrogen (B) matrices, in 10 K and after annealing at 30K with computational vibrational bands of chair conformer obtained from DFT/B3LYP/aug-cc-pVDZ method.

All spectroscopic parameters and assignment obtained from matrix isola-

tion experiment and calculations are listed in Table 12 in the APPENDIX I. The nitrogen matrix is more interactive than the argon, this is caused by the quadrupole moment. Two trans conformers of higher energy (axial and equatorial *trans*) have larger dipole moment thus can be better stabilized in the nitrogen matrix. The 750-950  $\text{cm}^{-1}$  regions of the spectra obtained from the matrix isolation experiment are depicted in Fig. 5.5. The spectra collected at 9K should reflect the population of the conformers at room temperature. Basing on the conversion energy barriers values, the only possible changes that can be observed after annealing process is the axial *gauche*  $\rightarrow$  axial *trans* and equatorial *gauche*  $\rightarrow$  equatorial *trans*. The energy barrier of the axial *trans*  $\rightarrow$  equatorial *trans* interconversion is too great to occur during the increase of the temperature. The annealing process should cause the increase of the axial *trans* conformer bands associated with the decrease of the axial *gauche* bands conformer bands. The same pattern should occur for the equatorial *gauche* and equatorial *trans* conformer pair. Therefore, after annealing the sample, an increase in intensity of the bands belonging to the first conformer is expected, along with the decrease in the intensity of the third conformer bands. The increase of the intensity is observed for the 810  $\text{cm}^{-1}$  860  $\text{cm}^{-1}$  bands. The 860  $\text{cm}^{-1}$  band intensity increase is much more significant than for the 810  $\text{cm}^{-1}$  band, thus we can describe them with vibrations belonging to the axial *trans* and equatorial *trans* conformers. Band at 875  $\text{cm}^{-1}$  decrease upon annealing and can be assigned to the axial *gauche* conformer. The 860  $\text{cm}^{-1}$  band intensity increase associated with the 875  $\text{cm}^{-1}$  band intensity decrease is the proof of the axial *gauche*  $\rightarrow$  axial *trans* inversion. In the argon matrix such big changes are not observable, the decrease of the 875  $\text{cm}^{-1}$  band intensity is not significant. Generally the annealing process does not significantly influence the obtained spectra. The slight increase in intensity can be observed for the bands at 780, 810, 860  $\text{cm}^{-1}$  accompanied with slight decrease of the low intensity bands at 800 and 872  $\text{cm}^{-1}$ . This is the proof of the stabilization of the axial and equatorial *trans* conformers in the nitrogen matrices and lowering of the *gauche* to *trans* inversion potential energy barrier.

### 5.1.5. Conclusions

According to the calculations the boat conformers due to the low potential barrier easily transform to the chair structures and the global potential minimum corresponds to the chair axial *trans* conformer. The potential energy barrier for the chair equatorial *trans* - chair axial *trans* transformation was estimated theoretically utilizing relaxed potential energy surface scans and equals to 4.68 kcal/mol. In the liquid and gas phase the presence of three lowest energy conformers, namely axial *trans*, equatorial *trans* and axial *gauche*, have been confirmed.

More detailed analysis of the spectra was possible with use of matrix isolation IR technique combined with annealing and hot nozzle experiments. Argon and nitrogen matrix isolation experiments confirmed the existence of additional axial gauche conformer. The conversion from axial gauche to the more stable axial trans conformer is observable only in the polar N<sub>2</sub> matrix while it is not possible in the more inert Ar matrix.

## 5.2. 1-chloro-1-chloromethyl-silacyclohexane (1-Cl-1-CIM-SiCH)

### 5.2.1. Density Functional Theory and Møller–Plesset based calculations

The 1-chloro-1-chloromethyl-silacyclohexane (1-Cl-1-CIM-SiCH) conformational analysis was performed for the 114 nondegenerate structures concerning the canonical ring shapes (boat, skew-boat, half-chair and chair) and the axial/equatorial and *trans/gauche-/gauche+* position of the substituents with use of the DFT/B3LYP/aug-cc-pVTZ method. Twelve representative local energy minimum conformers were successfully optimized including four chair, eight skew-boat structures.

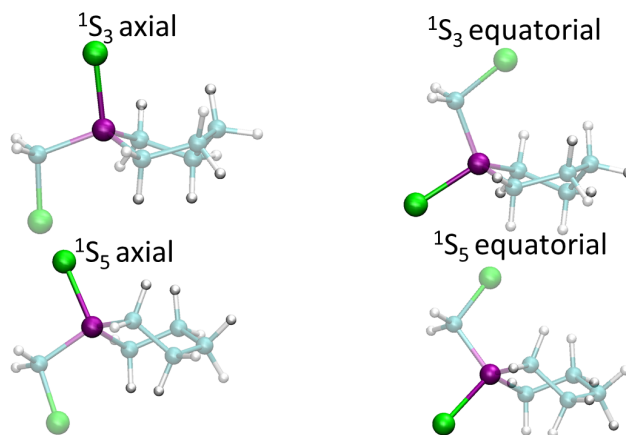


Figure 5.6: 1-chloro-1-chloromethyl-silacyclohexane skew-boat structures in axial/equatorial *trans* conformations derived from DFT B3LYP/aug-cc-pVTZ calculations. [A4]

Among the skew-boat structures, two representative ring shapes were investigated, namely  $^1S_5$  ( $C_2$  symmetry) and  $^1S_3$  ( $C_1$  symmetry) (see Fig. 5.6). In case of the  $^1S_5$  conformers, the axial/equatorial and *gauche-/gauche+* substituents position are degenerated. The energy of the conformers in pairs  $^1S_5$  axial *trans*- $^1S_5$  axial *trans* and  $^1S_5$  axial/equatorial *gauche+*- $^1S_5$  axial/equatorial *gauche+* are energetic with relative energy values equal to 3.92 and 5.36 kcal/mol, respectively. Conformers of with the  $^1S_3$  ring shape vary in energy and are nondegenerate. The relative energy rise in order:  $^1S_3$  axial

*trans* (4.50) <  $^1S_3$  equatorial *trans* (4.81) <  $^1S_3$  axial *gauche-* (6.20) <  $^1S_3$  axial *gauche-* (6.24) <  $^1S_3$  equatorial *gauche-* (6.28) <  $^1S_3$  equatorial *gauche+* (6.34 kcal/mol). The energy differences indicated that the skew-boat conformers can not be found in the matrix isolation experimental spectrum.

The most stable structure of the 1-Cl-1ClM-SiCH molecule is the chair  $^{Si}C_3$  axial *trans*, with the  $^{Si}C_3$  equatorial *trans*,  $^{Si}C_3$  equatorial *trans* and  $^{Si}C_3$  equatorial *gauche* (see Fig. 5.7) as the local energy minima. The *gauche-* and *gauche+* positions of the Cl-C-Si-Cl dihedral angle are degenerated, thus not further investigate.

The energies of all chair conformers and its structural parameters derived from the MP2/aug-cc-pVTZ and DFT/B3LYP/aug-cc-pVTZ method are listed in Table 13 in the APPENDIX I. The relative energy rise in order:  $^{Si}C_3$  axial *trans* <  $^{Si}C_3$  equatorial *trans* (1.04 MP2 0.88 DFT) <  $^{Si}C_3$  axial *gauche* (1.39 MP2, 1.53 DFT) <  $^{Si}C_3$  equatorial *gauche* (1.65 MP2, 1.77 DFT kcal/mol). The vibrational frequency assignment was done with use of the VMARD analysis procedure.

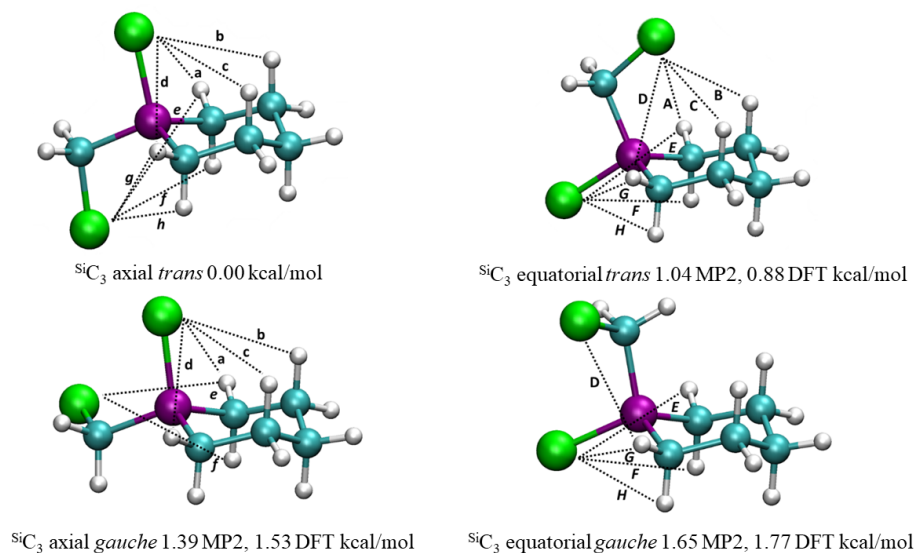


Figure 5.7: Non-degenerate chair conformers of the 1-chloro-1-chloromethyl-silacyclohexane in axial/equatorial, *trans*/*gauche* conformation, additionally marked Si-Cl $\cdots$ H-C and CH<sub>2</sub>-Cl $\cdots$ H-Cl hydrogen bonds. Obtained from MP2/aug-cc-pVTZ and DFT B3LYP/aug-cc-pVTZ method. [A4]

In the  $^{Si}C_3$  axial *trans* structure there are eight hydrogen bond like contacts, including four of Si-Cl $\cdots$ H-C and four of CH<sub>2</sub>-Cl $\cdots$ H-C type, the hydrogen bonding pattern for the  $^{Si}C_3$  axial *trans* is very similar (see Fig. 5.7). The different stability of mentioned conformers may be explained in terms of the C-H $\cdots$ Cl contacts strength (H $\cdots$ Cl atom distances) between the silicon atom

and equatorial hydrogen atoms from the silicon neighboring carbon (1C, 5C) atoms. The analogous H $\cdots$ Cl distances are 3.305 (3.312) (a, d) 3.305 (3.312) (d) for  $^{Si}C_3$  axial *trans* conformer and 3.717 (3.754) (A) and 3.717 (3.741) (D) [ $\text{\AA}$ ] for the  $^{Si}C_3$  axial *trans* structure. The decrease of the H $\cdots$ Cl distance is associate with the C-H $\cdots$ Cl interaction strength increase.

In the symmetric  $^{Si}C_3$  axial/equatorial *trans* conformers the C-H bonds have the same lengths in pairs 1C-H $_{ax/eq}$  - 5C-H $_{ax/eq}$  and 2C-H $_{ax/eq}$  /4C-H $_{ax/eq}$  (see Table 14 in the APPENDIX I). The C-H $\cdots$ Cl influences the 1/5C-H $_{eq}$  bonds lengths, for the equatorial *trans* become longer about 0.001  $\text{\AA}$ , what should cause the related vibrational frequencies shift to the lower frequencies in the computational spectrum. The 2/4C-H $_{ax}$  bond lengths are smaller by about 0.002  $\text{\AA}$  in the equatorial *trans* structure this should be followed with the vibrational frequencies shift to the higher frequency region. The decrease in the C-H bonds lengths as a result of hydrogen bonds contacts is clearly visible for the 2C-H $_{ax}$  and 4C-H $_{ax}$ , mentioned hydrogen atoms can form 2/4C-H $_{ax}\cdots$ Cl-Si contacts (b, c at Figure 5.7 and Table 14 in the APPENDIX I) which are stronger (shorter) in case of the  $^{Si}C_3$  axial *trans* structure.

In the  $^{Si}C_3$  axial *gauche* conformer, with the rotation of the CH $_2$ Cl group, the number of possible hydrogen bonds contacts is smaller and equal to six (two CH $_2$ -Cl $\cdots$ H-C (e, f) type and four of Si-Cl $\cdots$ H-C types).

$^{Si}C_3$  equatorial *gauche* only the number of possible hydrogen bonds contact is again reduced, and equal to 5. Only one CH $_2$ -Cl $\cdots$ H-C interaction is possible, namely the CH $_2$ -Cl $\cdots$ H $_{eq}$ -C (g) and cause increase of the 5C-Heq bond. While comparing its length to the analogous one from the  $^{Si}C_3$  equatorial *trans* conformer we can see that the difference is significant and equal to 0.651  $\text{\AA}$  for MP2 and 0.632  $\text{\AA}$  DFT calculations.

Calculated energy differences for the chair conformers were used to deliver the populations of each conformer in the sample. The amounts of conformers is as follow: axial *trans* - 79%, equatorial *trans* - 13%, axial *gauche* - 5% and equatorial *gauche* - 3%. While the degeneracy, based on the symmetry is taken into account for the Boltzmann population distribution is 73:12:9:6. While the computational spectra are taken into account we need to keep in mind the population of each conformer, which influence the bands intensity. The conformers with lower energy are most populated thus theirs intensity will be highest. The higher energy conformers has lower population in the sample, thus their intensity is smaller and are present in spectrum present near the strong bands of the most stable conformer in the matrix isolation experiment spectra.

### 5.2.2. Potential energy surface scan

During the potential energy surface scans calculation the Si-C1-C2-C3, C2-C3-C4-C5 and Cl-C-Si-C1 (see Fig. 5.8 and 5.9) dihedral angles change was traced.

The ring inversion and transition state structures were investigated. The geometry optimization was done at every scan step (every 10 degree dihedral angle change).

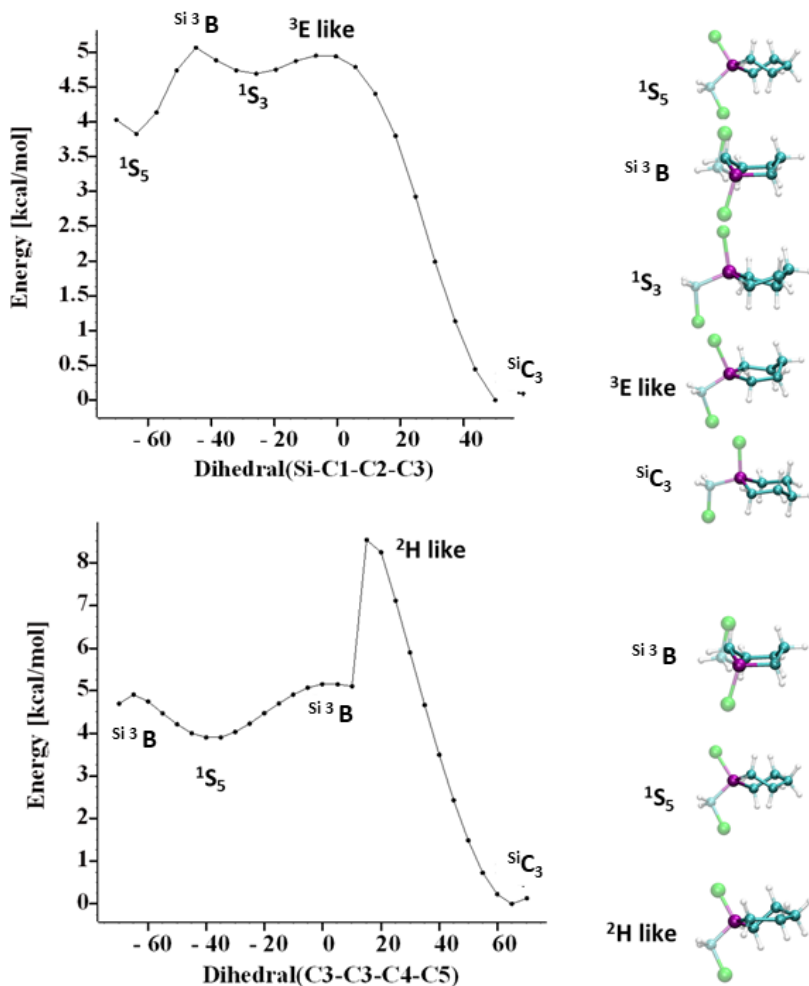


Figure 5.8: The potential energy relaxed surface scans the Si-C1-C2-C3 and C2-C3-C4-C5 dihedral angles change, derived from DFT/B3LYP/aug-cc-pVTZ method. The relative energy values are calculated for the lowest energy conformer for given scan,  $Si^3 C_3$  axial *trans* (top panel) and  $Si^3 C_3$  equatorial *trans* (bottom panel).[A4]

The  $Si^3 C_3 \rightarrow ^4 C_1$  inversion pathway is as follow: chair ( $Si^3 C_3$ )  $\rightarrow$  half-chair (TS)  $\rightarrow$  skew-boat ( $1S_3$  -  $C_1$  symmetry)  $\rightarrow$  boat (TS)  $\rightarrow$  skew-boat ( $1S_5$  -  $C_2$  symmetry). With the chair and skew-boat structures as the local energy minima and the half-chair and boat transition states (TS). The energy barriers for the  $Si^3 C_3 \rightarrow 1S_3$  transition and reverse process equals to 4.94 and 0.26 kcal/mol,

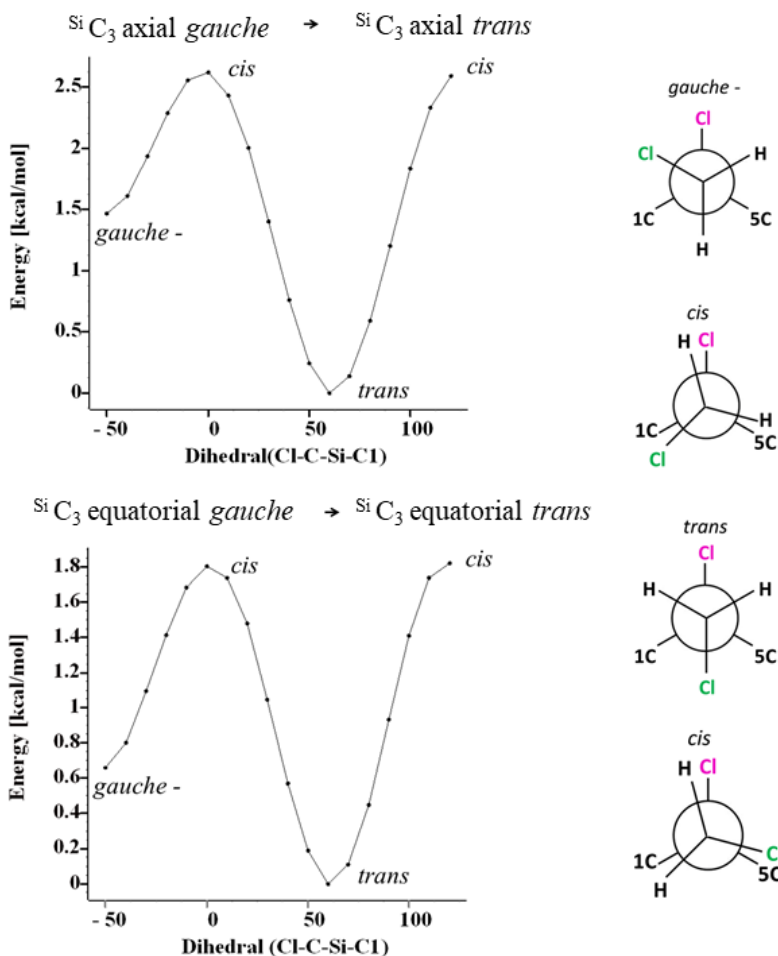


Figure 5.9: The potential energy relaxed surface scans for Cl-C-Si-C1 dihedral angle rotation for the axial (top) and equatorial (bottom) conformer DFT/B3LYP/aug-cc-pVTZ method. The relative energy values are calculated for the lowest energy conformer for given scan,  $^{Si}C_3$  axial *trans* (top panel) and  $^{Si}C_3$  equatorial *trans* (bottom panel).[A4]

respectively. The energy barrier for the  $^1S_3 \rightarrow ^1S_5$  interconversion via  $^1B_4$  transition state is equal to 0.37 kcal/mol, while for the  $^1S_5 \rightarrow ^1S_3$  is calculated to be 1.24 kcal/mol.

The Cl-C-Si-C1 dihedral angle rotation energetic values differs for the axial and equatorial. For the  $^{Si}C_3$  axial *gauche*  $\rightarrow$   $^{Si}C_3$  axial *trans* and reverse processes the potential energy barriers are equal to 1.15 and 2.62 kcal/mol, respectively. The  $^{Si}C_3$  equatorial *gauche*  $\rightarrow$   $^{Si}C_3$  equatorial *trans* transition is characterized by the energy value of 1.04 kcal/mol, while the reverse process is 1.86 kcal/mol.



Despite the energy difference the more probable rearrangement is from *gauche* to *trans* conformer for both axial and equatorial structures.

### 5.2.3. FT-IR vibrational analysis of sample in the liquid and gas phase

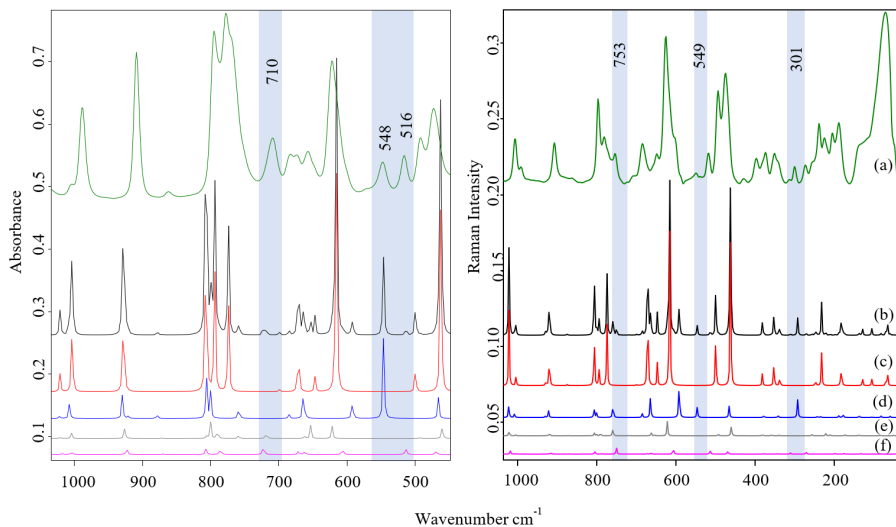


Figure 5.10: a) ATR (left) and Raman (right) experimental spectra of 1-Cl-1-ClMSiCH, calculated spectra (DFT/B3LYP/aug-cc-pVTZ) of b) all conformers, c) axial *trans*, d) equatorial *trans*, e) axial *gauche*, f) equatorial *gauche*. The calculated intensities of the spectral bands are scaled according to the expected abundance of the conformers at room temperature. Marker bands for different conformers are highlighted in gray color. [A4]

The FTIR ATR spectrum of the 1-Cl-1-ClMSiCH in the liquid phase along with the computational vibrational frequencies for chair conformers is presented in the left panel of Fig. 5.10.

Despite the fact that most of the bands in the ATR spectrum are broad and overlapped, several of them can be attributed to one or more conformers. Bands at 989 and 905  $\text{cm}^{-1}$  can be assigned to the ( $^{Si}C_3$ ) axial *trans* conformer (C-C bonds and rocking  $\text{CH}_2$  vibrations). The shoulder band at 791  $\text{cm}^{-1}$  and right slope of the 777  $\text{cm}^{-1}$  band can be attributed to the equatorial *trans* and axial *gauche* conformers. The 710  $\text{cm}^{-1}$  band is a marker for the axial *gauche* conformer (respective calculated band 719  $\text{cm}^{-1}$ ). The 658  $\text{cm}^{-1}$  spectral band as well can be assigned to 2 conformers - axial *gauche* with computed band at 654  $\text{cm}^{-1}$  and axial *trans* band at 647  $\text{cm}^{-1}$ , both assigned to stretching vibration of Si-C bond and ring deformation vibrations. Band 623  $\text{cm}^{-1}$  which is described with stretching vibrations of the Si-Cl and Si-C bonds from axial *trans* global energy minimum structure with computed spectral vibration at 616  $\text{cm}^{-1}$ ). Bands calculated at 592 and 547 and 616  $\text{cm}^{-1}$  for the  $^{Si}C_3$  equatorial

*trans* (rocking vibrations of the CH<sub>2</sub>Cl group, and Si-C stretching vibration of the Si-CH<sub>2</sub>Cl group) are associated with the 623 and 548 cm<sup>-1</sup> bands from experimental spectrum. The bands at 493 and cm<sup>-1</sup> are markers for the <sup>S<sub>i</sub></sup>C<sub>3</sub> equatorial *trans* conformers (the Si-Cl and Si-C stretching and ring deformation vibrations).

#### 5.2.4. Matrix isolation experiment

The matrix isolation experiment was performed to investigate unresolved regions, where we observe the bands overlap in the ATR spectrum. The spectral region of range 900-500 cm<sup>-1</sup> obtained for 1-Cl-1-CIMSiCH at neon and nitrogen matrices is depicted in Fig. 5.11.

Between 800 and 750 cm<sup>-1</sup> computational analysis indicates presence of three spectral bands for each chair conformer. The experimentally obtained bands at 804, 786 and 772 cm<sup>-1</sup> for both nitrogen and neon matrix environments can be described with 801 (equatorial *trans*), 801, 790 (axial *gauche*, 786 cm<sup>-1</sup> (equatorial *gauche*) computationally obtained vibrational modes (Si-C stretching and rocking vibrations of the ring CH<sub>2</sub> and CH<sub>2</sub>Cl groups). The band at 778 cm<sup>-1</sup> in nitrogen and 780 cm<sup>-1</sup> in neon matrix can be explained with the equatorial *gauche* conformer band at 786 cm<sup>-1</sup>, assigned to stretching vibrations of Si-C and C-C bonds. The experimentally obtained bands at 772 is associated to the axial *trans* conformer, while its shoulder band at 775 cm<sup>-1</sup> is caused by the matrix effect. The 765 cm<sup>-1</sup> band is a combination of the bands belonging to the equatorial *trans* and axial *gauche* conformers (759 cm<sup>-1</sup>). The band at 754 cm<sup>-1</sup> is a marker for the equatorial *gauche* conformer with calculated vibrational frequency at 750 cm<sup>-1</sup>. In 700-500 cm<sup>-1</sup> spectral region we can observe red-shifted spectral bands in comparison to those obtained from ATR experiment and theoretically. All bands are shifted about similar amount approximately 20 cm<sup>-1</sup>. The shift can be caused by the matrix influence on the vibrational bands which results from the motions of the heavy chlorine atom.

The bands at 690, 660 and 632 cm<sup>-1</sup> are associated to the 672 and 647 cm<sup>-1</sup> axial *trans* bands (stretching of Si-C bond and ring deformation modes). The same conformer has its marker band at the 632 cm<sup>-1</sup> with the calculated value at 616 cm<sup>-1</sup> (stretching of Si-Cl bond and ring deformation modes). For the equatorial *trans* conformer we can observe band at 684 cm<sup>-1</sup> (calculated band at 665 cm<sup>-1</sup> - ring deformation and stretching Si-C vibrations), 608 cm<sup>-1</sup> at neon and nitrogen (592 cm<sup>-1</sup> - stretching Si-Cl and Si-C, and ring deformation vibrations) and at 557 cm<sup>-1</sup> in the nitrogen and 532 cm<sup>-1</sup> for neon matrix (547 cm<sup>-1</sup> - stretching Si-Cl and Si-C, and ring deformation vibrations). The band at 674 cm<sup>-1</sup> in nitrogen matrix is shifted to 677 cm<sup>-1</sup> in neon environment and is assigned to the axial *gauche* 654 cm<sup>-1</sup> band (Si-C stretch and to ring deformation modes). The equatorial *gauche* conformer band at 607 cm<sup>-1</sup>

(attributed to Si-Cl stretch and rocking vibrations of ring CH<sub>2</sub> and CH<sub>2</sub>Cl groups) describes the presence of the 616 cm<sup>-1</sup> band in the nitrogen matrix (618 cm<sup>-1</sup> in the neon matrix) spectrum. The spectral marker bands characteristic for each conformer were integrated to calculate the conformers population distribution in the experimental sample and to compare the values with the computational results. For the <sup>Si</sup>C<sub>3</sub> axial *trans*, <sup>Si</sup>C<sub>3</sub> equatorial *trans*, <sup>Si</sup>C<sub>3</sub> equatorial *trans* and <sup>Si</sup>C<sub>3</sub> equatorial *gauche* structures were chosen bands at 632, 608, 674, 616 cm<sup>-1</sup>, respectively.

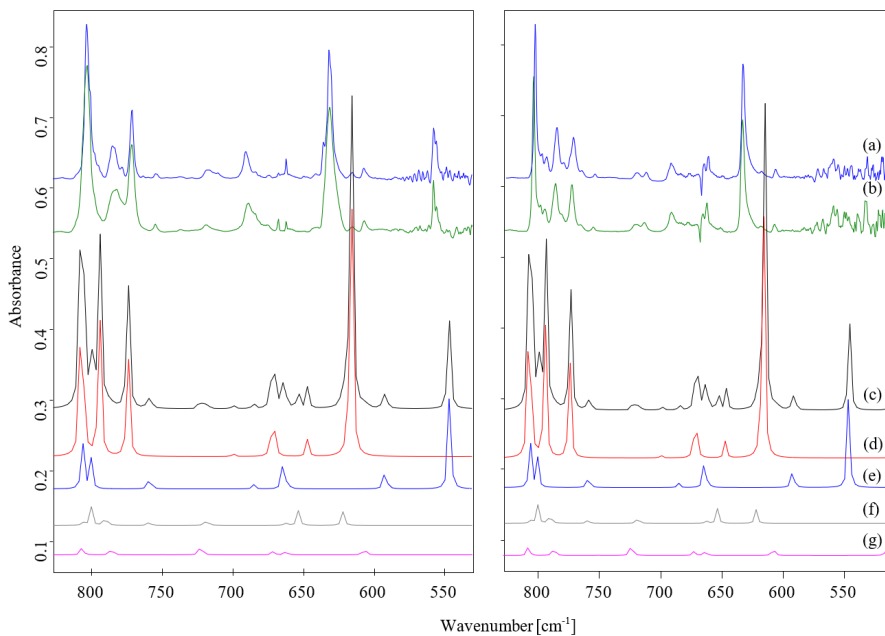


Figure 5.11: FTIR absorption spectra of 1-Cl-1-CIMSiCH isolated in neon at 3 K (left panel) and nitrogen (right panel) at 17 K, (b) after annealing at 9 K for neon and 35 K for nitrogen; and calculated spectra (DFT/B3LYP/aug-cc-pVTZ) of (c) all conformers, (d) axial *trans*, (e) equatorial *trans*, (f) axial *gauche*, (g) equatorial *gauche*. The calculated intensities of the spectral bands are scaled according to the expected abundance of the conformers at room temperature. [A4]

The integral intensity ratios comparison indicate that the concentration of the conformers in nitrogen (neon) matrix 81.3% (82%) , 12.2% (11%), 2.6% (5%), 3.9 % (2%) for conformer in increasing energy value order. Such a population distribution is with a good agreement with computationally obtained values, despite the axial *trans* structure is more populated than theoretically predicted. The annealing experiment was performed to investigate the conformational stability and check if the conformational rearrangements are present. The transitions with low energy barriers should occur during the annealing pro-

cess and conformer equilibrium should be changed. Nitrogen matrix in comparison with the neon has higher quadrupole moment, thus should stabilize the *gauche* conformers due to the bigger values of the dipole moment.

The annealing temperature for neon and argon matrices were 9K and 35K, respectively, the annealing time was 15 minutes. The band at  $786\text{ cm}^{-1}$  after annealing process is shifted to the lower wave numbers in nitrogen matrix, this is explained with the matrix effect, because is not present in the neon matrix. The spectral band at  $778\text{ cm}^{-1}$  which was assigned to the equatorial *gauche* does not loss its intensity, but due to the band broadening and overlap is poorly defined. The band related to the axial *gauche* conformer at  $710\text{ cm}^{-1}$ , almost disappear upon annealing, while the equatorial *gauche*  $718\text{ cm}^{-1}$  band intensity slightly decrease. The axial *trans* conformer related band at  $691\text{ cm}^{-1}$  become broader while for the  $685\text{ cm}^{-1}$  of equatorial *trans* conformer the raise in intensity is observable. For the  $616\text{ cm}^{-1}$  band associated with the equatorial *gauche* we observe the slight decrease.

In the neon matrix the majority of the *gauche* conformers related bands slightly decrease due to the *gauche*  $\rightarrow$  *trans* rearrangements. The shift of the  $760\text{ cm}^{-1}$  equatorial *gauche* band is accompanied with overlap with the axial *trans* band, but in contrary to the nitrogen matrix results we can observe the decrease in intensity. The bands related to the equatorial *trans* conformer become more broad and more intense in the neon matrix upon annealing. The axial *gauche* conformer band at  $620\text{ cm}^{-1}$  exhibits decrease after the annealing. The annealing process in both neon and nitrogen matrices prove the existence of the *gauche* to *trans* inversion.

### 5.2.5. Conclusions

Through the combination of experimental and theoretical results, it has been determined that 1-chloro-1-chloromethyl-silacyclohexane exists as a mixture of at least four conformers:  $^S i C_3$  axial *trans* (MP2/aug-cc-pVTZ 0, DFT/BLYP/aug-cc-pVTZ 0 kcal/mol),  $^S i C_3$  equatorial *trans* (1.04, 0.88 kcal/mol),  $^S i C_3$  axial *gauche* (1.39, 1.53 kcal/mol), and  $^S i C_3$  equatorial *gauche* (1.65, 1.77 kcal/mol). The conformers with the Cl atom in the *trans* position are more stable with lower energy due to the formation of intramolecular hydrogen bonds. The derived conformational path is consistent with previous reports for similar molecules, namely chair  $\rightarrow$  envelope/half-chair like (TS)  $\rightarrow$  skew-boat  $C_1 \rightarrow$  boat (TS)  $\rightarrow$  skew-boat  $C_2$ . The energy barrier between the  $^S i C_3$  and  $^1 S_3$  conformers is 4.94 kcal/mol and goes through a similar transition state to the envelope structure, while the reverse process ( $^1 S_3$  to  $^S i C_3$ ) barrier is only 0.26 kcal/mol.

Experiments using FTIR-ATR and Raman spectroscopy have shown the existence of higher energy conformers. FTIR spectra of the compound isolated in low-temperature neon and nitrogen matrices confirmed the presence

of four conformers in room-temperature samples. The axial trans conformer is the most stable and abundant in the experimental samples, but the other three conformers - equatorial trans, axial gauche, and equatorial gauche - can also be observed. Annealing experiments in both neon and nitrogen matrices demonstrated that only gauche to trans conformer interconversion is possible in those environments.

### 5.3. Car-Parrinello molecular dynamics of the 1-Cl-1-CIM-SiCH and 1-CIM-1-F-SiCH molecules

Static calculations refer to properties of molecules at the temperature of 0 K. Our experimental matrix isolation conditions are strictly related to the temperature changes, especially when the annealing procedure is applied. Therefore additional theoretical investigations have been performed, i.e. Car-Parrinello molecular dynamics (CP-MD) simulations. This technique enables simulations of systems of the size of hundreds of atoms at finite temperature and description of the atomic forces on the density functional theory level.

Car-Parrinello molecular dynamics simulations were done for 1-chloro-1-chloromethyl-silacyclohexane and 1-chloromethyl-1-fluoro-silacyclohexane molecules embedded in the nitrogen matrix. Simulations were performed at 20, 50 and 70 K temperatures utilizing periodic boundary conditions. The performed matrix isolation experiment refers to temperature range of 9-20K, thus for CP-MD calculations the temperature equal to 20K was chosen, to mimic the annealing temperature from the experiment. The supercell model consists of one 1-chloro-1-chloromethyl-silacyclohexane or 1-chloromethyl-1-fluoro-silacyclohexane molecule placed between nitrogen molecules in the cubic  $\alpha$ -phase. The molecule position was adjusted that its geometrical center fits the geometrical center of  $N_2$  molecule removed from the supercell. Supercell was optimized and then used as a starting point for further CP-MD simulations. The size of the supercell was chosen to prohibit any interactions between molecules (solute) and their images.

Figure 5.12 shows the time evolution of the Si-1C-2C-3C dihedral angle (this dihedral angle was chosen also for the PES scan calculations) of 1-chloromethyl-1-fluoro-silacyclohexane (1-CIM-1-F-SCH) and 1-chloro-1-chloromethyl-silacyclohexane (1-Cl-1-CIM-SCH) molecules. Si-1C-2C-3C dihedral angle values for the 1-CIM-1-F-SCH and 1-Cl-1-CIM-SCH molecules are equal to 54 and 53 degrees, respectively. Depending on the temperature, the dihedral angle deflection changes, the lower temperature the deflection decreases and revers.

For 1-Cl-1-CIM-SiCH molecule minimum and maximum values of respective dihedral angle are: 45 and 60 (20 K), 41 and 63 (50 K), 39 and 65 (70 K) degrees. Therefore, different amplitudes with respect to the temperature changes have

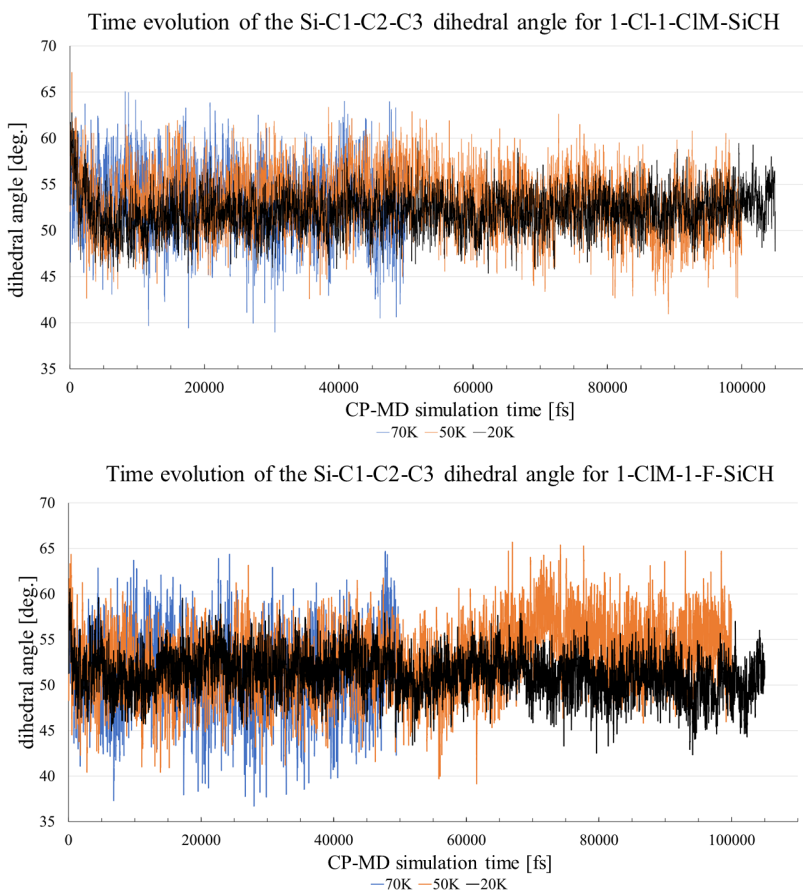


Figure 5.12: Time evolution of the Si-C1-C2-C3 dihedral angle of the 1-Cl-1-CIM-SiCH and 1-CIM-1-F-SiCH molecules at N<sub>2</sub> matrix derived from the Car-Parrinello molecular dynamics simulations at 20, 50, 70 K.

been obtained: 14 (20 K), 22 (50K) and 26 deg (70K). Static calculations refer to structure of the molecule in equilibrium where the bond lengths, valence and dihedral angle values are precisely defined. CP-MD simulations provide time-evolution of internal coordinates, therefore the averaged values of each structural parameter must be additionally calculated. In the 1-Cl-1-CIM-SiCH molecule Si-1C-2C-3C dihedral angles oscillate around averaged values of 52 deg (20 K) and 53 deg (50, 70K).

For 1-CIM-1-F-SiCH molecule increase of the dihedral angle has been observed in the middle part of the production run for the simulation at 50 K. At the beginning of the CP-MD simulation the Si-1C-2C-3C dihedral angle oscillates around 52 deg but then we observe an increase up to 55 deg of the equilibrium value. Analysis of the time evolution of this dihedral angle at 50 K

shows that one can not average all values and the simulation must be divided into two regions with different equilibrium values. For simulations at 20 K and 70 K the minimum, maximum and deflection range of the Si-1C-2C-3C dihedral angle are equal to 42, 60, 17 deg and 37, 65, 28 deg, respectively. For the simulation at 50 K the values equal to 39, 64, 25 deg (for the oscillation around 52 deg) and 45, 65, 20 deg (for the oscillation around 55 deg).

Generally, the higher the temperature the probability of the ring inversion increases for both molecules. The energy barriers for mentioned dihedral angle fluctuations do not exceed the chair  $\rightarrow$  skew-boat interconversion energy barriers which denote 4.94 and 4.68 kcal/mol for the 1-Cl-1-ClM-SiCH and 1-ClM-1-F-SiCH, respectively. Thus, the ring interconversion from chair to skew-boat structure can not occur in the nitrogen matrix environment.

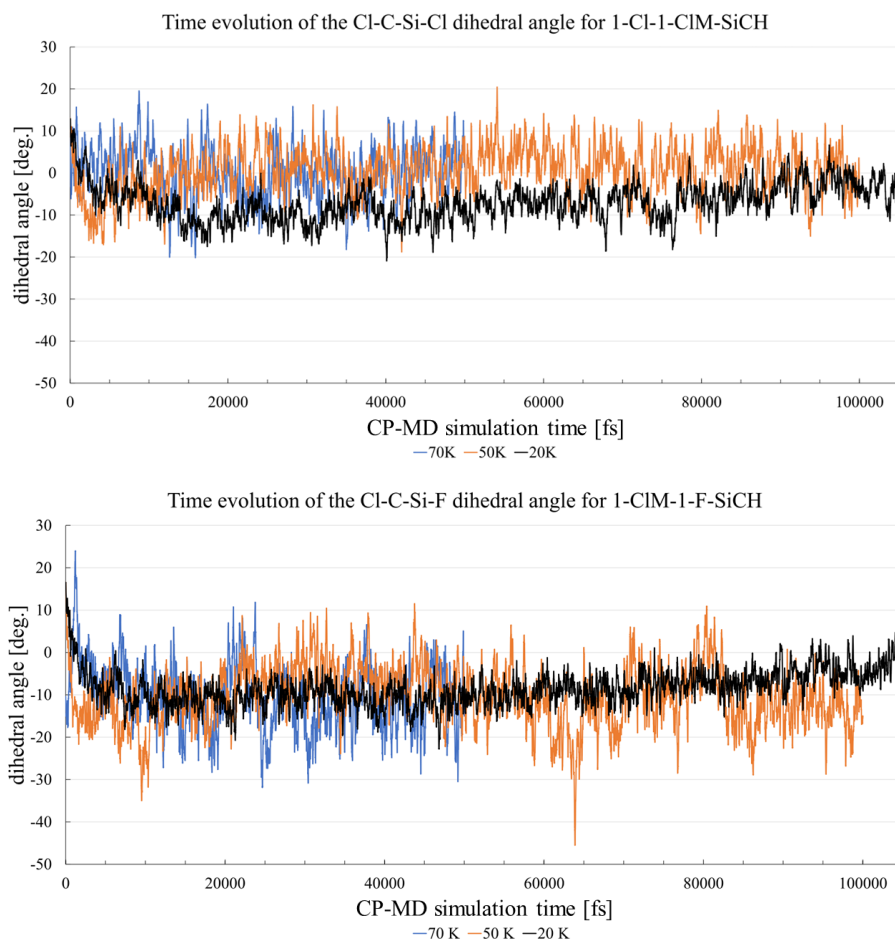


Figure 5.13: Time evolution of the Cl-C-Si-Cl and Cl-C-Si-F dihedral angles of the 1-Cl-1-ClM-SiCH and 1-ClM-1-F-SiCH molecules at N<sub>2</sub> matrix derived from the Car-Parrinello molecular dynamics simulations at 20, 50, 70 K.

The Cl-C-Si-F and Cl-C-Si-Cl dihedral angle time evolution (see Fig. 5.13) The averaged value of this dihedral angle differs slightly with respect to the temperature. Even though the Cl-C-Si-F/Cl dihedral angle oscillates with the amplitude of  $\pm 20$  deg it is an evidence this dihedral angle is planar. Exchange of substituent from -Cl to -F causes the decrease of the fluctuations of the dihedral angle averaged value. Within the analyzed time range the conformation of the molecule does not change, however at the time of the 64 ps a rapid decrease of the dihedral angle down to 135 deg has been observed. From one hand this fluctuation does end up in the conformational change but on the other hand it suggests a possibility of the CH<sub>2</sub>Cl group rotation.

So far we have investigated the time evolution of internal coordinates of the studied molecules, what generates information about the behavior of the system in the real time. Time evolution of the system however does not provide information about statistics and probability of structural properties. One of the ways to analyze the probability of events and distribution of different properties is a calculation of radial distribution functions (RDF). This function refers to the probability of occurrence of atom/particle at a specified distance from the reference atom/particle. In the case of a set of molecules studied the atom's choice is correlated to the existence of potential hydrogen bond donors and acceptors.

The influence of nitrogen matrix on structural properties of embedded molecule can be qualitatively and quantitatively measured by calculating RDF function based on R(N $\cdots$ H) distances. In such a way we take into account a possible formation of weak C-H $\cdots$ N intermolecular hydrogen bonds, where N atom from N<sub>2</sub> molecules serves as a proton acceptor. Nitrogen matrix consists of periodically arranged molecules as it is in N<sub>2</sub> crystalline  $\alpha$  phase and therefore has to adapt to embedded guest molecule. Calculation of  $g(R_{NH})$  radial distribution function for simulations at different temperatures enables to study the pattern of intermolecular interactions and temperature impact on matrix structure.

Figure 5.14 shows radial pair distribution function  $g(R_{NH})$  of the N $\cdots$ H distances calculated for 1-chloro-1-chloromethyl-silacyclohexane and 1-chloromethyl-1-fluoro-silacyclohexane molecules at different temperatures (20, 50, 70 K). The most important features of the plot for 1-Cl-1-ClM-SiCH molecule (upper panel of Fig. 5.14) are peaks located at the range of 3 Å. The peak marked with a blue color correspond to the nitrogen matrix at low temperature, namely 20 K and has the highest  $g(R)$  function value. This peak is shifted to the lower values of a N $\cdots$ H distance with respect to the positions of other peaks obtained for the CP-MD simulations for 50, 70 K temperatures. The increase of the temperature of the matrix causes the change of the shape of the peak, i.e. broadening. Apart from the analysis of the RDF function we can trace these structural changes by visualization of the trajectory obtained



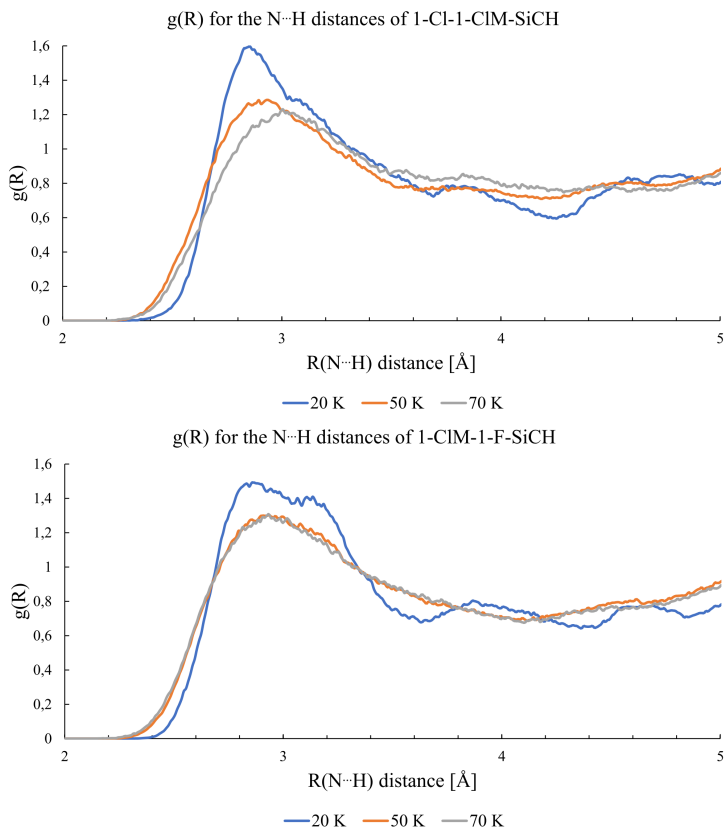


Figure 5.14: Radial pair distribution function  $g(R_{NH})$  of the  $N\cdots H$  distances for 1-chloro-1-chloromethyl-silacyclohexane and 1-chloromethyl-1-fluoro-silacyclohexane molecules from CP-MD simulations at  $N_2$  matrix, for 20, 50, 70 K.

from production run. CP-MD simulations give a direct possibility of the observation of formation/breaking of weak  $C-H\cdots N$  hydrogen bonds. In the case of 1-CIM-1-F-SiCH molecule (bottom panel of Fig. 5.14) a shift of the respective peaks is also observed. The present changes are not as pronounced as in the 1-Cl-1-CIM-SiCH molecule, what can be explained by the difference in atomic radius of fluorine with respect to the chlorine atom. It is worth to note that the subpeak at 20K was observed which can be assigned to different type of interactions with respect to the  $N_2$  position in crystalline  $\alpha$  phase.

## 5.4. 1-methyl-germacyclohexane

The literature data on the 1-methyl-germacyclohexane (1M-GeCH) molecule does not deliver vibrational spectroscopy data, thus the ATR, Raman and FT-IR at neon and nitrogen matrix spectroscopic studies deliver the detailed vibrational analysis for the first time.

### 5.4.1. Density Functional Theory and Møller–Plesset based calculations

The conformational landscape of the 1-methyl-1-germacyclohexane originates from the 38 canonical structures but the axial/equatorial positions of substituents enlarge this number. The DFT/B3LYP/aug-cc-pVTZ static calculations were done for 74 initial structures, including boat, chair, envelope, half-chair and skew-boat ring shape. The results indicate the presence of six local energy minima: two chair ( ${}^{Ge}C_3$  axial/equatorial), four skew-boats ( ${}^1S_5$  axial/equatorial and  ${}^1S_3$  axial/equatorial). All initial boat, envelope and half-chair structures resulted in the chair or skew-boat ring shapes. Due to the degeneracy representative skew boat structures were chosen:  ${}^1S_5={}^5S_1={}^2S_4={}^4S_2$  ( $C_2$  symmetry) and  ${}^1S_3={}^3S_1={}^{Ge}S_2={}^2S_{Ge}={}^{Ge}S_4={}^4S_{Ge}$  ( $C_2$  symmetry). The  ${}^1S_5$  axial and equatorial conformers have the same energy and structural parameters, thus are degenerated. The relative energy is equal to 2.32, 3.13 kcal/mol for MP2 and DFT/B3LYP methods respectively. The further analysis takes into account only  ${}^1S_5$  axial conformer. The  ${}^1S_3$  axial and equatorial differs are not energetic with energy values of 4.15 (MP2), 4.12 (DFT) for axial and 4.30 (MP2), 4.25 (DFT) for equatorial conformers.

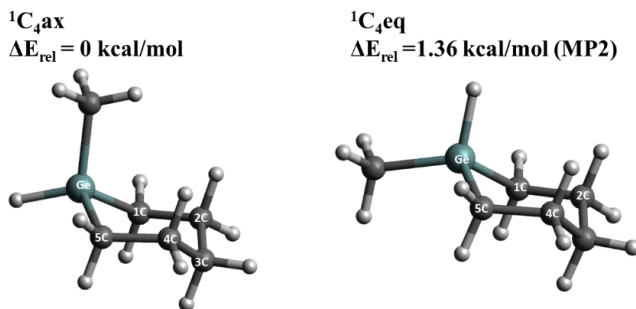


Figure 5.15: The  ${}^{Ge}C_3$  axial and equatorial conformers of the 1-methyl-germacyclohexane with ring atoms numbering derived from MP2/aug-cc-pVTZ calculations. [A5]

The relative energies were calculated with respect to the global energy minimum structure which is the  ${}^{Ge}C_3$  axial conformer. All structural parameters for the  ${}^{Ge}C_3$  axial and equatorial conformers are listed in Table 15 in the APPENDIX I. The first local energy minimum, the  ${}^{Ge}C_3$  equatorial structure vary in energy about 1.36 (MP2), 0.04 kcal/mol (DFT) (see Fig. 5.15). Taking into

account the relative energy differences we can calculate the conformer population distribution. The Boltzmann distribution equation indicate conformer concentration as follow:  ${}^G\text{C}_3$  axial - 67.84% (DFT), 92.99% (MP2),  ${}^G\text{C}_3$  equatorial - 31.71% (DFT), 4.69% (MP2),  ${}^1\text{S}_5$  axial - 0.35% (DFT), 1.86% (MP2),  ${}^1\text{S}_3$  axial - 0.06% (DFT), 0.42% (MP2) and  ${}^1\text{S}_3$  equatorial - 0.05% (DFT), 0.04%. Several computational studies, predict the  ${}^G\text{C}_3$  equatorial conformer to be the global minimum but previous experiments proved that the 1-M-GeCH molecule is the most abundant in the samples in the  ${}^G\text{C}_3$  axial conformation, thus should be considered as the global minimum structure. The vibrational bands intensities predicted computationally were scaled according to the Boltzmann distribution, to reflect the conformers concentration in the sample.

#### 5.4.2. Potential energy surface scan

During the potential energy surface scans calculation the Ge-C1-C2-C3 and C2-C3-C4-C5 (see Fig. 5.16) dihedral angles change was traced to investigate the ring inversion and transition state structures. The geometry optimization was done at every scan step (every 5 degree dihedral angle change).

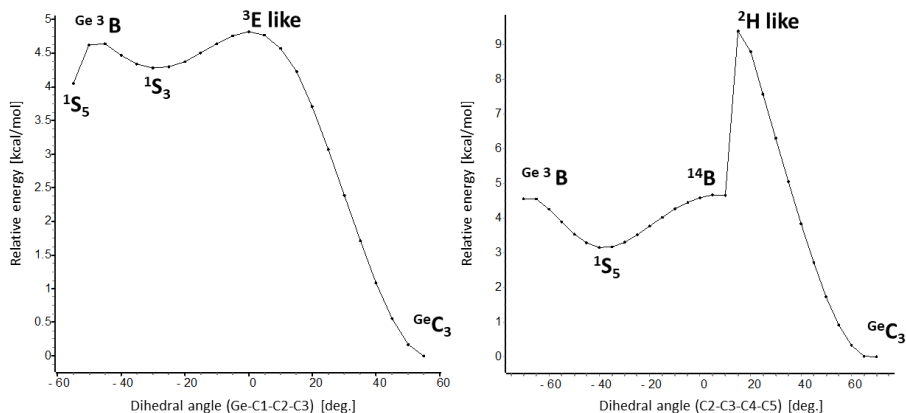


Figure 5.16: The potential energy surface scans for the Ge-C1-C2-C3 and C2-C3-C4-C5 dihedral angle change about 5 degree calculated with B3LYP/aug-cc-pVTZ method. [A5]

The  ${}^G\text{C}_3 \rightarrow {}^4\text{C}_1$  inversion pathway is as follow: chair ( ${}^G\text{C}_3$ )  $\rightarrow$  half-chair (TS)  $\rightarrow$  skew-boat ( ${}^1\text{S}_3$  -  $\text{C}_1$  symmetry)  $\rightarrow$  boat (TS)  $\rightarrow$  skew-boat ( ${}^1\text{S}_5$  -  $\text{C}_2$  symmetry) and is depicted in Fig. 5.17. The chair and skew-boat structures are the local energy minima and the half-chair and boat are transition states (TS). The energy barriers for the  ${}^G\text{C}_3 \rightarrow {}^1\text{S}_3$  transition and reverse process equals to 4.82 and 0.54 kcal/mol, respectively. The energy barrier for the  ${}^1\text{S}_3 \rightarrow {}^1\text{S}_5$  interconversion via  ${}^1\text{B}_4$  transition state is equal to 0.36 kcal/mol, while

for the  ${}^1S_5 \rightarrow {}^1S_3$  is calculated to be 0.59 kcal/mol. The calculated energy barriers for the  ${}^1S_3 \rightarrow {}^{Ge}C_3$ ,  ${}^1S_3 \rightarrow {}^1S_5$  and  ${}^1S_5 \rightarrow {}^1S_3$  are 0.54, 0.36 and 0.59 kcal/mol, thus the most probable interconversion for the  ${}^1S_3$  structure should be to the  ${}^1S_5$  conformer.

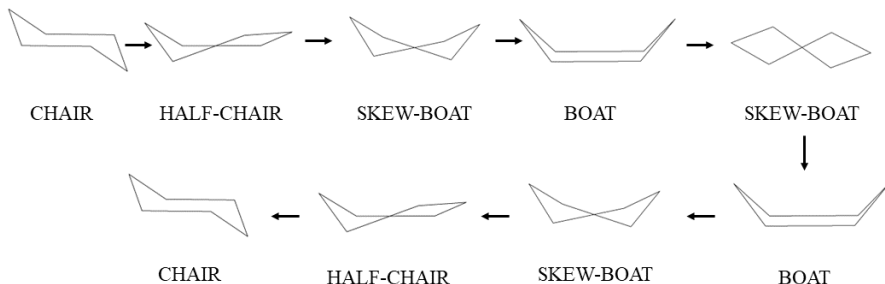


Figure 5.17: Schematic description of the full cycle of the  ${}^{Ge}C_3 \rightarrow {}^4C_1$  ring inversion for the 1-methyl-germacyclohexane.

#### 5.4.3. Matrix isolation experiment

The 2840–3000  $\text{cm}^{-1}$  region in the spectrum obtained from matrix isolation experiment represents vibrational modes related to the C-H bonds motion (see Fig. 5.18). Bands 2994 and 2988  $\text{cm}^{-1}$  are assigned the C-H asymmetric stretching. The intensity increase for the band at 2994  $\text{cm}^{-1}$  with the decrease of the intensity for 2988  $\text{cm}^{-1}$  band can be explained with the conformational changes occurring in the matrix. Both conformers have predicted with DFT/B3LYP method bands, namely:  ${}^{Ge}C_{3ax}$  at 3122, 3109  $\text{cm}^{-1}$  and  ${}^{Ge}C_{3eq}$  at 3109, 3103  $\text{cm}^{-1}$ . After annealing the amount of the  ${}^{Ge}C_{3ax}$  conformers increases.

The band at 2953  $\text{cm}^{-1}$  which becomes more intense upon annealing can be described with computational band 3074  $\text{cm}^{-1}$  of  ${}^{Ge}C_{3ax}$  conformer. The change is related to interconversion not only from  ${}^{Ge}C_{3eq}$  but as well with the interconversion from lower energy minima skew-boat structures. The drop of intensity of the 2942  $\text{cm}^{-1}$  and 2932  $\text{cm}^{-1}$  bands upon annealing is caused by the decrease of the amount of low energy skew-boat conformers. The band at 2942  $\text{cm}^{-1}$  from matrix isolation experiment is related with 3058  $\text{cm}^{-1}$  ( ${}^1S_{3ax}$ ), 3054 ( ${}^1S_{3eq}$ ) and 3053  $\text{cm}^{-1}$  ( ${}^1S_{5ax}$ ) bands obtained with DFT/B3LYP method. Bands at 2920 and 2915  $\text{cm}^{-1}$  which intensity grows upon annealing belongs to the  ${}^{Ge}C_{3ax}$  conformer. In the Neon matrix in this spectral region we observe no changes upon annealing. The comparison of the computational methods used for the calculations without doubts shows that the DFT/B3LYP method is better. The calculated peaks positions better matches the experimental ones.

In the region of 2050  $\text{cm}^{-1}$  we observe bands related to Ge-H stretching vibration (see Fig.5.18). The theoretical calculations predict presence of the

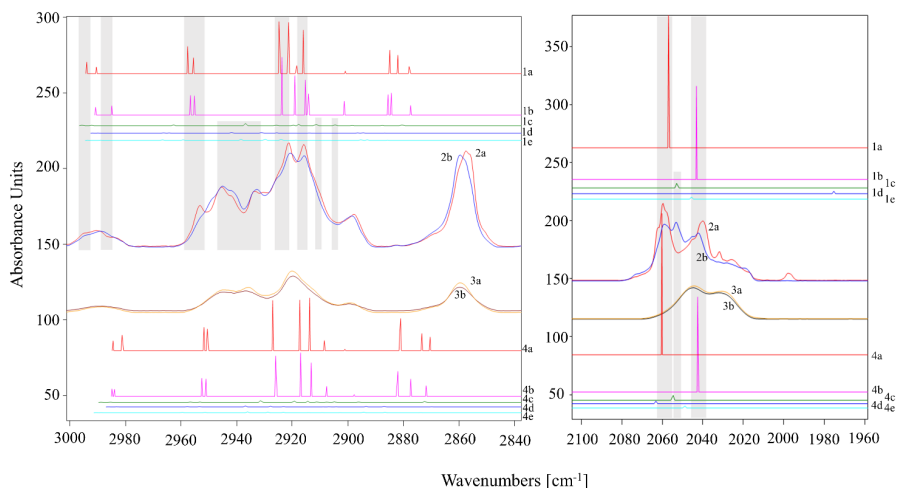


Figure 5.18: The vibrational analysis. 1: computational spectra (DFT/B3LYP/aug-cc-pVTZ) of  ${}^G e C_3$  axial (a),  ${}^G e C_3$  equatorial (b),  ${}^1 S_5$  axial (c),  ${}^1 S_3$  axial (d),  ${}^1 S_3$  equatorial (e) conformers. 2: FT-IR absorption spectra of  $N_2$  matrix isolated at 17K (b) and at 17K after annealing to 30 K (a). 3: FT-IR absorption spectra of Ne matrix isolated at 3K (b) and at 3K after annealing to 9 K (a). 4: computational spectra (DFT/M06-2X/aug-cc-pVTZ) of  ${}^G e C_3$  axial (a),  ${}^G e C_3$  equatorial (b),  ${}^1 S_5$  axial (c),  ${}^1 S_3$  axial (d),  ${}^1 S_3$  equatorial (e) conformers. The intensities of the theoretical spectra were scaled taking in to account Boltzmann distribution calculated from the DFT relative energy differences. [A5]

one spectral band for each conformer: 2080 ( ${}^G e C_3 ax$ ), 2066 ( ${}^G e C_3 eq$ ), 2076 ( ${}^1 S_5 ax$ ), 2076 ( ${}^1 S_3 ax$ ), 2915  $cm^{-1}$  ( ${}^1 S_3 eq$ ) for the DFT/B3LYP method and 2116 ( ${}^G e C_3 ax$ ), 2097 ( ${}^G e C_3 eq$ ), 2110 ( ${}^1 S_5 ax$ ), 2119 ( ${}^1 S_3 ax$ ), 2104  $cm^{-1}$  ( ${}^1 S_3 eq$ ) for the DFT/M06-2X method. In this experimental region, the positions and intensities of the vibrational bands obtained from DFT/M06-2X describe the position of the bands better. The spectral bands of decreasing intensity at 2920, 2053 and 2045  $cm^{-1}$  can be attributed respectively to the bands 2119 ( ${}^1 S_3 ax$ ), 2110 ( ${}^1 S_5 ax$ ) and 2104  $cm^{-1}$  ( ${}^1 S_3 eq$ ), leading to the conclusion that after annealing process the amount of these conformers in the sample is lower.

In the region of the 2840 – 3000  $cm^{-1}$  the band shapes and positions in the matrix experimental spectra results, are better described by the harmonic approximation, but in the both cases the bands increasing with the annealing process can be described with the frequencies obtained for the chair axial conformer. In region 1060 – 740  $cm^{-1}$ , it is troublesome to find the characteristic bands of the  ${}^1 S_3$  conformers. What can we observe is the increase in the intensity of the chair conformer bands.

Molecules in the skew-boat conformation can rearrange to lower energy minima structure: chair equatorial or chair axial (the rearrangement path-

ways are described in the PES calculation paragraph. In the spectral region of 1500–600  $\text{cm}^{-1}$  again the wavenumbers of the anharmonic spectra are closer to those obtained experimentally. The harmonic frequencies need to be scaled by the factor of 0.985 to describe the experimental spectra in this spectral region. The bands with the grown intensity are related with  ${}^G e C_{3ax}$  conformer bands due to the increase of the lower energy minima conformer in the experimental sample after the annealing process. Several bands in this spectral region, are becoming lower in intensity, this can be related either to the chair  ${}^G e C_{3eq}$  to  ${}^G e C_{3ax}$  or skew-boat to chair inversion. The Raman spectra do not contribute in the conformer search in the high frequency region, but allow for assignment of wavenumbers lower than 600  $\text{cm}^{-1}$ .

## 5.5. Conclusions

We have found that the lowest energy minimum structure of the 1-methylgermacyclohexane is  ${}^G e C_3$  axial conformer, regardless the computational method used. The first local energy minimum ( ${}^G e C_3$  equatorial) is only 0.04 kcal/mol higher in energy with respect to the global minimum structure. The  ${}^1 S_5$  axial and equatorial conformers are isoenergetic with the relative energy of 3.12 kcal/mol. The relative energies of  ${}^1 S_3$  axial and  ${}^1 S_3$  equatorial conformers are 4.15 and 4.30 kcal/mol, respectively. The conformational rearrangement path for the 1-methyl-1-germacyclohexane is as follow: chair ( $C_s$ )  $\rightarrow$  envelope/half-chair like (TS)  $\rightarrow$  skew-boat ( $C_1$ )  $\rightarrow$  boat (TS)  $\rightarrow$  skew-boat ( $C_2$ ).

The matrix isolation experiments revealed that in the 1-methylgermacyclohexane samples, the molecules exist only in the chair conformers, excluding the skew-boat configurations. The chair conformers with the axial structure are the most abundant in the FT-IR matrix isolation spectra, but it is possible to find spectroscopic bands belonging to the chair equatorial conformer as well. The annealing of the 1-methylgermacyclohexane sample allows to trace the chair axial to chair equatorial interconversion.

## 5.6. 1,3,5,2,4,6-triazatrisilinane and hexamethyl derivat

### 5.6.1. Density Functional Theory and Møller–Plesset based calculations

Conformational analysis of the possible conformers of the 1,3,5,2,4,6-triazatrisilinane (3A3S) 2,2,4,4,6,6-hexamethyl-1,3,5,2,4,6-triazatrisilinane was done taking the chair (C), boat (B), skew-boat (S), half-chair (H) and envelope (E) structures with the DFT/B3LYP/aug-cc-pVTZ method. Obtained energy minima structures were re-optimized with the MP2/aug-cc-pVDZ method. The vibrational analysis was performed at DFT/B3LYP/aug-cc-pVTZ level of theory with the VMARD method assignment.

The optimization of all investigated structures of the 1,3,5,2,4,6-triazatrisilinane resulted in the boat conformer (see Fig. 5.19) according to the DFT/B3LYP/aug-cc-pVTZ and MP2/aug-cc-pVDZ calculations.

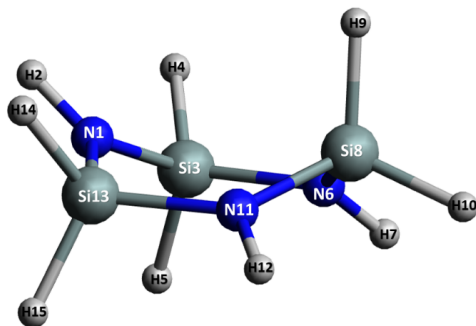


Figure 5.19: 1,3,5,2,4,6-triazatrisilinane boat conformer with ring atoms numbering, derived from DFT/B3LYP/aug-cc-pVTZ calculations. [A6]

The hexamethyl-1,3,5,2,4,6-triazatrisilinane (6M3A3S) global energy minimum structure is  ${}^1B^4$  conformer. According to the DFT/B3LYP/aug-cc-pVTZ calculations, the only local energy minimum is the skew-boat structure. The  ${}^1S_3$  and  ${}^1S_5$  conformers are degenerate, thus only  ${}^1B^4$  (boat) and  ${}^1S_3$  (skew-boat) conformers are investigated in details. The energy difference between global and local energy minimum structures is only 0.09 kcal/mol (DFT/B3LYP/aug-cc-pVTZ). On the other hand calculations performed at MP2/aug-cc-pVDZ level for boat and skew-boat conformers showed that only stable conformers are skew-boat.

Due to the fact that the global energy minimum for  $Si_3(NH)_3H_6$  and  $Si_3(NH)_3(CH_3)_6$  molecules is the boat structure, we can compare the structural parameters of the ring, such as respective dihedral angles values and bonds lengths (N-Si, N-H). The a, d N-Si-N-Si dihedral angles for 3A3S are -8.30, 8.82 kcal/mol (DFT) and -2.54, 2.83 kcal/mol (MP2), while for the (A,

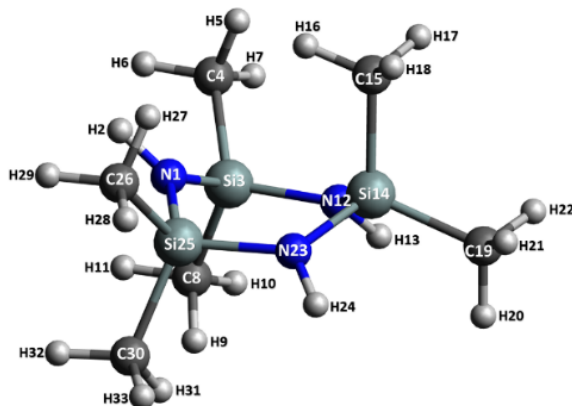


Figure 5.20: 2,2,4,4,6,6-hexamethyl-1,3,5,2,4,6-triazatrisilinane boat conformer with ring atoms numbering, derived from DFT/B3LYP/aug-cc-pVTZ calculations. [A6]

D) 6M3A3S: -7.28, 8.21 kcal/mol (B3LYP/aug-cc-pVTZ). The average dihedral angle values for the a/A, b/B, c/C, e/E, f/F for both molecules is the 42.9 deg. for 3A3S, and 42,6 deg for 6M3A3S. The N-H bond length, apart from the molecule investigated has the same values which are 1.008/1.009 Å B3LYP/aug-cc-pVTZ methods. The averaged length of the Si-N bonds, again in the same for both molecules and is equal to 1.74 (B3LYP/aug-cc-pVTZ).

The ring structure of both conformers has very similar parameters. The substitution of the H atoms attached to the Si atom with the -CH<sub>3</sub> group does not affect the structural parameters of the boat conformation but cause the presence of the skew-boat local energy minima for the 6M3A3S molecule. Nevertheless, the skew-boat structure vary only about 0.1 kcal/mol in the formation energy from the boat structure.

### 5.6.2. Potential energy surface scan

The potential energy surface scans were done for six dihedral angles of both 3A3S and 6M3A3S molecules.

For the 3A3S molecule the results indicates the presence of two transition state structures, namely half-chair and skew-boat. The interconversion pathways of the from one to another boat conformer may leads through one of the aforementioned transition states. The boat to half-chair interconversion energy barrier is 2.75 kcal/mol and make this transition impossible to occur in the experimental conditions. The second pathway consist of constant transition B → S (TS) → B → S (TS) → B, with the skew-boat structure as a transition state (TS). The barrier of the B → S transition is 0.68 kcal/mol, indicating that the ring inversion through the skew-boat structure is more probable.

The results indicate the ring inversion is based on the constant intercon-



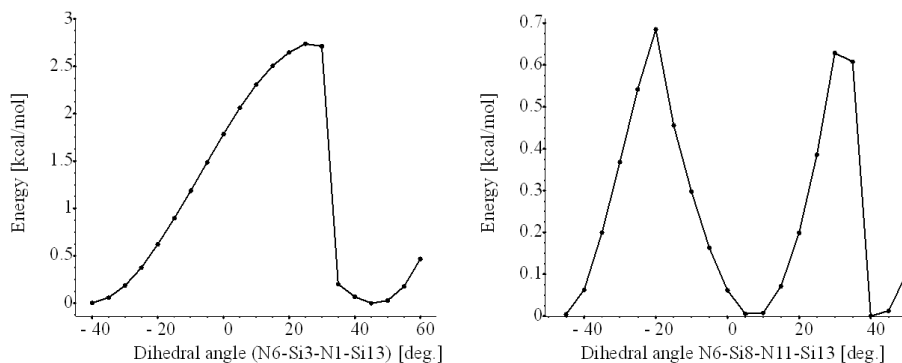


Figure 5.21: The relaxed potential energy surface scans along the N6-Si3-N1-Si13 and N6-N8-N11-Si13 dihedral angles of the 1,3,5,2,4,6-triazatrisilane, obtained from B3LYP/aug-cc-pVTZ method. [A6]

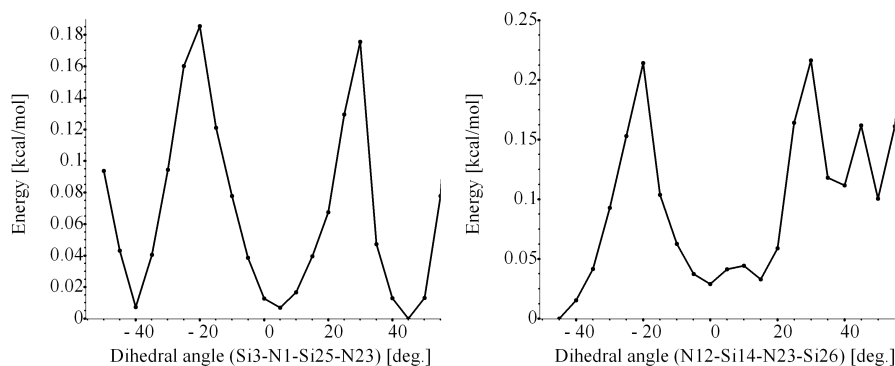


Figure 5.22: The relaxed potential energy surface scans along the Si3-N1-Si25-N23 and N12-Si14-N23-Si26 dihedral angles for the 2,2,4,4,6,6-hexamethyl-1,3,5,2,4,6-triazatrisilane, obtained from B3LYP/aug-cc-pVDZ method [A6]

version from the boat to the skew-boat structure (see Fig. 2). All results indicate that the global energy minimum structure is boat conformer, with the skew-boat conformer as the first local energy minimum structure. No transition structures were found, only skew-boat local energy minima conformers. The barrier of the  $B \rightarrow S$  conversion was found to be approx. 0.2 kcal/mol. The reverse process  $S \rightarrow B$  energy barrier was 0.18 kcal/mol. The low energy barriers may lead to the constant interconversion of both conformers in the experimental conditions.

### 5.6.3. Matrix isolation experiment

In the argon matrix spectra bands at  $3426\text{ cm}^{-1}$  and  $3419\text{ cm}^{-1}$ , can be described with bands  $3595\text{ cm}^{-1}$  and  $3584\text{ cm}^{-1}$  belonging to the skew-boat conformer. The band at  $3424\text{ cm}^{-1}$  which appears after annealing corresponds

to theoretically calculated  $3594\text{ cm}^{-1}$  band of the boat conformer. The bands of the neon matrix isolated sample in this spectral region are broad and difficult to assign. Matrix isolation band at  $2968\text{ cm}^{-1}$  is caused by C-H asymmetric stretching, for matrix isolation in argon matrix we can it splits to two bands:  $2970$  and  $2963\text{ cm}^{-1}$  upon annealing. These bands could be assigned to the  $3100$  and  $3093\text{ cm}^{-1}$  the calculated bands of the boat conformer, especially that the intensity of these bands increase upon annealing. Additionally, in this region, after the annealing process shoulder band at  $2976\text{ cm}^{-1}$  become visible, this band can be assigned to the calculated  $3108\text{ cm}^{-1}$  band of the boat conformer.

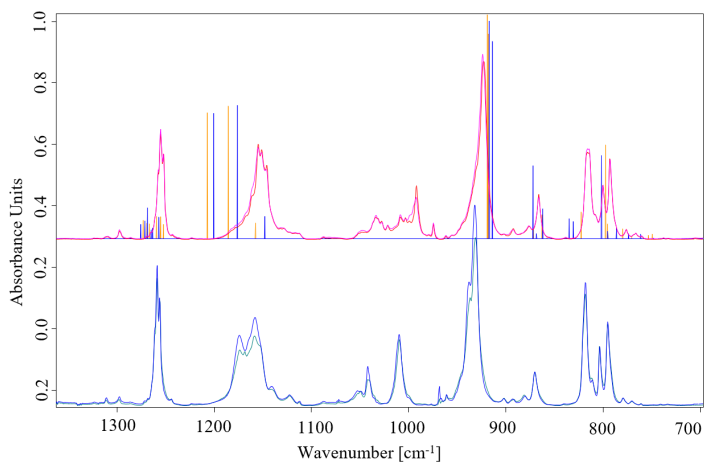


Figure 5.23: 1,3,5,2,4,6-triazatrisilinane boat conformer with ring atoms numbering, derived from DFT/aug-cc-pVTZ calculations. [A6]

The spectral bands in the region  $1460\text{-}1400\text{ cm}^{-1}$  for all experiments are assigned to computational bands  $1447\text{-}1422\text{ cm}^{-1}$  from both boat and skew-boat conformers, caused by the C-H stretching and twisting modes. It is impossible to attribute the bands to the specific conformer in this region. Bands in the region approximately  $1250\text{ cm}^{-1}$  in each experimental spectra can be assigned to  $1276\text{-}1255\text{ cm}^{-1}$  bands from the calculations and are a result of the C-H wagging vibration. None of the experimental bands can be assign to any of the conformer. In the argon matrix low intensity shoulder bands:  $1178$ ,  $1165$ ,  $1160\text{ cm}^{-1}$  decrease after annealing. The high intensity bands  $1155$ ,  $1151$  and  $1145\text{ cm}^{-1}$  increase after annealing. In the neon matrix we can observe only decrease of the high intensity bands. These bands are related to the N-H  $\rho$  motion.

## 5.7. Conclusions

The 2,2,4,4,6,6-hexamethyl-1,3,5,2,4,6-triazatrisilane (6M3A3S) have to stable conformations, namely boat (global energy minimum) and skew-boat (local energy minimum). The relative energy difference is equal to 0.1 kcal/mol. The conversion energy barrier (based on the PES calculations) for the B  $\rightarrow$  S process, was found to be 0.18 kcal/mol, thus it is possible to observe such a rearrangement under experimental conditions. The matrix isolation experiment proved the existence of both conformers. The annealing process allow to trace the boat  $\rightarrow$  skew-boat interconversion, the intensity of the bands belonging to the skew-boat conformer decrease after the sample annealing. The 1,3,5,2,4,6-triazatrisilane (3A3S) was investigated computationally, the results indicate that the only stable structure is the boat conformer. Despite the fact that the ring parameters of the 3A3S and 6M3A3S boat conformers are very similar, the conformational stability is affected by the introduction of the methyl groups at Si ring atoms. The PES analysis indicate two possible B  $\rightarrow$  B interconversion pathways, through the half-chair and skew-boat transition states. The energy barriers were found to be: 2.75 kcal/mol for the B  $\rightarrow$  H transition and 0.68 kcal/mol for the B  $\rightarrow$  S transition.

## 5.8. Summary on the influence of heteroatom/substituent to conformational stability

The six-member ring heterocyclic molecules were studied in detail before, but the differences in methodology do not allow for direct comparison of the obtained results. It was found that the conformational preference may vary basing on the computational method used. Additionally, most of the conformational searches omit the skew-boat conformers focusing only on the chair axial/equatorial conformers. That is why, we decided to perform detailed conformational analysis of the germacyclohexane, silacyclohexane and cyclohexane (see Fig.5.24), mono- and disubstituted with  $-\text{CH}_2\text{Cl}$ ,  $-\text{CH}_3$ ,  $-\text{Cl}$  and  $-\text{F}$  in a several configurations. All investigated molecules with energy values are presented in Tables 5.1, 5.2, 5.3 and 5.4 the detailed structural parameters of the chair conformers for all molecules are listed in Tables: 16, 17, 18, 19 and 20 in the APPENDIX I.

During the disubstituted cyclic molecules analysis firstly we focus on the  $-\text{Cl}/-\text{F}$  and  $-\text{CH}_2\text{Cl}$  substituents. Note that the axial/equatorial nomenclature in tables, describe the position of the  $-\text{Cl}/-\text{F}$  radicals. To make the description as clear as possible we introduced Clax/eq/Fax/eq and  $\text{CH}_2\text{Clax/eq}$  describing the position of the substituent which is not always consistent with the nomenclature in tables.

The global energy minimum structure for all  $-\text{Cl}$  and  $\text{CH}_2\text{Cl}$  substituted molecules, namely the 1-chloro-1-chloromethyl-germacyclohexane (1a),

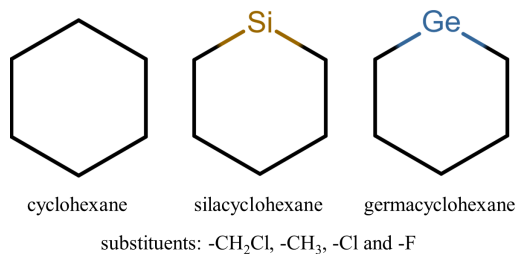


Figure 5.24: Scheme of the cyclohexane, silacyclohexane and germacyclohexane molecules and investigated substituents.

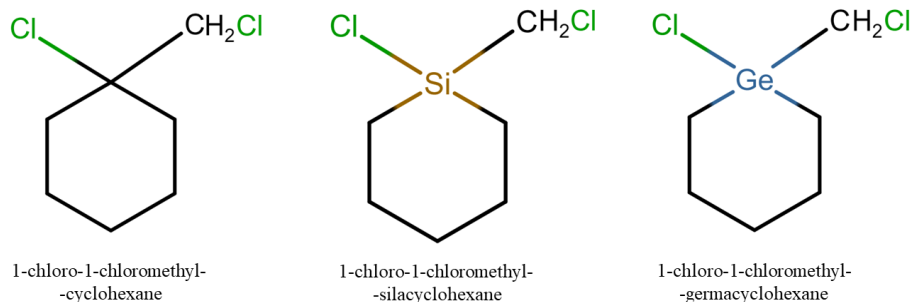


Figure 5.25: Scheme of the 1-chloro-1-chloromethyl-cyclohexane, 1-chloro-1-chloromethyl-silacyclohexane and 1-chloro-1-chloromethyl-germacyclohexane molecules.

1-chloro-1-chloromethyl-silacyclohexane (1b) and 1-chloro-1-chloromethyl-cyclohexane (1c) is the chair axial structure, where the -Cl is in axial and the CH<sub>2</sub>Cl in the equatorial position, the Cl atom from CH<sub>2</sub>Cl group is in trans conformation. Schematic structures of the molecules are depicted in the Fig. 5.25, the relative energies are listed in Table 5.1.

Table 5.1: Relative energy [kcal/mol] values for 1-chloro-1-chloromethyl-cyclohexane, 1-chloro-1-chloromethyl-silacyclohexane and 1-chloro-1-chloromethyl-germacyclohexane conformers calculated with DFT/B3LYP/aug-cc-pVTZ method.

Relative energy [kcal/mol] (DFT/B3LYP/aug-cc-pVTZ)					
(1a)	Cl-CIM-GeCH	(1b)	Cl-CIM-SiCH	(1c)	Cl-CIM-CH
Caxt	0	Caxt	0	Caxt	0
Ceqt	0.64	Ceqt	0.88	Caxg	1.63
Caxg	1.58	Caxg	1.53	Ceqg	2.51
Ceqg	2	Ceqg	1.77	Ceqt	4.23
<sup>1</sup> S <sub>5</sub> axt	3.49	<sup>1</sup> S <sub>5</sub> axt	3.92	<sup>1</sup> S <sub>3</sub> axt	6.22
<sup>1</sup> S <sub>3</sub> axt	4.06	<sup>1</sup> S <sub>3</sub> axt	4.5	<sup>1</sup> S <sub>5</sub> axt	6.38

continuation on next page

continuation					
${}^1S_3eqt$	4.26	${}^1S_3eqt$	4.81	${}^1S_5axg$	7.52
${}^1S_5axg$	5.08	${}^1S_5axg$	5.36	${}^1S_3axg-$	8.06
${}^1S_3axg-$	5.82	${}^1S_3axg-$	6.2	${}^1S_3axg+$	8.14
${}^1S_3axg+$	5.85	${}^1S_3axg+$	6.24	${}^1S_3eqg-$	8.49
${}^1S_3eqg-$	6.05	${}^1S_3eqg-$	6.28	${}^1S_3eqg+$	9.42
${}^1S_3eqg+$	6.06	${}^1S_3eqg+$	6.34		

The order of local energy minima structures for the 1-chloro-1-chloromethylcyclohexane molecule is as following:  $Caxt < Caxg < Ceqg < Ceqt < {}^1S_3axt < {}^1S_5axt < {}^1S_3axg- < {}^1S_3axg+ < {}^1S_3eqg- < {}^1S_3eqg+$ . During the optimization, the  ${}^1S_3eqt$  conformer rearrange to the  ${}^1S_5axt$  conformation, thus was not investigated. The trans conformations is more stable for Cax,  ${}^1S_3ax$  and  ${}^1S_5axt$  conformers, while for the Ceq conformer, gauche.

After introduction of the heteroatom, the conformers stability changes, see Table 5.2. In general, the results obtained for 1a and 1b are repeatable, with relative energy increases in order:  $Caxt < Ceqt < Caxg < Ceqg < {}^1S_5axt < {}^1S_3axt < {}^1S_3eqt < {}^1S_5axg < {}^1S_3axg- = {}^1S_3axg+ < {}^1S_3eqg- = {}^1S_3eqg+$ . The trans position of the -Cl in the -CH<sub>2</sub>Cl group is favored for all ring shapes (Cax/eq,  ${}^1S_5ax/eq$ ,  ${}^1S_3ax/eq$ ). The  ${}^1S_3axg- = {}^1S_3axg+$  as well as  ${}^1S_3eqg- = {}^1S_3eqg+$  pairs of conformers are isoenergetic despite the fact they slightly vary in the conformation. For 1c molecule energy differences in  ${}^1S_3axg- - {}^1S_3axg+$  and  ${}^1S_3eqg- - {}^1S_3eqg+$  pairs of conformers are bigger (1a: 0.03 and 0.01 kcal/mol, 1b: 0.04, and 0.06 kcal/mol, 1c: 0.08 and 0.93 kcal/mol), but the order of the relative energies decrease is the same.

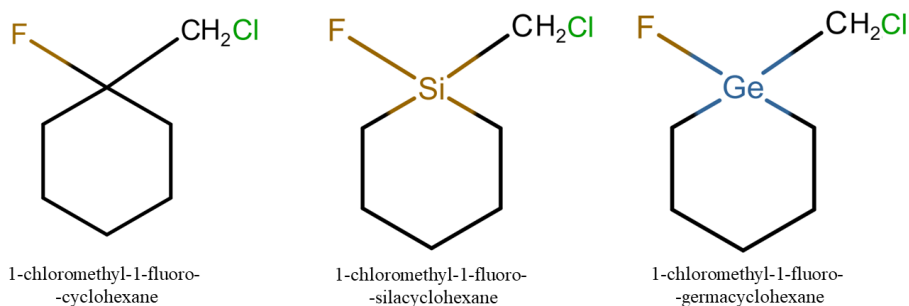


Figure 5.26: Scheme of the 1-chloromethyl-1-fluoro-cyclohexane, 1-chloromethyl-1-fluoro-silacyclohexane and 1-chloromethyl-1-fluoro-germacyclohexane molecules.

The change of the -Cl to -F substituent in the 1-chloromethyl-1-fluoro-silacyclohexane (2a), 1-chloromethyl-1-fluoro-germacyclohexane (2b) and 1-chloromethyl-1-fluoro-cyclohexane (2c) does not affect the global energy minima structure which is Caxt for 2a, 2b and 2c molecules. Schematic structures of

the 1-chloromethyl-1-fluoro substituted molecules are depicted in Fig. 5.26.

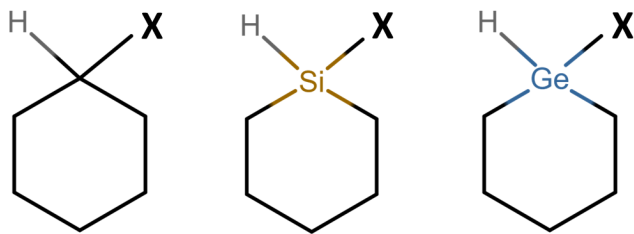
Table 5.2: Relative energy [kcal/mol] values for 1-chloromethyl-1-fluoro-cyclohexane, 1-chloromethyl-1-fluoro-silacyclohexane and 1-chloromethyl-1-fluoro-germacyclohexane conformers calculated with DFT/B3LYP/aug-cc-pVTZ method.

Relative energy [kcal/mol] (DFT/B3LYP/aug-cc-pVTZ)					
	(2a) CIM-F-GeC	(2b) CIM-F-SiCH		(2c) CIM-F-Hex	
Caxt	0	Caxt	0	Caxt	0
Ceqt	0.18	Ceqt	0.33	Caxg	0.77
Caxg	1.32	Ceqg	0.92	Ceqg	1.2
Ceqg	1.51	Caxg	1.08	Ceqt	3.16
<sup>1</sup> S <sub>5</sub> axt	3.27	<sup>1</sup> S <sub>5</sub> axt	3.5	<sup>1</sup> S <sub>3</sub> axt	5.38
<sup>1</sup> S <sub>3</sub> axt	3.7	<sup>1</sup> S <sub>3</sub> axt	4.04	<sup>1</sup> S <sub>5</sub> axt	5.52
<sup>1</sup> S <sub>3</sub> eqt	3.71	<sup>1</sup> S <sub>3</sub> eqt	4.12	<sup>1</sup> S <sub>5</sub> axg	5.94
<sup>1</sup> S <sub>5</sub> axg	4.6	<sup>1</sup> S <sub>5</sub> axg	4.5	<sup>1</sup> S <sub>3</sub> axg-	6.23
<sup>1</sup> S <sub>3</sub> axg-	5.21	<sup>1</sup> S <sub>3</sub> eqg-	5.26	<sup>1</sup> S <sub>3</sub> axg+	6.32
<sup>1</sup> S <sub>3</sub> axg+	5.24	<sup>1</sup> S <sub>3</sub> axg-	5.29	<sup>1</sup> S <sub>3</sub> eqg-	6.6
<sup>1</sup> S <sub>3</sub> eqg+	5.37	<sup>1</sup> S <sub>3</sub> eqg+	5.31	<sup>1</sup> S <sub>3</sub> eqg+	7.4
<sup>1</sup> S <sub>3</sub> eqg-	5.41	<sup>1</sup> S <sub>3</sub> axg+	5.32		

The biggest change is observable for the 2a and 2b where the order of chair conformers is changed from Caxt < Ceqt < Caxg < Ceqg to Caxt < Ceqt < Ceqg < Caxg, where Ceqg become more stable than Caxg conformer. In the table 3 we can see the differences in the order of the <sup>1</sup>S<sub>3</sub>axg-, <sup>1</sup>S<sub>3</sub>axg+, <sup>1</sup>S<sub>3</sub>eqg-, <sup>1</sup>S<sub>3</sub>eqg+, but again these structures can be treated as an isoenergetic pairs with energy change order: <sup>1</sup>S<sub>3</sub>axg- = <sup>1</sup>S<sub>3</sub>axg+ < <sup>1</sup>S<sub>3</sub>eqg- = <sup>1</sup>S<sub>3</sub>eqg+, being the same for 1a, 1b, 2a and 2c molecules. As it was in the case of 1c molecule, the <sup>1</sup>S<sub>3</sub>eqt conformer rearrange to <sup>1</sup>S<sub>5</sub>eqt therefore was not investigated. The order of the conformers energy for 1a/2a and 1c/2c molecules is the same, thus the change of the -Cl to -F substituent does not affect conformational stability of the disubstituted germacyclohexane and cyclohexane.

While considering the conformational stability of the monosubstituted molecules we investigate -Cl, -F, -CH<sub>3</sub> and CH<sub>2</sub>Cl substituents (see 5.3, Fig. 5.27).

The order of the -Cl and -F substituted germacyclohexane and silacyclohexane is the same, namely: Cax < Ceq < <sup>1</sup>S<sub>5</sub>eq = <sup>1</sup>S<sub>5</sub>ax < <sup>1</sup>S<sub>3</sub>ax < <sup>1</sup>S<sub>3</sub>eq, the <sup>1</sup>S<sub>5</sub>eq and <sup>1</sup>S<sub>5</sub>ax being degenerated (the same relative energy and structural parameters). The global energy minimum is the chair axial structure and the <sup>1</sup>S<sub>5</sub> structure is more stable than <sup>1</sup>S<sub>3</sub>ax/eq.



**X = -Cl, -F, -CH<sub>3</sub> or -CH<sub>2</sub>Cl**

Figure 5.27: Scheme of the investigated, monosubstituted with -Cl, -F, -CH<sub>3</sub> or -CH<sub>2</sub>Cl radicals, cyclohexane, silacyclohexane and germacyclohexane molecules.

Table 5.3: Relative energy [kcal/mol] values for cyclohexane, silacyclohexane and germacyclohexane molecules, monosubstituted with -Cl, -F and -CH<sub>3</sub> radicals calculated with DFT/B3LYP/aug-cc-pVTZ method.

Relative energy [kcal/mol] (DFT/B3LYP/aug-cc-pVTZ)					
(3a) Cl-GeCH		(3b) Cl-SiCH		(3c) Cl-CH	
Cax	0	Cax	0	Ceq	0
Ceq	0.95	Ceq	0.59	Cax	0.3
<sup>1</sup> S <sub>5ax</sub>	3.7	<sup>1</sup> S <sub>5ax</sub>	3.99	<sup>1</sup> S <sub>5ax</sub>	6.37
<sup>1</sup> S <sub>5eq</sub>	3.73	<sup>1</sup> S <sub>5eq</sub>	3.99	<sup>1</sup> S <sub>5eq</sub>	6.37
<sup>1</sup> S <sub>3ax</sub>	4.31	<sup>1</sup> S <sub>3ax</sub>	4.67	<sup>1</sup> S <sub>3ax</sub>	6.61
<sup>1</sup> S <sub>3eq</sub>	5.06	<sup>1</sup> S <sub>3eq</sub>	5.34	<sup>1</sup> S <sub>3eq</sub>	6.69
(4a) F-GeCH		(4b) F-SiCH		(4c) F-CH	
Cax	0	Cax	0	Ceq	0
Ceq	0.66	Ceq	0.21	Cax	0.27
<sup>1</sup> S <sub>5eq</sub>	3.47	<sup>1</sup> S <sub>5eq</sub>	3.65	<sup>1</sup> S <sub>3ax</sub>	5.81
<sup>1</sup> S <sub>5ax</sub>	3.47	<sup>1</sup> S <sub>5ax</sub>	3.66	<sup>1</sup> S <sub>5eq</sub>	5.9
<sup>1</sup> S <sub>3ax</sub>	3.96	<sup>1</sup> S <sub>3ax</sub>	4.28	<sup>1</sup> S <sub>5ax</sub>	5.9
<sup>1</sup> S <sub>3eq</sub>	4.56	<sup>1</sup> S <sub>3eq</sub>	4.85	<sup>1</sup> S <sub>3eq</sub>	6.51
(5a) M-GeCH		(5b) M-SiCH		(5c) M-CH	
Cax	0	Ceq	0	Ceq	0
Ceq	0.04	Cax	0.13	Cax	1.77
<sup>1</sup> S <sub>5ax</sub>	3.13	<sup>1</sup> S <sub>5ax</sub>	3.63	<sup>1</sup> S <sub>3eq</sub>	6.28
<sup>1</sup> S <sub>5eq</sub>	3.13	<sup>1</sup> S <sub>5eq</sub>	3.67	<sup>1</sup> S <sub>5eq</sub>	6.54
<sup>1</sup> S <sub>3ax</sub>	4.15	<sup>1</sup> S <sub>3ax</sub>	4.71	<sup>1</sup> S <sub>5ax</sub>	6.54
<sup>1</sup> S <sub>3eq</sub>	4.3	<sup>1</sup> S <sub>3eq</sub>	4.75	<sup>1</sup> S <sub>3ax</sub>	7.79

The axial position of the -Cl and -F radicals is favorable over equatorial for 3a, 3b, 4a, 4b molecules. In case of the substituted cyclohexanes, the order of conformers is different for both substitution. For the 3c molecule the order of

the relative energy is  $C_{eq} < C_{ax} < {}^1S_{5eq} = {}^1S_{5ax} < {}^1S_{3ax} < {}^1S_{3eq}$ . The global energy minima structure is  $C_{eq}$ , conformers  ${}^1S_{5eq}$  and  ${}^1S_{5ax}$  are isoenergetic and more stable than  ${}^1S_3$  conformers. In case of 4c molecule, the order is again changed, the global energy minimum structure is again  $C_{eq}$ , but the  ${}^1S_{3ax}$  is more stable than  ${}^1S_5$  conformer. The -Cl and -F radicals prefers the equatorial position in case of chair ring conformation and axial while the ring has skew-boat shape.

The substitution with methyl group gives different results for all 5a, 5b and 5c molecules (see Table 5.4). The 1-methyl-germacyclohexane (5a) have the same stability pattern as presented for 3a and 4a molecules. In case of the 1-methyl-silacyclohexane (5b), the global energy minimum is the  $C_{eq}$  conformer, but the local energy minima structures order is the same as in the 3b and 4b molecules. The methylcyclohexane molecule the most stable conformer is again  $C_{eq}$ , but we notice that this time more stable than  ${}^1S_5$  is the  ${}^1S_{3eq}$  conformer making the equatorial position more favorable for both chair and skew-boat structure. In case of the chloromethyl substituent we observe the change in the conformer stability for all molecules.

Table 5.4: Relative energy [kcal/mol] values for cyclohexane, silacyclohexane and germacyclohexane molecules, monosubstituted with  $-CH_2Cl$  calculated with DFT/B3LYP/aug-cc-pVTZ method.

Relative energy [kcal/mol] (DFT/B3LYP/aug-cc-pVTZ)					
(6a) ClM-GeCH		(6b) ClM-SiCH		(6c) ClM-CH	
Ceqt	0	Ceqt	0	Ceqg	0
Caxt	0.17	Caxg	0.31	Ceqt	0.21
Caxg	0.2	Caxt	0.47	Caxg	1.54
Ceqg	0.66	Ceqg	0.6	Caxt	4.08
${}^1S_{5axt}$	3.14	${}^1S_{5axt}$	3.55	${}^1S_{3eqg+}$	5.97
${}^1S_{5eqt}$	3.15	${}^1S_{5eqt}$	3.57	${}^1S_{5axg+}$	6.13
${}^1S_{5eqg+}$	3.51	${}^1S_{5axg+}$	3.95	${}^1S_{5eqg+}$	6.13
${}^1S_{5axg+}$	3.52	${}^1S_{5eqg+}$	3.97	${}^1S_{3eqg-}$	6.21
${}^1S_{5eqg-}$	3.66	${}^1S_{5axg-}$	4.06	${}^1S_{3eqt}$	6.21
${}^1S_{5axg-}$	3.7	${}^1S_{5eqg-}$	4.16	${}^1S_{5axg-}$	6.39
${}^1S_{3axt}$	3.9	${}^1S_{3eqt}$	4.41	${}^1S_{5eqg-}$	6.41
${}^1S_{3eqt}$	3.94	${}^1S_{3axt}$	4.44	${}^1S_{5eqt}$	6.46
${}^1S_{3axg-}$	4.27	${}^1S_{3axg-}$	4.7	${}^1S_{5axt}$	6.47
${}^1S_{3axg+}$	4.35	${}^1S_{3axg+}$	4.82	${}^1S_{3axg-}$	6.98
${}^1S_{3eqg+}$	4.8	${}^1S_{3eqg-}$	5.22	${}^1S_{3axg+}$	7.47
${}^1S_{3eqg-}$	4.82	${}^1S_{3eqg+}$	5.22		

For the 1-chloromethyl-silacyclohexane the relative energy rise in order:  $C_{eqt} > C_{axt} > C_{axg} > C_{eqg} > {}^1S_{5axt} > {}^1S_{5eqt} > {}^1S_{5eqg+} > {}^1S_{5axg+} >$



${}^1S_5eqg^- > {}^1S_5axg^- > {}^1S_3axt > {}^1S_3eqt > {}^1S_3axg^- > {}^1S_3axg^+ > {}^1S_3eqg^+ > {}^1S_3eqg^-$ . The global energy minimum structure is chair equatorial, the trans conformers are more stable within one ring shape, and the  ${}^1S_5$  conformers are more stable than  ${}^1S_3$ . The 1-chloromethyl-silacyclohexane (6b) global energy minimum is a differ only in chair equatorial trans conformer. When comparing with the 6a molecule only the order of chair conformers is different, namely,  $Ceqt > Caxg^- > Caxt > Ceqq$ . The skew boat conformers stability is the same as in the 6a, with the preference of the trans position and the  ${}^1S_5$  ring conformation. For both 6a and 6b molecules, we can find isoenergetic pairs of conformers:  ${}^1S_5axt = {}^1S_5eqgt$ ,  ${}^1S_5eqg^+ = {}^1S_5axg^+$ ,  ${}^1S_5eqg^- = {}^1S_5axg^-$ ,  ${}^1S_3axt = {}^1S_3eqt$ ,  ${}^1S_3axg^- = {}^1S_3axg^+$ ,  ${}^1S_3eqg^+ = {}^1S_3eqg^-$ . The reason of keeping them in analysis is the fact that for the chloromethyl-cyclohexane (6c) it occurs only for the skew-boat conformers, namely:  ${}^1S_5eqg^+ = {}^1S_5axg^+$ ,  ${}^1S_5eqg^- = {}^1S_5axg^-$  and  ${}^1S_5axt = {}^1S_5eqgt$ . The 6c conformers stability differ from the 6a and 6b. The global energy minimum structure is the  $Ceqg$ , the order of the increase of the relative energy is  $Ceqg > Ceqt > Caxg > Caxt > {}^1S_3eqg^+ > {}^1S_5axg^+ > {}^1S_5eqg^+ > {}^1S_3eqg^- > {}^1S_3eqt > {}^1S_5axg^- > {}^1S_5eqg^- > {}^1S_5eqt > {}^1S_5axt > {}^1S_3axg^- > {}^1S_3axg^+$ . The *gauche* position is favored in case of the 6c molecule conformers, the  ${}^1S_3eqg^+$  is more stable than  ${}^1S_5$  conformer. Despite the fact that conformers  ${}^1S_3eqg^- > {}^1S_3eqt$  have the same energy, are not degenerated, the structure differs in the position of the chloromethyl group. Additionally, the conformer  ${}^1S_3axt$  during the geometry optimalization rearrange to  ${}^1S_5axt$  conformer.

## CONCLUSIONS

1. Characteristic marker bands for envelope ( $C_s$ ) and twisted ( $C_2$ ) conformers of tetrahydrofuran (THF) were found in the FT-IR nitrogen matrix isolation spectrum. The estimated relative energy difference between the  $C_s$  and  $C_2$  conformers is 0.12 kcal/mol, what is in a very good agreement with theoretical calculations. Changes of characteristic bands intensity prove the envelope to twisted rearrangement (pseudorotation) under experimental conditions.
2. The structure of the most populated THF conformer, found in the CP-MD simulations, is neither envelope nor twisted, but a superposition of both of them, with the averaged C-C-C-C dihedral angle value equal to  $24^\circ$ . Results from the CP-MD simulations show constant conformational rearrangements (pseudorotation), namely  $C_2 \rightarrow C_s$  and  $C_s \rightarrow C_2$  transitions of the length of 2.6 ps and 1.2 ps, respectively. The increase of temperature to 100 K causes that the time of  $C_2 \rightarrow C_s \rightarrow C_2$  interconversion process is much shorter, and equals to 0.4 ps. The pseudorotation process is affected by the matrix environment, i.e. formation of the C-H $\cdots$ N hydrogen bonds.
3. From the Fourier transform of the dipole moment autocorrelation function, obtained from the trajectory of Car-Parrinello molecular dynamics simulations, anharmonic IR spectrum of THF embedded in  $N_2$  matrix was generated. Spectroscopic parameters obtained from matrix isolation experiment agree very well with the theoretically obtained anharmonic IR spectrum, what indicates that the model of the matrix is correct.
4. In the FT-IR matrix isolation spectra of 1-chloromethyl-1-fluoro-silacyclopentane molecule, characteristic marker bands for twisted *trans*, twisted *gauche-* and twisted *gauche+* conformers were found. In the experimental sample upon annealing procedure the twisted *gauche-* and twisted *gauche+* energy conformers rearrange to twisted *trans* structure (intensities of respective marker bands were changed).
5. Relative energy differences of 1-chloromethyl-1-fluoro-silacyclopentane conformers are equal to 3.57 kcal/mol (twisted *gauche-*) and 4.17 kcal/mol (twisted *gauche+*), with respect to the twisted *trans* structure. The conformational stability originates from Cl-C-Si-F dihedral angle change which influences a possibility of blue-shifting improper bonds formation. The stability of the *trans* conformer has its origin in the 3C-H<sub>ax</sub> $\cdots$ Cl interaction. The proof for the blue-shifting hydrogen bonds formation

is the decrease of the C-H bonds length when comparing with *gauche* structures.

6. The characteristic marker bands for 1-chloromethyl-1-fluoro-silacyclohexane conformers (axial *trans*, equatorial *trans*, axial *gauche* and axial *gauche*) have been found in the spectra obtained from FT-IR ATR measurements. Argon and nitrogen matrix isolation experiments confirmed the existence of additional axial *gauche* conformer which was not observed in the liquid phase spectra.
7. Matrix isolation experiments show influence of different gasses, i.e. argon and nitrogen, on axial *gauche*  $\rightarrow$  axial *trans* conformational change of 1-chloromethyl-1-fluoro-silacyclohexane molecule (intensities of the respective marker bands were changed). The conversion from *gauche*  $\rightarrow$  axial *trans* is observable only in the polar nitrogen matrix while it is not present in the more inert argon matrix.
8. The existence of chair axial *trans*, chair equatorial *trans*, chair axial *gauche* and chair equatorial *gauche* conformers of 1-chloro-1-chloromethyl-silacyclohexane molecule was proved with the presence of characteristic marker bands in the FT-IR spectra obtained from neon and nitrogen matrix isolation experiment.
9. Trajectories obtained from Car-Parrinello molecular dynamics simulations calculated for 1-chloromethyl-1-fluoro-silacyclohexane and 1-chloro-1-chloromethyl-silacyclohexane molecules do not show transitions between global energy minima structures (chair axial *trans*) to other local energy minima (chair axial *gauche*). Analysis of radial distribution functions calculated for different types of intermolecular distances, obtained from CP-MD simulations at various temperatures, shows changes of the arrangement of nitrogen atoms in the matrix.
10. In the FT-IR matrix isolation spectra (at neon and nitrogen matrix) of 1-methyl-germacyclohexane characteristic marker bands for chair axial and chair equatorial conformers were found, which implies that the chair axial conformer is the most abundant. The annealing procedure shows that of the chair equatorial to chair axial occurs in the matrix environment (intensities of respective marker bands were changed).
11. According to the found characteristic marker bands, in the spectra obtained from matrix isolation experiments in argon and neon matrix at low temperatures, the 2,2,4,4,6,6-hexamethyl-1,3,5,2,4,6-triazatrisilinane molecule may exist in two conformations, namely boat (global energy minimum) and skew-boat (local energy minimum). After annealing pro-

cess the intensities of respective marker bands were changed, thus the skew-boat to boat interconversion occur.

12. Static DFT calculations indicate that the introduction of methyl substituents to silicon ring atoms of 1,3,5,2,4,6-triazatrisilinane molecule affects the conformational stability, reducing the number of stable conformers.

# SANTRAUKA LIETUVIŲ KALBA

## DISERTACIJOS STRUKTŪRA

Disertacija yra parašyta anglų kalba. Jos aprašas susideda iš įvado ir penkių skyrių. Įvado dalyje aprašomi tyrimo tikslai ir uždaviniai, praktinis ir mokslinis naujumas ir pateikiami darbo metu gautais rezultatais paremti ginamieji teiginiai. Be to, aprašytas autorės indėlis ir pateiktas publikacijų sąrašas. Pirmame skyriuje yra pateikta bendra sočiųjų heterociklinių molekulių apžvalga, kuri disertacijoje naudojama kaip pagrindas šiame darbe atliktiems naujai susintetintų molekulių tyrimams. Aprašomos oksolanų, silicio ir germanio turinčios heterociklinės molekulės bei jų konformacinė įvairovė. Antrame skyriuje aprašomos heterociklinių molekulių spektriniais tyrimams darbe naudotos eksperimentinės ir skaičiavimo metodikos. Darbe naudotos eksperimentinės metodikos yra Ramano sklaidos ir infraraudonosios sugerties spektroskopija. Taip pat darbe buvo taikomos pažeistojo vidaus atspindžio (angl. attenuated total reflection, ATR) ir matricinės izoliacijos technikos. Buvo atliekami statiniai DFT/MP2 ir dinaminiai Car-Parrinello skaičiavimai, pasitelkiant Python matematinį modelį. Trečiame skyriuje pateikti aukščiau paminėtų metodikų parametrai. Ketvirtas ir penktas skyriai apima rezultatus, gautus penkių penkianarių (tetrahidrofuranas, 1-chlorometil-1-fluorociklopentanas) ir šešianarių ciklų (1-chloro-1-chlorometilsilacikloheksanas, 1-chlorometil-1-fluorosilacikloheksanas, 1-metil-germacikloheksanas ir 2,2,4,4,6,6-hexametil-1,3,5,2,4,6-triazatrisilinanas) heterociklinėms molekulėms, įskaitant konformacijų ir energetinio stabilumo tyrimus, virpesinę analizę ir Car-Parrinello molekulinės dinamikos simuliacijas. Visi disertacijos teiginius pagrindžiantys rezultatai pateikiami išvadų skyriuje.

## ĮVADAS

Heterociklinių molekulių konformacinė įvairovė yra labai svarbi cheminiams ir biocheminiams procesams. Pilnam daugumos cheminių reakcijų supratimui yra būtina atsižvelgti į skystos ar kietos aplinkos įtaką. Todėl cheminius procesus reikia traktuoti kaip sudėtingą kompleksą, sudarytą iš tarpusavyje sąveikaujančių molekulinę sistemų. Šiuo požiūriu, tam, kad būtų galima sukurti tinkamą tiriamų procesų modelį, būtina įskaityti sąveikas su labai dideliu skaičiumi atomų. Daugelių atvejų, tokia kompleksinė analizė reikalauja labai daug išteklių arba yra tiesiog neįmanoma. Vienas iš labiausiai paplitusių būdų, kaip išspręsti šią problemą, yra sudaryti daug mažesnį modelį, kuris turėtų tas pačias savybes kaip ir sudėtingesnės sistemos. Penkių ir šešių narių sočiosios heterociklinės molekulės yra labai svarbios įvairiuose gamtoje vykstančiuose procesuose.

ose bei pramoniniuose taikymuose. Laikantis aukščiau paminėtos idėjos, galima bandyti suprasti charakteringų šios grupės molekulių struktūrinės ir energinės savybes ir daryti išvadas apie struktūrinių parametrų įtaką šiai grupei priklausančių molekulių darinių stabilumui. Todėl, norint nustatyti sąsajas tarp penkių ir šešių narių sočiųjų heterociklinių molekulių struktūros ir energijos, buvo pasirinkti tam tikri molekuliniai dariniai, apie kurių konformacinę įvairovę bei konformacinius virsmus iki šiol nėra pakankamai gerai žinoma. Atsižvelgiant iš ciklinių molekulių struktūrą bei galimus ciklo heteroatomus, spektriniam tyrimams buvo pasirinkti tokie molekuliniai dariniai: tetrahidrofuranoi, sočiosios heterociklinės penkianarės ar šešianarės molekulės su siliciu ar germaniu, taip pat šešianariai Si-N cikliniai neutralūs klasteriai. Tetrahidrofurano žiedas gali egzistuoti dvejose konformacijose:  $C_s$  simetrijos ir  $C_2$  simetrijos. Žemas energijos barjeras tarp konformerų slygoja  $C_s \leftrightarrow C_2$  konformerų konversiją (pseudorotaciją). Pirmą kartą šis procesas buvo aprašytas ciklopentano molekulės atveju. [6, 7] Tetrahidrofurano konformaciniuose tyrimuose yra daugybė prieštaraujančių mokslinių eksperimentų ir skaičiavimų rezultatų, kurie sukėlė diskusiją apie stabiliausią šios molekulės konformero struktūrą.

Naudojant šiame darbe tiriamas heterociklines molekules kaip modelines sistemas, galima gauti informaciją apie kompleksinių makrociklinių sistemų „host“ ir „guest“ tipo sąveikas, ir ši informacija galėtų būti naudinga sudėtingų vaistinių molekulių sintezėje. [8–16] Plati silicio pagrindu susintetintų molekulių junginių panaudojimo sritis padaro šiuos junginius svarbia modeline sistema struktūriniam tyrimams. Plačiausia šių junginių naudojimo sritis yra daugelio medžiagų, tokių kaip stiklo, keramikos, cemento, šviesolaidinės optika, silikono ir daugelio kitų polimerų, gamyba. [17–26] Pavyzdžiui, anglies atomo pakeitimas silicio atomu biozosteruose, gali padidinti šios molekulės efektyvumą membranų pralaidumui. [83–86] Silicio atomai biologiškai aktyviose molekulėse keičia jų elektroninę struktūrą, sukelia skirtingas sąveikas su žmogaus organizmo fermentais. Tokios savybės naudojamos modeliuojant specifinius vaistus, tokius kaip fermentų inhibitoriai (silanedioliai ir silantriooliai) ir pan. [87–91]

Penkių ir šešių narių ciklinės molekulės, turinčios vieną silicio atomą, gali būti laikomos didesnių biologiškai aktyvių bei įvairiems medicininiam taikymams tinkančių molekulių dalimi. Šios mažesnės molekulės yra intensyviai tiriamos, siekiant rasti veiksmingų fungicidų, priešauglinių, priešmaliarinių ir į steroidus panašių vaistų. [27–32] Dėl gerų adsorbcinių savybių, silicio turinčios molekulės yra hidrofobinės ir gali būti naudojamos kaip naujos kartos hidrofobinės dangos. Silicio turintys molekuliniai dariniai paprastai yra mažiau toksiški ir gali būti naudojami kaip Teflono pakaitalai. [17, 33]

Silacikloheksanų ir silaciklopentanų spektroskopinių savybių ir konformacinės įvairovės tyrinėjimas yra svarbus, siekiant sukurti specializuotas molekules medicinai ir pramonei.

Germanis, dar vadinamas "technologiskai kritiniu elementu", naudojamas šviesolaidinės optikos pramonėje, infraraudonosios spinduliuotės optikoje, kaip polimerizacijos katalizatorius, elektronikos ir saulės energijos taikymuose, o taip pat net ir tokiose srityse kaip metalurgija bei chemoterapija. [34, 35] Germanio atomo įvedimas į cikloheksano žiedą keičia žiedo struktūrinius parametrus, konformacinį stabilumą bei jo reaktyvumą. Germacikloheksanų konformacinė įvairovė iki šiol dar nėra detaliai iširta. Germanio elektroneigiamumas yra mažesnis negu anglies atomo, o van der Waals spindulys yra didesnis, dėl ko pailgėja cheminės jungtys. Cikliniame žiede cheminių jungčių pailgėjimas gali padidinti žiedo lankstumą. Germacikloheksanas yra labai svarbus komponentas gaminant nematinių skystųjų kristalų ekranus. Iki šiol, germacikloheksanas buvo tirtas dujinės fazės elektronų difrakcijos, mikrobangų spektroskopijos [36] ir infraraudonosios ir Ramano sklaidos spektroskopijos metodais, ši molekulė taip pat buvo teoriškai modeliuota DFT metodu. [37] Buvo nustatyta, kad kėdės (chair) ir valtys (skew-boat) konformacijos yra stabilios, tačiau dėl per mažos koncentracijos mažiau stabilios struktūros negalima stebėti eksperimentinėmis sąlygomis.

Šešių narių  $Si_nN_m$  ciklinės sistemos, taip pat vadinamos mišriais silicio klasteriais, yra labai intensyviai tyrinėjamos tiek eksperimentiškai, tiek teoriškai. [38–42] Šie klasteriai dažnai yra tyrinėjami dėl jų svarbaus vaidmens, kuriant medžiagas, skirtas astrofiziniams, aplinkos ir biomedicininiais taikymams. [38] Šešių narių silicio nitrido ciklinių sistemų tyrimai atliekami, siekiant įgyti žinių apie tūrinio silicio nitrido morfologiją ir savybes. Šio straipsnio autoriai tyrinėjo eilę  $Si_nN_m$  klasterių, naudodami DFT su TZ2P metodus. Jie padarė išvadą, kad šios struktūros didinant atomų skaičių evoliucionuoja iš plokščių į trimates.

Ankstesniuose moksliniuose tyrimuose, skirtuose penkių ir šešių narių heterociklinių molekulių struktūrinių ir energetinių savybių analizei, buvo akcentuojami difrakcijos ir spektroskopijos eksperimentiniai metodai. Dujų fazės medžiagų struktūrinius parametrus galima gana tiksliai nustatyti rotacinės spektroskopijos metodais. Spektriniai cheminių junginių, esančių skysčių fazėje, tyrimai yra daug sudėtingesni dėl aplinkos įtakos. FT-IR spektrai gali tapti labai sudėtingi dėl didelio spektrinių juostų skaičiaus ir jų tarpusavio persiklojimo. Tarp kitų konformacinės įvairovės analizei naudojamų eksperimentinių metodų, yra taikomas matricos izoliacijos infraraudonųjų spindulių sugerties spektroskopijos metodas. Greitai užšaldant matricinį mišinį kriogeninėje temperatūroje yra išlaikoma dujinio mišinio prieš užšalimą temperatūros (t.y. kambario temperatūros) termodinaminė pusiausvyra. Dėl nykstanti mažų sąveikų su matricine terpe joje izoliuotas molekules galima tirti kaip nesąveikaujančias su aplinka, tokiu būdu eliminuojant aplinkos poveikį. [43–45] Spektrinės juostos, užregistruotos pasinaudojant matricinės izoliacijos metodą, yra daug siauresnės negu juostos užregistruotos standartiniais metodais, t.y. kai tiriamas bandinys yra kambario temperatūros. Dėl šios priežasties konformacinėje anal-

izėje matricinės izoliacijos metodas yra žymiai informatyvesnis už standartinius spektrinius metodus.

Per paskutinius du dešimtmečius ženkliai padidėjo kompiuterių našumas. Naujų aukšto našumo skaičiavimo klasterių, pagreitintų paralelizuota programine įranga, panaudojimas cheminių procesų modeliavimui kvantinės chemijos metodais leido pasiekti aukštą molekulių darinių struktūrinių ir energinių parametrų skaičiavimo tikslumą net ir atliekant skaičiavimus didelėms, siekiančioms kelis šimtus atomų, sistemoms. Tokie skaičiavimai iš esmės pagerina eksperimentinių virpesinių spektrinių juostų priskyrimą skirtingų konformerų molekuliniais virpesiais.

Penkių ir šešių narių heterociklinės molekulės yra tinkamos kombinuotam eksperimentiniam ir teoriniam tyrimui dėl jų pakankamai mažo dydžio. Tyrimui pasirinktos molekulės turi skirtingus heteroatomus ir gali gerai reprezentuoti heterociklinius molekulinis junginius su penkianariais ir šešianariais ciklais. Išsamūs ir sistemingi stabilų konformerų struktūros ir energijos tyrimai gali būti atliekami tik tyrimuose naudojant plačią tokių junginių klasę. Iki šiol tokie tyrimai buvo atliekami gretinant matricinės izoliacijos FT-IR spektrus su statinių DFT/MP2 skaičiavimų rezultatais. Papildžius šiuos tyrimus Car-Parrinello molekulinės dinamikos simuliacijomis, galima aprašyti tokių molekulių sistemų kinetiką, ko negalima padaryti naudojant tik statinius skaičiavimus. Molekulinės dinamikos simuliacijų pagalba galima sekti molekulių pokyčių dinamiką bei gauti kokybinį ir kiekybinį vidujmolekulių ir tarpmolekulių sąveikų aprašymą.

Šioje disertacijoje buvo sprendžiamos dvi pagrindinės problemos - naujai susintetintų heterociklinių molekulių darinių struktūrinių ir spektroskopinių parametrų nustatymas; statinių kvantinės chemijos skaičiavimų tikslumo pagerinimas, atsižvelgiant į molekulių dinamiką ir sąveikas su aplinka. Tam darbe buvo panaudotos Car-Parrinello molekulinės dinamikos simuliacijos, kurios suteikia informaciją apie šių molekulių konformacinių šuolių dinamiką.

## DARBO TIKSLAI IR UŽDAVINIAI

Pagrindinis disertacijos tikslas – nustatyti sočiųjų heterociklinių molekulių struktūrinius, energetinius ir spektroskopinius parametrus ir atlikti šių molekulių sistemingą konformacinę analizę, taikant tiek eksperimentinius, tiek ir teorinių skaičiavimų metodus. Disertacijos tikslui pasiekti buvo sprendžiami žemiau išvardinti uždaviniai:

- • Tetrahidrofurano, 1-chlorometil-1-fluoro-silaciklopentano, 1-chlorometil-1-fluorosilacikloheksano, 1-chloro-1-chlorometil-silacikloheksano, 1-metil-1-germacikloheksano ir 2,2,4,4,6,6-heksametil-1,3,5,2,4,6-triazatrisililano konformacinė analizė eksperimentiniu FTIR matricinės izoliacijos metodu.



- Šių molekulių išsami teorinė konformacinė analizė, naudojant DFT ir MP2 statinius skaičiavimo metodus.
- CP-MD simuliacijos N2 matricose izoliuotiems tetrahidrofuranui, 1-chlorometil-1-fluoro-silacikloheksanui ir 1-chloro-1-chlorometil-silacikloheksanui.
- Heterociklinių junginių su šešianariu ciklu konformacinio stabilumo sisteminis tyrimas, naudojant vienodus skaičiavimo metodus. Heteroatomų (Ge, Si) ir pakaitinių atomų (-Cl, -F, -CH<sub>3</sub>, -CH<sub>2</sub>Cl) įtakos konformerų stabilumui nustatymas.
- Sistemine stabilių Si<sub>3</sub>(NH)<sub>3</sub>H<sub>6</sub> (1,3,5,2,4,6-triazatrisilino) Si<sub>3</sub>(NH)<sub>3</sub>(CH<sub>3</sub>)<sub>6</sub> (2,2,4,4,6,6-hexametil-1,3,5,2,4,6-triazatrisilino) konformerų paieška naudojant DFT ir MP2 metodus.

## GINAMIEJI TEIGINIAI

1. FTIR matricinės izoliacijos spektrinis metodas įgalina ženkliai sumažinti heterociklinių sočiųjų junginių su penkianariais ir šešianariais ciklais virpesinių spektrinių juostų pločius ir yra tinkamas šių junginių konformacinei analizei.
2. Car-Parrinello molekulinės dinamikos simuliacijos suteikia informaciją apie penkianarių heterociklinių molekulių envelope ir twisted tipo konformerų santykio priklausomybę nuo temperatūros. Šios simuliacijos gerai aprašo tetrahidrofurano konformacijų gyvavimo trukm ir C<sub>2</sub> → C<sub>s</sub> ir C<sub>s</sub> → C<sub>2</sub> konformacinius virsmus.
3. Matricinės izoliacijos eksperimentuose matricinių dujų tipas įtakoja axial-gauche → axial-trans konformacinius virsmus nearomatiniuose heterocikliniuose molekulinuose dariniuose, o polinė N<sub>2</sub> matrica stabilizuoja konformerus su didesniu dipoliniu momentu.
4. Car-Parrinello molekulinės dinamikos simuliacijos atskleidžia, kad 1-chlorometil-1-fluoro-silacikloheksano ir 1-chloro-1-chlorometilsilacikloheksano molekulių chair axial-trans tipo konformerai yra stabilūs azoto matricoje ir konformaciniai virsmai atkaitinant matricą nestebimi. Sukurtas matricos modelis patvirtina silpnų C-H...N vandenilio ryšių susidarymą tarp matricos ir joje izoliuotų molekulių.
5. Prie silicio prijungti metilo radikalai 1,3,5,2,4,6-triazatrisilino klasteryje mažina stabilių klasterio konformerų skaičių.

## PUBLIKACIJŲ SĄRAŠAS

### APIE DISERTACIJOS TEMĄ

- [A1] **J. Stocka**, J. Čeponkus, V. Šablinskas, P. Rodziewicz, Conformational diversity of the THF molecule in N<sub>2</sub> matrix by means of FTIR matrix isolation experiment and Car-Parrinello molecular dynamics simulations, *Spectrochimica Acta Part A: Molecular and Biomolecular Spectroscopy* **238**, (2020).
- [A2] T.M.C. McFadden, R. Platakytė, **J. Stocka**, J. Čeponkus, V. Aleksa, T. Carrigan-Broda, V. Šablinskas, P. Rodziewicz, G.A. Guirgis, Experimental (Raman and IR) and computational (DFT, MP2) studies of conformational diversity of 1-chloromethyl-1-fluorosilacyclohexane, *Journal of Molecular Structure*, **1221** (2020).
- [A3] **J. Stocka**, R. Platakytė, T.M.C. McFadden, J. Čeponkus, V. Aleksa, A.G. Hanna, V. Šablinskas, P. Rodziewicz, G.A. Guirgis, Conformational diversity of 1-chloro-1-chloromethylsilacyclohexane with experimental (Raman and IR) and computational (DFT, MP2) methods, *Journal of Molecular Structure*, **1249** (2022).
- [A4] **J. Stocka**, R. Platakytė, D. Hickman, T. Carrigan-Broda, J. Čeponkus, V. Šablinskas, P. Rodziewicz, G.A. Guirgis, Experimental (Raman and IR) and computational (DFT, MP2) studies of the conformational diversity of 1-chloromethyl-1-fluorosilacyclopentane molecule.) and computational (DFT, MP2) methods, *Journal of Molecular Structure*, **1272** (2023).
- [A5] **J. Stocka**, R. Platakytė, J. Macyte, V. Šablinskas, P. Rodziewicz, G.A. Guirgis, Influence of heteroatoms and substituents on structural and spectroscopic parameters of saturated six-member ring heterocycles: experimental and theoretical study of 1-methyl-1-germacyclohexane, *Journal of Molecular Structure*, **xx** (2023), under review.
- [A6] **J. Stocka**, J. Čeponkus, V. Šablinskas, P. Rodziewicz, G.A. Guirgis, Influence of methyl substituents on the conformational stability of Si<sub>3</sub>N<sub>3</sub>(CH<sub>3</sub>)<sub>6</sub> cluster: first principles and FT-IR matrix isolation study, *Journal of Molecular Structure*, **xx** (2023), submitted.

### KITOS PUBLIKACIJOS

- [A7] **J. Lach (Stocka)**, J. Goclon, P. Rodziewicz, Structural flexibility of the sulfur mustard molecule at finite temperature from Car-Parrinello molecular dynamics simulations, *J. Hazard. Mater.* **306**, 269–277 (2016).

- [A8] Y. Vaskivskyi, Y. Chernolevska, A. Vasylieva, V. Pogorelova, R. Platakytė, **J. Stocka**, I. Doroshenko, 1-Hexanol conformers in a nitrogen matrix: FTIR study and high-level ab initio calculations, *Journal of Molecular Liquids* **278**, 356–362 (2019).

#### TYRIMAI UŽSIENYJE, PRAKTIKOS

- [B1] **Tyrinėjimai Bialystoko universitete** Erasmus praktikos stažuotė, Bialystokas, Lenkija, 2016 m. balandis – rugsėjis.
- [B2] **Toruńska Molekularna Szkoła Modelowania**, Molekulinio modeliavimo stažuotė, Supraśl, Lenkija, 2016 m. balandžio 11-15 d.
- [B3] **Tyrinėjimai Jano Kochanowskio universitete Kielce mieste**, Erasmus praktikos stažuotė, Kielce, Lenkija, 2020 m. vasaris – rugsėjis.
- [B4] **Nuo teorijos iki eksperimento: molekulių sąveikų vaidmuo molekulių savitvarkos procese**, seminaras / webinaras, Chemijos fakultetas, Vroclavo universitetas, Lenkija, 2022 m. vasario 16 d.
- [B5] **Klasikinio molekulinio dinamikos praktinis požiūris**, stažuotė, Chemijos fakultetas, Vroclavo universitetas, Lenkija, 2022 m. vasario 16 d.

#### PRANEŠIMAI KONFERENCIJOSE

- [C1] **J. Lach (Stocka)**, P. Rodziewicz, M. Kozłowska, M. Baradyn, Differences in the structural flexibility of the sulfur and oxygen mustards molecules from Car-Parrinello molecular dynamics simulations, *Deutsche Physikalische Gesellschaft, Regensburg, Germany*, 2016.
- [C2] **J. Lach (Stocka)**, J. Čeponkus, V. Šablinskas, P. Rodziewicz, Tetrahydrofuran conformational diversity: FT-IR matrix isolation spectra and the theoretical study, *EUCMOS 2016 33rd European Congress on Molecular Spectroscopy, Szeged, Hungary*, 2016.
- [C3] **J. Lach (Stocka)**, J. Čeponkus, V. Šablinskas, P. Rodziewicz, FT-IR matrix isolation and theoretical study of tetrahydrofuran pseudorotation, *Deutsche Physikalische Gesellschaft, Regensburg, Germany*, 2016.
- [C4] **J. Lach (Stocka)**, R. Platakytė, J. Čeponkus, V. Šablinskas, V. Pavardenis, Conformational analysis of tetrahydrofuran by means of FT-IR matrix isolation spectra - hot nozzle experiment, *Open Readings, Vilnius, Lithuania*, 2016.

- [C5] R. Platakytė, **J. Lach (Stocka)**, J. Čeponkus, C. Crepin-Gilbert, A. Gutierrez, M. Chevalier, V. Šablinskas, Study of water-acetylacetone complexes by the means of matrix isolation infrared absorption spectrometry, Open Readings, Vilnius, Lithuania, 2016.
- [C6] **J. Stocka**, FTIR Matrix Isolation and CPMD methods in conformational analysis of THF molecule, Open Readings, Vilnius, Lithuania, 2017.
- [C7] **J. Stocka**, THF pseudorotation under FTIR Matrix Isolation and CPMD study, COINS International conference of Life sciences, Vilnius, Lithuania, 2017.
- [C8] **J. Stocka**, R. Platakytė, J. Čeponkus, V. Šablinskas, G. A. Guirgis, P. Rodziewicz, Computational and experimental vibrational study of 1-chloromethyl-1-fluorosilacyclohexane and its rearrangements, Open Readings, Vilnius, Lithuania, 2021.
- [C9] **J. Stocka**, R. Platakytė, J. Macyte, J. Čeponkus, V. Šablinskas, P. Rodziewicz, Kinetics of the conformational changes of the valeric acid in the nitrogen matrix: experiment meets theory at finite temperature, ACCORD 2022. Interdisciplinary Conference on Drug Sciences Synergy of interdisciplinary innovations - **apdovanotas kaip geriausias prisitatumas**, Warsaw, Poland, 26-28 May, 2022.
- [C10] **J. Stocka**, V. Šablinskas, Conformational diversity of non-aromatic heterocyclic molecular compounds as studied by means of matrix isolation infrared spectroscopy, International Symposium on Molecular Spectroscopy, Champaign-Urbana, 20-24 June, 2022.
- [C11] **J. Stocka**, P. Rodziewicz, V. Šablinskas, G. A. Guirgis, Kinetics of the conformational changes of the nitrogen matrix isolated disubstituted silacyclohexanes: experiment meets theory at finite temperatures, Open Readings, Vilnius, Lithuania, 18-21 May, 2023.
- [C12] **J. Stocka**, J. Macyte, P. Rodziewicz, V. Šablinskas, G. A. Guirgis, Experimental (Raman and IR) and computational (DFT,MP2) studies of the 1-chlorosilacyclopentane as saturated five-member ring molecule, Open Readings, Vilnius, Lithuania, 18-21 May, 2023.

## PRAKTINIS IR MOKSLINIS NAUJUMAS

Šis eksperimentinis ir teorinis mokslinis darbas yra skirtas heterociklinių sočiųjų molekulinėms dariniams konformacinei analizei. Darbe buvo tirta: tetrahidrofuranas, 1-chlorometil-1-fluorosilacikloheksanas, 1-chloro-1-chlorometil-silacikloheksanas, 1-chlorometil-1-fluorosilaciklopentanas

ir 2,2,4,4,6,6-heksametil-1,3,5,2,4,6-triazatrisilinas. Visos darbe tirtos molekulės išskyrus tetrahidrofuraną, yra naujai susintetintos ir jų struktūra bei konformacinė įvairovė nėra žinomi. Matricos izoliacijos technika buvo naudojama kompleksiniam ir sistematiškam eksperimentinių virpesinių juostų priskyrimui konformerų normaliesiems virpesiams. Matricos atkaitinimo eksperimentai įgalino eksperimentiškai identifikuoti konformacinius virsmus. Šiame darbe konformacinių šuolių analizėje pirmą kartą buvo panaudotos Car-Parrinello molekulinės dinamikos simuliacijos. Silaciklomolekulėms pirmą kartą buvo nustatytas silpnų vandenilinio ryšio jungčių virpesinių spektrinių juostų mėlynasis poslinkis. Darbe buvo pasiūlytas azoto matricos modelis, pagal kurį ši matrica priklausomai nuo temperatūros yra kristalinėje alfa arba beta fazėje. Taip pat Car-Parrinello molekulinės dinamikos simuliacijos leido giliau suprasti konformacijos stabilumo kinetiką atsižvelgiant į temperatūros pokyčius, t. y. nustatyti konformerų gyvavimo trukmes. Molekulinių dinamikos simuliacijų trajektorijų analizei buvo sukurta nauja programinė įranga. Programos parašytos „Python“ programavimo kalba ir jos gali būti panaudojamos kitokių fizikinių procesų aprašymui. Darbe tirtos molekulės priklauso šešianarių heterociklinių junginių klasei – tokio tipo junginių yra daug. Šių junginių teoriniams tyrimams ankstesniuose darbuose buvo naudojami skirtingi teoriniai metodai, ir todėl buvo sunku palyginti tokių tyrimų rezultatus gautus skirtingose laboratorijose. Šiame darbe siekiant metodiškai palyginti šešianarių ciklų heterociklinių junginių energetines, struktūrines ir spektroskopines savybes, kai kurie iš jau anksčiau ištirtų molekulių struktūriniai ir energiniai parametrai buvo perskaičiuoti šiame darbe naudotais teoriniais metodais.

## MEDŽIAGOS IR METODAI

### EXPERIMENTINIAI METODAI

Tetrahidrofurano mėginys buvo įsigytas iš Sigma Aldrich (grynumas 99,9%). Azotas (99,995%), argonas (99,995%), neonas ir ksenonas iš Elme Messer Gaas buvo naudojami kaip matricinės dujos. Heterocikliniai junginiai, t.y. 1-metilgermacikloheksanas, 1-chloro1-chlorometilsilacikloheksanas, 1-chlorometil-1-fluoro-silacikloheksanas, 1-chlorometil-1-fluoro-silaciklopentanas ir 2,2,4,4,6,6-heksametil-1,3,5,2,4,6triazatrisilinas buvo neseniai susintetinti Guirgis grupės Čarlstono koledže (Charleston SC). Sintezės procedūra nėra įtraukta į disertacijoje aprašomus tyrimus.

Heterocikliniai junginiai buvo išvalomi vakuuminėje sistemoje juos užšaldant skysto azoto temperatūroje, atsiurbiant ir tada vėl atitirpinant. Visi matricinės izoliacijos bandiniai buvo paruošti vakuuminėje sistemoje su pastoviu tūriu (mišinio kameroje). Tiriamų junginių garai buvo sumaišyti su matricinėmis dujomis tam tikrais santykiais, kontroliuojant dujų slėgį dujų kameroje. Paruoštas analitės:matricos dujų mišinys buvo nusodinamas ant CsI

lango. Tetrahidrofuranui buvo naudojamas He kriostatas (Leybold-Heraeus RW2). Kitų junginių atveju naudotas naujas trijų ciklų šaldymo sistemos (Janis SHI4-1) kriostatas (veikimo temperatūra 3–300 K). Nusodinimo trukmė buvo parenkama priklausomai nuo naudojamo junginio, paprastai apie 1 valandą. Nusodinimo greitis buvo reguliuojamas prisukant adatinę sklendę nusodinimo linijoje. IR sugerties spektrai buvo registruojami iškart po nusodinimo ir po temperatūros reguliavimo proceso. Temperatūros nusodinimo ir reguliavimo metu buvo parenkamos priklausomai nuo naudojamų matricos dujų, atsižvelgiant į tai, kad pasiekus tam tikras temperatūras dėl neišvengiamų procesų gali būti pažeista kieta matricinio mišinio struktūra. Pavyzdžiui, gali įvykti analito molekulių klasterizacija ar greitas mišinio išgaravimas nuo nusodinto paviršiaus.

Matricinės izoliacijos eksperimentams buvo naudojamas infraraudonųjų spindulių spektrometras Bruker IFS 113 (Bruker Optik GmbH, Ettlingen, Vokietija) su 1 cm1 rezoliucija, KBr spinduliuotės dalikliu, šviesos šaltiniu – globaru ir MCT detektoriumi. Kiekvienai matavimo operacijai buvo vidutiniškai apdorojami 256 spektrai. Tie patys fono ir bandinių spektrai buvo matuojami tokiomis pačiomis sąlygomis.

Ramano sklaidos eksperimentai buvo atlikti naudojant Bruker MultiRAM FT-Raman spektrometrą (Bruker Optik GmbH, Ettlingen, Vokietija), naudojant Nd:YAG (1064 nm) lazerį kaip sužadinimo šaltinį ir germanio diodą, aušintą skystu azotu, kaip detektorį. Naudota lazerio galia – 1000 mW. Spektrai buvo matuojami su 4 cm1 rezoliucija ir vidutiniškai vieno matavimo metu buvo apdorota 1000 spektrų. Matavimo metu bandinys buvo uždareme stikliniame buteliuke skystoje būsenoje.

Pažeistojo visiško vidaus atspindžio technika (ATR) buvo naudojama gauti infraraudonųjų spindulių sugerties spektrus bandiniams skystoje būsenoje. Visi spektrai buvo užregistruoti naudojant Bruker Alpha spektrometrą su deimantine vieno atspindžio prizme, globaru kaip šviesos šaltiniu ir DTGS detektoriumi. Pasirinkta rezoliucija buvo 4 cm1, matavimo metu vidutiniškai buvo apdorota 256 spektrai.

## SKAIČIAVIMO METODAI

Visi statiniai skaičiavimai buvo atlikti naudojant ORCA 4.1.1 programinę įrangą. [207] Skaičiuotos energijos ir virpesiniai dažniai. Skaičiuojant heterociklinių junginių atveju buvo naudojamas tankio funkcionalo teorijos (DFT) metodas (DFT), su hibridine B3LYP [208] funkcija ir Dunning bazinius rinkinius (angl. Dunning's augmented triple zeta correlation consistent basis set) [209]. Gerai aprašyti nekovalentinės sąveikos buvo taikoma Grimme (DFTD3) dispersijos korekcija. [193, 210] Skaičiavimo parametrai potencinės energijos paviršiaus skenavimui ir konformerų konversijos barjerams buvo

aprašyti aukščiau. Skenuojant potencinės energijos paviršių, struktūros buvo optimizuojamos kiekviename skenavimo žingsnyje. Normaliosios virpesinės būsenos, gautos naudojant DFT/B3LYP/augccpVTZ metodą, buvo aprašytos naudojant Vipresinės būsenos automatinio svarbos nustatymo (angl. Vibrational Mode Automatic Relevance Determination, VMARD) metodą. Šis metodas yra Bayes Ridge regresijos variantas ir gerai įvertina pagrindines vidines koordinates. [211]

Tetrahidrofurano, 1-chloro-1-chlorometil-silacikloheksano ir 1-chlorometil-1-fluoro-silacikloheksano molekulėms buvo atliktos Car-Parrinello molekulinės dinamikos (CP-MD) simuliacijos, naudojant gradientinį Becke-Lee-Yang-Parr (BLYP) mainų-koreliacijos funkcionalą. [212,213] Izoliuotiems THF konformerams ( $C_2$  ir  $C_s$ ) buvo atlikti papildomi DFT plokščiųjų bangų (PW) skaičiavimai su 70 Ry riba ir kitais parametrais tokiais pačiais kaip ir molekulių dinamikos simuliacijose. Car-Parrinello molekulinės dinamikos (angl. Car-Parrinello molecular dynamics, CP-MD) simuliacijos buvo atlikta naudojant CPMD programinę įrangą [215] su žemiau išvardintais parametrais:

- standartiniai normos išlaikantys Troullier–Martins pseudopotencialai atomų branduolių aprašymui [216],
- Brillouin zonos aprašymas tik  $\Gamma$ -taške,
- empirinė D2 dispersijos korekcija pagal Grimme [192],
- kanoninis ansamblis (NVT), Nosé–Hoover grandinės termostatai [203, 217] branduoliniams laisvės laipsniams,
- fiktyvioji elektroninė masė nustatyta ties 400 a. v. vienetais,
- judėjimo lygtys integruotos 4 a.v. laiko žingsniu,
- temperatūra nustatyta ties 20 K THF ir 20, 50, 70 K 1-Cl-1-ClM-SiCP ir 1-ClM-1-F-SiCP molekulėms,
- molekulės dedamos į kubinę dėžę, kurios kraštinė yra 11,288 Å, kad imituotų vieną kubinę  $\alpha$ -fazę tūriniam azoto kristale [218],
- CP-MD simuliacijos trukmė tetrahidrofuranui: 50 ps (pusiausvyros procedūra), 100 ps (produkcijos fazė), o 1-chloro-1-chlorometilsilacikloheksanui ir 1-chlorometil-1-fluoro-silacikloheksanui: 50 ps (pusiausvyros procedūra) ir 50 ps (70 K), 100 ps (20, 50 K).

Izoliuotiems tetrahidrofurano  $C_2$  ir  $C_s$  konformerams atliktos papildomos Car-Parrinello molekulinės dinamikos (CP-MD) simuliacijos su 15.0 Å kraštinės ilgio kubais ir temperatūra 10 K temperatūra. Simuliacijų trukmė buvo 10 ps (pusiausvyros fazė) ir 80 ps (produkcijos fazė).

Anharmoniniai THF konformerų ir bandinyje įterptos THF molekulės virpesiniai dažniai buvo skaičiuojami naudojant dipolinių momentų autokoreliacijos funkcijos Furjė transformaciją (programinė įranga, sukurta Kohlmeyer [219]), gaunamą iš CP-MD simuliacijos ir toliau koreguojamą harmoniniu kvantų korekcijos faktoriumi. [220] Trajektorijos vizualizavimui buvo naudojamas VMD programinės įrangos paketas [221], o statinių skaičiavimų rezultatų vizualizavimui buvo naudojamos ChemCraft [222] ir Avogadro [223] programos.



## APPENDIX I: TABLES

Table 5: Spectroscopic bands obtained from THF at N matrix at 9K before and after annealing. Frequencies are given in  $\text{cm}^{-1}$ . The strength described with very strong (vs), strong (s), medium (m), weak (w) and very weak (vw) relative intensity description. [A1]

THF@N 9 K		THF@N 9 K ann	
Freq.	Strength	Freq.	Strength
2987.9	m	2987.8	m
2969.8	w	2970.2	w
2962.2	w	2963.6	w
2946.2	w	2946.2	w
2938.8	w	2938.6	w
2925.6	w	2925.4	w
2921.1	w	2920.4	w
2891.5	w	2890.9	w
2884.4	w	2884.0	w
2863.3	m	2863.5	m
2860.7	m	2860.4	m
2856.0	m	2856.0	m
2724.9	w	2723.9	w
2705.6	w	2705.6	w
2348.8	s	2348.9	m
2342.4	w	2344.7	w
2328.2	w	2328.2	w
2283.0	w	2283.1	w
1994.8	w	1994.8	w
1597.1	w	1596.9	w
1468.1	w	1468.1	w
1450.5	w	1456.6	w
1404.4	w	1404.3	w
1368.3	w	1368.8	w
1286.0	w	1286.1	w
1211.8	w	1211.1	w
1195.8	w	1195.3	w
1130.2	w	1130.2	w
1079.1	vw		
1077.4	vs	1077.4	vs
1073.1	m		
1041.8	w	1041.8	w
952.5	w		
954.8	w	955.0	w
936.8	w	937.0	w
926.6	s	926.7	s
916.8	w	916.9	w
903.2	w	903.3	m
898.9	w		
667.6	w		
662.2	m	662.2	m
648.3	w		
638.4	w	638.5	w
631.6	w	631.6	w

Table 6: Vibrational analysis of the tetrahydrofuran  $C_2$  and  $C_s$  conformers derived with the DFT/BLYP aug-cc-pVTZ calculations. [A1]

envelope ( $C_s$ )				twisted ( $C_2$ )			
mode nr	Freq	Int	description	mode nr	Freq	Int	description
1	52.8	0.0	Ring. def.	1	27.0	4.4	Ring. def.
2	262.0	6.9	Ring. def.	2	237.5	0.0	Ring. def.
3	625.4	5.1	Ring. def.	3	568.5	0.9	Ring. def.
4	635.9	0.2	Ring. def.	4	653.2	3.5	Ring. def.
5	775.5	6.6	Ring. def.	5	808.7	13.1	Ring. def.
6	837.8	8.0	$r_{CO}$	6	845.1	14.6	COC rocking
7	865.3	6.7	$\nu_{CC}$	7	852.8	17.3	$r_{CO}$
8	880.9	34.0	$\nu_{CO}$	8	875.8	6.0	$\nu_{CO}$
9	898.6	1.6	$\nu_{CO}$	9	889.3	6.2	$\nu_{CO}$
10	921.3	4.0	$\nu_{CO}$	10	942.4	0.6	$\nu_{CO}$
11	1009.5	4.4	$\nu_{CO}$	11	997.7	4.2	$\nu_{CO}$
12	1013.9	71.4	$\nu_{CO}$	12	1008.4	92.3	$\nu_{CO}$
13	1115.9	0.7	$r_{CC}$	13	1136.6	0.2	$r_{CC}$
14	1179.9	4.1	$w_{CC}$	14	1142.9	1.9	$t_{CC}$
15	1191.3	4.1	$t_{CC}$	15	1148.7	5.1	$t_{CC}$
16	1220.5	4.0	$r_{CC}$	16	1218.8	0.2	$t_{CC}$
17	1232.3	4.1	$w_{CC}$	17	1225.4	5.9	$t_{CC}$
18	1268.8	0.9	$t_{CC}$	18	1285.5	0.3	$t_{CC}$
19	1287.7	0.2	$w_{CC}$	19	1301.0	0.2	$w_{CC}$
20	1315.2	0.3	$w_{CC}$	20	1321.8	0.0	$w_{CC}$
21	1347.8	4.1	$w_{CC}$	21	1350.7	2.4	$w_{CC}$
22	1457.9	0.8	$s_{CC}$	22	1456.0	2.9	$s_{CC}$
23	1469.4	3.7	$s_{CC}$	23	1462.9	3.9	$s_{CC}$
24	1470.2	0.0	$s_{CC}$	24	1484.0	0.8	$s_{CC}$
25	1486.0	0.7	$s_{CC}$	25	1494.0	0.0	$s_{CC}$
26	2884.7	48.7	$\nu_{sym}(CH)$	26	2908.1	145.8	$\nu_{sym}(CH)$
27	2889.1	110.0	$\nu_{sym}(CH)$	27	2913.0	1.4	$\nu_{sym}(CH)$
28	2978.6	24.7	$\nu_{sym}(CH)$	28	2962.0	20.2	$\nu_{sym}(CH)$
29	2988.4	42.0	$\nu_{sym}(CH)$	29	2966.5	6.4	$\nu_{sym}(CH)$
30	3003.7	18.3	$\nu_{asym}(CH)$	30	2981.2	112.0	$\nu_{asym}(CH)$
31	3016.3	0.4	$\nu_{asym}(CH)$	31	2983.5	0.5	$\nu_{asym}(CH)$
32	3020.1	31.6	$\nu_{asym}(CH)$	32	3011.8	21.0	$\nu_{asym}(CH)$
33	3032.5	67.2	$\nu_{asym}(CH)$	33	3021.0	54.2	$\nu_{asym}(CH)$

Table 7: Parameters for the  ${}^2T_3$  *trans*,  ${}^2T_3$  *gauche-* and  ${}^2T_3$  *gauche+* energy minima structures of the 1-chloromethyl-1-fluoro-silacyclopentan. Relative energy of formation [kcal/mol], bonds lengths [Å] and ring dihedral angle [deg.] derived from the MP2/aug-cc-pVTZ and DFT/B3LYP/aug-cc-pVTZ methods. [A2]

structure		${}^2T_3$ <i>trans</i>		${}^2T_3$ <i>gauche-</i>		${}^2T_3$ <i>gauche+</i>	
		MP2	DFT	MP2	DFT	MP2	DFT
Rel. E [kcal/mol]		0	0	3.57	1.40	4.17	1.52
bonds length [Å]	1C-Heq	1.084	1.089	1.084	1.089	1.085	1.089
	1C-Hax	1.088	1.092	1.087	1.093	1.090	1.094
	2C-Hax	1.090	1.094	1.089	1.093	1.089	1.093
	2C-Heq	1.086	1.091	1.086	1.091	1.085	1.091
	3C-Heq	1.086	1.091	1.085	1.091	1.086	1.091
	3C-Hax	1.087	1.093	1.091	1.094	1.089	1.094
	4C-Hax	1.088	1.093	1.087	1.093	1.088	1.093
	4C-Heq	1.085	1.089	1.085	1.089	1.084	1.089
	CH <sub>2</sub> Cl Hg-	1.083	1.087			1.084	1.088
	CH <sub>2</sub> Cl Hg+	1.082	1.087	1.083	1.088		
	CH <sub>2</sub> Cl Ht			1.084	1.088	1.085	1.088
	5C-Cl	1.787	1.820	1.783	1.818	1.781	1.817
Si-F	1.621	1.627	1.614	1.622	1.616	1.62	
dih. angle [deg.]	C1-C2-C3-C4	-54.72	-48.93	-58.13	-49.25	-57.06	-49.29
	C2-C3-C4-Si	38.91	34.93	49.09	35.88	37.45	35.2
	C3-C4-Si-C1	-13.20	-11.76	-25.09	-12.84	-9.52	-11.82
	C4-Si-C1-C2	-14.96	-13.58	-4.49	-12.68	-19.82	-13.69
	Si-C1-C2-C3	40.02	36.21	34.10	35.77	44.62	36.47
	Cl-C-Si-F	-172.91	-175.77	71.43	70.98	-73.00	-66.58

Table 8: Intramolecular contacts formed in the  ${}^2T_3$  *trans*,  ${}^2T_3$  *gauche-* and  ${}^2T_3$  *gauche+* energy minima structures of the 1-chloromethyl-1-fluoro-silacyclopentan calculated with MP2/aug-cc-pVTZ and DFT/B3LYP/aug-cc-pVTZ method. [A2]

contact type		${}^2T_3$ <i>trans</i>		${}^2T_3$ <i>gauche-</i>		${}^2T_3$ <i>gauche+</i>	
		length [Å]		length [Å]		length [Å]	
		MP2	DFT	MP2	DFT	MP2	DFT
a	1C-Hax...F-Si	3.693	3.720	3.627	3.715	3.720	3.720
b	1C-Heq...F-Si	3.001	3.009	3.020	3.021	2.965	3.005
c	2C-Hax...F-Si	3.508	3.604	3.803	3.628	3.262	3.587
d	4C-Hax...F-Si	2.926	2.884	3.053	2.877	2.858	2.883
e	4C-Heq...F-Si	3.545	3.580	3.482	3.570	3.549	3.574
f	5C-Hg+...F-Si	3.117	3.028	2.943	2.992		
g	5C-Ht...F-Si			3.717	3.751	3.743	3.755
h	5C-Hg-...F-Si	3.209	3.099			3.007	3.027
A	1C-Hax...Cl-CH <sub>2</sub>	2.909	3.212	2.913	3.396		
B	1C-Heq...Cl-CH <sub>2</sub>			3.653	3.878		
C	3C-Hax...Cl-CH <sub>2</sub>	2.779	3.405				
D	4C-Heq...Cl-CH <sub>2</sub>	2.994	3.362			2.991	3.355
E	4C-Hax...Cl-CH <sub>2</sub>					3.988	4.282
F	5C-Hg+...Cl-CH <sub>2</sub>	2.352	2.376	2.348	2.373		
G	5C-Ht...Cl-CH <sub>2</sub>			2.350	2.373	2.351	2.372
H	5C-Hg-...Cl-CH <sub>2</sub>	2.350	2.375			2.351	2.373

Table 9: Calculated (B3LYP aug-cc-pVTZ) vibrational modes of the twisted trans conformer of 1-chloromethyl-1-fluoro-silacyclopentane molecule. Mode description:  $\rho$ -rocking,  $\omega$ -wagging,  $\tau$ -twisting,  $\delta$ -scissoring,  $\nu$ -stretching, def-ring deformation, dispersed-contributions lower than 10%.

Freq	IR Int.	Raman Act.	Dep. ratio	VMARD	description
3132	0.60	71.60	0.75	49.1S16 + 48.8S 17	5CH <sub>2</sub> vas
3097	14.00	126.70	0.38	51.2S1 + 23.0S2	1CH <sub>2</sub> vas
3095	17.00	51.80	0.48	51.4S12 + 18.5S11	4CH <sub>2</sub> vas
3077	7.00	163.40	0.07	44.7S17 + 44.6S16	5CH <sub>2</sub> vs
3070	40.40	58.60	0.72	24.5S6 + 20.0S8 + 18.1S9 + 15.9S5	2CH <sub>2</sub> vas, 3CH <sub>2</sub> vas
3065	39.90	212.40	0.14	29.4S8 + 27.8S6 + 11.1S9	2CH <sub>2</sub> vas, 3CH <sub>2</sub> vas
3040	10.80	68.30	0.28	56.1S2 + 25.8S1 + 18.1S6	1CH <sub>2</sub> vs, 2CH <sub>2</sub> vas
3030	17.20	67.70	0.44	38.2S11 + 19.9S8 + 15.8S12 + 14.3S9	3CH <sub>2</sub> vs, 4CH <sub>2</sub> vs
3026	14.70	73.90	0.20	28.8S9 + 20.6S11 + 16.1S8 + 12.8S5 + 12.1S6	2CH <sub>2</sub> vs, 3CH <sub>2</sub> vs, 4CH <sub>2</sub> vs,
3019	18.50	196.70	0.11	45.4S5 + 22.9S9 + 15.2S6	2CH <sub>2</sub> vs, 3CH <sub>2</sub> vs
1506	2.90	1.10	0.55	35.8S36 + 34.0S30	2CH <sub>2</sub> $\delta$ , 3CH <sub>2</sub> $\delta$
1499	5.20	8.70	0.74	38.3S30 + 35.5S36	2CH <sub>2</sub> $\delta$ , 3CH <sub>2</sub> $\delta$
1453	9.20	4.50	0.74	49.9S18	1CH <sub>2</sub> $\delta$
1446	10.30	4.00	0.75	54.0S42	4CH <sub>2</sub> $\delta$
1441	11.40	4.10	0.75	72.2S50	5CH <sub>2</sub> $\delta$
1354	0.60	1.20	0.71	12.9S38 + 12.4S34 + 11.6S31 + 9.3S24	2CH <sub>2</sub> $\omega$ , 3CH <sub>2</sub> $\omega$
1348	0.90	0.20	0.64	11.7S33 + 11.6S32 + 10.3S24	2CH <sub>2</sub> $\omega$ , 3CH <sub>2</sub> $\omega$
1290	1.60	3.00	0.74	dispersed	ring CH <sub>2</sub> $\tau$
1286	7.10	2.40	0.65	dispersed	ring CH <sub>2</sub> $\tau$
1227	0.10	1.60	0.07	dispersed	def., 1CH <sub>2</sub> $\tau$ , 4CH <sub>2</sub> $\tau$ , 2CH <sub>2</sub> $\rho$ , 3CH <sub>2</sub> $\rho$
1194	2.80	1.70	0.40	28.0S49 + 27.4S48 + 16.4S15 + 11.5S76 + 11.1S75	5CH <sub>2</sub> $\omega$ , Si-5C $\nu$
1185	4.30	1.90	0.73	dispersed	1CH <sub>2</sub> $\omega$ , 4CH <sub>2</sub> $\omega$ , 1CH <sub>2</sub> $\tau$ , 4CH <sub>2</sub> $\tau$ , Si-1C $\nu$ , Si-4C $\nu$
1106	34.10	2.20	0.49	dispersed	1CH <sub>2</sub> $\omega$ , 4CH <sub>2</sub> $\omega$ , 2CH <sub>2</sub> $\tau$ , 3CH <sub>2</sub> $\tau$ , Si-4C $\nu$
1106	11.40	1.20	0.60	13.5S93 + 11.8S68 + 11.1S32 + 10.2S33	ring CH <sub>2</sub> $\omega$ , 5CH <sub>2</sub> $\tau$
1052	14.50	0.30	0.49	dispersed	ring CH <sub>2</sub> $\tau$
1027	13.90	3.30	0.60	22.6S7 + 8.4S3 + 18.0S10	ring C-C $\nu$
957	0.90	2.90	0.75	14.9S3 + 14.1S10	ring C-C $\nu$ , def.
936	0.50	0.20	0.73	dispersed	1CH <sub>2</sub> $\tau$ , 4CH <sub>2</sub> $\tau$ , 2CH <sub>2</sub> $\rho$ , 3CH <sub>2</sub> $\rho$
875	27.20	0.90	0.67	12.2S3 + 10.5S10	ring C-C $\nu$ , def., Si-F $\nu$
864	130.10	2.70	0.44	30.8S14	Si-F $\nu$ , ring C-C $\nu$ , Si-4C $\nu$ , def.
852	13.10	9.80	0.06	20.8S7 + 17.4S10 + 16.3S3	Si-F $\nu$ , ring C-C $\nu$ , def.
816	77.60	0.50	0.68	20.6S14 + 15.9S15 + 13.4S4	Si-F $\nu$ , ring C-C $\nu$ , Si-4C $\nu$ , Si-1C $\nu$ , def.
779	44.00	3.20	0.32	25.5S15 + 17.7S13 + 12.1S14	Si-5C $\nu$ , Si-4C $\nu$
740	4.30	2.60	0.64	17.9S15 + 15.4S29 + 14.4S14 + 10.3S50	Si-5C $\nu$ , Si-F $\nu$
716	16.40	4.20	0.07	22.7S4 + 11.1S14	Si-1C $\nu$ , Si-F $\nu$ , def.
679	36.10	3.90	0.55	28.7S13 + 18.8S93 + 11.5S72 + 10.4S47	Si-5C $\nu$ , def.
659	14.90	3.90	0.25	20.6S4 + 15.6S13 + 10.9S48	Si-1C $\nu$ , Si-5C $\nu$ , def.
604	2.80	18.40	0.02	15.6S15 + 14.8S4 + 10.3S13	Si-1C $\nu$ , Si-4C $\nu$ , Si-5C $\nu$ , def.
501	3.50	0.80	0.75	12.9S4 + 10.7S41	Si-1C $\nu$ , Si-4C $\nu$ , def.
403	12.90	6.60	0.10	25.0S27 + 12.5S15 + 10.8S14	def., Si-5C $\nu$ , Si-F $\nu$

continuation on next page

continuation								
Freq	IR Int.	Raman Act.	Dep. ratio	VMARD			description	
287	7.90	0.40	0.72	21.5S29 + 17.6S14 + 15.9S46	+	19.4S28 + 10.1S14	+	def., Si-F $\nu$ , out of plane
278	3.50	0.40	0.58	24.6S45 + 20.8S45				def., Si-F $\nu$ , out of plane
252	6.40	0.50	0.62	24.8S67 + 14.5S93 + 10.5S85	+	20.1S92 + 11.4S28	+	def., out of plane
230	3.60	1.30	0.62	18.7S29 + 14.4S46	+	15.1S45	+	def.
167	1.20	0.50	0.74	20.8S94 + 17.5S39 + 10.3S66	+	19.0S47	+	def., out of plane
129	6.00	0.20	0.17	27.6S71 + 19.4S93 + 10.0S22	+	26.1S68	+	CH <sub>2</sub> Cl $\tau$
71	2.80	1.00	0.75	27.1 S85 + 17.6S72 + 11.6S67	+	26.2S92	+	def., out of plane
58	0.30	0.70	0.62					

Table 10: Experimental (FT-IR gas phase, Raman liquid, matrix isolation at argon and nitrogen matrices at 17K and after annealing to 35K) and computational (B3LYP/cc-pVTZ) frequencies and intensities (in parentheses) of 1-chloromethyl-1-fluoro-silacyclopentane molecule chair conformers. The intensity described with: s – strong, m – medium, w – weak, v – very, sh – shoulder, b – broad.

IR gas	experimental					computational		
	Ar	Ar ann	N	N ann	Raman	t	g-	g+
2957 w	2957 w	2957 vw	2963 vw	2963 vw		3097	3102	3101
						3095	3090	3094
2954 m	2953 w	2953 vw	2952 w	2952 w		3077		
						3070		
2949 m	2950 w	2950 vw	2949 w	2949 w			3066	
						3065	3065	3065
								3063
								3062
								3060
2913 vw b			2912 vw b	2921 vw		3040	3036	3037
				2901 vw			3032	
2877 vw b	2877 vw	2877 vw	2880 vw	2880 vw		3030		
	2868 vw	2868 vw				3026		3027
	2861 vw	2861 vw	2871 vw	2871 vw		3019	3022	3021
			sh	sh				3012
			2349 vw	2349 vw				3006
				sh				
	2344 vw b	2344 vw b		2345				
			2328 vw	2328 vw				
		1602 vw b		1608 vw				
		1599 vw b	1597 vw	1597 vw				
1460 vw	1465 vw	1465 vw	1465 vw	1465 vw	1460 m	1506	1507	1507
	1455 vw	1455 vw	1455 vw	1455 vw		1499	1498	1498
1406 vw			1438 vw	1438 vw				
			1420 vw	1420 vw				1453
	1416 vw	1416 vw	1416 vw	1416 vw	1418 m	1452	1452	
							1450	1451
	1407 vw	1407 vw	1407 vw	1407 vw	1409 m	1446		
	1404 vw	1404 vw	1404 vw	1404 vw	1398 w	1441		
	1397 vw	1397 vw	1397 vw	1397 vw			1432	
								1432
	1378 vw	1378 vw	1378 vw	1378 vw	1372 vw			
1310 vvw	1310 vw	1310 vw	1310 vw	1310 vw		1354	1349	1348
						1348	1345	1344

continuation on next page

continuation								
IR gas	experimental					computational		
	Ar	Ar ann	N	N ann	Raman	t	g-	g+
1257 w	1258 vw	1258 vw	1258 vw	1258 vw	1260 m	1290	1287	1286
	1255 vw	1255 vw	1255 vw	1255 vw	1252 w sh	1285	1282	1284
	1204 vw	1204 vw	1204 vw	1204 vw	1202 w			
	1196 vw	1196 vw	1196 vw	1196 vw			1222	1223
			1187 vw	1187 vw			1200	1201
			sh	sh				
1181 vw b	1181 vw	1181 vw	1182 vw	1182 vw		1194		
	1174 vw	1174 vw	1176 vw	1176 vw		1185	1182	1280
1161 vw	1160 vw	1160 vw	1160 vw	1161 vw	1161 w		1121	1120
			1109 vw		1107 vw			
1083 m b	1081 w	1081 m		1084 m	1084 w	1106		
			1082 m				1101	1101
1034 s	1032 w	1032 w	1033 w	1033 w		1052		
1030 vs	1025 w	1025 w	1026 w				1045	1045
1022 m sh	1022 w	1022 w	1022 m		1023 m			
	1019 w	1019 w	1019 w	1019 w	1015 w sh	1027	1027	1028
				1010 w				
				1006 w				
937 vw b	945 vw	945 vw	945 vw	945 vw	950 m	957	956	956
	930 vw	930 vw	926 vw	926 vw		925		
919 vw b	917 vw	917 vw	917 vw	917 vw				
899 m sh	906 vw	906 vw	903 vw				929	929
	892 w	892 w						
	889 w	889 w						
875 s			887 w	890 vw	884 vw		883	885
	873 vs	873 vs	874 sh			875		
			870 vs	870 vs				
862 w sh			862 m	862 s	854 s	862	864	865
				858 m sh				
			849	849		851	852	851
812 w	812 m	812 s	812 s	812 s	815 w	816	814	
			801 vw		805 w			802
			784 vw					792
778 w	778 w	778 m	778 m	778 m	782 w	778		
			760 vw		767 w		761	
727 vw b	727 w	727 w	727 w	727 w	728 w	740	731	
711 vw b	711 w	711 w	711 w	711 m	715 m	716	714	720
	702 wv	702 wv	702 wv					702
693 w b	692 vw sh	692 vw sh	692 vw sh	692 vw sh				694
687	687 w	687 m	687 m	687 m	688 m	678		
655 b	656 vw	656 vw	656 vw	656 vw	659 m	659	655	646
					607 s	607	590	609
					502 w	501	497	497
					429 w		431	424
					409 m	403		



Table 11: DFT/BLYP/aug-cc-pVDZ and MP2/aug-cc-pVDZ relative energies for 1-chloromethylo-1-fluoro-silacyclohexane (kcal/mol). Dipole moment [D], internal axes [a.u.] and C-H bond length (Å) for ring carbon hydrogens, numbering according to the carbon number (Fig. 1), ax – hydrogen in axial position, eq – hydrogen in equatorial position. [A3]

	Axial trans	Equatorial trans	Equatorial gauche	Axial gauche
Erel [kcal/mol]		0.33	0.92	1.08
Bonds lengths [Å]				
1 C-H ax	1.094	1.095	1.094	1.095
1 C-H eq	1.092	1.092	1.092	1.091
2 C-H ax	1.094	1.092	1.095	1.094
2 C-H eq	1.092	1.092	1.092	1.092
3 C-H ax	1.096	1.096	1.096	1.096
3 C-H eq	1.093	1.093	1.093	1.093
4 C-H ax	1.094	1.092	1.095	1.094
4 C-H eq	1.092	1.092	1.092	1.092
5 C-H ax	1.094	1.095	1.094	1.095
5 C-H eq	1.092	1.092	1.090	1.092
C (Met)-Yg+	1.088	1.088	1.088	1.088
C (Met)- Yg-	1.088	1.088	1.817	1.818
C (Met)- Yt	1.820	1.820	1.088	1.088
X-F	1.631	1.629	1.621	1.625
X-C (Met)	1.888	1.890	1.889	1.886
X-C1	1.865	1.869	1.871	1.865
C1-C2	1.543	1.543	1.545	1.543
C2-C3	1.535	1.534	1.534	1.535
C3-C4	1.535	1.534	1.534	1.535
C4-C5	1.543	1.544	1.544	1.544
C5-X	1.865	1.869	1.864	1.871
Dihedral angles values [deg.]				
C1-C2-C3-C4	-65.85	-66.44	-64.76	-65.3
C2-C3-C4-C5	65.81	66.37	65.47	65.6
C3-C4-C5-X	-53.34	-50.62	-54.92	-54.19
C4-C5-X-C1	41.57	35.96	44.05	42.95
C5-X-C1-C2	-41.62	-36.05	-43.63	-42.78
X-C1-C2-C3	53.43	50.77	53.79	53.82
Possible hydrogen bond distances [Å]				
a	3.00	3.73		3.02
b	3.15	3.05		3.12
c	3.15	3.05	3.85	3.10
d	3.00	3.72	3.10	3.01
e	4.16	3.28	3.24	3.35
f	3.20	2.88	2.98	3.68
g	4.16	3.28	3.24	
h	4.16	2.88	3.00	

Table 12: Experimental and calculated frequencies and intensities (in parentheses) of 1-chloromethyl-1-fluoro-silacyclohexane molecule and their vibrational assignment.

Ar matrix	experimental		calculated			assignment	
	Raman	ATR	axial trans	equatorial trans	axial gauche		equatorial gauche
			58.2	54.7	44.2	44.3	$\Gamma$ ( $\gamma$ C-Si-ring)
	68.5		66.7	79.0		79.7	C2Cl b.o.p. $\Gamma$ ( $\gamma$ C-Si-ring)
					92.2	88.5	
			123.1	111.0	97.11		C2Cl, SiF, CH <sub>2</sub> (ring) b.o.p.
			132.9	143.6	155.2	145.0	C2Cl, CH <sub>2</sub> (ring) b.i.p.
	160.0		185.9		191.6	191.2	C2Cl, CH <sub>2</sub> (ring) b.i.p.
	201.6		197.4			212.5	SiF, CH <sub>2</sub> (ring) b.i.p.
				217.0	220.8	217.8	SiF, CH <sub>2</sub> (ring) b.i.p.
	216.2			219.6			SiF, CH <sub>2</sub> (ring) b.i.p.
				232.4	246.6		C2Cl, SiF, CH <sub>2</sub> (ring) b.i.p.
	230.7		257.7			281.8	C2Cl, SiF, CH <sub>2</sub> (ring) b.o.p.
						(10)	
				249.2			C2Cl, SiF, CH <sub>2</sub> (ring) b.o.p.
	266.1		269.3		295.5		C2Cl, CH <sub>2</sub> (ring) b.i.p.
						338.9	C2Cl, CH <sub>2</sub> (ring) b.o.p.
						373.9	CH <sub>2</sub> (ring) b.o.p.
	299.4		337.8	339.8			CH <sub>2</sub> (ring) b.i.p.
					334.1		CH <sub>2</sub> (ring) b.o.p.
				342.3		383.9	CH <sub>2</sub> (ring) b.o.p.
	345.1		359.8		344.4		C2Cl, CH <sub>2</sub> (ring) b.i.p.
						491.4	CH <sub>2</sub> (ring) b.o.p.
	368.0		377.5	376.4			CH <sub>2</sub> (ring) b.i.p.
	388.8				375.9		CH <sub>2</sub> (ring) b.i.p.
	488.7	487.6	493.9	487.3	483.3	595.8	CH <sub>2</sub> (ring) b.o.p.
						642.0	C2Cl, CH <sub>2</sub> (ring) b.i.p.
	584.3	585.7	588.3	584.3			C2Cl, CH <sub>2</sub> (ring) b.o.p.
604.9	604.2	602.1			573.4		C2Cl, CH <sub>2</sub> (ring) b.o.p.
612.8	609.9	609.5	635.6				C2Cl, CH <sub>2</sub> (ring) b.i.p.
632.2	641.6			646.9	652.5		C2Cl, CH <sub>2</sub> (ring) b.i.p.
						651.1	CH <sub>2</sub> b.o.p.
651.7		655.1			666.3		$\nu$ C-Cl, CH <sub>2</sub> b.i.p.
661.8			669.5	666.9			$\nu$ C-Cl, CH <sub>2</sub> b.o.p.
674.3		671.6	682.4	685.1			CH <sub>2</sub> Cl, CH <sub>2</sub> (ring) b.i.p.
691.7	685.9	684.1			701.1	693.1	CH <sub>2</sub> Cl, CH <sub>2</sub> (ring) b.i.p.
755	750.5	753.1	755.9	747.5		758.0	CH <sub>2</sub> Cl, CH <sub>2</sub> (ring) b.o.p.
					749.2		CH <sub>2</sub> Cl, CH <sub>2</sub> (ring) b.i.p.
						761.1	$\rho$ CH <sub>2</sub> b.o.p.
770.5	768.7	768.3	777.0				$\nu$ Si-C, CH <sub>2</sub> b.i.p.
781.4		780.7			783.3		$\rho$ CH <sub>2</sub> (ring) b.i.p.
				798.5		793.6	$\nu$ Si-C, CH <sub>2</sub> b.o.p.
	797.1		805.1	808.4	804.0	805.2	$\nu$ Si-C, CH <sub>2</sub> (ring) b.o.p.
808.9		798.3	810.8	811.0	806.7		CH <sub>2</sub> Cl, CH <sub>2</sub> b.i.p.
835.2		845.4	825.2	819.2			CH <sub>2</sub> Cl, CH <sub>2</sub> b.o.p.
855.9		859.5					
875.9					843.7	843.7	$\nu$ Si-F, CH <sub>2</sub> b.o.p.
			869.9	868.8	863.8	865.2	CH <sub>2</sub> (ring) b.i.p.
			918.5	920.6	916.2	918.6	CH <sub>2</sub> (ring) b.i.p.
886.8	882.1						CH <sub>2</sub> (ring) b.o.p.
913.2			927.6	928.4	923.7	926.2	CH <sub>2</sub> (ring) b.i.p.
						(35)	
	907.1	910.0					CH <sub>2</sub> (ring) b.i.p.
				1004.2	997.7		CH <sub>2</sub> (ring) b.o.p.
993.4	994.5	990.8	1005.1		1019.5	1001.4	CH <sub>2</sub> (ring) b.o.p.
						(17)	
					1044.1		CH <sub>2</sub> (ring) b.o.p.
	1006.9		1021.7	1023.9		1021.3	CH <sub>2</sub> (ring) b.i.p.
						(3)	
						1050.1	CH <sub>2</sub> (ring) b.o.p.
1026.2			1051.6	1051.4			CH <sub>2</sub> (ring) b.i.p.
	1077.0	1078.8	1088.8		1091.8		C2Cl, CH <sub>2</sub> (ring) b.i.p.
						1092.1	C2Cl, CH <sub>2</sub> (ring) b.o.p.
				1095.3	1109.3		C2Cl, CH <sub>2</sub> (ring) b.i.p.
1092.8	1097.3		1095.9	1099.6			C2Cl, CH <sub>2</sub> (ring) b.i.p.

continuation on next page

continuation								
Ar matrix	Raman	ATR	axial trans	equatorial trans	axial gauche	equatorial gauche		assignment
					1113.9	1103.4		C2Cl. CH <sub>2</sub> (ring) b.o.p.
1103.3	1104.1	1101.4	1120.5	1119.9	1186.0	1117.4		C2Cl. CH <sub>2</sub> (ring) b.o.p.
		-19						C2Cl. CH <sub>2</sub> (ring) b.i.p.
1109.9								
1186.9	1183.8	1199.2	1180.3	1185.7	1200.6	1187.4		C2Cl b.i.p.
1201.2	1200.7	1199.2	1200.9	1204.6	1213.6	1202.5		CH <sub>2</sub> (ring) b.o.p.
1208.9			1222.2		1267.8	1218.1		CH <sub>2</sub> (ring) b.i.p.
				1222.6				CH <sub>2</sub> (ring) b.o.p.
					1288.6			CH <sub>2</sub> (ring) b.o.p.
1240.2			1273.5	1270.9		1272.1		CH <sub>2</sub> (ring) b.i.p.
1255.6	1255.0		1292.7	1291.9	1308.3	1291.8		CH <sub>2</sub> (ring) b.i.p.
1273.8	1271.9	1271	1314.1	1317.2	1351.7	1312.0		CH <sub>2</sub> (ring) b.o.p.
					1365.2			CH <sub>2</sub> (ring) b.o.p.
1299.4	1295.7	1294.9	1353.4	1354.0		1353.2		CH <sub>2</sub> (ring) b.i.p.
	1333.0		1366.8	1369.4	1365.8	1366.5		CH <sub>2</sub> (ring) b.i.p.
1348.7	1344.8	1343.5	1369.0	1372.2	1408.5	1368.7		vCC. CH <sub>2</sub> (ring) b.i.p.
1384.7			1409.2	1410.8	1422.6	1403.0		C2Cl. CH <sub>2</sub> (ring) b.o.p.
1402.8			1422.3	1423.1	1429.0	1421.6		CH <sub>2</sub> (ring) b.i.p.
1405.9	1404.2	1401.2	1423.5	1428.0	1471.7	1423.0		CH <sub>2</sub> (ring) b.o.p.
1448.9	1451.6	1447.6	1474.4	1473.8	1475.8	1474.3		CH <sub>2</sub> (ring) b.o.p.
1466.3	1463.9	1463.1	1475.4	1476.3	1485.8	1475.3		CH <sub>2</sub> (ring) b.i.p.
	1483.2		1486.0	1490.2		14784.7		CH <sub>2</sub> (ring) b.o.p.
	2656.6	2656.9	3008.0	3006.1	3007.3	3005.3		vasCH (ring)
	2675.0	2669.3	3016.6	3017.0	3009.8	3010.3		vasCH (ring)
			3019.0	3019.1	3015.7	3015.3		vasCH (ring)
			3024.4	3026.1	3021.4	3020.5		vasCH (ring)
	2728.4		3029.1	3027.9	3031.2	3021.9		vasCH (ring)
2795.7	2787.6	2789.0	3059.9	3063.6	3056.8	3061.3		vasCH (ring)
2811.5			3063.1	3065.0	3060.9	3063.9		vsCH (ring)
2868.1	2860.2	2858.4	3065.7	3068.0	3062.8	3067.6		vCH (ring)
2898.6	2889.4	2885.2	3078.3	3074.8	3071.4	3069.7		vCH (all)
2940.5	2932.7	2924.5	3080.3	3078.4	3074.0	3075.2		vasCH (ring)
2982.3	2977.0	2980	3082.2	3079.2	3094.7	3089.8		vCH (all)
2992.5			3145.1	3143.8	3134.8	3134.4		vasCH (CH <sub>2</sub> Cl)

Table 13: Structural and energetic properties of the 1-chloro-1-chloromethyl-silacyclohexane chair conformers obtained from MP2/aug-cc-pVTZ (DFT/B3LYP/aug-cc-pVTZ is vary) method (DFT in parenthesis if there is a variation from MP2). Relative energy [kcal/mol], C-H length [Å] and ring dihedral angle values [deg.]. [A4]

		<sup>1</sup> C <sub>4</sub> ax t	<sup>1</sup> C <sub>4</sub> eq t	<sup>1</sup> C <sub>4</sub> ax g-	<sup>1</sup> C <sub>4</sub> eq g-
Erel [kcal/mol]		0.00	1.04 (0.88)	1.39 (1.53)	1.65 (1.77)
C-H length [Å]	1C-Hax	1.095 (1.094)	1.095 (1.094)	1.096	1.094
	1C-Heq	1.092 (1.091)	1.092	1.091 (1.090)	1.092
	2C-Hax	1.094	1.092	1.094	1.095
	2C-Heq	1.092	1.092 (1.093)	1.092	1.092 (1.093)
	3C-Hax	1.096	1.096	1.096	1.095
	3C-Heq	1.092	1.092 (1.093)	1.092	1.092
	4C-Hax	1.094	1.092	1.094 (1.093)	1.095
	4C-Heq	1.092	1.092 (1.093)	1.092 (1.093)	1.092
	5C-Hax	1.095 (1.094)	1.095 (1.094)	1.096	1.094 (1.093)
	5C-Heq	1.092 (1.091)	1.092	1.092 (1.091)	1.091 (1.090)
	CH <sub>2</sub> Cl Hg-	1.088 (1.087)	1.088 (1.087)		
	CH <sub>2</sub> Cl Hg+	1.088 (1.087)	1.088 (1.087)	1.088	1.089
CH <sub>2</sub> Cl Ht			1.089	1.089	
dih. angle [deg.]	C1-C2-C3-C4	-67.26 (-65.72)	-68.15 (-64.84)	-66.72 (-65.29)	-66.14 (-66.54)
	C2-C3-C4-C5	67.26 (65.73)	68.15 (65.58)	66.99 (65.44)	67.11 (66.45)
	C3-C4-C5-Si	-55.30 (-53.81)	-52.27 (-55.45)	-55.80 (-54.39)	-56.94 (-51.47)
	C4-C5-Si-C1	44.02 (42.33)	37.54 (44.75)	44.92 (43.37)	46.35 (37.41)
	C5-Si-C1-C2	-44.09 (-42.35)	-37.54 (-44.30)	-44.77 (-43.28)	-45.70 (-37.49)
	Si-C1-C2-C3	55.30 (53.82)	52.27 (54.27)	55.46 (54.22)	55.35 (51.63)

Table 14: 1-chloro-1-chloromethyl-silacyclohexane hydrogen bonds lengths [ $\text{\AA}$ ] formed in the  ${}^1\text{C}_4$  axial trans,  ${}^1\text{C}_4$  equatorial trans,  ${}^1\text{C}_4$  axial gauche and  ${}^1\text{C}_4$  equatorial gauche conformers calculated with MP2/aug-cc-pVTZ and DFT/B3LYP/aug-cc-pVTZ method (DFT in parenthesis if there is a variation from MP2). [A4]

		${}^1\text{C}_4$ axial trans	${}^1\text{C}_4$ axial gauche
contact type		H-bond length [ $\text{\AA}$ ]	H-bond length [ $\text{\AA}$ ]
a	1C-Heq...Cl-Si	3.305 (3.312)	3.311 (3.321)
b	2C-Hax...Cl-Si	3.219 (3.319)	3.196 (3.287)
c	4C-Hax...Cl-Si	3.219 (3.318)	3.180 (3.274)
d	5C-Heq...Cl-Si	3.305 (3.312)	3.307 (3.314)
e	1C-Heq...Cl-CH <sub>2</sub>	4.096 (4.153)	3.282 (3.350)
f	1C-Hax...Cl-CH <sub>2</sub>	3.172 (3.199)	3.706 (3.680)
g	5C-Heq...Cl-CH <sub>2</sub>	4.096 (4.153)	
h	5C-Hax...Cl-CH <sub>2</sub>	3.172 (3.198)	
A	1C-Heq...Cl-CH <sub>2</sub>	3.717 (3.754)	
B	2C-Hax...Cl-CH <sub>2</sub>	2.957 (3.022)	
C	4C-Hax...Cl-CH <sub>2</sub>	2.957 (3.017)	
D	5C-Heq...Cl-CH <sub>2</sub>	3.717 (3.741)	3.066 (3.109)
E	1C-Heq...Cl-Si	3.593 (3.608)	3.541 (3.560)
F	1C-Hax...Cl-Si	3.181 (3.190)	3.312 (3.290)
G	5C-Heq...Cl-Si	3.593 (3.610)	3.532 (3.557)
H	5C-Hax...Cl-Si	3.181 (3.189)	3.323 (3.301)

Table 15: Structural and energetic properties of the 1-methylgermacyclohexane chair conformers obtained from MP2/aug-cc-pVTZ (DFT/B3LYP/aug-cc-pVTZ is vary) method (DFT in parenthesis if there is a variation from MP2). Relative energy [kcal/mol], C-H length [Å] and ring dihedral angle values. [A5]

		<sup>1</sup> C <sub>4ax</sub>		<sup>1</sup> C <sub>4eq</sub>	
		DFT	MP2	DFT	MP2
Erel [kcal/mol]		0.00	0.00	0.04	1.36
C-H length [Å]	1C-Hax	1.093	1.088	1.093	1.089
	1C-Heq	1.091	1.087	1.091	1.086
	2C-Hax	1.095	1.091	1.095	1.091
	2C-Heq	1.094	1.089	1.094	1.089
	3C-Hax	1.096	1.092	1.094	1.092
	3C-Heq	1.093	1.088	1.093	1.088
	4C-Hax	1.095	1.091	1.095	1.091
	4C-Heq	1.094	1.089	1.094	1.089
	5C-Hax	1.093	1.088	1.093	1.089
	5C-Heq	1.091	1.087	1.091	1.086
	CH <sub>3</sub> Hg-	1.090	1.088	1.090	1.085
	CH <sub>3</sub> Hg+	1.090	1.086	1.090	1.085
	CH <sub>3</sub> Ht	1.090	1.085	1.090	1.086
dih. angle [deg.]	C1-C2-C3-C4	-67.66	-70.73	-67.46	-70.63
	C2-C3-C4-C5	67.67	70.73	67.42	70.63
	C3-C4-C5-Ge	-55.67	-60.32	-55.37	-59.65
	C4-C5-Ge-C1	42.81	50.19	42.44	48.44
	C5-Ge-C1-C2	-42.82	-50.19	-42.49	-48.44
	Ge-C1-C2-C3	55.66	60.32	55.45	59.65

Table 16: Parameters of the chair conformers of 1-chloro-1-chloromethyl-germacyclohexane, 1-chloro-1-chloromethyl-silacyclohexane and 1-chloro-1-chloromethyl-cyclohexane. Relative energies [kcal/mol], bonds lengths [Å], ring dihedral angle values [deg.] and distances of the atoms which may form weak hydrogen bonds [Å] calculated with DFT/B3LYP/aug-cc-pVTZ method. Y – atom attached to the C in the chloromethyl group, X – heteroatom (Si, Ge or C).

Erel [kcal/mol]	CIM-Cl-GeCH				CIM-Cl-SiCH				CIM-Cl-CP			
	Caxt	Ceqt	Caxg	Ceqg	Caxt	Ceqt	Caxg	Ceqg	Caxt	Caxg	Ceqg	Ceqt
	0	0.64	1.58	2	0	0.88	1.53	1.77	0	1.63	2.51	4.23
Bonds lengths [Å]												
1 C-H ax	1.093	1.091	1.093	1.091	1.094	1.094	1.096	1.094	1.093	1.096	1.091	1.091
1 C-H eq	1.089	1.09	1.088	1.09	1.091	1.092	1.09	1.092	1.091	1.088	1.091	1.091
2 C-H ax	1.093	1.093	1.093	1.095	1.094	1.092	1.094	1.095	1.092	1.092	1.093	1.089
2 C-H eq	1.093	1.093	1.093	1.093	1.092	1.093	1.092	1.093	1.091	1.091	1.091	1.092
3 C-H ax	1.096	1.096	1.096	1.095	1.096	1.096	1.096	1.095	1.095	1.096	1.095	1.095
3 C-H eq	1.092	1.092	1.092	1.092	1.092	1.093	1.092	1.092	1.092	1.092	1.092	1.092
4 C-H ax	1.093	1.093	1.093	1.095	1.094	1.092	1.093	1.095	1.092	1.091	1.093	1.089
4 C-H eq	1.093	1.093	1.093	1.093	1.092	1.093	1.093	1.092	1.091	1.091	1.091	1.092
5 C-H ax	1.092	1.091	1.094	1.091	1.094	1.094	1.096	1.093	1.093	1.095	1.091	1.091
5 C-H eq	1.089	1.09	1.089	1.088	1.091	1.092	1.091	1.09	1.091	1.09	1.088	1.091
C (CIM)-Yg+	1.085	1.086	1.085	1.086	1.087	1.087	1.088	1.089	1.085	1.085	1.085	1.084
C (CIM)- Yg-	1.085	1.086	1.809	1.808	1.087	1.087	1.813	1.813	1.085	1.805	1.805	1.084
C (CIM)- Yt	1.815	1.816	1.087	1.087	1.818	1.821	1.089	1.089	1.818	1.088	1.085	1.821
X-Cl	2.207	2.203	2.199	2.192	2.102	2.098	2.092	2.084	1.861	1.846	1.842	1.869
X-C (CIM)	1.972	1.974	1.974	1.979	1.888	1.892	1.889	1.893	1.524	1.521	1.523	1.528
X-C1	1.956	1.959	1.954	1.962	1.869	1.873	1.869	1.876	1.526	1.528	1.535	1.531
C1-C2	1.537	1.539	1.536	1.539	1.542	1.543	1.541	1.544	1.528	1.528	1.535	1.535
C2-C3	1.536	1.535	1.536	1.536	1.535	1.534	1.535	1.535	1.529	1.529	1.53	1.529
C3-C4	1.536	1.536	1.536	1.536	1.535	1.534	1.535	1.535	1.53	1.529	1.53	1.529
C4-C5	1.537	1.539	1.537	1.538	1.542	1.543	1.542	1.543	1.528	1.529	1.532	1.535
C5-X	1.956	1.959	1.962	1.954	1.869	1.873	1.875	1.867	1.526	1.535	1.527	1.531
Dihedral angles values [deg.]												
C1-C2-C3-C4	-69	-70	-69	-68	-66	-65	-65	-67	-55	-55	-53	-56
C2-C3-C4-C5	69	70	69	68	66	66	65	66	55	55	55	56
C3-C4-C5-X	-53	-52	-54	-55	-54	-55	-54	-51	-53	-54	-56	-52
C4-C5-X-C1	39	36	40	42	42	45	43	37	50	51	55	48
C5-X-C1-C2	-39	-36	-40	-42	-42	-44	-43	-37	-50	-51	-54	-48
X-C1-C2-C3	53	52	54	54	54	54	54	52	53	53	53	52
Possible hydrogen bonds lengths [Å]												
a	3.40	3.82	3.41		3.31	3.75	3.32		2.86	2.88		3.51
b	3.41	3.17	3.36		3.32	3.02	3.29		2.88	2.87		2.72
c	3.41	3.16	3.34	3.77	3.32	3.02	3.27		2.88	2.86	3.42	2.72
d	3.40	3.81	3.40	3.11	3.31	3.74	3.31	3.11	2.86	2.86	2.72	3.50
e	4.31	3.77	3.44	3.73	4.15	3.61	3.35	3.56	3.62	2.79	2.93	2.99
f	3.36	3.30	3.67	3.39	3.20	3.19	3.68	3.29	2.77	3.38	2.77	2.70
g	4.31	3.78		3.73	4.15	3.61		3.56	3.62		2.93	2.99
h	3.36	3.30		3.39	3.20	3.19		3.30	2.77		2.79	2.70

Table 17: Parameters of the chair conformers of 1-chloromethyl-1-fluoro-germacyclohexane, 1-chloromethyl-1-fluoro -silacyclohexane and 1-chloromethyl-1-fluoro -cyclohexane. Relative energies [kcal/mol], bonds lengths [Å], ring dihedral angle values [deg.] and distances of the atoms which may form weak hydrogen bonds [Å] calculated with DFT/B3LYP/aug-cc-pVTZ method. Y – atom attached to the C in the chloromethyl group, X – heteroatom (Si, Ge or C).

	CIM-F-GeCH				CIM-F-SiCH				CIM-F-CP			
	Caxt	Ceqt	Caxg	Ceqg	Caxt	Ceqt	Caxg	Ceqg	Caxt	Caxg	Ceqg	Ceqt

continuation on next page

continuation												
Erel	0	0.18	1.32	1.51	0	0.33	0.92	1.08	0	0.77	1.2	3.16
[kcal/mol]												
Bonds lengths [Å]												
1 C-H ax	1.092	1.092	1.093	1.092	1.094	1.095	1.094	1.095	1.092	1.094	1.092	1.092
1 C-H eq	1.09	1.09	1.089	1.09	1.092	1.092	1.092	1.091	1.092	1.089	1.092	1.092
2 C-H ax	1.094	1.093	1.094	1.095	1.094	1.092	1.095	1.094	1.092	1.092	1.094	1.09
2 C-H eq	1.093	1.093	1.093	1.093	1.092	1.092	1.092	1.091	1.091	1.091	1.091	1.091
3 C-H ax	1.096	1.096	1.096	1.096	1.096	1.096	1.096	1.096	1.096	1.096	1.095	1.095
3 C-H eq	1.092	1.093	1.092	1.093	1.093	1.093	1.093	1.093	1.092	1.092	1.092	1.092
4 C-H ax	1.094	1.093	1.093	1.095	1.094	1.092	1.095	1.094	1.092	1.092	1.094	1.09
4 C-H eq	1.093	1.093	1.093	1.093	1.092	1.092	1.092	1.092	1.091	1.091	1.091	1.091
5 C-H ax	1.092	1.092	1.093	1.092	1.094	1.095	1.094	1.095	1.092	1.093	1.092	1.092
5 C-H eq	1.09	1.09	1.09	1.088	1.092	1.092	1.09	1.092	1.092	1.092	1.088	1.092
C (Met)-Yg+	1.086	1.086	1.086	1.087	1.088	1.088	1.088	1.088	1.086	1.086	1.086	1.086
C (Met)- Yg-	1.086	1.086	1.812	1.81	1.088	1.088	1.817	1.818	1.086	1.808	1.807	1.086
C (Met)- Yt	1.815	1.818	1.087	1.087	1.82	1.82	1.088	1.088	1.807	1.086	1.084	1.809
X-F	1.773	1.771	1.768	1.764	1.631	1.629	1.621	1.625	1.427	1.416	1.413	1.43
X-C (Met)	1.971	1.972	1.972	1.977	1.888	1.89	1.889	1.886	1.525	1.519	1.521	1.529
X-C1	1.953	1.956	1.951	1.959	1.865	1.869	1.871	1.865	1.523	1.525	1.531	1.527
C1-C2	1.539	1.54	1.538	1.54	1.543	1.543	1.545	1.543	1.53	1.529	1.533	1.533
C2-C3	1.536	1.536	1.536	1.536	1.535	1.534	1.534	1.535	1.529	1.529	1.53	1.529
C3-C4	1.536	1.536	1.536	1.536	1.535	1.534	1.534	1.535	1.53	1.529	1.53	1.529
C4-C5	1.539	1.539	1.539	1.539	1.543	1.544	1.544	1.544	1.53	1.53	1.531	1.533
C5-X	1.953	1.956	1.959	1.951	1.865	1.869	1.864	1.871	1.522	1.531	1.523	1.527
Dihedral angles values [deg.]												
C1-C2-C3-C4	-70	-70	-69	-68	-66	-66	-65	-65	-56	-55	-53	-56
C2-C3-C4-C5	69	70	69	68	66	66	65	66	56	56	55	56
C3-C4-C5-X	-52	-51	-53	-54	-53	-51	-55	-54	-54	-55	-56	-52
C4-C5-X-C1	37	34	38	41	42	36	44	43	52	53	54	47
C5-X-C1-C2	-37	-34	-38	-41	-42	-36	-44	-43	-52	-53	-53	-47
X-C1-C2-C3	52	51	52	54	53	51	54	54	54	54	53	52
Possible hydrogen bonds lengths [Å]												
a	3.11	3.80	3.12		3.00	3.73		3.02	2.58	2.60		3.48
b	3.27	3.23	3.22		3.15	3.05		3.12	2.67	2.66		2.78
c	3.27	3.22	3.19	3.74	3.15	3.05	3.85	3.10	2.66	2.64	3.49	2.77
d	3.11	3.79	3.10	3.09	3.00	3.72	3.10	3.01	2.58	2.59	2.71	3.48
e	4.34	3.47	3.44	3.42	4.16	3.28	3.24	3.35	3.61	2.76	2.66	2.71
f	3.38	2.99	3.63	3.07	3.20	2.88	2.98	3.68	2.84	3.45	2.48	2.40
g	4.34	3.46		3.43	4.16	3.28	3.24		3.60		2.65	2.71
h	3.38	2.98		3.07	4.16	2.88	3.00		2.84		2.50	2.40

Table 18: Parameters of the chair conformers of 1-chloromethyl-germacyclohexane, 1-chloromethyl-silacyclohexane and 1-chloromethyl-cyclohexane, Relative energies [kcal/mol], bonds lengths [Å], ring dihedral angle values [deg.] and distances of the atoms which may form weak hydrogen bonds [Å] calculated with DFT/B3LYP/aug-cc-pVTZ method, Y – atom attached to the C in the chloromethyl group, X – heteroatom (Si, Ge or C).

Erel [kcal/mol]	CIM-GeCH				CIM-SiCH				CIM-CP			
	Ceqt	Caxt	Caxg	Ceqg	Ceqt	Caxg	Caxt	Ceqg	Ceqt	Caxg	Caxt	Ceqg
	0	0.17	0.2	0.66	0	0.31	0.47	0.6	0	0.21	1.54	4.08
Bonds lengths [Å]												
1 C-H ax	1.092	1.093	1.092	1.093	1.094	1.095	1.095	1.095	1.096	1.093	1.094	1.094
1 C-H eq	1.09	1.091	1.091	1.089	1.092	1.092	1.092	1.091	1.09	1.093	1.093	1.093
2 C-H ax	1.09	1.092	1.095	1.095	1.095	1.095	1.092	1.095	1.095	1.095	1.094	1.09
2 C-H eq	1.093	1.094	1.093	1.093	1.093	1.093	1.093	1.093	1.092	1.092	1.092	1.092
3 C-H ax	1.096	1.096	1.096	1.096	1.095	1.096	1.096	1.096	1.096	1.095	1.096	1.096
3 C-H eq	1.093	1.093	1.093	1.093	1.093	1.093	1.093	1.093	1.092	1.092	1.092	1.092
4 C-H ax	1.095	1.092	1.095	1.095	1.095	1.095	1.092	1.095	1.095	1.095	1.094	1.09
4 C-H eq	1.093	1.094	1.093	1.094	1.093	1.093	1.093	1.093	1.092	1.092	1.092	1.092
5 C-H ax	1.092	1.093	1.092	1.093	1.094	1.094	1.095	1.095	1.096	1.093	1.094	1.094
5 C-H eq	1.09	1.091	1.089	1.09	1.092	1.091	1.092	1.092	1.093	1.093	1.09	1.093
C (Met)-Yg+	1.086	1.087	1.086	1.086	1.088	1.088	1.088	1.088	1.087	1.087	1.087	1.087
C (Met)- Yg-	1.086	1.087	1.816	1.817	1.088	1.82	1.088	1.821	1.82	1.087	1.819	1.087
C (Met)- Yt	1.817	1.818	1.086	1.087	1.822	1.087	1.822	1.088	1.088	1.823	1.085	1.826
X-F	1.549	1.548	1.54	1.542	1.493	1.486	1.492	1.488	1.095	1.1	1.092	1.098
X-C (Met)	1.983	1.985	1.984	1.98	1.898	1.9	1.9	1.896	1.518	1.519	1.523	1.522
X-C1	1.967	1.97	1.974	1.966	1.88	1.887	1.883	1.88	1.532	1.532	1.541	1.54
C1-C2	1.537	1.537	1.537	1.536	1.541	1.542	1.542	1.541	1.529	1.53	1.541	1.532
C2-C3	1.535	1.535	1.535	1.535	1.535	1.534	1.534	1.534	1.53	1.53	1.533	1.529
C3-C4	1.535	1.535	1.535	1.535	1.534	1.535	1.534	1.534	1.53	1.53	1.531	1.53
C4-C5	1.537	1.537	1.536	1.537	1.541	1.541	1.542	1.542	1.53	1.53	1.531	1.532
C5-X	1.967	1.97	1.966	1.974	1.879	1.88	1.883	1.886	1.537	1.532	1.536	1.54
Dihedral angles values [deg.]												
C1-C2-C3-C4	-68	-70	-68	-68	-65	-65	-67	-65	-54	-55	-54	-56
C2-C3-C4-C5	68	69	68	68	65	65	66	65	54	55	55	56
C3-C4-C5-X	-54	-52	-55	-55	-55	-55	-51	-55	-55	-55	-55	-52
C4-C5-X-C1	41	35	42	42	43	44	37	45	55	55	53	46
C5-X-C1-C2	-41	-35	-41	-42	-43	-43	-37	-44	-55	-55	-53	-46
X-C1-C2-C3	54	52	54	55	55	54	52	55	55	55	54	52
Possible hydrogen bonds lengths [Å]												
a		3.82					3.77					3.50
b		3.06					3.00					2.77
c		3.05	3.96				3.96	3.00			3.74	2.77
d		3.81	3.21				3.18	3.76			2.81	3.49
e												
f	4.29			3.54	4.16				3.41	2.84	3.60	
g	3.22			3.78	3.17				3.78	3.62	2.86	
h	4.28				4.16						3.60	



Table 19: Parameters of the chair conformers of monosubstituted (with - Cl and -F) germacyclohexane, silacyclohexane and cyclohexane, Relative energies [kcal/mol], bonds lengths [Å], ring dihedral angle values [deg.] and distances of the atoms which may form weak hydrogen bonds [Å] calculated with DFT/B3LYP/aug-cc-pVTZ method, Where X indicates heteroatom (Si, Ge or C).

Erel [kcal/mol]	Cl						F					
	Si		Ge		C		Si		Ge		C	
	Cax	Ceq	Cax	Ceq	Ceq	Cax	Cax	Ceq	Cax	Ceq	Ceq	Cax
	0	0.59	0	0.95	0	0.3	0	0.21	0	0.66	0	0.27
	Bonds lengths [Å]											
1 C-H ax	1.096	1.094	1.094	1.092	1.093	1.096	1.095	1.094	1.094	1.092	1.093	1.094
1 C-H eq	1.091	1.091	1.089	1.089	1.09	1.09	1.092	1.091	1.09	1.089	1.091	1.091
2 C-H ax	1.093	1.095	1.093	1.095	1.095	1.092	1.094	1.095	1.093	1.095	1.095	1.091
2 C-H eq	1.093	1.093	1.093	1.093	1.091	1.091	1.093	1.092	1.093	1.093	1.091	1.092
3 C-H ax	1.096	1.095	1.096	1.095	1.095	1.096	1.096	1.096	1.096	1.096	1.095	1.096
3 C-H eq	1.092	1.093	1.092	1.092	1.092	1.092	1.093	1.093	1.092	1.093	1.092	1.092
4 C-H ax	1.093	1.095	1.093	1.095	1.095	1.092	1.094	1.095	1.093	1.095	1.095	1.092
4 C-H eq	1.093	1.093	1.093	1.093	1.091	1.091	1.093	1.092	1.093	1.093	1.091	1.092
5 C-H ax	1.096	1.094	1.094	1.091	1.093	1.096	1.095	1.094	1.094	1.092	1.093	1.094
5 C-H eq	1.091	1.091	1.089	1.089	1.09	1.09	1.092	1.091	1.09	1.089	1.091	1.091
X-ax	2.098	2.091	2.204	2.195	1.831	1.843	1.629	1.624	1.77	1.766	1.41	1.417
X-eq	1.483	1.484	1.537	1.54	1.089	1.086	1.484	1.485	1.539	1.541	1.095	1.092
X-C1	1.874	1.873	1.96	1.962	1.52	1.523	1.871	1.87	1.957	1.958	1.517	1.52
C1-C2	1.541	1.543	1.536	1.538	1.534	1.529	1.542	1.544	1.538	1.539	1.533	1.531
C2-C3	1.535	1.534	1.536	1.536	1.53	1.531	1.535	1.534	1.536	1.536	1.531	1.531
C3-C4	1.535	1.535	1.536	1.536	1.53	1.531	1.535	1.534	1.536	1.536	1.531	1.531
C4-C5	1.541	1.543	1.536	1.538	1.534	1.529	1.542	1.544	1.538	1.539	1.533	1.531
C5-X	1.874	1.873	1.96	1.962	1.52	1.523	1.871	1.87	1.957	1.958	1.517	1.52
	Dihedral angles values [deg.]											
C1-C2-C3-C4	-65	-65	-68	-68	-55	-55	-65	-65	-69	-69	-54	-55
C2-C3-C4-C5	65	65	68	68	55	55	65	65	69	68	55	55
C3-C4-C5-X	-54	-56	-54	-55	-55	-53	-54	-55	-53	-54	-55	-53
C4-C5-X-C1	43	46	41	42	57	51	43	46	39	40	56	52
C5-X-C1-C2	-43	-46	-41	-42	-57	-51	-43	-46	-39	-40	-56	-52
X-C1-C2-C3	54	56	54	55	55	53	54	55	53	54	55	53
	Possible hydrogen bonds lengths [Å]											
a	3.32		3.41			2.88	3.02		3.11			2.58
b	3.27		3.29			2.92	3.12		3.16			2.72
c	3.27		3.29			2.92	3.12		3.16			2.72
d	3.32		3.41			2.87	3.02		3.11			2.58
e		3.56		3.73	2.91			3.24		3.43	2.64	
f		3.31		3.35	2.90			3.01		3.03	2.59	
g		3.56		3.73	2.91			3.24		3.42	2.64	
h		3.31		3.35	2.90			3.01		3.02	2.59	

Table 20: Parameters of the chair conformers of monosubstituted 1-methyl-germacyclohexane, 1-methyl-silacyclohexane and 1-methyl-cyclohexane. Relative energies [kcal/mol], bonds lengths [ $\text{\AA}$ ], ring dihedral angle values [deg.] and distances of the atoms which may form weak hydrogen bonds [ $\text{\AA}$ ] calculated with DFT/B3LYP/aug-cc-pVTZ method. Where X indicates heteroatom (Si, Ge or C).

	-CH <sub>3</sub>					
	Si		Ge		C	
	Ceq	Cax	Cax	Ceq	Ceq	Cax
Erel [kcal/mol]	0	0.13	0	0.04	0	1.77
	Bonds lengths [ $\text{\AA}$ ]					
1 C-H ax	1.095	1.094	1.093	1.091	1.096	1.095
1 C-H eq	1.092	1.092	1.091	1.094	1.093	1.093
2 C-H ax	1.095	1.095	1.095	1.095	1.095	1.094
2 C-H eq	1.093	1.093	1.094	1.094	1.092	1.092
3 C-H ax	1.096	1.096	1.096	1.096	1.096	1.096
3 C-H eq	1.093	1.093	1.093	1.093	1.092	1.092
4 C-H ax	1.095	1.095	1.095	1.095	1.095	1.094
4 C-H eq	1.093	1.093	1.094	1.094	1.092	1.092
5 C-H ax	1.095	1.094	1.093	1.094	1.096	1.095
5 C-H eq	1.092	1.092	1.091	1.091	1.093	1.093
C (Met)-Hg+	1.092	1.091	1.09	1.09	1.092	1.092
C (Met)- Hg-	1.092	1.091	1.09	1.09	1.092	1.092
C (Met)- Ht	1.092	1.091	1.09	1.09	1.093	1.09
X-ax	1.494	1.491	1.546	1.55	1.097	1.094
X-eq	1.881	1.885	1.972	1.966	1.525	1.531
X-C1	1.887	1.889	1.974	1.974	1.533	1.538
C1-C2	1.54	1.541	1.536	1.536	1.53	1.531
C2-C3	1.534	1.534	1.535	1.535	1.53	1.531
C3-C4	1.534	1.535	1.535	1.535	1.53	1.531
C4-C5	1.54	1.541	1.536	1.536	1.53	1.531
C5-X	1.887	1.889	1.974	1.974	1.533	1.538
	Dihedral angles values [deg.]					
C1-C2-C3-C4	-65	-65	-68	-68	-54	-54
C2-C3-C4-C5	65	65	68	68	54	54
C3-C4-C5-X	-55	-56	-56	-55	-55	-55
C4-C5-X-C1	45	45	43	42	54	54
C5-X-C1-C2	-45	-45	-43	-42	-54	-54
X-C1-C2-C3	55	56	56	55	55	55

## BIBLIOGRAPHY

- [1] B. Thiemer, J. Andreesen, T. Schraeder, Cloning and characterization of a gene cluster involved in tetrahydrofuran degradation in pseudonocardia sp. strain, *Arch.Microbiol.* **179**, 266–277 (2003).
- [2] Y. Aoki, A preparation method of thermoreversible poly(vinyl chloride) gels, *Macromolecules* **34**, 3500 (2001).
- [3] N. Werawattanachai, P. Towiwat, S. Unchern, T. Maher, Neuropharmacological profile of tetrahydrofuran in mice, *Life Sci.* **80**, 1656 (2007).
- [4] A. Aouissi, S. Al-Deyab, H. Al-Shahri, The cationic ring-opening polymerization of tetrahydrofuran with 12-tungstophosphoric acid, *Molecules* **15**, 1398 (2010).
- [5] M. Lepage, S. Letarte, M. Michaud, F. Motte-Tollet, M.-J. Hubin-Franskin, D. Roy, L.Sanche, Electron spectroscopy of resonance-enhanced vibrational excitations of gaseous and solid tetrahydrofuran, *J. Chem. Phys.* **109**(14), 2915 (1998).
- [6] W. Lafferty, D. Robinson, R. Louis, J. Russell, H. Strauss, Far infrared spectrum of tetrahydrofuran: spectroscopic evidence for pseudorotation, *J. Chem. Phys.* **42**(8), 2915 (1965).
- [7] J. Kilpatrick, K. Pitzer, R. Spitzer, The thermodynamics and molecular structure of cyclopentane, *J. Am. Chem. Soc.* **69**(10), 2483 (1947).
- [8] G. J. Davies, A. Planas, C. Rovira, Conformational analyses of the reaction coordinate of glycosidases, *Acc. Chem. Res.* **45**(0), 308–316 (2012).
- [9] R. D. Hancock, A. E. Martell, Ligand design for selective complexation of metal ions in aqueous solution, *Chem. Rev.* **89**(8), 1875–1914 (1989).
- [10] S. Begel, R. Puchta, R. van Eldik, Host-guest complexes of calix[4]tubes - prediction of ion selectivity by quantum chemical calculations, *J. Mol. Model.* **20**, 280 (2014).
- [11] H.-Y. Gong, D.-X. Wang, G.-Y. Zheng, M.-X. Wang, Highly selective complexation of metal ions by the self-tuning tetraazacalixpyridine macrocycles., *Tetrahedron* **65**, 87–92 (2009).
- [12] E. Marsault, M. L. Peterson, Macrocycles are great cycles: Applications, opportunities, and challenges of synthetic macrocycles in drug discovery, *J. Med. Chem.* **54**, 1961–2004 (2011).
- [13] F. Giordanetto, J. Kihlberg, Macrocyclic drugs and clinical candidates: What can medicinal chemists learn from their properties., *J. Med. Chem.* **57**, 278–295 (2014).
- [14] E. A. Villar, D. Beglov, S. Chennamadhavuni, J. A. Porco, D. Kozakov, S. Vajda, A. Whitty, How proteins bind macrocycles, *Nat. Chem. Biol.* **10**, 723–731 (2014).

- [15] E. M. Driggers, S. P. Hale, J. Lee, N. K. Terrett, The exploration of macrocycles for drug discovery-an underexploited structural class, *Nat. Rev. Drug Discovery* **7**, 608–624 (2008).
- [16] C. Altona, M. M. Sundaralingam, Conformational analysis of the sugar ring in nucleosides and nucleotides. new description using the concept of pseudorotation., *J. Am. Chem. Soc.* **94**(8205-8212) (1972).
- [17] W. Bains, R. Tacke, Silicon chemistry as a novel source of chemical diversity in drug design, *Curr. Opin. Drug Discovery Devel.* **6**(4), 526–543 (2003).
- [18] R. Ramesh, D. Srinivasa, Quest for novel chemical entities through incorporation of silicon in drug scaffolds, *J. Med. Chem* **61**(9), 3779–3798 (2018).
- [19] J. Salem, Transparent armor ceramics as spacecraft windows, *J. Am. Ceram. Soc.* **96**(1), 281–289 (2012).
- [20] C. B. Carter, M. G. Norton, *Ceramic materials: Science and engineering* (Springer, 2007).
- [21] J. Ballato, T. Hawkins, P. Foy, R. Stolen, B. Kokuoz, M. Ellison, C. McMillen, J. Reppert, A. M. Rao, M. Daw, S. Sharma, R. Shori, O. Stafsudd, R. R. Rice, D. R. Powers, Silicon optical fiber, *OSA Publishing* **16**, 18675. (2008).
- [22] A. J. Snell, K. D. Mackenzie, W. E. Spear, P. G. LeComber, A. J. Hughes, Application of amorphous silicon field effect transistors in addressable liquid crystal display panels, *Appl. Phys. A* **24**, 357–362 (1981).
- [23] R. R. LeVier, M. C. Harrison, R. Cook, T. Lane, What is silicone?, *J. Clinical Epidimiology* **48**, 513–517. (1995).
- [24] A. M. Muzafarov, *Advances in Polymer Science: Silicon Polymers* (Springer, 2010).
- [25] R. D. Miller, Polysilane high polymers, *Chem. Rev.* **89**, 1359–1410 (1989).
- [26] R. J. Hoffman, M. Vlatkovic, F. Wiesbrock, Fifty years of hydrosilylation in polymer science. a review of current trends of low-cost transition-metal and metal-free catalysts, non-thermally triggered hydrosilylation reactions, and industrial applications, *Polymers* **9**(10), 543 (2017).
- [27] S. Inayama, K. Mamoto, T. Shibata, T. Hirose, Structure and antitumor activity relation of 2-arylidene-4-cyclopentene-1, 3-diones and 2-arylideneindan-1, 3-diones, *J. Med. Chem.* **19**(3), 433 (1975).
- [28] G. R. Jachak, R. Ramesh, D. G. Sant, S. U. Jorwekar, M. R. Jadhav, S. G. Tupe, M. V. Deshpande, D. S. Reddy, Silicon incorporated morpholine antifungals: Design, synthesis, and biological evaluation, *ACS Med. Chem. Lett* **6**(11), 1111–1116 (2015).

- [29] T. Ouchi, K. Hagita, M. Kwashima, T. Inoi, T. Tashiro, Synthesis and anti-tumor activity of vinyl polymers containing 5-fluorouracils attached via carbamoyl bonds to organosilicon groups, *J. Controlled Release* **8**(2), 141–150 (1988).
- [30] R. Lekphrom, K. Kanokmedhakul, F. Schevenels, S. Kanokmedhakul, Antimalarial polyoxygenated cyclohexene derivatives from the roots of *uvaria cherrevensis*, *Fitoterapia* **127**, 420–424 (2018).
- [31] V. M. Dembitsky, T. A. Loriozova, V. V. Porikov, Biological activities of organometalloid (as, at, b, ge, si, se, te) steroids, *J. App. Pharm. Sci.* **7**(11), 184–202 (2017).
- [32] J. T. Edward, N. E. Lawon, D. L'Anglais, Optical activities of two steroids containing a chiral cyclopentene ring, *Can. J. Chem.* **50**, 766 (1972).
- [33] R. Tacke, H. Zilch, Sila-substitution – a useful strategy for drug design?, *Endeavour* **10**, 191–197 (1986).
- [34] U. G. Survey, "germanium – statistics and information", U.S. Geological Survey, Mineral Commodity Summaries. (2008).
- [35] K. Avarmaa, L. Klemettinen, H. O'Brien, P. Taskinen, A. Jokilaakso, Critical metals ga, ge and in: Experimental evidence for smelter recovery improvements, *Minerals* **9**(6), 367 (2019).
- [36] Q. Shen, S. Rhodes, Y. Takeuchi, K. Tanaka., Molecular structures of germacyclohexane and 1,1-dimethylgermacyclohexane as determined by gas-phase electron diffraction, *Organometallics* **11**(4), 1752–1754 (1992).
- [37] V. Aleksa, D. Ozerenskis, M. Pucetaite, C. Cotter, G. A. Guirgis, V. Sablinskas, Infrared and raman spectra. dft-calculations and spectral assignments of germacyclohexane, *AIP Conference Proceedings* (2015).
- [38] A. C. Reber, S. Paranthaman, P. A. C. amd S. A. Khanna, A. W. C. Jr., From sio molecules to silicates in circumstellar space: Atomic structures. growth patterns. and optical signatures of sinom clusters, *ACS Nano* **2**(8) (2008).
- [39] A. C. Reber, P. A. Clayborne, J. U. Reveles, S. N. Khanna, A. W. Castleman, A. Ali, Silicon oxide nanoparticles reveal the origin of silicate grains in circumstellar environments., *Nano Lett.* **6**(6), 1190–1195 (2006).
- [40] N. M. Tam, H. T. Pham, N. T. Cuong, N. T. Tung, A dft investigation on geometry and chemical bonding of isoelectronic  $si_8n_6v$ .  $si_8n_6cr$ . and  $si_8n_6mn+$  clusters., *Chem. Phys. Lett.* **685**, 410–415 (2017).
- [41] Y. Zhu, B. Li, G. Ye, First principle study on  $simnm$  and  $simmm\pm 1$  ( $m=2-10$ ) clusters., *Comput. Theor. Chem.* **1017**(162-167) (2013).
- [42] E. Owusu-Ansah, Y. M. Wang, Y. J. Shi, A theoretical study of the structures and electronic transitions of small silicon nitride clusters ( $sinnm$ .  $n + m$  4), *J. Mol. Spectrosc.* **330**, 200–210 (2016).

- [43] E. Whittle, D. A. Dows, G. C. Pimentel, Matrix isolation method for the experimental study of unstable species, *J. Chem. Phys.* **22**(11), 1943 (1954).
- [44] E. D. Becker, G. C. Pimentel, Spectroscopic studies of reactive molecules by the matrix isolation method, *J. Chem. Phys.* **22**(224) (1956).
- [45] I. Norman, G. Porter, Trapped atoms and radicals in a glass cage, *Nature* **174**, 508 (1954).
- [46] L. Chan, G. Hutchison, G. M. Morris, Understanding ring puckering in small molecules and cyclic peptides, *J. Chem. Inf. Model.* **61**(2), 1549–9596 (2021).
- [47] D. Cremer, J. A. Pople, General definition of ring puckering coordinates, *J. Am. Chem. Soc.* **97**(6), 1345–1358 (1975).
- [48] L. Paoloni, S. Rampino, V. Barone, Potential-energy surfaces for ring-puckering motions of flexible cyclic molecules through cremer–pople coordinates: Computation, analysis, and fitting, *J. Chem. Theory Comput.* **15**, 4280–4294 (2019).
- [49] D. Cremer, J. A. Pople, Molecular orbital theory of the electronic structure of organic compounds. xxiii. pseudorotation in saturated five-membered ring compounds, *J. Am. Chem. Soc.* **97**(6), 1358–1367 (1975).
- [50] Y. K. Kang, H. Park, Puckering transitions in cyclohexane: revisited, *Chem. Phys. Lett.* **702**, 82–89 (2018).
- [51] C. A. G. Haasnoot, The conformation of six-membered rings described by puckering coordinates derived from endocyclic torsion angles., *J. Am. Chem. Soc.* **114**, 882–887 (1992).
- [52] H. B. Mayes, L. J. Broadbelt, G. T. Beckham, How sugars pucker: Electronic structure calculations map the kinetic landscape of five biologically paramount monosaccharides and their implications for enzymatic catalysis., *J. Am. Chem. Soc.* **136**(3), 1008–1022 (2014).
- [53] A. Ionescu, A. Bérces, M. Zgierski, D. Whitfield, T. Nukada, Conformational pathways of saturated six-membered rings. a static and dynamical density functional study, *J. Phys. Chem. A* **109**, 8096 (2005).
- [54] A. Bérces, D. Whitefield, T. Nukada, Quantitative description of six-membered ring conformations following the iupac conformational nomenclature, *Tetrahedron* **57**, 477–491 (2001).
- [55] J. Schwarz, Rules for conformation nomenclature for five- and six-membered rings in monosaccharides and their derivatives, *J.C.S. Chem. Comm.* **14**, 505–508 (1973).
- [56] F. Taddei, E. Kleinpeter, The anomeric effect in substituted cyclohexanes. i. the role of hyperconjugative interactions and steric effect in monosubstituted cyclohexanes, *J. Mol. Struct.: THEOCHEM* **683**(1-3), 29–41 (2004).

- [57] F. Freeman, C. Fang, B. A. Shainyan, Relative energies, stereoelectronic interactions, and conformational interconversion in silacycloalkanes, *Int. J. Quantum Chem.* **100**, 720–732 (2004).
- [58] I. Arnason, G. Thorarinnsson, E. Matern, Conformations of silicon-containing rings: part 1. a conformational study on 1,3,5-trisilacyclohexane. comparison of ab initio, semiempirical, and molecular mechanics calculations. conformational energy surface of 1,3,5-trisilacyclohexane, *J. Mol. Struct.: THEOCHEM* **454**, 91–102 (1998).
- [59] B. Cadioli, E. Gallinella, C. Coulombeau, H. Jobic, G. Berthier, Geometric structure and vibrational spectrum of tetrahydrofuran, *J. Phys. Chem.* **97**, 7844 (1993).
- [60] S. Han, Y. Kang, Pseudorotation in heterocyclic five-membered rings: tetrahydrofuran and pyrrolidine, *J. Mol. Struct. THEOCHEM* **396**, 157 (1996).
- [61] M. Strajbl, J. Florian, Density functional calculations of the pseudorotational flexibility of tetrahydrofuran, *Theor. Chem. Accounts* **99**, 166 (1998).
- [62] D. Melnik, S. Gopalakrishnan, T. Miller, F. Lucia, The absorption spectroscopy of the lowest pseudorotational states of tetrahydrofuran, *J. Chem. Phys.* **118**, 3589 (2000).
- [63] V. Rayon, J. Sordo, Pseudorotation motion in tetrahydrofuran: an ab initio study, *J. Chem. Phys.* **122**, 204–303 (2005).
- [64] T. Ford, The evolution of the structural, vibrational and electronic properties of the cyclic ethers – on ring size. an ab initio study, *J. Mol. Struct.* **1073**, 125–133 (2014).
- [65] A. D. Boese, R. Boese, Tetrahydrothiophene and tetrahydrofuran, computational and x-ray studies in the crystalline phase, *Cryst. Growth Des.* **15**(3), 1073–1081 (2014).
- [66] T. Yang, G. Su, C. Ning, J. Deng, F. Wang, S. Zhang, X. Ren, Y. Huang, New diagnostic of the most populated conformer of tetrahydrofuran in the gas phase, *J. Phys. Chem. A* **111**, 4927 (2007).
- [67] F. Billes, H. Boehlig, M. Ackermann, M. K. ", A vibrational spectroscopic study on furan and its hydrated derivatives, *J. Mol. Struct. THEOCHEM* **672**, 1 (2004).
- [68] R. Meyer, J. C. López, J. L. Alonso, S. Melandri, P. G. Favero, W. Caminati, Pseudorotation pathway and equilibrium structure from the rotational spectrum of jet-cooled tetrahydrofuran, *J. Chem. Phys.* **111**, 7871 (1999).
- [69] A. H. Mamleev, L. N. Gunderova, R. V. Galeev, Microwave spectrum and hindered pseudorotation of tetrahydrofuran, *J. Struct. Chem.* **42**, 365 (2001).

- [70] J. Chandrasekhar, W. L. Jorgensen, Monte carlo simulations of liquid tetrahydrofuran including pseudorotation, *J. Chem. Phys.* **77**, 5073 (1982).
- [71] L. T. da Silva, J. R. S. Politi, R. Gargano, Theoretical study of tetrahydrofuran: Comparative investigation of spectroscopic and structural properties between gas and liquid phases, *Int. J. Quant. Chem.* **111**, 2914 (2011).
- [72] R. Weast, *CRC, Handbook of Chemistry and Physics* (Boca Raton, Florida: Chemical Rubber Company Publishing, 1984).
- [73] L. Pauling, The nature of the chemical bond. iv. the energy of single bonds and the relative electronegativity of atoms, *J. Am. Chem. Soc.* **54**, 3570–3582 (1931).
- [74] B. R. Luke, J. A. Pople, M. B. Krogh-Jespersen, Y. Apeloig, J. Chandrasekhar, P. von. R Schleyer, A theoretical survey of singly bonded silicon compounds. comparison of the structures and bond energies of silyl and methyl derivatives, *J. Am. Chem. Soc.* **108**, 260–269 (1986).
- [75] K. I. Jentzsch, T. Min, J. I. Etcheson, J. C. Fettinger, A. K. Franz, Silyl fluoride electrophiles for the enantioselective synthesis of silylated pyrrolidine catalysts, *J. Org. Chem.* **76**, 7065–7075 (2011).
- [76] E. W. Colvin, *Silicon in Organic Synthesis* (Butterworths: London, 1981).
- [77] E. J. Corey, X.-M. Cheng, *The logic of chemical synthesis* (JOHN WILEY SONS, 1986).
- [78] H. E. Suess, H. C. Urey, Abundances of the elements, *Rev. Modern Phys.* **28**, 53–74. (1956).
- [79] G. Busch, Early history of the physics and chemistry of semiconductors – from doubts to fact in a hundred years, *Eur. J. Phys.* **10**(4), 254–263 (1989).
- [80] M. Riordan, L. Hoddeson, The origins of the p-n junction, *IEEE Spectrum* **34**(6), 46 (1997).
- [81] W. Monch, *Semiconductor Surfaces and Interfaces* (Berlin-Heidelberg: Springer, 2001).
- [82] D. Laws, 13 sextillion counting: The long winding road to the most frequently manufactured human artifact in history, Computer History Museum (2020).
- [83] J. S. Millership, M. L. Shanks, Prodrugs utilizing a reversible silyl linkage, *Int. J. Pharm.* **28**, 1–9 (1982).
- [84] S. Fujii, Expanding the chemical space of hydrophobic pharmacophores: the role of hydrophobic substructures in the development of novel transcription modulators, *Med. Chem. Comm* **7**, 1082–1092 (2016).



- [85] B. Vivet, F. Cavelier, J. Martinez, Synthesis of silaproline, a new proline surrogate, *Eur. J. Org. Chem* 807–811 (2000).
- [86] M. Mortensen, R. Husmann, E. Veri, C. Bolm, Synthesis and applications of silicon-containing  $\alpha$ -amino acids, *Chem. Soc. Rev* **38**, 1002–1010 (2009).
- [87] C. A. Chen, S. M. Sieburth, A. Glekas, G. W. Hewitt, G. L. Trainor, S. Erickson-Viitanen, S. S. Garber, B. Cordova, S. Jeffry, R. M. Klabe, Drug design with a new transition state analog of the hydrated carbonyl: silicon-based inhibitors of the hiv protease, *Chem. Biol.* **8**, 1161–1166 (2001).
- [88] S. M. Sieburth, T. Nittoli, A. M. Mutahi, L. Guo, Silanediols: a new class of potent protease inhibitors, *Angew. Chem., Int. Ed* **37**, 812–814 (1988).
- [89] S. M. Sieburth, C. A. Chen, Silanediol protease inhibitors: from conception to validation., *Eur. J. Org. Chem.* (2), 311–322 (2006).
- [90] D. H. Juers, J. Kim, B. W. Matthews, S. M. Sieburth, Structural analysis of silanediols as transition-state-analogue inhibitors of the benchmark metalloprotease thermolysin, *Biochemistry* **44**, 16524–16528 (2005).
- [91] J. Kim, K. Glekas, S. M. Sieburth, Silanediol-based inhibitor of thermolysin, *Bioorg. Med. Chem. Lett.* **12**, 3625–3627 (2002).
- [92] S. Clarson, J. Fitzgerald, M. Owen, S. Smith, M. V. Dyke, *Advances, Silicones and Silicone Modified Materials. ACS Symposium Series* (2010).
- [93] J. Blitz, C. Little, *Fundamental and Applied Aspects of Chemically Modified Surfaces* (The Royal Society of Chemistry, 1999).
- [94] J. El-Maiss, T. Darmanin, E. T. D. Givenchy, S. Amigoni, J. Eastoe, M. Sagisaka, F. Guittard, Superhydrophobic surfaces with low and high adhesion made from mixed (hydrocarbon and fluorocarbon) 3,4-propylenedioxythiophene monomers, *J. Polym. Sci. Part B: Polym. Phys.* **52**(11), 782–788 (2014).
- [95] H. A. Taha, M. R. Richards, T. L. Lowary, Conformational analysis of furanoside-containing mono- and oligosaccharides, *Chem. Rev.* **113**, 1851 (2013).
- [96] K. Nester, K. Gaweda, W. Plazinski, A gromos force field for furanose-based carbohydrates, *J. Chem. Theory Comput.* **15**, 1168 (2019).
- [97] C. Cabrele, O. Reiser, The modern face of synthetic heterocyclic chemistry, *J. Org. Chem.* **81**, 10109 (2016).
- [98] J. Jampilek, Heterocycles in medicinal chemistry, *Molecules* **24**, 3839 (2019).

- [99] H. J. Chun, L. F. Colegrove, J. Laane, Theoretical calculations, far-infrared spectra and the potential energy surfaces of four cyclic silanes, *Chem. Phys.* **431–432**, 15–19 (2014).
- [100] Z. Chen, J. van Wijngaarden, Theoretical calculations, far-infrared spectra and the potential energy surfaces of four cyclic silanes, *J. Mol. Spectrosc.* **269**, 137–140 (2011).
- [101] C. A. Stortz, A. M. Sarotti, Exhaustive exploration of the conformational landscape of mono- and disubstituted five-membered rings by dft and mp2 calculations, *RSC Advances* **9**, 24134 (2019).
- [102] N. Sakhaee, S. A. Jalili, F. Darvish, Spherical conformational landscape shed new lights on fluxional nature of cyclopentane and its derivatives, confirmed by their raman spectra, *Comput. Theor. Chem.* **1090**, 193–202 (2016).
- [103] S. Sakhaee, M. H. Sakhaee, A. Takallou, F. Forouzanfar, N. Sakhaee, Fluxional nature in cyclohexane and cyclopentane: spherical conformational landscape model revisited, *J Chem Sci* **132**, 11 (2020).
- [104] J. Durig, W. Lafferty, V. Kalasinsky, Spectra and structure of small-ring molecules. 33. microwave spectrum of silacyclopentane, *J. Phys. Chem.* **80**, 1199–1202 (1976).
- [105] G. A. Guirgis, A. M. E. Defrawy, T. K. Gounev, M. S. Soliman, J. R. Durig, Conformational stability, r0 structural parameters, ab initio calculations, and vibrational assignment for silacyclopentane, *J. Mol. Struct.* **832**, 73–83 (2007).
- [106] L. F. Colegrove, J. C. Wells, J. Laane, Far-infrared spectra and two-dimensional potential energy surface of silacyclopentane and its deuterated isotopomers, *Chemical Physics* **93**, 6291–6302 (1990).
- [107] I. O. C. Ekejiuba, H. E. Hallam, Spectroscopic studies of cyclopentyl compounds—i. infra-red and raman spectra of cyclopentyl mono-halides, *Spectrochim. Acta A Mol. Spect.* **26**(1), 59–66 (1970).
- [108] I. O. C. Ekejiuba, H. E. Hallam, Spectroscopic studies of cyclopentyl compounds—ii. conformational isomerism and  $\nu(\text{c-hal})$  frequencies of cyclopentyl mono-halides, *Spectrochim. Acta A Mol. Spect.* **26**(1), 67–75 (1970).
- [109] J. R. Durig, A. M. E. Defrawy, A. Ganguly, T. K. Gounev, G. A. Guirgis, Conformational stability, r0 structural parameters, ab initio calculations, and vibrational assignment for fluorocyclopentane, *J. Phys. Chem. A* **113**, 9675–9683 (2009).
- [110] J. R. Durig, S. S. Panikar, K. A. Glenn, Y. Y. Zheng, G. A. Guirgis, Infrared and raman spectra, conformational stability and vibrational assignment of 1-chloro-1-silacyclopentane, *Vib. Spectrosc.* **55**, 250 (2011).

- [111] G. A. Guirgis, S. S. Panikar, J. J. Klaassen, S. S. Purohit, M. D. Johnston, J. R. Durig, Infrared and raman spectra, ab initio calculations, conformational stability and vibrational assignment of 1-bromo-1-silacyclopentane, *Spectrochim. Acta A* **79**, 858 (2011).
- [112] S. Bel, H. D. Stidham, A. J. LaPlante, Y. Y. Zheng, G. A. Guirgis, Conformational stability, ab initio calculations and vibrational assignment for 1,1-difluoro- and 1,1-dichloro-1-silacyclopentane, *J. Mol. Struct.* **992**(1-3), 1–8 (2011).
- [113] D. L. Philen, T. H. Chao, J. Laane, Vibrational analyses of silacyclopentanes, *J. Mol. Struct.* **16**, 417–431 (1973).
- [114] H. Pickett, H. Strauss, Conformational structure. energy. and inversion rates of cyclohexane and some related oxanes, *J. Am. Chem. Soc.* **92**(25), 7281–7290 (1970).
- [115] E. Eliel, S. Wilen, *Stereochemistry of Organic Compounds* (John Wiley Sons, 2008).
- [116] J. Durig, C. Zheng, A. E. Defrawy, R. Ward, T. Gounev, K. Ravindranath, N. Rao, On the relative intensities of the raman active fundamentals. structural parameters. and pathway of chair-boat interconversion of cyclohexane and cyclohexane-d<sub>12</sub>, *J. Raman Spectros.* **40**, 197–204 (2009).
- [117] G. Brugger, H.-M. Frey, P. Steinegger, F. Balmer, S. Leutwyler, Accurate determination of the structure of cyclohexane by femtosecond rotational coherence spectroscopy and ab initio calculations, *J. Phys. Chem. A* **115**, 9567–9578, (2011).
- [118] G. Brugger, P. S. H.-M. Frey, P. Kowalewski, S. Leutwyler, Femtosecond rotational raman coherence spectroscopy of cyclohexane in a pulsed supersonic jet, *J. Phys. Chem. A* **115**(44), 12380–12389 (2011).
- [119] D. Dixon, A. Komornicki, Ab initio conformational analysis of cyclohexane, *J. Phys. Chem.* **94**, 5630 (1990).
- [120] E. Białkowska-Jaworska, M. Jaworski, Z. Kisiel, The structure of cyclohexane, f-, cl-, br- and i-cyclohexane, *J. Mol. Struct.* **350**(3), 247–254 (1995).
- [121] B. Smith, From cyclohexane to 2-hydroxy-3-oxanone: A conformation study, *J. Phys. Chem. A* **102**, 3756 (1998).
- [122] C. Riehn, V. Matyilitsky, W. Jarzaba, B. Brutschy, P. Tarakeshwar, K. Kim, Insights into the structure of cyclohexane from femtosecond degenerate fourwave mixing spectroscopy and ab initio calculations, *J. Am. Chem. Soc.* **125**, 16455 (2003).
- [123] K. Kakhiani, U. Lourderaj, W. Hu, D. Birney, W. Hase, Cyclohexane isomerization. unimolecular dynamics of the twist-boat intermediate, *J. Phys. Chem. A* **113**, 4570 (2009).

- [124] J. Demaison, N. Craig, P. Groner, P. Écija, E. Cocinero, A. Lesarri, H. Rudolph, Accurate equilibrium structures for piperidine and cyclohexane, *J. Phys. Chem. A* **119**, 1486 (2015).
- [125] F. Cortés-Guzmán, J. Hernández-Trujillo, G. Cuevas, The nonexistence of repulsive 1,3-diaxial interactions in monosubstituted cyclohexanes, *J. Phys. Chem. A* **107**(44), 9253–9256 (2003).
- [126] J. Dommen, T. Brupbacher, G. Grassi, A. Bauder, Microwave spectra of isotopicspecies and substitution structure of cyclohexane, *J. Am. Chem. Soc.* **112**, 953–957 (1990).
- [127] R. Peters, W. Walker, A. Weber, High resolution raman spectroscopy of gases with laser sources. vii: The rotational spectrum of cyclohexane- $c_6h_{12}$  and  $c_6d_{12}$ , *J. Raman Spectrosc.* **1**, 159 (1973).
- [128] E. Juaristi, G. Cuevas, A. Vela, Stereoelectronic interpretation for the anomalous  $^1h$  nmr chemical shifts and one-bond  $c-h$  coupling constants (perlin effects) in 1,3-dioxanes, 1,3-oxathianes, and 1,3-dithianes. spectroscopic and theoretical observations, *J. Am. Chem. Soc.* **116**, 5796 (1994).
- [129] G. Cuevas, E. Juaristi, A. Vela, Density functional calculation of  $^1j_c-h$  coupling constants in cyclohexane and diheterocyclohexanes. repercussion of stereoelectronic effects on coupling constants, *J. Phys. Chem. A* **103**, 932 (1999).
- [130] F. Anet, D. O’Leary, P. Williams, Tritium nmr in conformational analysis: isotopic perturbation of the ring inversion equilibrium in  $[^3h]$ cyclohexane, *J. Chem. Soc. Chem. Commun.* **20**, 1427–1429 (1990).
- [131] J. Ewbank, G. Kirsch, L. S. 1, Electron-diffraction study of hydrogen isotope effects in cyclohexane, *J. Mol. Struct.* **31**(1), 39–45 (1976).
- [132] N. Leventis, S. Hanna, C. Sotiriou-Leventis, A three-dimensional energy surface for the conformational inversion of cyclohexane, *J. Chem. Educ.* **74**(7), 813 (1997).
- [133] U. Salzner, P. v. R. Schleyer, Ab initio examination of anomeric effects in tetrahydropyrans, 1,3-dioxanes, and glucose, *J. Org. Chem.* **59**(8), 2138–2155 (1994).
- [134] A. J. L. Jesus, J. S. Redinha, Charge-assisted intramolecular hydrogen bonds in disubstituted cyclohexane derivatives, *J. Phys. Chem. A* **115**(48), 14069–14077 (2011).
- [135] U. Burkert, *Molecular mechanics*, ACS monograph **177** (1982).
- [136] A. Weldon, T. Vickrey, G. Tschumper, Intrinsic conformational preferences of substituted cyclohexanes and tetrahydropyrans evaluated at the ccSD(T) complete basis set limit: implications for the anomeric effect, *J. Phys. Chem.* **109**(48), 11073–11079 (2005).

- [137] Z. Smith, A. Almenningen, E. Hengge, D. Kovar, Investigating the microstructure of poly(cyclosilane) by  $^{29}\text{Si}$  solid-state nmr spectroscopy and dft calculations, *J. Am. Chem. Soc.* **104**(16), 4362–4366 (1982).
- [138] M. R. Frierson, M. R. Imam, V. B. Zalkow, L. N. Allinger, Themm2 force field for silanes and polysilanes, *J. Org. Chem.* **53**(22), 5248–5258 (1988).
- [139] K. Chen, N. Allinger, Molecular mechanics calculations (mm3) on silanes, *J. Phys. Org. Chem.* **10**(9), 697–715 (1997).
- [140] N. Allinger, Y. Yuh, J. Lii, Molecular mechanics—the mm3 force-field for hydrocarbons 0.1, *J. Am. Chem. Soc.* **111**(23), 8551–8566 (1989).
- [141] Q. Shen, R. Hilderbrandt, V. Mastryukov, Molecular structures of silacyclohexane and silacyclopentane as determined by gas phase electron diffraction, *J. Mol. Struct.* **54**, 121–134 (1979).
- [142] L. Goodman, V. Pophristic, Where does the dimethyl ether internal rotation barrier come from?, *Chem. Phys. Lett.* **259**, 287 (1996).
- [143] O. Sovers, C. Kern, R. Pitzer, M. Karplus, Bond-function analysis of rotational barriers: Ethane, *J. Chem. Phys.* **49**, 2592 (1968).
- [144] R. Bader, J. Cheeseman, K. Laidig, K. Wiberg, C. Breneman, Origin of rotation and inversion barriers, *J. Am. Chem. Soc.* **112**, 6530 (1990).
- [145] E. Knight, L. Allen, Rotational barriers originate from energy changes in individual atoms, *J. Am. Chem. Soc.* **117**, 440 (1995).
- [146] I. Arnason, G. Thorarinnsson, E. Matern, A conformational study on silacyclohexane. comparison of ab initio (hf, mp2), dft, and molecular mechanics calculations. conformational energy surface of silacyclohexane, *Anorganische und Allg. Chem.* **626**(4), 853–862 (2000).
- [147] G. Guirgis, C. Nielsen, A. Horn, V. Aleksa, P. Klaeboe, Infrared and raman spectra. dft-calculations and spectral assignments of silacyclohexane, *J. Mol. Struct.* **1023**(12), 189–196 (2012).
- [148] L. Favero, B. Velino, W. Caminati, I. Arnason, A. Kvaran, Structures and energetics of axial and equatorial 1-methyl-1-silacyclohexane, *Organometallics* **25**(16), 3813–3816 (2006).
- [149] A. Bodi, A. Kvaran, S. Jonsdottir, E. Antonsson, S. Wallevik, I. Arnason, A. Belyakov, A. Baskakov, M. H. and H. Oberhammer, Conformational properties of 1-fluoro-1-silacyclohexane. c5h10sihf: gas electron diffraction. low-temperature nmr. temperature-dependent raman spectroscopy and quantum chemical calculations, *Organometallics* **26**, 6544–6550 (2007).
- [150] S. Wallevik, R. Bjornsson, A. Kvaran, S. Jonsdottir, G. Girichev, N. Giricheva, K. Hassler, I. Arnason, Conformational properties of 1-fluoro-1-methylsilacyclohexane and 1-methyl-1-trifluoromethyl-1-silacyclohexane: gas electron diffraction. low-temperature nmr.

- temperature-dependent raman spectroscopy. and quantum chemical calculations, *J. Mol. Struct.* **1-3**, 209–219 (2010).
- [151] A. Belyakov, A. Baskakov, R. Berger, N. Mitzel, H. Oberhammer, I. Arnason, S. Wallevik, Molecular structure and conformational preferences of gaseous 1-iodo-1-silacyclohexane, *J. Mol. Struct.* **1012**, 126–130 (2012).
- [152] A. Belyakov, A. Baskakov, V. Naraev, Molecular structure and conformational preferences of 1-chloro-1-silacyclohexane, *ch<sub>2</sub>(ch<sub>2</sub>ch<sub>2</sub>)<sub>2</sub>sih-cl*, as studies by gas-phase electron diffraction and quantum chemistry, *Russ. J. Gen. Chem.* **81**, 2257–2261 (2011).
- [153] V. Aleksa, G. A. Guirgis, A. Horn, P. Klæboe, R. J. Liberatore, C. J. Nielsen, Vibrational spectra, conformations, quantum chemical calculations and spectral assignments of 1-chloro-1-silacyclohexane, *J. Mol. Struct.* **61**, 167–175 (2012).
- [154] R. Bjornsson, I. Arnason, Conformational properties of six-membered heterocycles: accurate relative energy differences with dft. the importance of dispersion interactions and silicon substitution effects, *Phys. Chem. Chem. Phys.* **11**, 8689–8697 (2009).
- [155] I. Arnason, A. Kvaran, S. Jonsdottir, P. Gudnason, H. Oberhammer, Conformations of silicon-containing rings. 5. conformational properties of 1-methyl-1-silacyclohexane: gas electron diffraction, low-temperature nmr, and quantumchemical calculations, *J. Org. Chem.* **67**, 3827 (2002).
- [156] P. Klæboe, A. Horn, C. Nielsen, V. Aleksa, G. Guirgis, J. Wyatt, H. Dukes, Infrared and raman spectra, conformations, quantum chemical calculations and spectral assignments of 1-methyl-1-silacyclohexane, *J. Mol. Struct.* **1034**, 207–215 (2013).
- [157] P. Jena, Q. Sun, Super atomic clusters: Design rules and potential for building blocks of materials, *Chem. Rev.* **11**, 5755–5870 (2018).
- [158] J. U. Reveles, P. A. Clayborne, A. C. Reber, S. N. Khanna, K. Pradhan, P. Sen, M. R. Pederson, Designer magnetic superatoms, *Nat. Chem.* **4**, 310–315 (2009).
- [159] F. Oba, K. Tatsumi, H. Adachi, I. Tanaka, N- and p-type dopants for cubic silicon nitride, *Appl. Phys. Lett.* **78**, 1577–1579 (2001).
- [160] J. Emsley, *Nature's Building Blocks* (Oxford: Oxford University Press, 2001).
- [161] Y. Takeuchi, M. Shimoda, K. Tanaka, S. Tomoda, K. Ogawa, H. Suzuki, Nuclear magnetic resonance spectra of organogermanium compounds. part 4. nuclear magnetic resonance spectra and molecular mechanics calculations of germacyclohexane, methylgermacyclohexanes, and dimethylgermacyclohexanes, *J Chem Soc Perkin Trans (1)*, 7–13 (1988).

- [162] N. Jonsdottir, A. Kvaran, S. Jonsdottir, I. Arnason, R. Bjornsson, Conformational properties of 1-methyl-1-germacyclohexane: Low-temperature nmr and quantum chemical calculations, *Struct. Chem.* **24**, 769–774 (2013).
- [163] N. B. Colthup, L. H. Daly, S. E. Wiberley, *Introduction to Infrared and Raman Spectroscopy* (1990).
- [164] P. Larkin, *Infrared and Raman Spectroscopy: Principles and Spectral Interpretation* (Elsevier, 2011).
- [165] J. Wang, W. Huang, S. Jiang, Raman spectroscopy for structural analysis of biomolecules., *Analyst.* **144**(16), 4871–4888 (2019).
- [166] K. Maquelin, C. Kirschner, L. P. Choo-Smith, Prospects for the application of raman spectroscopy in clinical microbiology, *J Biomed Opt* **7**(1), 1–11 (2002).
- [167] Y. Ozaki, K. Nakamoto, H. Takeuchi, Raman spectroscopic studies on the conformational changes in proteins induced by ligand binding., *Biopolymers* **74**(6), 406–413 (2004).
- [168] X. Li, S. Li, Y. Li, W. Lu, Z. Liu, Conformational analysis of small peptides and their interaction with metal ions using raman spectroscopy., *J. Raman Spectrosc.* **48**(7), 952–959 (2017).
- [169] B. H. Stuart, *Infrared Spectroscopy: Fundamentals and Applications* (John Wiley Sons, 2004).
- [170] P. R. Griffiths, J. A. D. Haseth, G. S. Hammond (eds.), *Infrared Spectroscopy: Theory, Practice and Applications* (CRC Press, 2001).
- [171] M. R. Derrick, D. Stulik, J. M. Landry, *Infrared Spectroscopy in Conservation Science* (The Getty Conservation Institute, 1999).
- [172] J. Workman, H. Mark, *Modern Fourier Transform Infrared Spectroscopy* (John Wiley Sons, 2001).
- [173] E. K. Potter, K. E. J. Barrett (eds.), *ATR-FTIR Spectroscopy in Polymer Research* (Blackwell Science, 1998).
- [174] T. Bally, *Matrix isolation in reactive intermediate chemistry* (John Wiley Sons, Inc., 2004).
- [175] L. Khriachtchev, *Physics and Chemistry at Low Temperatures* (Pan Stanford, Singapore, 2011).
- [176] A. Barnes, W. J. Orville-Thomas, A. M. R. Gaufrès, *Matrix Isolation Spectroscopy* (Springer Science Business Media, New York, 2012).
- [177] P. Klaeboe, Conformational studies by vibrational spectroscopy: a review of various methods, *Vib. Spectrosc.* **9**, 3–17 (1995).
- [178] A. Barnes, Matrix isolation vibrational spectroscopy as a tool for studying conformational isomerism, *J. Mol. Struct.* **113**, 161–174 (1984).

- [179] P. Klaeboe, C. J. Nielsen, Recent advances in infrared matrix isolation spectroscopy. invited lecture, *Analyst* **117**(3), 335–341 (1992).
- [180] I. R. Dunkin, *Matrix Isolation Techniques: A Practical Approach* (Matrix Isolation Techniques: A Practical Approach, 1998).
- [181] T. Tsuneda, *Density Functional Theory in Quantum Chemistry* (Springer, New York, 2014).
- [182] D. R. Hartree, The wave mechanics of an atom with a non-coulomb central field, *Mathematical Proceedings of the Cambridge Philosophical Society* **24**(1), 89–110 (1928).
- [183] W. Koch, M. C. Holthausen, *A Chemist's Guide to Density Functional Theory* (Wiley-VCH Verlag GmbH, 2001).
- [184] W. J. Hehre, *A Guide to Molecular Mechanics and Quantum Chemical Calculations* (Wavefunction, Inc., 2003).
- [185] A. Kaczmarek-Kedziera, M. Ziegler-Borowska, D. Kedziera, *Chemia obliczeniowa w laboratorium organicznym* (Wydawnictwo Naukowe Uniwersytetu Mikołaja Kopernika, 2014).
- [186] F. Jensen, *Intoduction to Computational Chemistry* (John Wilet & Sons, Ltd, 2007).
- [187] R. F. Nalewajski, *Podstawy i metody chemii kwantowej* (Wydawnictwo Naukowe PWN, 2001).
- [188] P. Hohenberg, W. Kohn, Inhomogenous electron gas), *Phys. Rev.* **136**, B864 (1964).
- [189] R. O. Jones, *Computational Nanoscience: Do It Yourself! Introduction to Density Functional Theory and Exchange-Correlation Energy Functionals* (John von Neumann Institute for Computing, 2006).
- [190] J. P. Perdew, K. Schmidt, Jacob's ladder of density functional aapproximation fot the exchange-correlation energy, *AIP Conf. Proc.* **5777**, 1 (2001).
- [191] C. Fiolhais, F. Nogueira, M. Marques, *A Primer in Density Functional Theory* (Springer-Verlag Berlin Heidelberg, 2003).
- [192] S. Grimme, Semiempirical GGA-type density functional constructed with a long-range dispersion correction, *J. Comp. Chem.* **27**, 1787 (2006).
- [193] S. Grimme, Accurate description of van der waals complexes by density functional theory including empirical corrections, *J. Comp. Chem.* **25**, 1463 (2004).
- [194] T. Shwabe, S. Grimme, Double-hybrid density functionals with long-range dispersion corrections: higher accuracy and extended applicability, *Phys. Chem. Chem. Phys.* **9**, 3397 (2007).



- [195] D. Marx, J. Hutter, *Modern Methods and Algorithms of Quantum Chemistry. Ab initio molecular dynamics: Theory and Implementation* (John von Neumann Institute for Computing, 2000).
- [196] G. B. Bachelet, D. R. Hamann, M. Schluter, Pseudopotentials that work: From h to pu, *Phys. Rev. B* **28**(8), 4199 (1982).
- [197] I. Morrison, D. M. Bylander, L. Kleinman, Nonlocal hermitian norm-conserving vanderbilt pseudopotential, *Phys. Rev. B* **47**(11), 6728 (1993).
- [198] D. Vanderbilt, Soft self-consistent pseudopotentials in a generalized eigenvalue formalism, *Phys. Rev. B* **41**, 7892 (1990).
- [199] L. Piela, *Idee Chemii Kwantowej* (Wydawnictwo Naukowe PWN, 2003, 2011).
- [200] M. C. Payne, M. Teter, D. C. Allan, T. Arias, J. D. Joannopoulos, Iterative minimization techniques for ab initio total-energy calculations: molecular dynamics and conjugate gradients, *Rev. Mod. Phys. Chem. Chem. Phys.* **64**, 1045 (1992).
- [201] R. Car, M. Parrinello, Unified approach for molecular dynamics and density-functional theory, *Phys. Rev. Lett.* **55**, 2471 (1985).
- [202] D. K. Remler, P. A. Madden, Molecular dynamics without effective potentials via car-parrinello approach, *Mol. Phys.* **70**, 921 (1990).
- [203] S. Nosé, *J. Chem. Phys.* **81**, 511 (1984).
- [204] G. B. G. Levine, J. E. Stone, A. Kohlmeyer, Fast analysis of molecular dynamics trajectories with graphicsprocessing units—radial distribution function histogramming, *Journal of Computational Physics* **230**, 3556–3569 (2011).
- [205] S. Holden, D. Beazly, *Python Web Programming* (New Riders Publishing, 2002).
- [206] D. M. Beazley, *Python Essential Reference* (Sams Publishing, 2006).
- [207] F. Neese, Software update: the orca program system, version 4.0: software update, *WIREs Comput. Mol. Sci.* **8**, 1327 (2017).
- [208] A. Becke, Density-functional thermochemistry. iii. the role of exact exchange, *J. Chem. Phys.* **98**, 5648–5652 (1993).
- [209] T. Dunning, Gaussian basis sets for use in correlated molecular calculations. i. the atoms boron through neon and hydrogen, *J. Chem. Phys.* **90**, 1007–1023 (1989).
- [210] S. Grimme, J. Antony, S. Ehrlich, H. Krieg, A consistent and accurate ab initio parametrization of density functional dispersion correction (dft-d) for the 94elements h-pu, *J. Chem. Phys.* **132**, 154104 (2010).

- [211] F. Teixeira, M. Natália, D. Cordeiro, Improving vibrational mode interpretation using bayesian regression, *J. Chem. Theory Comput.* **15**(1), 456–470 (2019).
- [212] A. D. Becke, Density-functional exchange-energy approximation with correct asymptotic behavior, *Phys. Rev. A* **38**, 3098 (1988).
- [213] C. Lee, W. Yang, R. G. Parr, Development of the colle-salvetti correlation-energy formula into a functional of the electron density, *Phys. Rev. B* **37**, 785 (1988).
- [214] R. Car, M. Parrinello, Unified approach for molecular dynamics and density-functional theory, *Phys. Rev. Lett.* **55**, 2471 (1985).
- [215] I. C. 1990-2008, *CPMD*, <http://www.cpmc.org/>, *Copyright IBM Corp 1990-2008* (Copyright MPI fuer Festkoerperforschung Stuttgart 1997-2001, 2011).
- [216] N. Troullier, J. L. Martins, Efficient pseudopotentials for plane-wave calculations, *Phys. Rev. B* **43**, 1993 (1991).
- [217] W. G. Hoover, *Phys. Rev. A* **31**, 1695 (1985).
- [218] J. Kjems, G. Dolling, Crystal dynamics of nitrogen: the cubic alpha-phase, *Phys. Rev. B* **11**, 1639 (1975).
- [219] A. Kohlmeyer, <http://www.theochem.ruhr-uni-bochum.de/axel.kohlmeyer/index.html> .
- [220] R. Ramirez, T. Lopez-Ciudad, P. Kumar, D. Marx, Quantum corrections to classical time-correlation functions: Hydrogen bonding and anharmonic floppy modes, *J. Chem. Phys.* **121**, 3973 (2004).
- [221] W. Humphrey, A. Dalke, K. Schulten, Vmd - visual molecular dynamics, *J. Molec. Graphics* **14**, 33 (1996).
- [222] ChemCraft, Graphical software for visualization of quantum chemistry computations, <https://www.chemcraftprog.com> .
- [223] A. Chemistry, Avogadro, <http://avogadro.cc/> (2016).
- [224] P. Rodziewicz, B. Meyer, Interplay between molecule–molecule and molecule–substrate interactions: first-principles study of fluoroform aggregates on a hexagonal ice (0001) surface, *Phys. Chem. Chem. Phys.* **16**, 940 (2014).
- [225] S. Batsanov, Van der waals radii of elements, *Inorg. Mater.* **37**, 871–885 (2001).
- [226] P. Rodziewicz, S. M. Melikova, K. S. Rutkowski, A. Koll, Ab initio studies of electron acceptor-donor interactions with blue- and red-shifted hydrogen bonds, *ChemPhysChem* **6**, 1282 (2005).
- [227] S. M. Melikova, K. S. Rutkowski, P. Rodziewicz, A. Koll, Comparative studies of blue shifting and red shifting effects in fluoroform and acetylene cryogenic solutions, *J. Mol. Struct.* **705**, 49 (2004).

## CURRICULUM VITAE

**Name:** Joanna  
**Surname:** Stocka  
Date of birth: 1990-03-04  
Place of birth: Białystok, Poland  
E-mail: joana.stocka@gmail.com

### Education:

2015-2022 Vilnius University, Faculty of Physics, Lithuania, *PhD studies*,  
2013-2015 University of Białystok, Institute of Chemistry, Poland *MSc*,  
2010-2013 University of Białystok, Institute of Chemistry, Poland *BSc*,  
2007-2009 3 Liceum Ogólnokształcące, Białystok.

### Practice, workshops

2022 „The practical approach of the classical molecular dynamics”, Traineeship,  
The Chemistry Department, University of Wrocław, Poland,  
2022 „From theory to the experiment: role of the molecular interactions in  
self-organization of the molecules”, seminar/webinar,  
The Chemistry Department, University of Wrocław, Poland,  
2020 Erasmus Practice, Jan Kochanowski University of Kielce, Poland,  
2016 Erasmus Practice, University of Białystok, Poland,  
2016 Molecular Modeling Traineeship  
Toruń School of Molecular Modeling, Supraśl, Poland,  
2015 Molecular modeling, technical course, University of Białystok, Poland,  
2015 A molecule in media, workshop,  
Wrocław Center for Networking and Supercomputing, Wrocław, Poland,  
2015 LLP Erasmus Practice, Erasmus Internship, Vilnius University, Lithuania,  
2015 “Absolwent w Transferowni” training project,  
Group award and personal award as a leader of the group  
2014 LLP Erasmus Practice, Erasmus Internship, Vilnius University, Lithuania,  
2014 Advanced analysis with VisNow programme usage, training,  
Interdisciplinary Center for Mathematical and Computational Modelling,  
2013 Certificate of professional teacher training No. 2329,  
University of Białystok, Poland.

### Work experience:

2023 - now IT Specialist, Roche Global IT Solution Center, Warsaw Poland  
2015 Laboratory, Technician, CEDC International, Białystok, Poland  
2012 Practice: Institute of Plant Protection,  
National Research Institute in Białystok

## NOTES

## NOTES

Vilnius University Press  
Saulėtekio al. 9, LT-10222 Vilnius  
e-mail: [info@leidykla.vu.lt](mailto:info@leidykla.vu.lt),  
[www.leidykla.vu.lt](http://www.leidykla.vu.lt)  
Print run copies 15